Silesian University of Technology

Faculty of Chemistry

Department of Physical Chemistry and

Technology of Polymers

Welisson de Pontes Silva

DOCTORAL DISSERTATION

Design, Synthesis, and Investigation of the Photophysical and Electrochemical Properties of Selected Conjugated Molecules Belonging to Various Classes of Compounds

Promoter: Prof. Dr hab. inż. Mieczysław Łapkowski

Assistant Promoter: Dr inż. Radosław Motyka

Gliwice 2023

Acknowledgments

Firstly, I would like to thank my supervisor Prof. Mieczysław Łapkowski, who believed in my success and ideas and always motivated me to continue my development as a researcher. Thank you for your time, patience, and guidance. In the same way, I would like to thank my co-supervisor, Dr. Radosław Motyka for all valuable discussions about organic synthesis and all contribution to the work.

To Prof. P. Data for all support in the project and encourage to try new applications. I Also want to acknowledge the support received from the National science Centre-NCN under project number 2018-31-B-ST5-03085 (NCN1/2020).

In particular, I also would like to thank my Brazilian family in Poland: Nicolas, Marli, Leandro, Gabi, Leko and Paola, for all valuable discussions about work and also for all friendship that make the days in Poland happier. It was pleasure to work in Prof. Łapkowski group and in the Red Chemistry building, and for that, I would like to thank all my colleagues from our group: Dawid, Klaudia, Ola, Agata, Sandra, Pavel, Kinga, Kumar, Prassana, Jay, Matheus, Szymon, Magdalena, Pyotr, Damian, Sara, Agnieska, Taral, Paulos, Massimiliano, Gosha, Patryk, Abdulla, Ivan, Karolina, for all friendship, as well as time spent in long, fruitful discussions about chemistry and life.

To all my friends who have always been with me in difficult and joyful moments.

And of course, to my girlfriend Suelly for all the love, patience, support, and for always believe in my success in the journey.

E finalmente à toda minha família, em especial aos meus pais, Bina e Edivaldo, por todo o suporte, carinho e cuidado. Amo vocês.

Welisson de Pontes Silva

Abstract

Developing new organic materials for optoelectronic applications such as OLED and OPV continues to be a challenge due to the market demand for more efficient devices that operate with minimum energy consumption. Designing purely organic molecules exhibiting TADF properties may be an excellent strategy for obtaining efficient OLED devices. The design of TADF emitters covers mainly the combinations of electron-acceptor (A) and electron-donor (D) units in twisted D-A structures, obtaining spatially separated HOMO and LUMO orbitals and small singlet-triplet energy gap, which can allow efficient RISC process in molecules.

This work brings the design and synthesis of different A, belonging to various classes of compounds and commonly D moieties (diphenylamine, carbazole, phenothiazine, phenoxazine, acridine derivatives, and azepine derivatives), displaying different configurations of D-A structures to investigate the photophysical and electrochemical properties and consequently suitability to optoelectronic applications. The final compounds were synthesized mainly using N-C and C-C cross-coupling reactions between the brominated acceptors and donors, obtaining moderate to good yields. The acceptor design strategy covered mainly the construction of N-rich systems, such as acenaphtopyridopyrazine, naphthalene benzimidazole, diquinoxaline, diphenazine, derivatives of pyridobenzotriazole isomers, benzopyridoimidazoisoquinolinone, and perylene dianhydride/tetraesthers and triphenylphosphanimine.

All the acceptors were connected with common donors, and their molecular structures were characterized by ^{1}H and ^{13}C Nuclear Magnetic Resonance (NMR) and High-Resolution Mass Spectrometry (HRMS). The electrochemical properties were investigated by cyclic voltammetry (CV), and the energies of HOMO and LUMO levels were estimated from oxidation and reduction potentials, respectively. Additionally, the susceptibility of some compounds to the electrochemical polymerization process was displayed. The photophysical parameters were investigated by UV-Vis and photoluminescence in solution and in the solid state in Zeonex matrix. The profile of the emission was examined in different solvent polarities to understand the nature of the emission (CT and/or LE) of the compounds. Moreover, aggregation-induced emission (AIE) properties were investigated in THF solutions with different water fractions for the acenaphtopyridopyrazine and triphenylphosphanimine derivatives. The properties of the obtained materials indicated that the compounds can be excellent candidates for applications in optoelectronic devices.

Welisson de Pontes Silva

Abstrakt

Opracowywanie nowych materiałów organicznych do zastosowań optoelektronicznych, takich jak OLED czy OPV, nadal stanowi wyzwanie ze względu na zapotrzebowanie rynku na bardziej wydajne urządzenia, które mogą działać przy minimalnym zużyciu energii. Projektowanie związków czysto organicznych, wykazujących właściwości TADF może być doskonałą strategią otrzymywania wydajnych urządzeń OLED. Projektowanie emiterów TADF polega na takim łączeniu związków o charakterze elektronoakceptorowym (A) ze związkami o charakterze elektronodonorowym (D), aby ich końcowa struktura (D-A) przyjęła formę skręconą. Uzyskuje się w ten sposób przestrzenne rozdzielenie orbitali HOMO i LUMO, oraz zwężenie przerwy energetycznej pomiędzy stanami singletowym a trypletowym, co może umożliwić wydajny proces RISC.

W pracy przedstawiono projektowanie i syntezę połączeń akceptorów (A) należących do różnych klas związków oraz powszechnie używanych ugrupowań donorowych (D) (difenyloamina, karbazol, fenotiazyna, fenoksazyna, pochodne akrydyny i pochodne azepiny), w wielu konfiguracjach typu donor-akceptor (D-A), w celu zbadania ich właściwości fotofizycznych oraz elektrochemicznych, a w konsekwencji przydatności do zastosowań w optoelektronice. Końcowe związki zsyntetyzowano stosując reakcje sprzęgania krzyżowego typu N-C i C-C pomiędzy bromowanymi akceptorami i związkami donorowymi, uzyskując umiarkowane bądź dobre wydajności. Plan projektowania akceptorów obejmował tworzenie układów bogatych w azot, takich jak: acenaftopirydopirazyna, naftalenobenzimidazol, dichinoksalina, difenazyna, pochodne izomerów pirydobenzotriazolu, benzopirydo-imidazoizochinolinon, dibezwodnik i tetraestry perylenu oraz trifenylofosfanimina.

Wszystkie akceptory łączono z powszechnie stosowanymi donorami, a strukturę molekularną produktów scharakteryzowano za pomocą magnetycznego rezonansu jądrowego ^{1}H i ^{13}C (NMR) oraz wysokorozdzielczej spektrometrii masowej (HRMS). Właściwości elektrochemiczne badano za pomocą woltamperometrii cyklicznej (CV), a energie poziomów HOMO i LUMO oszacowano, odpowiednio, na podstawie potencjałów utleniania i redukcji. Dodatkowo niektóre związki wykazały podatność na proces polimeryzacji elektrochemicznej. Parametry fotofizyczne badano metodą UV-Vis i fotoluminescencji w roztworze oraz w stanie stałym w matrycy Zeonex. W celu zrozumienia natury emisji związków (CT i/lub LE), badania prowadzono w rozpuszczalnikach o różnej polarności. Ponadto dla pochodnych acenaftopirydopirazyny i trifenylofosfaniminy zbadano właściwości emisji indukowanej agregacją (AIE) w mieszaninach THF-u i wody w różnych proporcjach. Właściwości otrzymanych materiałów wykazały, że związki te mogą być doskonałymi kandydatami do zastosowań w urządzeniach optoelektronicznych.

Welisson de Pontes Silva

Table of contents

Welisson de Pontes Silva

Welisson de Pontes Silva

List of Figures

List of tables

List of Schemes

List of abbreviations and symbols

LE	Locally Excited
Bu_4NBF_4	Tetrabutylammonium Tetrafluoroborate
CE	Counter Electrode
CT	Charge Transfer
D-A	Donor-Acceptor
D-A-D	Donor-Acceptor-Donor
DCM	Dichloromethane
DF	Delayed Fluorescence
EA	Electron Affinity
EBL	Electron-Blocking Layer
E_{HOMO}	Energy level of Highest Occupied Molecular Orbital
E_{LUMO}	Energy level of Lowest Occupied Molecular Orbital
E_{ox}	Oxidation Potential

EQE	External Quantum Efficiency
E_{red}	Reduction Potential
ETL	Electron-Transporting Layer
eV	Electron Volt
OPV	Organic Photovoltaic
HBL	Hole-Blocking Layer
HIL	Hole-Injecting Layer
HOMO	Highest Occupied Molecular Orbital
HTL	Hole-Transporting Layer
ICT	Intramolecular Charge Transfer
IQE	Internal Quantum Efficiency
ISC	Intersystem Crossing
ITO	Indium Tin Oxide
IP	Ionization Potential
TADF	Thermally Activated Delayed fluorescence
RTP	Room-Temperature Fluorescence
RISC	Reverse Intersystem-Crossing
WE	Working Electrode
ΔE_{ST}	Singlet-Triplet Energy Gap
λ_{onset}	Onset Wavelength
S_0	Singlet Ground State
S_1	Singlet Excited State
SOC	Spin-Orbit Coupling
T_1	Triplet Excited State
PL	Photoluminescence
PLQY	Photoluminescence Quantum Yield

1. *Introduction*

The human society is largely dependent on artificial light. Light is in almost everything daily, from illuminating to electronic devices. This shows the relationship of dependence to searching for more technologies related to eco-friendly sources to increase life quality and reduce energy consumption in our society. Therefore, the search for more economical and environmentally friendly light sources is entirely justified. Recently, researches in the field of semiconductors has focused in organic light-emitting diodes (OLEDs), which appear as an alternative strategy to achieve efficient lighting emitters. This shows that the technologies based on organic conjugated materials are related to the future of the OLED market.[1]

Various fields of research into light sources are developing in order to reduce global energy consumption. The future of the lighting market is walking in the search of more efficient devices that can operate at lower voltages and have a wide range of accessible colors. π-Conjugated organic materials have been used in electronic devices and presenting excellent results concerning typical inorganic semiconductors. The flexibility and processability that organic materials can offer to electronic devices minimize the costs and increase the possibilities of applications in electronic industries due to the versatility of functionalization that can be made in conjugated organic molecules.[2] The durability, stability, and preferable solubility in common organic solvents for inkjet printing are the main requirements for prototype applications. Organic materials can already be encountered in commercial OLED display devices, and organic photovoltaic cells (OPVs). The versatility of π-conjugated organic materials consists in the possibility of using them as active organic layers simultaneously in diodes, transistors, solar cells, and others.[3,4]

In this context, searching for new materials that can attend to the parameters necessary to be applied in such devices with high efficiency, color purity, and stability is still challenging. Also, other applications such as OPVs and organic field effect transistors (OFETs) had the necessity of designing and synthesizing more and more compounds to understand the mechanisms involved and improve the efficiencies in using light. To OPVs, the molecular design is based on donor-acceptor structures aiming at the minimization of the band gap. Absorption mainly in the visible region is also requirement, such as solubility in common organic solvents to solution processed techniques. In this way, the design and synthesis of new conjugated organic

compounds is the future of this field. Related to OLEDs, the leading researchers around the world in organic electronics are focusing on Thermally activated delayed fluorescence (TADF) materials which appear as an alternative to high-cost materials based on a metal complex with Iridium, Platinum, and others which are very expensive and scarce.[3,5] TADF materials can achieve 100% internal quantum efficiency (IQE) through triplet harvesting mechanisms. Therewith, the synthesis of new ambipolar organic compounds that can present TADF properties is very important to the development of new low-cost and efficient materials to be applied in optoelectronic devices.

In this way, this work focuses on the design and synthesis of new purely organic ambipolar compounds as candidates to be applied as optoelectronic materials, especially in OLED and OPVs devices. The acceptors (A) will be synthesized covering a wide range of chemical reactions and belong to different classes of compounds. Such as N-rich acenaphtopyridopyrazine (NQPy), flexible diquinoxalines (DQ), rigid diphenazine (NQ), derivatives of pyridobenzotriazole (PyBTZ) isomers, perylene dianhydride (PDA), naphthalene benzimidazole (BTNA), triphenyl phosphanimine (Ph$_3$PN) and benzopyridoimidazoisoquinolinone (PyNA). All the acceptors units will be connected by N-C or C-C cross-coupling reactions with different donor (D) moieties in different D-A structures configurations in order to investigate the structure/properties relationship between them. In addition, the photophysical and electrochemical characterizations performed will give an understanding of the mechanisms involved in light generation and will be supported by the evaluation of electrochemical stability.

Welisson de Pontes Silva

2. Background Theory

2.1 Electronic transitions in organic emitters

The researchers' interest in organic materials capable of exhibiting electroluminescent properties began with the anthracene crystals.[6] This pioneering research led to the exploration of others π-conjugated compounds as potential organic emitters for application in organic electronics. While organic compounds can exhibit high fluorescence quantum efficiencies, purely organic systems presented challenges due to the high voltage requirements for charge injection into organic crystals. In comparison to inorganic systems, these devices demonstrated significantly lower efficiencies and lifetimes.[7] Just at the end of the 1980s, the use of purely organic compounds in optoelectronics was established.[8] As a result, the search for new organic functional materials through the design and synthesis of various π-conjugated compounds that exhibit luminescent properties became crucial for the future of research in materials science.

Considering the photoluminescence process, with light absorption (photon) with the necessary amount of energy, it undergoes electronic transitions from the ground state to excited states. The relaxation to the fundamental state can happen through several processes, which could be described by Jablonski's diagram as shown in **Figure 2.1**.[9]
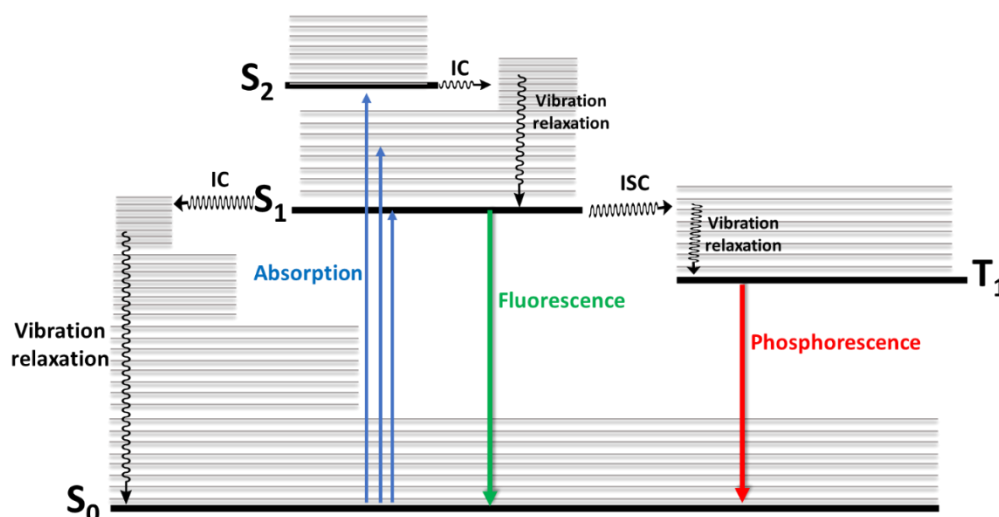
Figure 2.1. *Jablonski diagram for photoluminescence process with absorption, fluorescence, phosphorescence, and vibrational relaxation as non-radiative process. Adapted from*

literature.[6] IC – Internal Conversion; ISC – Intersystem Crossing, S_0 – singlet ground state; S_1 and S_2 – singlet excited states; T_1 – triplet excited state.

When the molecule is excited by photon absorption from the ground state (S_0) to the singlet excited states (S_1, S_2, …S_n), the absorbed energy can be released through radiative and non-radiative deactivation pathways. The vibrational relaxation is a non-radiative deactivation process occurring by dispersion of thermal energy.[10] In the context of energy release by radiative pathways, it may happen with light emission, which is required in organic light-emitting devices. Following the excitation to an excited state in a molecule, one of the electrons is moved from the highest occupied molecular orbital (HOMO) to the lowest unoccupied molecular orbital (LUMO). Generally, the electrons in the ground states have an antiparallel configuration. Based on this configuration, it can be inferred that the total spin number is 0 (-½ + ½), and the corresponding spin multiplicity (2S+1) is equal to 1, indicating a singlet state. However, in the event of an electron spin inversion, the total spin number changes to 1 (½ + ½), and the spin multiplicity increases to 3, denoting a triplet state.[11]

An excited state molecule may exhibit the relaxation from the S_1 state to the ground state ($S_1 \rightarrow S_0$) with the release of energy in the form of a photon, achieving a phenomenon known as fluorescence, as a very fast radiative deactivation process (10^{-10}-10^{-7}s).[12] The electrons in the S_1 state could populate the excited triplet state (T_1) by the intersystem crossing (ISC) process. The ISC presents two states with the same vibrational energy and different spin multiplicity. Generally, the T_1 state presents lower energy than the S_1 state. The electrons in the excited triplet state could undergo de-excitation by radiative decay to the fundamental state ($T_1 \rightarrow S_0$), which is the phosphorescence phenomenon. Due to the parallel spins exhibited by electrons in triplet excited states and the antiparallel spins in singlet states, the transition from T_1 to S_0 (phosphorescence) is characterized by its spin-forbidden nature. Despite being a formally forbidden process, the transition can occur due to spin-orbit coupling (SOC).[13] This transition takes longer time (10^{-6} – 10s), which could increase the quenching of the triplet excited states. Consequently, the rate constants associated with triplet emission are significantly smaller at room-temperature, extending several orders of magnitude compared to those observed in fluorescence. The quenching of excited triplet states by thermal deactivation can be reduced at very low temperatures, which increases the probability of the transition $T_1 \rightarrow S_0$.[14]

Welisson de Pontes Silva

2.2. Organic light-emitting diodes

An organic light-emitting diode (OLED) is a type of light-emitting diode (LED) that incorporates organic compounds as an emitter layer within its structure, enabling the emission of light through excitation by an electric current.[15] The device structures of OLEDs have presented numerous modifications since the initial reports. Typically, the construction involves a thin organic emitting layer that is sandwiched between two electrodes, with one of them being transparent. The Anode is transparent and made of indium tin oxide (ITO) and the cathode is reflective and made of metal.[16] When a driving voltage of 5 to 10 V or lower, is applied across the electrodes, positive and negative charges are injected. To enhance the efficiency of OLED devices, considerable attention has been directed towards multi-layer systems, wherein the additional layers play a crucial role in executing various functions within the device structure.[17] In this particular structure, additional layers, such as Electron-injecting Layers (EIL), Electron-Transporting Layers (ETL), Hole-Injecting Layers (HIL), and Hole-Transporting Layers (HTL) can be observed, as shown in **Figure 2.2**.[15] These layers play a crucial role in facilitating the electron-hole recombination into the emission layer (EML). The EML consists of organic compounds with a high photoluminescence quantum yield, which is aimed at enhancing the efficiency of the device.[18] The operational principle is based on the application of a potential difference, which induces the separation and migration of charge carriers (negative electrons and positive holes) between the layers until they recombine in the emissive layer, forming excitons. Once formed into the EML, these excitons can relax to lower energy levels with the emission of light.[19] The additional layers serve to ensure a higher probability of exciton formation within the EML, preventing the loss of injected charge carriers that may otherwise reduce the device efficiency. The EML plays a crucial role in the performance of the OLED, because it determines the mechanism of relaxation of the excitons in the emission of light. In this way, the efficiency will be directly related to the organic compound used.[20]
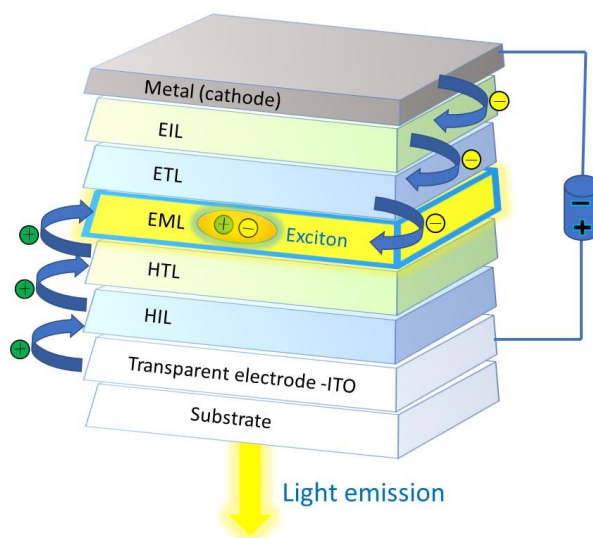
Figure 2.2. *Example of device structure in a multi-layer OLED. Adapted from literature.*[15]

The performance and stability of organic electronics are still in development with the research in the design and synthesis of new organic materials. The most appropriate operations in organic lighting emitting diodes (OLEDs) are dependent on the regular distribution of negative (electrons) and positive (holes) charge carriers.[21] The efficiency of the devices is directly related to the recombination of these charge carriers that will give light properties. The equilibrium in the recombination process can be affected by a high ionization potential or low electron affinity and a large HOMO-LUMO energy gap from materials.[22] These characteristics are influenced by the control of the conjugation length and the introduction of electron-donors (D) and electron-acceptors (A) groups to the materials.[23] There are several kinds of research developments in new materials for OLEDs. Conjugated linear organic molecules, star-shaped and dendritic structures are being investigated as active layers in these kinds of devices. However, significant changes in the molecular design are achieving enhanced properties in the mobility of charge carriers, photophysical and electronic behaviors.[24]

The materials properties to be applied as emitter layer in these devices need to combine high charge-transporting properties and high electroluminescence. These properties can be encountered in molecules with a good level of electron π-conjugation. To obtain good efficiency in OLEDs, the organic active layer needs to attend to some important parameters such as high photoluminescence quantum yields (PLQY) and semiconducting properties. Recently researchers worldwide have been

focusing on the increment of the External Quantum Efficiency (EQE) in OLEDs through mechanisms of thermally activated delayed fluorescence (TADF) or room-temperature phosphorescence (RTP).[25,26]

2.2.1 OLEDs based on purely organic emitters

The OLED devices are commonly divided into phosphorescence and fluorescence emitters.[20] The fluorescence is a fast relaxation process where the emitting energy is related to the returns of the excited molecule in the singlet state (S_1) to the ground state (S_0) by emission in the form of photons. Phosphorescence is a longer relaxation process, associated with the forbidden transition by spin from the excited triplet state (T_1) to the ground state.[27] In organic lighting emitting devices, the electrons and holes formed by the application of potential can recombine to form singlet and triplet excitons or excited states. Due to charge injection, the ratio between singlets and triplets formations is theoretically one to three. According to quantum mechanics, the intrinsic spin quantum number of electrons and holes can exist in two states $m_s = + \frac{1}{2}$ or $m_s = - \frac{1}{2}$. If we consider the combination of two electrons, we can observe the statistical formation of four combinations of spin: $S = 0$ ($m_s = 0$), with non-parallel spin number; and $S = 1$ ($m_s = -1, 0, +1$), with parallel spin number; obtaining a rate of one singlet to three triplet (25% to 75%) excitons.[9]

Hence in fluorescence devices the emission is related to singlet excitons decay and in phosphorescence devices with triplet excitons decay, the internal quantum efficiency (IQE) of the devices will be limited to 25% and 75%, respectively, for each type of device, as we can see in the Jablonski diagram in **Figure 2.3**. It means that each device is wasting excitons which reduces the device efficiency.[24,28,29]
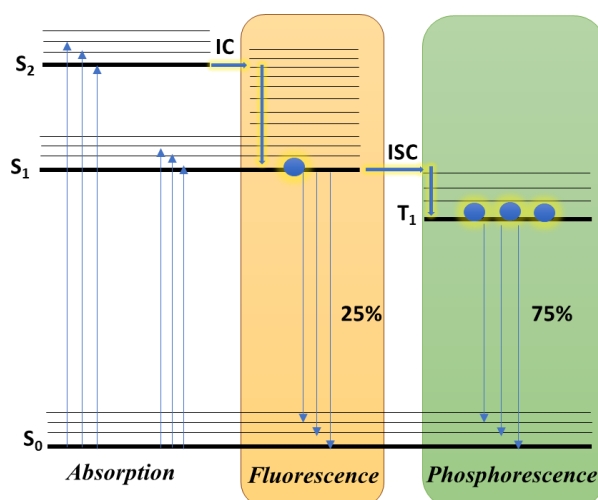
Figure 2.3. *The Jablonski diagram of absorption, fluorescence, and phosphorescence with electric excitation. S_0: the ground state; S_1 and S_2: the first and second excited singlet states, respectively; T_1: the first excited triplet state. The following conversion routes are possible: an internal conversion (IC) and an intersystem crossing (ISC). Adapted from P. Data and Y. Takeda.*[23]

Three generations of OLEDs have been developed in parallel aiming at the construction of efficient and low-cost devices (**Figure 2.4**). The first and second generations of OLED devices had limitations. The first was related to efficiency because all the light came from singlet excitons, which is theoretically limited to 25% which can achieve EQEs up to 5% in the device. The emission layer based on this kind of device presented π-conjugated molecular design with rigid chemical structure and good thermal stability. The challenges are related to the aggregation-cause quenching in solid state, that may result in weakly emissive systems due to effective molecular π-stacking and attractive dipole-dipole interactions.[15]

The second generation (phosphorescent OLEDs) was based on the remaining 75% of triplet excitons. These devices are typically based on phosphorescent heavy metal complexes. The heavy metals atoms, such as Iridium or Platinum, can enhance the spin-orbit coupling (SOC) and facilitate the process of Intersystem Crossing (ISC). If the ISC is very effective, the singlet excitons can be used to achieve 100% IQE. But the challenge with phosphorescent OLEDs are the necessity to use expensive and scarce metals to obtain them.[23,30]

The third generation of OLEDs is based on the delayed fluorescence process. The strategy to increase the efficiency of the device is to use mechanisms to harvest triplets to singlet states to achieve 100% IQE. For that, the reverse intersystem crossing (RISC) from triplet (T_1) to singlet (S_1) states need to be effective to have an

efficient delayed fluorescence process.[31] The mechanism to harvest triplets to singlets states is possible by Thermally Activated Delayed Fluorescence (TADF). This mechanism can be achieved with the use of purely organic emitters. Because of that various research groups starts to focus on the design and synthesis of TADF emitters to be applied in organic light-emitting devices.[32]
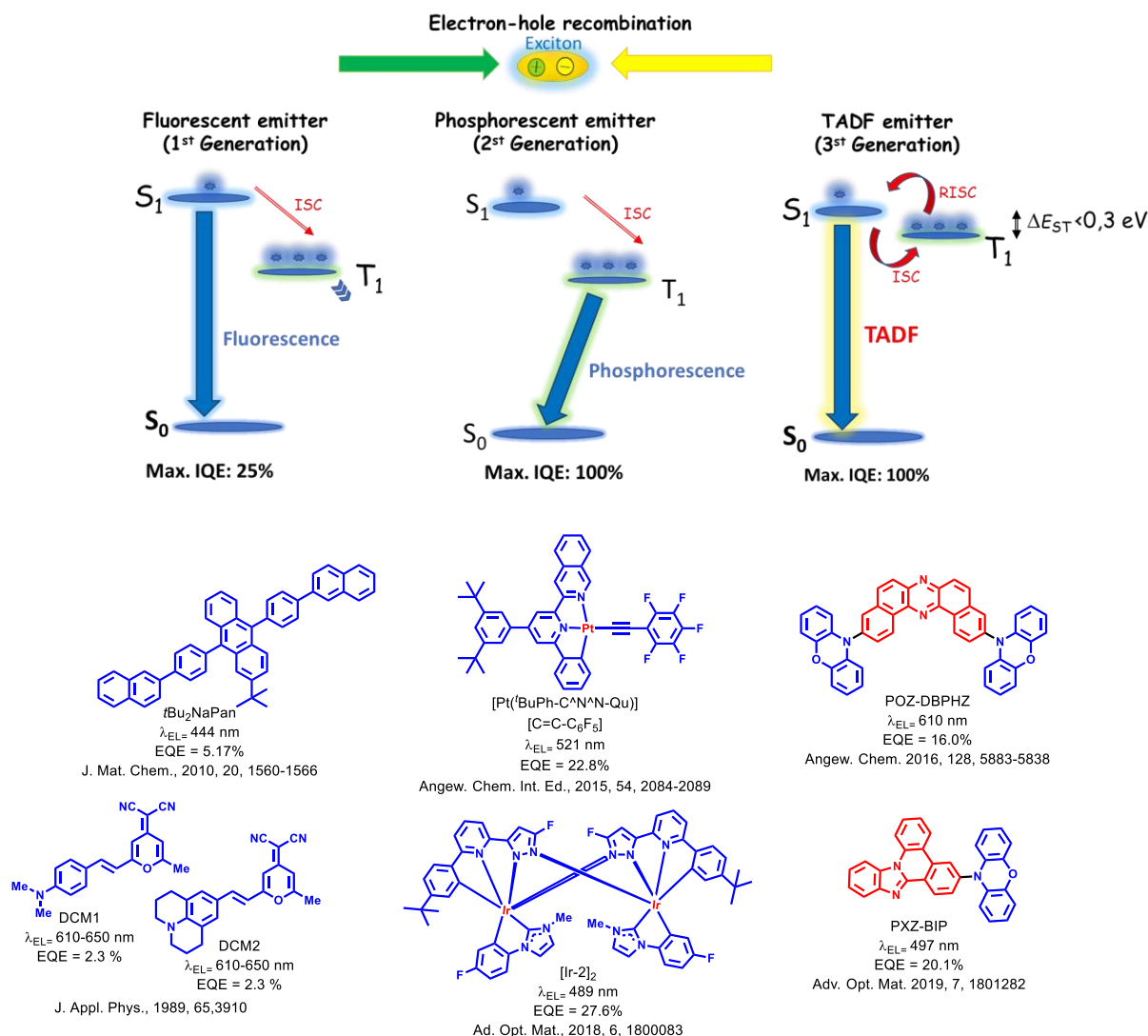
Figure 2.4. *Generations of OLEDs devices and examples of compounds used for each type. Adapted from literature.*[15]

The delayed fluorescence (DF) process can occur by two mechanisms (**Figure 2.5**). The first E-type delayed fluorescence (or Thermally Activated Delayed Fluorescence – TADF) is associated with the energy between the singlets and triplets states. This energy gap needs to be very small ($\Delta E_{ST} < 0.3$ eV). In these conditions, the excited molecules in triplets states can move to singlets states by reverse intersystem crossing (RISC). The process of RISC is thermally supported by the proper

energy from the molecule, where a strong charge transfer process can lead the energy necessary to harvest the excitons from T_1 to S_1 state. The maximum efficiency of this mechanism can reach 100%. The second p-type delayed fluorescence (Triplet-Triplet Annihilation -TTA) is associated with two molecules in the excited triplet state that can annihilate to yield one molecule in the ground state (S_0) and one in the excited singlet state (S_1) (triplet fusion), that can relax to the ground state by emission of photons in the delayed fluorescence mechanism. The main problem with this process is related to the low (less than 50%) efficiency.[15,23]
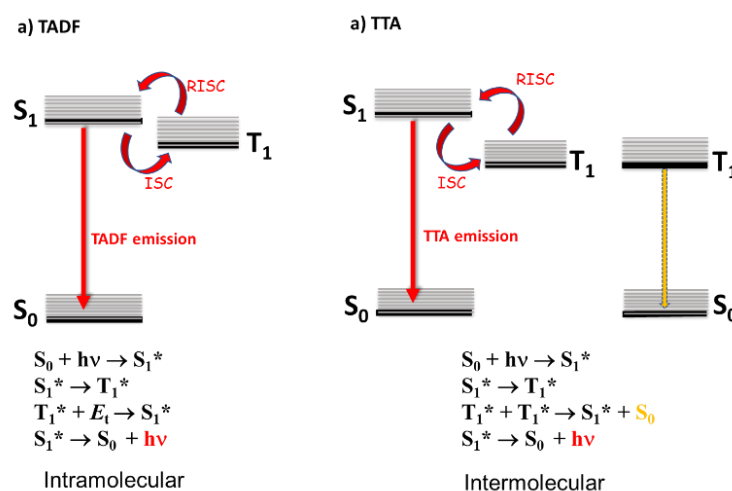
Figure 2.5. Representation of the possible mechanisms of delayed fluorescence. a) TADF, intramolecular process; b) TTA, intermolecular process.

The room-temperature phosphorescence mechanism occurs in the opposite way to the delayed fluorescence (DF) process. To observe delayed fluorescence it is necessary to increment the thermal energy through molecular vibration to obtain efficient reverse intersystem crossing from the local triplet state to the ground state (S_0), supported by the CT process. As for phosphorescence, because of the long lifetime of the relaxation process, it was needed to decrease the possibility of non-radiative deactivation from the T_1 state, which is achieved by cooling down the molecule or decreasing the possibility of molecular vibration by steric hindrance between donor and acceptor unitis.[33] In these systems, the T_1 state can be populated by intersystem crossing (ISC) from the S_1 state and achieved 100% IQE from the radiative relaxation from excited triplet state (T_1) to the singlet ground state (S_0).[34,35] These parameters are obtained in a metal complex with strong spin-orbit coupling (SOC).[36] To obtain these characteristics at room temperature with pure organic

compounds, new approaches for the design of RTP-active organic materials are required.

2.3.1 TADF and AIE properties

The concept of aggregation-induced emission (AIE) was first proposed by Tang et al in 2001.[37] This phenomenon is related to the restriction of the intramolecular rotation or vibration through block and rigid molecular conformation. Hence, the decrease of the molecular relaxation can suppress the non-radiative pathways, it can lead to the enhancement emission in the solid state. This mechanism can be an alternative to the standard aggregation caused quenching (ACQ) effect. For TADF based OLEDs, the addition of the AIE effect can decrease the efficiency roll-off and consequently increases the devices performance.[38] The development of aggregation-induced delayed fluorescence (AIDF) materials also can be used in host-free OLEDs which could reduce the device construction costs.[38]

The first TADF compounds with AIE properties were reported by Wang et al. using thioxanthone as an acceptor core.[39] They investigated it in different water fractions (f_w) in water/acetonitrile mixtures obtaining high PLQY in direct relation to the increase of f_w content and consequently presented good EQE performances up to 21.5%. Non-doped OLED devices using acridine donor derivatives with restricted structure via C---H---π interactions, presenting AIDF properties were reported by Tang et al. showing very small non-radiative decay.[40] Due to AIE nature, the devices showed high EQEs up to 14.2%, and significantly decreased roll-off ratio. In this way, the AIDF materials are proven to be a great alternative in the obtention of low-cost devices maintaining good EQE performances. In the sequence year, Tang et al also reported four more AIDF materials with superior efficiencies and with 100% of excitons harvesting.[41] These TADF emitters based on 4-(phenoxazine-10- yl)benzoyl moiety showed high EQEs up to 22.2% in non-doped OLEDs with negligible efficiency roll-offs, very low turn-on voltages (2.5 V) and good stability. This validates the AIE-TADF materials design as a strategy to obtain efficient and stable devices based on the characteristics in the aggregate state. Additionally, the polymorphism was studied as associated with AIDF properties, where Lee et al. showed a phenothiazine derivative presenting different aggregate states in crystal structures. With AIE properties increasing the PLQY as well as decreasing the ΔE_{ST}.[42] Hence, the inhibition of intramolecular rotations with modulation of the aggregate states can be a great

strategy in emission layers for OLEDs applications based on AIE-active compounds. It also open potential applications in various fields including fluorescent imaging, chemical sensors, photonic drugs, optoelectronics, etc.[43–45] Thus the development of new molecules with AIE properties is very important for study and understand of the mechanisms involved, which can increase the knowledge in the molecular design to be applied in systems with more efficiency.

2.3 Molecular design of TADF molecules

The design of new TADF compounds is a challenging task involving several essential conditions simultaneously.[46] These conditions include:

a) the minimization of the energy gap (ΔE_{ST}) between the singlet and triplet excited states;

b) Minimizing non-radiative decay pathways to ensure that the triplet excited state persists for an extended lifetime, improving the probability of efficient triplet harvesting through the thermally activated reverse intersystem crossing (RISC) mechanism;

c) Maximizing the photoluminescence quantum yield (PLQY).

The reduction of ΔE_{ST} is fundamental in maximizing the RISC rate constant (k_{RISC}), as indicated by **Equation 2.1** in dependence of temperature:

$$k_{RISC} \propto e^{\frac{(-\Delta E_{ST})}{K_B T}} \qquad (\textbf{Equation 2.1})$$

where k_B is Boltzmann constant and T is the temperature. From this equation, we can observe that for higher ΔE_{ST}, we will have the lower value of k_{RISC}, and vice versa.[47] This relation is very important to design the TADF materials. So, the decrease of ΔE_{ST} is directly related to RISC rate.

According to quantum mechanics, when estimating the energy of the excited singlet state (E_{S1}) and triplet state (E_{T1}), we can consider three different terms: the energy referring to an electron's orbital (E_{orb}); the electrostatic Coulomb repulsion energy (K) from electron; and also the exchange energy (J), that is associated with two unpaired electrons in the HOMO and LUMO molecular orbitals and their electron-electron repulsion, based on the Pauli principle. For the S_1 and T_1 with the same electron configuration, these terms have similar contribution, but due to the spin

configuration the exchange component (J) has an increment in the contribution for S_1 state, while is opposite for the T_1 state, as shown in the **equations 2.2** and **2.3**.

$$E_S = E_{orb} + K + J \qquad \text{(Equation 2.2)}$$

$$E_T = E_{orb} + K - J \qquad \text{(Equation 2.3)}$$

In this way, the singlet-triplet energy gap (ΔE_{ST}) is based on **equation 2.4**:

$$\Delta E_{ST} = E_S - E_T = 2J \qquad \text{(Equation 2.4)}$$

J, that is the exchange energy, is directly related with spatial distributions of the wave functions of the HOMO and LUMO.[48] Thus, to decrease ΔE_{ST} in organic molecules, it is necessary to reduce the overlap of the HOMO and LUMO orbitals in compounds. This spatial separation can be encountered in twisted molecules containing parts of electron-donors (D) and electron-acceptors (A), which can induce the charge-transfer (CT) from D to A in the excited state.[49] Therewith, the design of TADF materials involves generally donor-acceptor units connected directly or with an aromatic π-spacer bridge, in order to form excited states with strong CT character. The ΔE_{ST} also can be decreased in twisted D-A systems with orientation close to orthogonality, decreasing the overlapping between HOMO and LUMO.[32]

The selection of D and A units is fundamental in the design of TADF emitters, which implies direct photophysical behavior of the compounds. Normally, the connection between twisted strong acceptors and donors are required, in order to obtain the orientation close to orthogonality associated with strongly localized HOMO and LUMO orbitals and increasing RISC.[50] On the other hand, there is an antagonistic topic related to the efficiency in the RISC and the electron coupling in the fundamental state and singlet excited state. Where, the low orbital overlap also implies the decrease of radiative rates and in consequence low PLQY. In another way, the use of weak acceptors and donors leads to low separation between the HOMO and LUMO, and consequently increases the ΔE_{ST} and decreases the TADF mechanism performance.[51]

Therefore, the molecular design to obtain molecules with TADF properties is based on the balance of control of the bandgap values, such as HOMO-LUMO and singlet-triplet energy that are related to the light emission wavelength, the PLQY and the efficiency of RISC process. The focus on the well π-conjugated molecular system with the possibility of intensive charge transfer to support the RISC process in D-A systems have been applied successfully to obtain a high CT process and good

separation between HOMO and LUMO levels.[31,52] **Figure 2.6** summarizes some important parameters in the development of TADF compounds and some commonly used donors and acceptors.
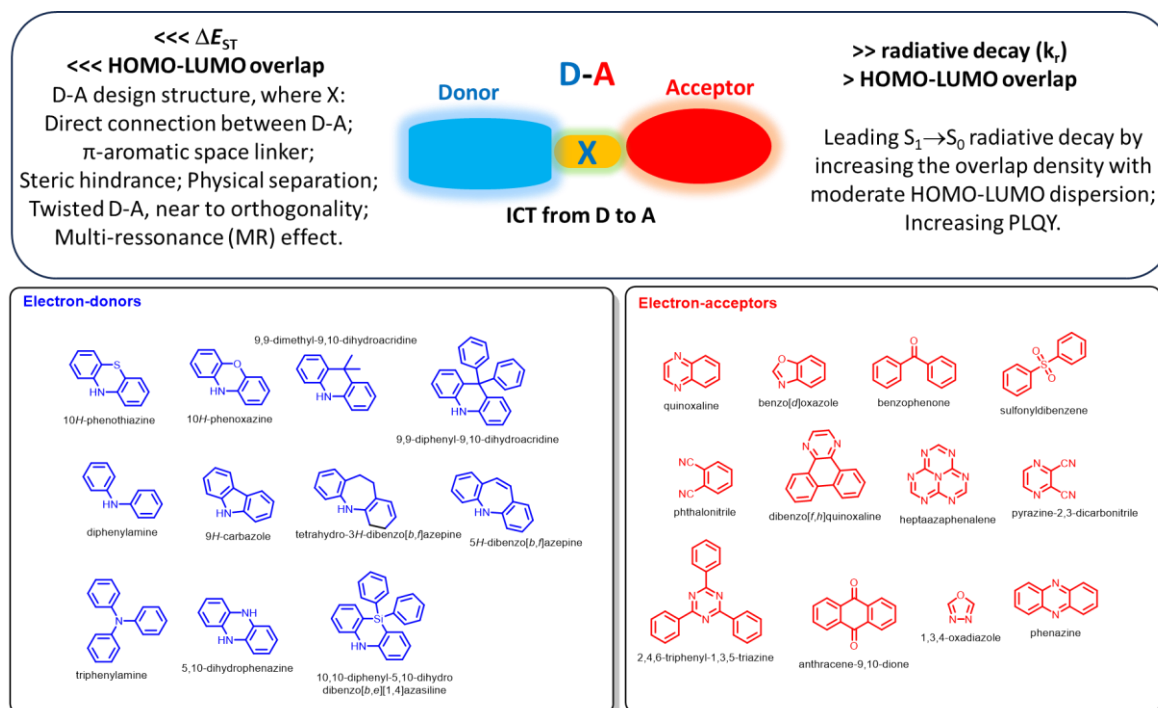
Figure 2.6. *Strategies to design TADF materials in D-A structures with small ΔE_{ST} and moderate radiative decay constant (k_r) (top). Molecular structures of common electron-donors (blue) and electron-acceptors (red) units based TADF molecules. Adapted from literature.*[53,54]

The development of new organic materials based on TADF properties is based on the synthesis of ambipolar compounds, but not only in specific standard D-A arrangement. The ambipolar compounds can present different arrangements such as: Donor-Acceptor (D-A), Donor-Acceptor-Donor (D-A-D), Donor-π-spacer-Acceptor-π-spacer-Donor (D-π-A-π-D), D$_3$-A, D$_3$-π-A, D$_4$-A and others arrangements that can present intense intermolecular charge transfer (ICT) process, mediating the ΔE_{ST} to achieve thermally activated RISC process.[55,56]

Further investigations become necessary to find structures with balanced efficient RISC and PLQY values. These kinds of parameters can be obtained in systems with strong acceptor and several weaker donors, for example in D-A-D and D$_3$A configurations, to increase the donor character in the structures. Recently, ΔE_{ST} control has also been performed in systems with a multi-resonance effect.[57] Additionally, the extension of the π-conjugation degree and the redox potentials are also important in the design of efficient TADF compounds. Which can help to cover the

emission wavelength in the visible region from blue to red with stability and color purity.[12]

Other parameters related to stability in OLED devices should also be considered for improvement. Various works are focusing on the investigation of ambipolar structures to achieve low ΔE_{ST} by TADF mechanism to obtain good EQE in purely organic OLED devices. The molecules need to have good processability to be used in the preparation of the devices. Its construction can be realized by deposition process that requires molecules with low molecular mass and good thermal stability to be sublimed without decomposition or by solution-processed techniques which requires molecules with good solubility in common organic solvents.[58] For that, the design of new materials and investigations of the photophysical/electrochemical parameters behavior involved is fundamental to the knowledge of the mechanisms associated in light generation.

Actually, the density functional theory (DFT) and time-dependent density functional theory (TD-DFT) calculations are good tool to improve the efficiency in TADF molecular design.[59] The theoretical estimates allow for the selection of the best candidate compounds to be synthesized, which can help in the better use of synthetic time, decreasing the costs in the development of new compounds.[60] Different parameters such as singlet-triplet energies gaps and their nature, HOMO-LUMO levels and contours, oscillator strength, can be estimated by several methods using DFT and TD-DFT theories.[61] Functionals such as B3LYP, LC-ωPBE, CAM-B3LYP, PBE0, M06-2X and others are currently used to obtain certain estimates from TADF parameters.[62] These calculations also help to elucidate the TADF mechanism, by calculation of the nature of excited states and with correlation with experimental data.[63,64]

3. D-A compounds derived from Pyridoquinoxalines: Synthesis and investigation of photophysical and electrochemical properties

This chapter will demonstrate the design and synthesis of 8 new compounds derived from acenaphtopyridoquinoxaline as acceptor core, and different donor moieties attached by N-C cross-coupling reactions. These materials were synthesized aiming multifunctional properties, such as TADF to OLEDs application. In this chapter the author was responsible for all the molecular design, synthesis, structural characterizations (NMRs), and partially for the electrochemical and photophysical investigations.

3.1 Introduction

High-performance organic light-emitting diodes (OLEDs) with purely organic emission materials have gained a lot of interest in recent years due to easy processability, flexibility, low production cost, and lightness. All these properties can be tailored by modifying their molecular structures to suitable parameters. Small organic molecules with Donor-Acceptor (D-A) characteristics and very small singlet-triplet (ΔE_{ST}) energy gap are attractive strategies to harvest triplets states by reverse intersystem crossing (RISC).[65–67] High efficient TADF-based OLEDs have been implemented with EQE comparable with the phosphorescent emitters-based organometallic complex that had limitations in the cost due to the use of heavy metals which are rare and expensive. D-A molecules with spatially separated highest occupied molecular orbitals (HOMO) and lowest unoccupied molecular orbitals (LUMO) are conducive to low ΔE_{ST} values, because they facilitate the RISC by excited-state intramolecular charge transfer (ICT).[68–70]

N-rich acceptor cores are a useful strategy to optimize the spin-orbit coupling (SOC) that is related to the rate increase in the RISC and consequently minimize the ΔE_{ST}.[31–33] Materials based on quinoxaline core have been largely investigated for application in optoelectronic devices due to the high level of charge transport carriers and intrinsic high photoluminescence quantum yields (PLQY).[71,72] Pyridoquinoxalines presented a higher acceptor character in relation to quinoxalines due to the addition of one more nitrogen atom in the system which increases the electronegativity in the core.

Ambipolar compounds based on quinoxalines as acceptor and common donor units were used to obtain efficient TADF materials.[73–75]

The synthetic versatility of the pyridoquinoxalines family is very attractive due to the easy synthetic approach by condensation reaction of 2,3-diaminopyridines and dicarbonyl derivatives, being simple and low cost. Various substituents can be used in the diaminopyridines and in the dicarbonyl part in order to functionalize the core. Different D-A molecules based on these systems were investigated to obtain multifunctional materials.[76,77] Although, the dicarbonyls based on acenaphto-1,2-dione have not been much investigated so far,[63] the naphthalene endows them with a rigid planar structure, with abundant delocalization of the π electrons. In this way the condensation with acenaphto-1,2-dione can be an excellent strategy to obtain a new core aiming multifunctional properties.

In this way, this chapter is based on the design, synthesis, and investigation of the photophysical and electrochemical properties of one new series of compounds based on acenaphtopyridoquinoxaline as acceptor core and donor units such as carbazole, diphenylamine, phenothiazine, phenoxazine, acridine derivatives and azepine derivatives in order to define the relation between molecular structure and photophysical properties to be applied in OLEDs devices with a wide range of accessible colors. **Figure 3.1** shows the molecules that were synthesized.
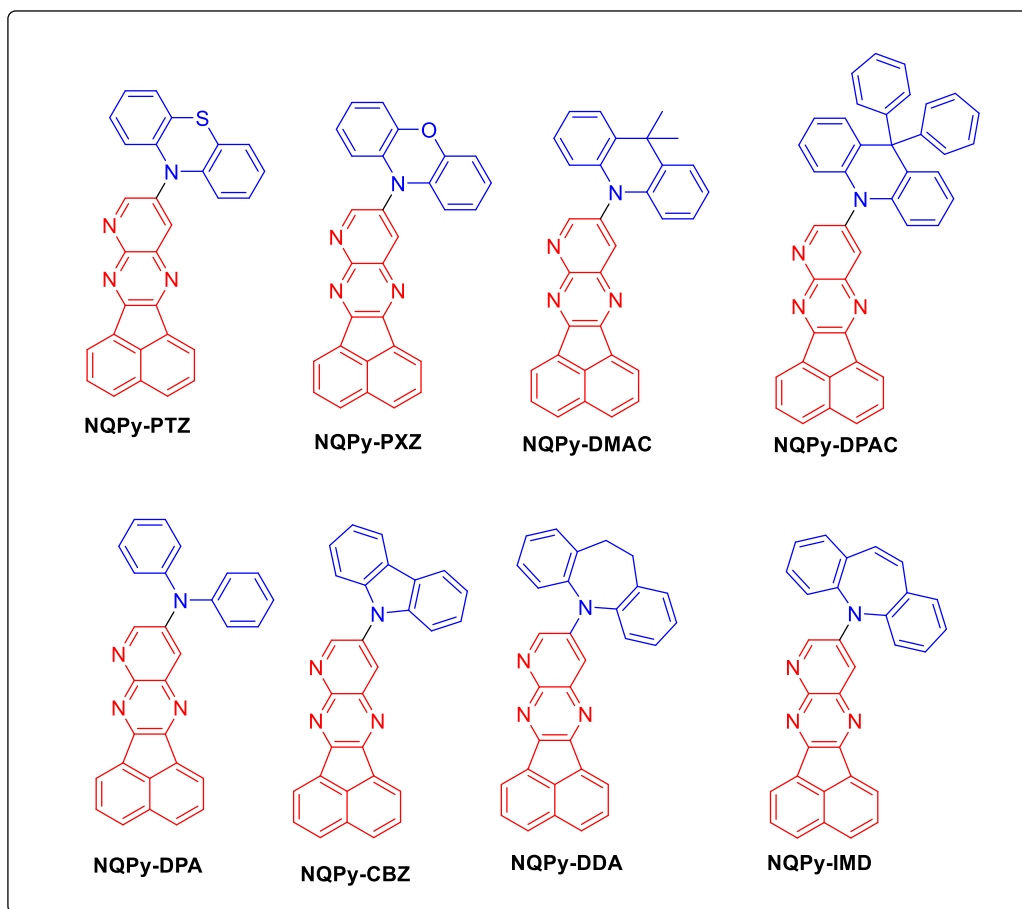
Figure 3.1. *The molecular structures of the pyridoquinoxaline derivatives.*

3.2 Design, synthesis and characterization

The frontier molecular orbitals (MOs) HOMO and LUMO of the **NQPy-Donor** compounds were predicted using density functional theory (DFT) calculations. As shown in **Figure 3.2**, the LUMOs of all compounds are spatially localized on the acenaphtopyridopyrazine core. On the other hand, their HOMOs are concentrated preferentially on the donor units, showing a clear spatial separation of the frontier MOs. The HOMO-LUMO energy gap (E_g) follows the expected behavior determined by the strength of the donor unit: **NQPy-PXZ** < **NQPy-PTZ** < **NQPy-DMAC** < **NQPy-DPAC** < **NQPy-DDA** < **NQPy-IMD** < **NQPy-DPA** < **NQPy-CBZ**. These theoretical estimates showed good correlation with the experimental electrochemical data. We used time-dependent DFT (TD-DFT) to estimate the energy of the lowest singlet and triplet states. The lowest ΔE_{ST} value was obtained for **NQPy-PXZ**, **NQPy-PTZ**, **NQPy-DMAC** and **NQPy-DPAC**, which we expect to display TADF properties. ΔE_{ST} values above 0.35 eV were observed for **NQPy-DDA**, **NQPy-IMD**, **NQPy-CBZ** and **NQPy-DPA**, which we

expect to either display RTP or a mixed TADF+RTP luminescence. Although we generally observe a minimum HOMO-LUMO overlap, for **NQPy-CBZ** and **NQPy-DPA** this overlap is more substantial. Thus, we expect these two molecules to display a stronger fluorescent behavior.
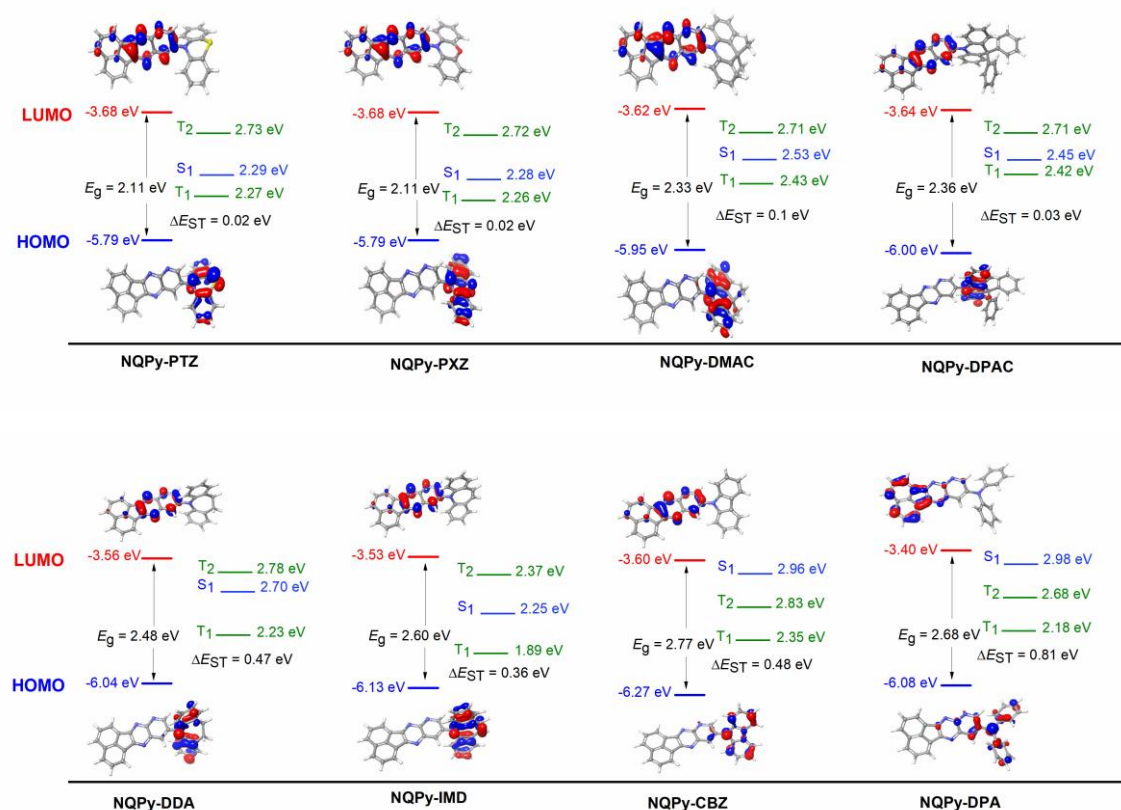
Figure 3.2. *Molecular optimized geometries of HOMO and LUMO spatial distributions and* ΔE_{ST} *of **NQPy-Donors** optimized via DFT and TD-DFT at the B3LYP/6-31G** level.*

The designed compounds were synthesized in two steps (**Scheme 3.1**). The key intermediate 10-bromoacenaphtho[1,2-*b*]pyrido[2,3-*b*]pyrazine (**NQPy-Br**) was synthesized by a dehydration condensation reaction between acenaphthylene-1,2-dione and 5-bromopyridine-2,3-diamine. The second step was based on the Buchwald-Hartwig cross-coupling reaction (N-C coupling) using 3 mol% of the palladium catalyst Pd$_2$(dba)$_3$ and 6 mol% of the phosphine derivative [(*t*-Bu)$_3$PH]BF$_4$ as ligand with different donors in excess (1.2 eq): 10*H*-phenothiazine (**PTZ**), 10*H*-phenoxazine (**PXZ**), 9,9-dimethyl-9,10-dihydroacridine (**DMAC**), 9,9-diphenyl-9,10-dihydroacridine (**DPAC**), 9*H*-carbazole (**CBZ**), diphenylamine (**DPA**), 10,11-dihydro-5*H*-dibenzo[*b,f*]azepine (**DDA**) and 5*H*-dibenzo[*b,f*]azepine (**IMD**) to obtain all final **NQPy-Donors** compounds in good yields after purification.
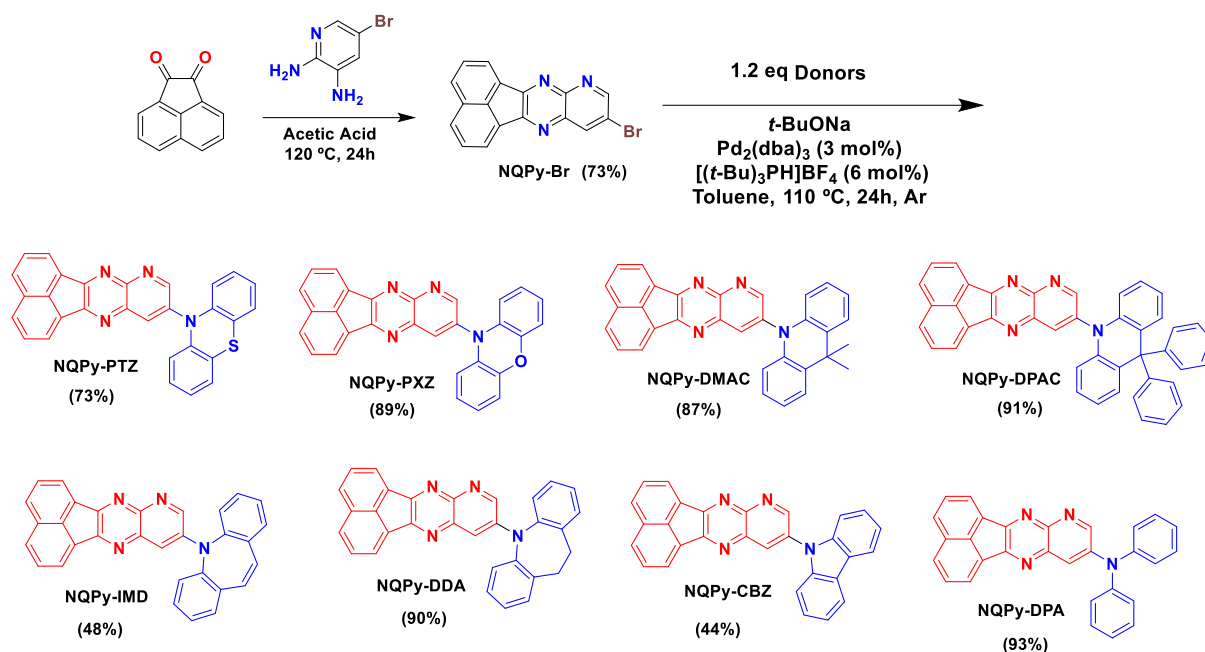
Scheme 3.1. *Synthetic routes to obtain NQPy-Donors. Donors: PTZ, PXZ, DMAC, DPAC, IMD, DDA, CBZ and DPA.*

The structures of all compounds were confirmed by nuclear magnetic resonance (NMR) spectroscopy and High-Resolution Mass Spectrometry (HRMS). All experimental procedures are described in the synthetic details of this chapter (**section 3.6**) and all the spectra are provided in the appendices section. As an example, **Figure 3.3** shows the ^{1}H NMR spectrum of the compound **NQPy-PXZ** indicating the success of the C-N coupling. On this spectrum, we can clearly observe signals for hydrogens from the acceptor unit in the range of 9.2-7.8 ppm and the phenoxazine donor part in the range of 6.9-6.0 ppm. The most chemically shifted was the hydrogen signal assigned as Ha doublet (*J*= 2.5 Hz) and Hb doublet (*J*= 2.5 Hz) due to proximity to piridoquinoxaline system. Followed by doublets Hd (*J*= 7 Hz) and Hc (*J*= 7 Hz) from naphthalene part close to piridoquinoxaline system. The typical signals referring to phenoxazine system with integration for 8H at 6.9-6.0 ppm confirm the success of the N-C coupling reaction.
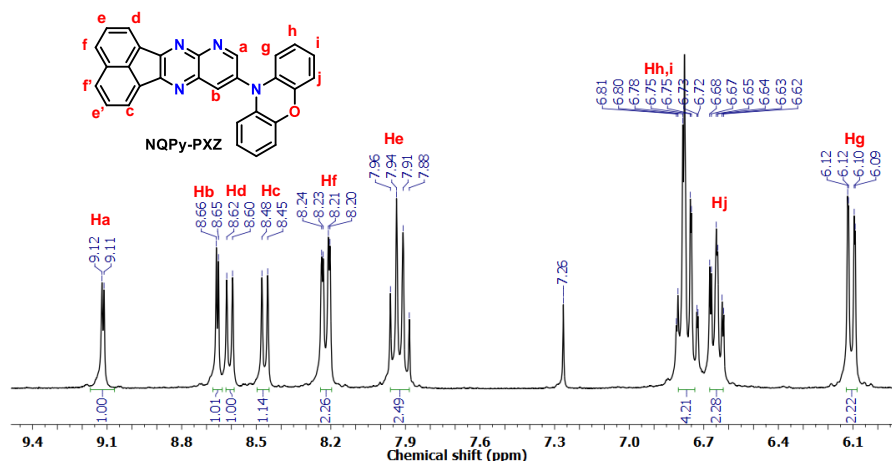
Figure 3.3. ^{1}H NMR (300 MHz) of the **NQPy-PXZ** in CDCl$_3$.

3.3 Electrochemical properties

The electrochemical properties of the **NQPy-Donors** were investigated by cyclic voltammetry (CV) to estimate the ionization potential (IP) and electron affinity (EA) (from onset oxidation (E$_{ox}$) and reduction (E$_{red}$) potentials), that are correlated with the HOMO (E_{HOMO}) and LUMO (E_{LUMO}) energy levels, respectively, using the following equations: E_{HOMO} = -(E$_{ox}$ + 5.1); E_{LUMO} = -(E$_{red}$ + 5.1).[78] The results are summarized in **Table 3.1** and the voltammograms are compiled in **Figure 3.4**.

Table 3.1. *HOMO and LUMO energy levels obtained from CV measurements and DFT calculations.*

Compound	Cyclic Voltammetry[a]			Theory[b]		
	HOMO (eV)	LUMO (eV)	E_g (eV)	HOMO (eV)	LUMO (eV)	E_g (eV)
NQPy-PTZ	-5.49	-3.45	2.04	-5.79	-3.68	2.11
NQPy-PXZ	-5.56	-3.56	2.00	-5.79	-3.68	2.11
NQPy-DMAC	-5.68	-3.44	2.24	-5.95	-3.62	2.33
NQPy-DPAC	-5.77	-3.44	2.33	-6.00	-3.64	2.36
NQPy-DDA	-5.90	-3.19	2.69	-6.04	-3.56	2.48
NQPy-IMD	-5.87	-3.18	2.71	-6.13	-3.53	2.60
NQPy-CBZ	-6.01	-3.49	2.52	-6.27	-3.60	2.77
NQPy-DPA	-5.85	-3.41	2.44	-6.08	-3.40	2.68

[a] *Measurements were performed for 1 mM solutions of investigated compounds in the presence of 100 mM tetrabutylammonium tetrafluoroborate and calibrated using ferrocene/ferrocenium redox couple.* [b] *Results obtained at the B3LYP/6-31G** level of theory.*

All materials showed good stability and reversibility in the applied voltage range especially in the reduction process that involved acenaphtopyridoquinoxaline unit. The LUMO levels of the investigated compounds did not present many differences in the

values. But appears to be affected by a partial conjugation with the donor and hence it varies according to its type. The first oxidation process was more clearly reversible for **NQPy-PTZ** and **NQPy-PXZ**. While it was more irreversible for the other compounds. The donor character of the materials can be evaluated considering the HOMO levels energy varying with **NQPy-CBZ** < **NQPy-DDA** < **NQPy-IMD**, **NQPy-DPA** < **NQPy-DPAC** < **NQPy-DMAC** < **NQPy-PXZ** < **NQPy-PTZ**. The electrochemical band gap (E_g) follows the small values for D-A combinations of the acceptor and strong donors, while for the donors with a lower electron-donating strength, E_g increases. The results obtained by DFT calculations show a good correlation with the experimental electrochemical data as we can observe in **Table 3.1**.
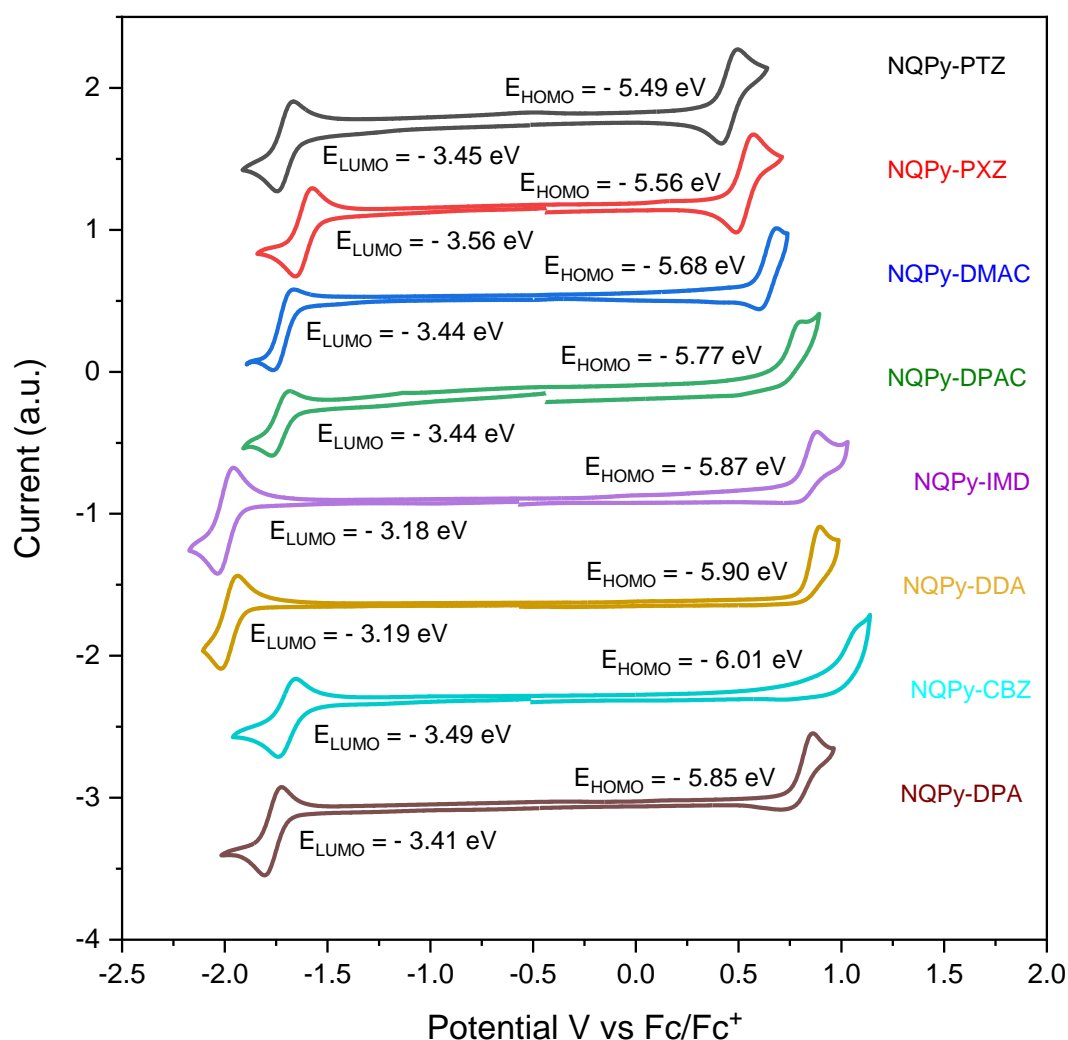
*Figure 3.4. Voltammograms of the 1mM solutions of compounds **NQPy-Donors** in 100mM tetrabutylammonium tetrafluoroborate in DCM. Pt disk as working, Pt wire as counter and Ag/AgCl as reference electrode, at 50 mv s^{-1} scan rate.*

3.4 Photophysical properties

3.4.1 Photophysical properties in diluted solutions

The absorption spectra (UV-Vis) in dichloromethane (DCM) and photoluminescence (PL) spectra in DCM and toluene are shown in **Figure 3.5** and the data are summarized in **Table 3.2.** We can observe strong absorption bands in 290-330 nm, that can be signed to the $\pi \rightarrow \pi^*$ transitions in the donor-acceptor structures.[79–81] Lower intense broad bands can be observed from 390 to 510 nm and can be attributed to a CT transition from the donor units to the acceptor.[82] For the molecules with more conjugation degree in the D-A systems (**NQPy-DDA**, **NQPy-IMD**, **NQPy-DPA**, and **NQPy-CBZ**) the CT bands are more evident contributing to a higher HOMO-LUMO overlap. On the other hand, for the compounds **NQPy-DMAC, NQPy-DPAC**, **NQPy-PXZ**, and **NQPy-PTZ** these said CT bands are less intense attributed to more twisted conformation with minimum HOMO-LUMO overlap. Analyzing the PL spectra we can observe emission for all compounds, except for **NQPy-PXZ** in DCM. Which can be attributed to the polarity of the DCM that could stabilize the ^{1}CT excited state leading to a quench of the emission. [70,83] All the compounds showed CT (with gaussian profile) or CT+LE (with vibronic profile) emission in solution. The solvents polarities effects promote redshift from toluene to DCM in the PL emission. Which is in agreement with the sensitivity of ^{1}CT states in the D-A molecules. The vibronic profile in the emission was more pronounced for **NQPy-DDA** and **NQPy-IMD,** mainly in toluene, showing higher ^{1}LE contribution to the excited singlet states. The dual emission showed by **NQPy-PTZ** in toluene solution with maxima at $\lambda_{PL} = 476$ nm and at $\lambda_{PL} = 656$ nm is in agreement with other examples in the literature.[83–85] This could be related with the possibility of phenothiazine adopting two stable conformations, such as *quasi*-axial and *quasi*-equatorial, showing two distinct CT energies. [86–90] The compounds **NQPy-PTZ** and **NQPy-PXZ** have very low PLQY in both solvents. **NQPy-IMD**, **NQPy-DMAC** and **NQPy-DPAC** show higher PLQY in less polar solvent (toluene) than in more polar solvent (DCM) which can be associated with polarity quenching of ^{1}CT states. **NQPy-DPA** and **NQPy-CBZ** showed the highest values of PLQY (>80%).

Table 3.2. *Summary of photophysical characteristics of the studied D-A luminophores.*

Compounds	λ_{abs}/nm [ϵ/10^3M^{-1} cm^{-1}][a]	λ_{em} [nm] DCM	λ_{em} [nm] Toluene	PLQY [%] DCM/TOL
NQPy-PTZ	322 [30.1], 418 [8.4], 485sh [2.6]	518	476, 656	<1/<1

NQPy-PXZ	322 [63.9], 472 [2.3], 566sh [0.8]	-	638	-/1.7
NQPy-DMAC	322 [80.4], 447 [3.9]	657	586	<1/19.1
NQPy-DPAC	322[14.2], 440 [1.3]	627	557	3.8/26.5
NQPy-DDA	307 [25.1], 348 [16.2], 426 [12.5]	500, 624	473, 545	10.3/31.2
NQPy-IMD	304 [31.2], 345 [21.2], 417 [14.8]	495	472	2.9/11.8
NQPy-CBZ	292[10.4], 317 [19.0], 419 [4.76]	537	485	81.9/43.8
NQPy-DPA	312 [69.7], 351 [24.6], 444 [26.3]	581	529	77.5/99.6

[a] Absorption spectra recorded in DCM solutions 1x10^{-5} M.
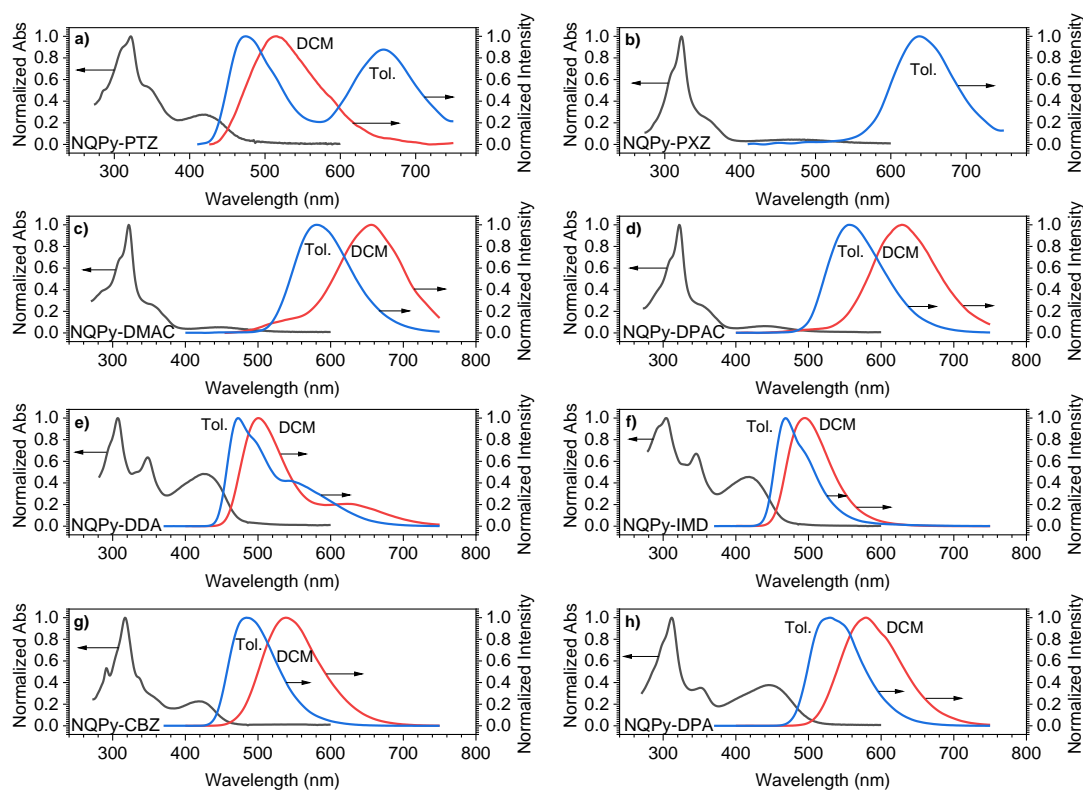
Figure 3.5. *Normalized absorption and photoluminescence spectra in DCM and toluene, c = 10^{-5} M. a) **NQPy-PTZ**; b) **NQPy-PXZ** (not emissive in DCM); c) **NQPy-DMAC**; d) **NQPy-DPAC**; e) **NQPy-DDA**; f) **NQPy-IMD**; g) **NQPy-CBZ**; g) **NQPy-DPA**.*

3.4.2 Photophysical properties in solid state

Figure 3.6 shows the emission spectra for the compounds **NQPy-donors** in a solid state in zeonex, a non-polar polymeric matrix. We can observe that the materials presented a large range of emission wavelengths from blue to orange which is indicative that the control of the donor can influence the color emission of the materials. The compound **NQPy-CBZ** shows maximum wavelength emission (472 nm) in the blue region and the compound **NQPy-PTZ** shows maximum of wavelength emission (574 nm) close to yellow. It shows that the control of the donor strength can modulate the photophysical properties. The gaussian profiles were more pronounced in **NQPy-**

Welisson de Pontes Silva

DMAC and **NQPy-DPAC** indicating strong [1]CT character. While **NQPy-PTZ** and **NQPy-PXZ** showed a mixture CT+LE characters for the excited single state. The less strong donors, shift the emission from green to blue, presenting mixture CT+LE for emission profile. The less strong donors in the compounds **NQPy-CBZ**, **NQPy-IMD** and **NQPy-DDA** show the minimum PLQYs in opposite way as observed in solution, which can be attributed to the aggregation effects. The compound **NQPy-PXZ** presented the highest PLQY (30.6%) and the compound **NQPy-CBZ** the smallest (4.3%).
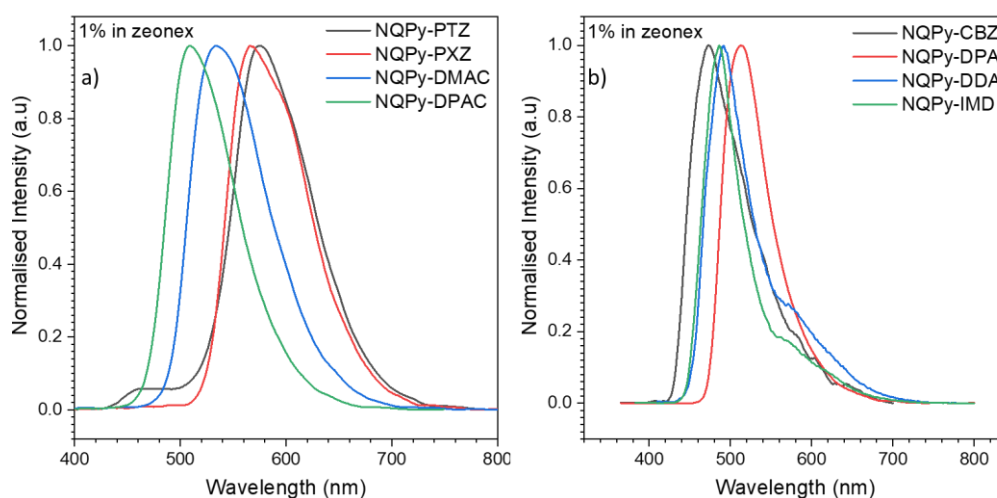
Figure 3.6. *Photoluminescence spectra of the final compounds (1% **NQPy-Donors** in Zeonex matrix) with excitation in 355 nm.*

To investigate the TADF properties is very important to perform measurements in a degassed system to avoid the quenching interactions between the triplet excited states and the oxygen, which decreases the RISC rates. When the materials present the TADF mechanism there are contributions of the triplet states in the mechanism. In this way the emission intensity will be increased in the degassed systems due to possibility of the RISC process.
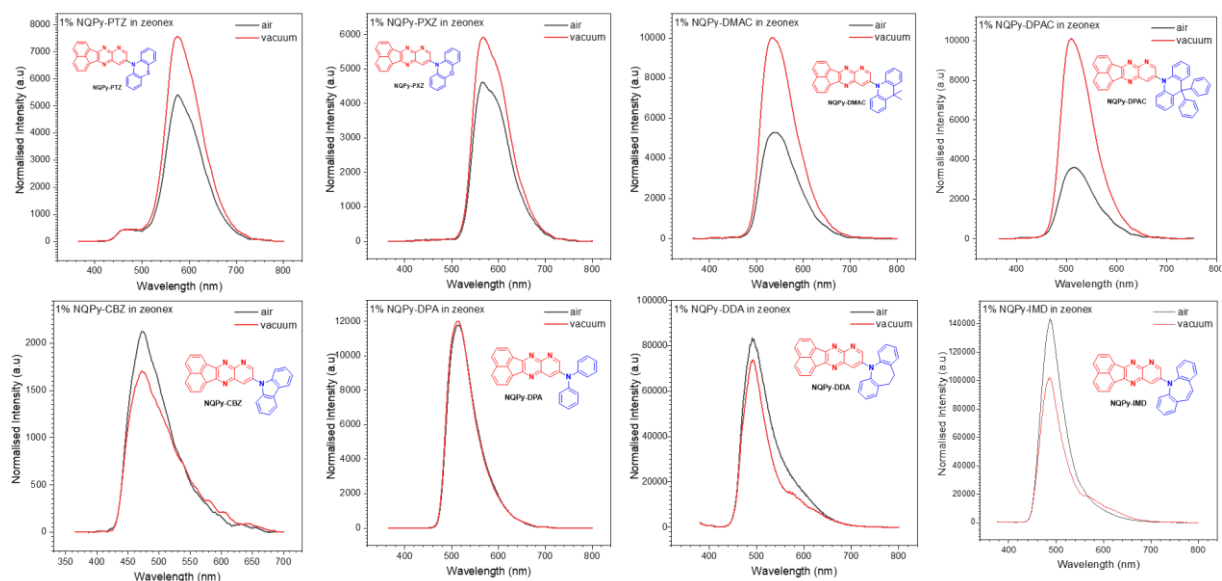
Figure 3.7. *Photoluminescence spectra of the final compounds (1% NQPy derivatives in Zeonex matrix) with excitation in 355 nm in degassed (red line) and no degassed (black line) conditions.*

Figure 3.7 shows the emission spectra from all molecules comparing the intensity in the degassed (under vacuum) and no degassed (air conditions) systems. The compounds **NQPy-PTZ**, **NQPy-PXZ**, **NQPy-DMAC** and **NQPy-DPAC** presented an increment in emission intensity in degassed measurements indicating that the molecules can present mechanisms involving the triplet states which are consistent with TADF properties. The compounds **NQPy-DMAC** and **NQPy-DPAC** showed the highest values in the emission increment, 1.8x and 2.5x, respectively, which can be associated with more efficient RISC process for these compounds. As we can see in **Table 3.3** all materials presented moderate PLQYs in solid-state, but it can be increased in degassed measurements, considering the increment in the emission area. On the other hand, the compounds with less strong donors (**NQPy-CBZ**, **NQPy-DPA**, **NQPy-IMD** and **NQPy-DDA**) did not show an increment in the emission which is in agreement with the absence of TADF behavior.

Table 3.3. *Photophysical properties of the 1% NQPy-Donor in the Zeonex matrix under aerated and deaerated conditions.*

Compound	λ_{em} (nm)	PLQY (%)	Increase[a]	PLQY x Increase (%)
NQPy-DMAC	533	19.0	1.81	34.5
NQPy-DPAC	508	12.0	2.56	30.7

NQPy-PXZ	566	30.6	1.26	38.6
NQPy-PTZ	574	21.9	1.37	30.1
NQPy-DPA	512	23.6	1.01	23.8
NQPy-CBZ	473	4.3	0.90	3.9
NQPy-IMD	486	6.2	0.78	4.8
NQPy-DDA	492	4.3	0.77	3.3

[a] Increase in the PL emission after degassing the system under vacuum.

3.4.3 Aggregation-induced emission (AIE) and aggregation-induced emission enhancement (AIEE)

To better understand the optical properties of the **NQPy-donors** compounds in the aggregated state, we investigated their photoluminescent behavior in THF/water mixtures with different water fractions (f_w) at a concentration of 100 µM. The experimental results and photographs (**Figure 3.8**) show that the emission spectra of the compounds show different behavior in THF/water mixtures. **NQPy-PTZ** and **NQPy-PXZ** display low emission in THF solutions, while the emission increases upon addition of water (f_w = 80-90%) indicating evident aggregation-induced emission enhancement (AIEE) behavior. When the concentration of **NQPy-PTZ** is between 0-80%, the upper [1]CT state dominates its photoluminescence, whereas the lower [1]CT state is suppressed because of a polar environment. However, when the concentration reaches 90%, the lower [1]CT state photoluminescence becomes more noticeable because the **NQPy-PTZ** is no longer in contact with the polar environment of the solvent. Additionally, we have observed that **NQPy-PXZ** has a very low PLQY in toluene, around 2%, and an even lower photoluminescence yield in DCM or THF. However, we noticed that the PL intensity of **NQPy-PXZ** increases up to 50 to 100-fold upon precipitation. This indicates that **NQPy-PXZ** exhibits AIE behavior rather than AIEE.[91] We can observe that **NQPy-DMAC**, **NQPy-DPAC**, and **NQPy-DPA** exhibit an interesting behavior, where initial relatively strong luminescent THF solutions show much lower PL intensities (near complete quenching) upon initial addition of water. This behavior can be interpreted as CT PL quenching due to increases of solvent polarity caused by addition of highly polar water. Addition of further amounts of water induces a relative increase in PL intensity by ~100-900 fold, which is commonly interpret as AIE.[91] **NQPy-DDA**, **NQPy-IMD**, and **NQPy-CBZ**, showed a similar

behavior to **NQPy-DMAC**, **NQPy-DPAC**, and **NQPy-DPA**, however the overall increase in PL intensity upon aggregation (f_w > 60%) is lower. Importantly, for **NQPy-CBZ** we observe PL intensity at high water content to be significantly lower than in dry THF, an effect in line with aggregation-caused quenching (ACQ). For the compounds **NQPy-DMAC** and **NQPy-DPAC** we observe a blue shift in the luminescence at high f_w = 80-90% related to THF solution. This behavior can be interpreted as an effect of molecular interactions between fluorophores being less strong than with the solvent when completely dispersed in a solution. In addition, the aggregate environment is much more rigid than the solution, what can also contribute to the PL blue shift.[92–94]
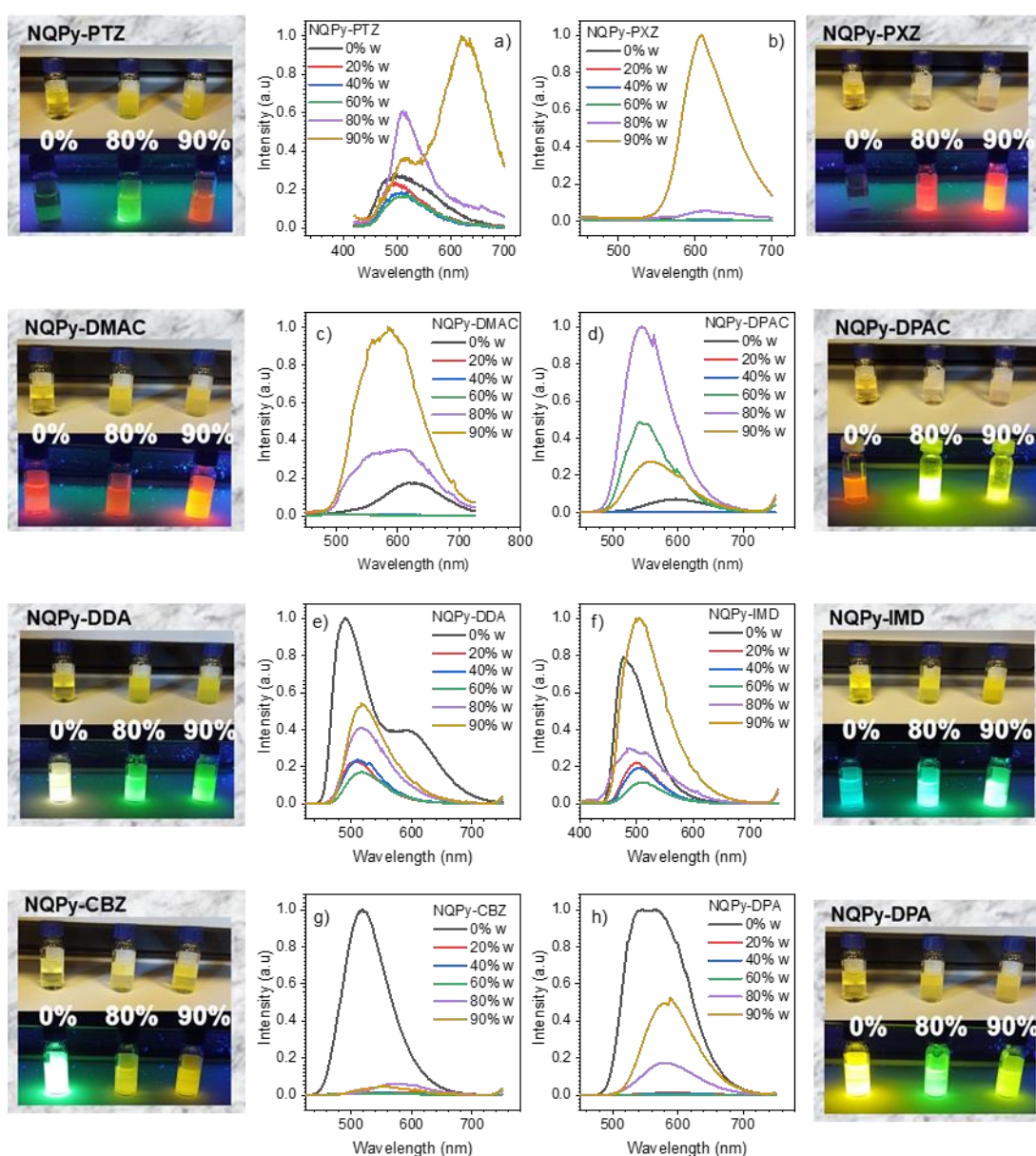
Figure 3.8. *a-g) Emission spectra recorded in THF/water mixtures for water fractions f_w = 0-90%. On the sides photographs of solutions and dispersions of the **NQPy-Donors** compounds*

in THF (f_w = 0%) and THF/water mixtures, f_w = 80-90 %. Top images show photographs under ambient light, while the bottom was recorded with UV light illumination.

The experiments show that results obtained from the "classic AIE experiment" should be treated with caution when CT emissive states in D-A molecules are involved. The aggregates emerging from an almost non-emissive solution will appear photoluminescent due to the expulsion of polar solvent acting as a quencher and not necessarily from restriction of intramolecular rotation (RIR). The molecules often display high PLQY in solvents less polar than THF, as in the case of **NQPy-DMAC** and **NQPy-DPAC**. For D-A luminophores, including TADF and RTP emitters will display the common *polarity-reduced emission*, but remain highly emissive in non-polar environments.

3.5 Conclusions

This chapter described the design successfully synthesis of 8 new D-A molecules based on pyridoquinoxaline as acceptor core and different donor moieties attached via N-C Buchwald-Hartwig cross-coupling reaction. All structural characterizations were realized by NMR spectroscopy and additionally by high-resolution mass spectrometry in the case of final molecules. The materials were obtained in good to moderate yields (44-93%) depending on the donor attached. The electrochemical investigations showed that the materials display good stability in the applied voltage range, which possibilities the modulation of the HOMO-LUMO gap by different combinations with the acceptor and donor. The molecules showed spatial separation between the frontier molecular orbitals indicating the possibility of charge transfer process and minimization of singlet-triplet energy gap. The photophysical properties were investigated, presenting good PLQYs and an increase in the PL intensity under degassed conditions for the materials with stronger donor moieties indicating that they are great candidates for OLEDs based on TADF properties. The choice of the donor allowed for tuning the PL wavelength from 473 to 607 nm, exhibiting a great range of accessible colors depending on the donors attached. The compounds **NQPy-DMAC**, **NQPy-DPAC**, **NQPy-PTZ**, **NQPy-PXZ** and **NQPy-IMD** show AIE or AIEE properties in water/THF mixtures. It demonstrates the control of photophysical parameters by changes in the molecular design to obtain multifunctional materials.

3.6 Synthetic details

10-bromoacenaphtho[1,2-b]pyrido[2,3-e]pyrazine (**NQPy-Br**)

NQPy-Br

A mixture of acenaphthylene-1,2-dione (1.00 g; 5.48 mmol) and 5-bromopyridine-2,3-diamine (1.08 g; 5.76 mmol) were refluxed in 30 ml of glacial acetic acid for 24h. After the reaction was completed, the reaction mixture was filtrated and the solid obtained was washed with water and methanol. The solid was dissolved in 100 ml of chloroform and washed three times with sodium hydroxide solution (1M) and water. The organic layer was separated and dried with $MgSO_4$. The solvent was evaporated to give the compound **NQPy-Br** in 73% of yield. ^{1}H NMR (300 MHz, CDCl$_3$) δ 9.11 (d, J = 2.4 Hz, 1H), 8.68 (d, J = 2.4 Hz, 1H), 8.52 (d, J = 7.0 Hz, 1H), 8.40 (d, J = 6.9 Hz, 1H), 8.19 – 8.14 (m, 2H), 7.90 – 7.84 (m, 2H). ^{13}C NMR (75 MHz, CDCl$_3$) δ 157.2, 155.6, 153.3, 149.1, 139.8, 137.4, 136.8, 130.9, 130.5, 130.5, 130.4, 129.9, 129.0, 128.8, 123.6, 122.8, 119.9.

General procedure for Buchwald-Hartwig Cross-Coupling Reaction in the NQPy-Br core

To a Schlenk tube equipped with a reflux condenser was added a mixture of compounds **NQPy-Br** (0.299 mmol), the respective aryl amine (0.389 mmol), _t_-BuONa (0.72 mmol), Pd$_2$(dba)$_3$ (0.0089 mmol), [(t-Bu)$_3$PH]BF$_4$ (0.018 mmol) and 10 mL of degassed toluene. The mixture was stirred at 110 °C for 24h under Argon atmosphere. After the completed reaction the mixture was filtered through celite and washed with dichloromethane. The solvents were evaporated, and the residue was purified by column chromatography using dichloromethane as eluent.

10-(acenaphtho[1,2-b]pyrido[2,3-e]pyrazin-10-yl)-10H-phenothiazine (**NQPy-PTZ**)

Welisson de Pontes Silva
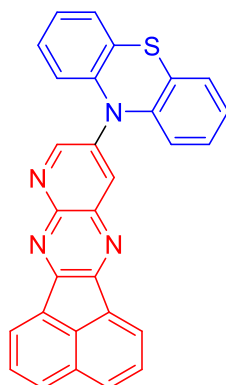
NQPy-PTZ

Yellow solid (73 %). ^{1}H NMR (300 MHz, CDCl$_3$) δ/ppm: 9.03 (d, J = 2.9 Hz, 1H), 8.52 (d, J = 6.4 Hz, 1H), 8.40 (d, J = 6.6 Hz, 1H), 8.20 (d, J = 2.9 Hz, 1H), 8.15 (dd, J = 7.9, 4.1 Hz, 2H), 7.87 (ddd, J = 8.3, 7.0, 5.2 Hz, 2H), 7.42 (dd, J = 7.7, 1.2 Hz, 2H), 7.30 (m, 3H), 7.25 – 7.16 (m, 3H). ^{13}C NMR (75 MHz, CDCl$_3$) δ/ppm: 147.1, 147.0, 141.7, 141.173, 136.9, 131.5, 131.1, 130.6, 130.1, 130.0, 129.8, 128.9, 128.7, 128.6, 127.6, 125.7, 125.5, 123.8, 122.9, 122.2. HRMS: m/z calcd for C$_{29}$H$_{16}$N$_4$S (M+H)$^+$: 453.1174; found: 453.1175.

10-(acenaphtho[1,2-b]pyrido[2,3-e]pyrazin-10-yl)-10H-phenoxazine (**NQPy-PXZ**)
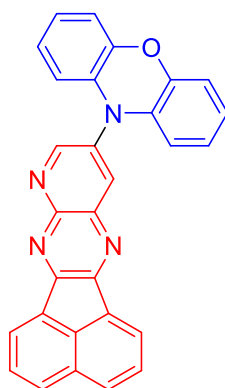
NQPy-PXZ

Red solid (89 %). ^{1}H NMR (300 MHz, CDCl$_3$) δ 9.11 (d, J = 2.6 Hz, 1H), 8.65 (d, J = 2.6 Hz, 1H), 8.61 (d, J = 7.0 Hz, 1H), 8.47 (d, J = 7.0 Hz, 1H), 8.22 (dd, J = 8.1, 2.0 Hz, 2H), 7.93 (dt, J = 8.2, 7.1 Hz, 2H), 6.82 – 6.72 (m, 4H), 6.65 (ddd, J = 7.9, 7.0, 2.0 Hz, 2H), 6.11 (dd, J = 8.0, 1.3 Hz, 2H). ^{13}C NMR (75 MHz, CDCl$_3$) δ/ppm: 156.3, 155.2, 155.1, 149.9, 144.3, 140.4, 137.2, 135.9, 133.6, 131.1, 130.7, 130.6, 130.2, 129.2, 129.0, 123.8, 123.6, 122.9, 122.7, 116.2, 113.6. HRMS: m/z calcd for C$_{29}$H$_{16}$N$_4$O (M+H)$^+$: 437.1402; found: 437.1400.

Welisson de Pontes Silva

*N,N-diphenylacenaphtho[1,2-b]pyrido[2,3-e]pyrazin-10-amine (**NQPy-DPA**)*
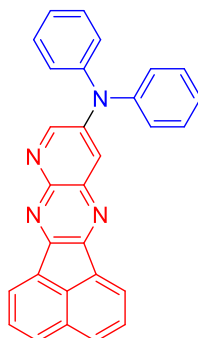
NQPy-DPA

Yellow solid (93 %). ^{1}H NMR (300 MHz, CDCl$_3$) δ/ppm: 8.94 (d, J = 2.9 Hz, 1H), 8.48 (d, J = 7.0 Hz, 1H), 8.34 (d, J = 7.0 Hz, 1H), 8.12 (dd, J = 8.2, 5.2 Hz, 2H), 7.93 (d, J = 2.9 Hz, 1H), 7.84 (td, J = 8.2, 7.1 Hz, 2H), 7.42 – 7.36 (m, 4H), 7.27 (d, J = 1.3 Hz, 2H), 7.25 – 7.17 (m, 4H). ^{13}C NMR (75 MHz, CDCl$_3$) δ/ppm: 161.5, 155.3, 154.4, 153.0, 148.5, 146.2, 145.9, 145.1, 137.4, 136.7, 131.9, 131.4, 130.13, 130.0, 129.6, 129.0, 128.7, 125.6, 125.2, 124.5, 122.7, 122.1. HRMS: m/z calcd for C$_{29}$H$_{18}$N$_4$ (M+H)$^+$: 423.1610; found 423.1611.

*10-(acenaphtho[1,2-b]pyrido[2,3-e]pyrazin-10-yl)-10H-carbazole (**NQPy-CBZ**)*
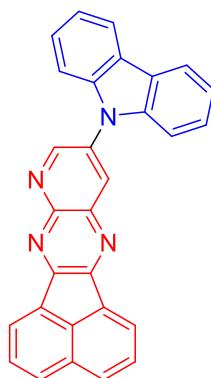
NQPy-CBZ

Yellow solid (54%). ^{1}H NMR (300 MHz, CDCl$_3$) δ/ppm: 9.42 (d, J = 2.6 Hz, 1H), 8.77 (d, J = 2.6 Hz, 1H), 8.59 (d, J = 6.9 Hz, 1H), 8.44 (d, J = 6.9 Hz, 1H), 8.29 – 8.08 (m, 4H), 7.90 (td, J = 8.4, 7.1 Hz, 2H), 7.61 (d, J = 8.2 Hz, 2H), 7.53 – 7.44 (m, 2H), 7.43 – 7.32 (m, 2H). ^{13}C NMR (75 MHz, CDCl$_3$) δ/ppm: 157.3, 155.9, 152.5, 151.0, 149.2, 140.5, 137.5, 136.8, 134.8, 134.2, 131.2, 130.8, 130.8, 130.7, 130.6, 130.5, 130.9, 130.17, 130.16, 129.2, 128.9, 126.7, 124.3, 123.7, 122.9, 121.3, 120.8. HRMS: m/z calcd for C$_{29}$H$_{16}$N$_4$ (M+H)$^+$: 421.1453; found: 421.1454.

Welisson de Pontes Silva

*10-(9,9-dimethylacridin-10(9H)-yl)acenaphtho[1,2-b]pyrido[2,3-e]pyrazine (**NQPy-DMAC**)*
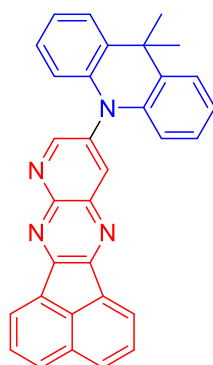
NQPy-DMAC

Yellow solid (87 %). ^{1}H NMR (300 MHz, CDCl$_3$) δ/ppm: 9.09 (d, *J* = 2.6 Hz, 1H), 8.67 (d, *J* = 2.6 Hz, 1H), 8.62 (d, *J* = 6.7 Hz, 1H), 8.47 (d, *J* = 6.8 Hz, 1H), 8.22 (dd, *J* = 8.0, 2.4 Hz, 2H), 7.97 – 7.87 (m, 2H), 7.54 (dd, *J* = 6.1, 3.2 Hz, 2H), 7.06 – 6.99 (m, 4H), 6.44 (dd, *J* = 6.2, 3.3 Hz, 2H), 1.75 (s, 6H). ^{13}C NMR (75 MHz, CDCl$_3$) δ/ppm: 157.4, 155.4, 155.4, 155.3, 149.7, 140.5, 139.9, 138.0, 137.5, 137.2, 131.3, 131.1, 130.7, 130.5, 130.4, 130.1, 129.1, 128.9, 126.6, 125.5, 123.6, 122.7, 121.8, 114.6, 36.2, 30.9. HRMS: m/z calcd for C$_{32}$H$_{22}$N$_4$ (M+H)$^+$: 463.1923; found: 463.1923.

*10-(9,9-diphenylacridin-10(9H)-yl)acenaphtho[1,2-b]pyrido[2,3-e]pyrazine (**NQPy-DPAC**)*
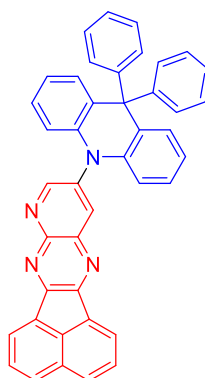
NQPy-DPAC

Yellow solid (91 %). ^{1}H NMR (300 MHz, CDCl$_3$) δ/ppm: 8.62 (d, *J* = 2.6 Hz, 1H), 8.60 (dd, *J* = 7.0, 0.4 Hz, 1H), 8.47 – 8.43 (m, 2H), 8.23 – 8.18 (m, 2H), 7.91 (dt, *J* = 8.2, 7.0 Hz, 2H), 7.32 – 7.27 (m, 6H), 7.15 – 7.09 (m, 2H), 7.03 – 6.98 (m, 8H), 6.64 – 6.59 (m, 2H). ^{13}C NMR (75 MHz, CDCl$_3$) δ/ppm: 157.4, 155.5, 155.0, 149.6, 145.9, 141.9, 139.0, 137.8, 137.5, 136.9, 131.8, 131.3, 130.9, 130.5, 130.4, 130.2, 129.1,

128.9, 127.9, 127.2, 126.7, 123.7, 122.7, 121.5, 115.1. HRMS: m/z calcd for $C_{42}H_{26}N_4$ (M+H)$^+$: 587.2236; found: 587.2233.

*10-(10,11-dihydro-5H-dibenzo[b,f]azepin-5-yl)acenaphtho[1,2-b]pyrido[2,3-e]pyrazine (**NQPy-DDA**)*
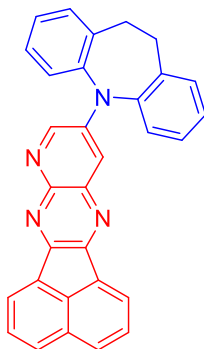
NQPy-DDA

Yellow solid (90 %).^{1}H NMR (300 MHz, CDCl$_3$) δ/ppm: 8.68 (d, *J* = 3.1 Hz, 1H), 8.43 (d, *J* = 7.0 Hz, 1H), 8.31 (d, *J* = 7.0 Hz, 1H), 8.08 (t, *J* = 8.6 Hz, 2H), 7.81 (dd, *J* = 15.0, 6.8 Hz, 2H), 7.54 (dd, *J* = 7.0, 2.2 Hz, 3H), 7.36 (qd, *J* = 6.1, 3.7 Hz, 6H), 3.07 (s, 4H). ^{13}C NMR (75 MHz, CDCl$_3$) δ/ppm: 155.3, 153.1, 145.5, 144.4, 142.1, 137.9, 137.5, 136.4, 132.1, 131.6, 131.5, 129.9, 129.7, 129.11 129.0, 128.9, 128.5, 128.2, 127.8, 122.2, 121.8, 115.0, 30.7. HRMS: m/z calcd for $C_{31}H_{21}N_4$ (M+H)$^+$: 449.1766; found: 449.1761.

*10-(5H-dibenzo[b,f]azepin-5-yl)acenaphtho[1,2-b]pyrido[2,3-e]pyrazine (**NQPy-IMD**)*
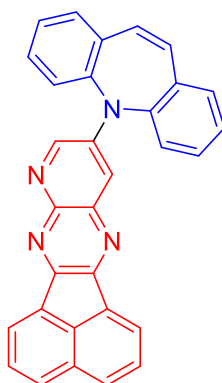
NQPy-IMD

Yellow solid (48 %).^{1}H NMR (300 MHz, CDCl$_3$) δ/ppm: 8.41 (dd, *J* = 7.0, 0.5 Hz, 1H), 8.35 (d, *J* = 3.1 Hz, 1H), 8.29 (d, *J* = 7.1 Hz, 1H), 8.07 (t, *J* = 8.5 Hz, 2H), 7.80 (ddd, *J* = 8.2, 7.0, 6.2 Hz, 2H), 7.65 – 7.58 (m, 4H), 7.55 – 7.44 (m, 4H), 7.24 (dd, *J* = 2.8, 1.8 Hz, 1H), 6.89 (s, 2H). ^{13}C NMR (75 MHz, CDCl$_3$) δ/ppm: 155.2, 153.1, 145.3,

144.7, 141.5, 141.5, 137.3, 136.4, 135.9, 132.0, 131.5, 130.8, 130.6, 130.5, 129.9, 129.7, 129.5, 129.0, 128.8, 128.5, 128.0, 122.2, 121.7, 114.6. HRMS: m/z calcd for $C_{31}H_{19}N_4$ $(M+H)^+$: 447.1610; found: 447.1610.

4. New D-A-D compounds derived from perylene: design, synthesis and characterization

This chapter will demonstrate the design and synthesis of four new compounds derived from perylene as acceptor core, and phenothiazine and phenoxazine as electron donors. These functional materials were synthesized for optoelectronic applications via Pd-catalyzed C−N cross-coupling reactions. In this chapter the author was responsible for all the molecular design, synthesis, structural characterizations (NMRs), and partially for the electrochemical and photophysical investigations.

4.1 Introduction

Perylenes are an important class of compounds that present a high level of π-conjugation. Materials containing derivatives of perylene have been largely applied in strategies to obtain organic photovoltaic cells (OPVs),[95] liquid crystals (LC),[96] photo-emissive materials,[97] sensors, [98] and others.[98–100] Devices based on OLEDs, OPVs, OFETs are very important nowadays and research focused on the use of perylene core can be an excellent strategy to get smart materials with multifunctional properties due to the tunning of photophysical and electrochemical parameters.[101] Studies of perylene derivatives with the TADF effect are not yet widely explored in the literature, which opens new possibilities for research using this acceptor core in combination with various donor moieties. TADF properties in molecules with a high conjugation degree in the acceptor part can be an excellent strategy to control the emission wavelength by the connection of the appropriate donors units and modulation of HOMO-LUMO band gap values and ΔE_{ST}. Perylene dianhydride (PDA) core is very attractive due to its versatility to perform functionalization by different types of organic reactions as well as the usefulness of its photophysical properties in optoelectronic applications, due to its exceptional photochemical stability, and strong and broad absorption in the visible region.[102]

The functionalization of the perylene core with anhydride (PDA), ester (PTE), and imide (PDI) groups is very common in perylene chemistry due to their synthetic versatility and facile interconversion. Furthermore, positions 1,6,7, and 12 (bay positions) are very electropositive, to which halides can be easily attached, allowing for subsequent functionalization through various reaction types. (**Figure 4.1**)
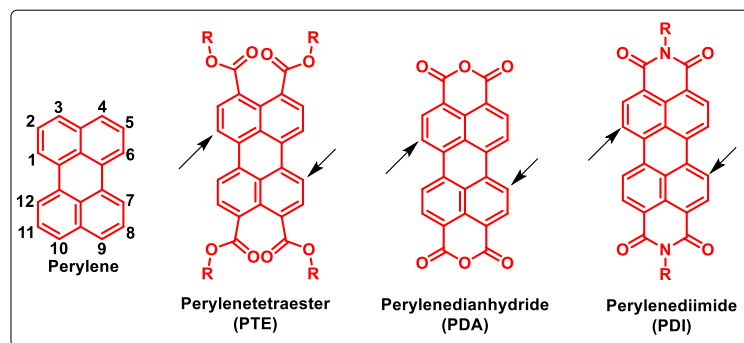
Figure 4.1. *Common functionalizations associated with perylene chemistry. In positions 3, 4 and 9, 10 with ester, anhydride, and imide; in positions 1, 6, 7, and 12 (bay positions) indicated by the arrows with other moieties.*

Despite that, various challenges in molecular design of perylene derivatives materials with appropriate properties are necessary due to search for more efficient devices. PTEs and PDAs derivatives are very interesting due to the modulation of electron-acceptor character by easy and low-cost inter-convection reactions which promotes the tunning of photophysical behavior. Positions 1 and 7 in PTE/PDA also can be functionalized in order to add donor unities which can affect HOMO-LUMO separation and intramolecular charge transfer from donor to acceptor. This strategy also is very useful due to the enhancement in solubility of PDA in common organic solvents. Substituents can increase the solubility by enforcing a twisted conformation, limiting the face-to-face π-π stacking in perylenes systems and being pushed out of the PDA plane by steric interactions.[97,102]

The bay positions are often subjected to regioselective bromination reaction, especially in positions 1,7 and 1,6 which are typically obtained with high yields, and often studied and used, as mixtures of isomers due to the difficulty of separation.[103] Nucleophilic substitution of bromo bay substituents, mainly in PTEs and PDIs due to solubility, is relatively straightforward, and normally, products can be isolated in relatively good yields.[99] Moreover, dibromo-PDIs, dibromo-PTEs and dibromo-PDAs have also been used in palladium catalyzed C-C couplings, such as Suzuki,[104] Stille,[105] and Sonogashira reactions,[106] to obtain various aryl-, heteroaryl-, and alkynyl-functionalized perylene derivatives. On the other hand, the N-C palladium catalyzed reactions have not been explored so far using typical TADF donors such as phenothiazine and phenoxazine, for example.

Based on that, it was designed and synthesized a new series of D-A-D molecules with perylenetetraester (**PTE**) and perylenedianhydride (**PDA**) as acceptor

core and phenothiazine (**PTZ**) and phenoxazine (**PXZ**) as the donors in the positions 1,7, as we can see in the **Figure 4.2**. The addition of the donors by palladium catalyzed N-C coupling reactions can increase the solubility of the materials. The focus is to obtain new functional materials based on PTE/PDA as acceptor core, which can aggregate high electron-negative character and modulation of the HOMO-LUMO gap by low-cost inter-conversion reactions.
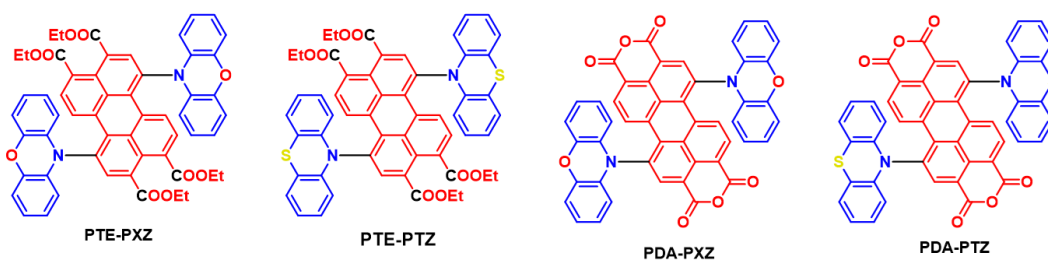
*Figure 4.2. Molecular structures of the compounds derived from perylene-tetraester (**PTE-donor**) and perylene-dianhydride (**PDA-donor**). Donors: phenothiazine (**PTZ**) or phenoxazine (**PXZ**).*

4.2 Molecular design, synthesis, and characterization

The structures were thought to present the perylene core with donor units attached in order to favor CT process by spatial separation of HOMO-LUMO. Also the donors attached can help in the increment of solubility in the standard PDA system, due to the twisted conformation obtained in the final molecules. The phenothiazine and phenoxazine donors were chosen due to their higher electron donation ability in order to equilibrate the high electron deficiency in PTE and PDA systems. The connection in 1,7 bay positions was thought due to the good reaction yields leading to the preparation of the dibrominated PTE and the possibility of isolating any resulting isomers. Due to the ethyl chains in **PTE-donors** we expected more solubility of these compounds in relation to **PDA-donors**.

The design of the molecules was based preliminary on the predictions by DFT and TD-DFT at the B3LYP/6-31G level of theory using Schrodinger 2018-1 software. They allowed for the estimation of the FMOs spatial distributions, S-T gaps, and band gap of the compounds as we can observe in **Figure 4.3**. The HOMO of all the molecules is spatially localized on the donor moieties, with twisted structures near orthogonality. The LUMO is preferentially localized in the perylene core. From **PTE-Donors** to **PDA-Donors,** the band gap (E_g) is decreasing. The ST gaps also are

influenced by the structure and vary between tetraester and dianhydride, with the lowest value of ΔE_{ST} for the compound **PDA-PTZ**.
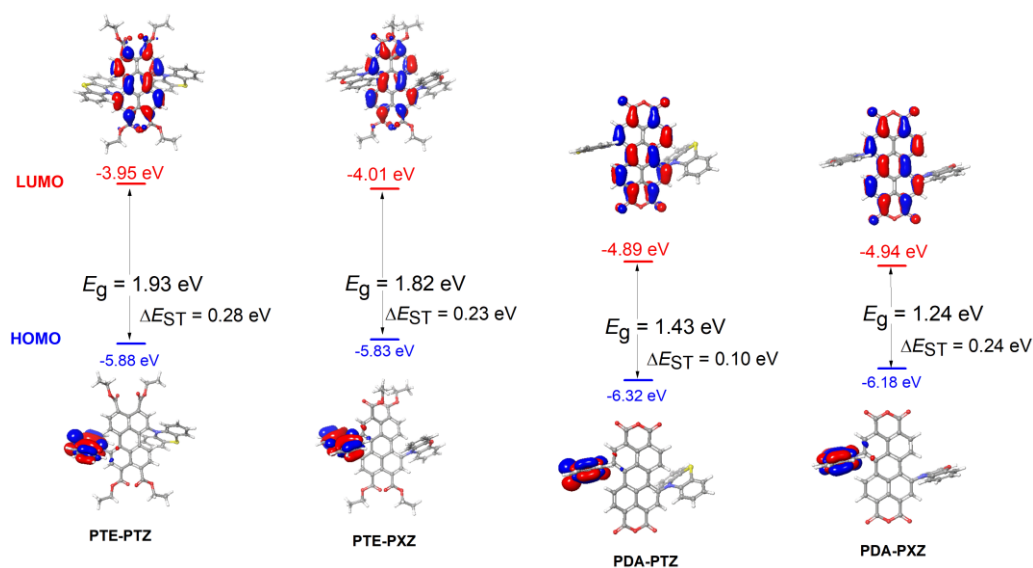
Figure 4.3. *HOMO and LUMO spatial distributions, excited singlet-triplet energy (ΔE_{ST}) and HOMO-LUMO energy gap (E_g) for the **PTE-donor** and **PDA-donor** molecules using DFT and TD-DFT at the B3LYP/6-31G level. Isovalue 0.02.*

The synthesis of the new molecules derived from perylene follows **Scheme 4.1**. The first step of the reaction was the esterification of **PDA** by using ethyl iodide in an alcoholic solution in a basic medium (potassium carbonate) to obtain the compound **PTE** which is very soluble in common organic solvents. The bromination of **PTE** in DCM as solvent provides the mix of isomers (mono- and dibrominated compounds) that were isolated by column chromatography to give the compound dibrominated in positions 1,7 **PTE-Br**. With the dibrominated perylenetetraester (**PTE-Br**) it was possible to realize the nitrogen-carbon coupling. The strategy was the use of the Buchwald-Hartwig Cross-Coupling Reaction using a palladium catalyst and a phosphine derivative as a ligand. The reactions were performed using the respective donor unit (phenothiazine (**PTZ**) or phenoxazine (**PXZ**)) and the base was sodium *tert*-butoxide. For the catalyst was used 3 mol% of the tris(dibenzylideneacetone)dipalladium(0) (Pd$_2$dba$_3$) and 6 mol% of the ligand tri-*tert*-butylphosphonium tetrafluoroborate (HP(*t*-Bu)$_3$BF$_4$) under Argon atmosphere and reflux (110 °C) in toluene for 48h to obtain the compounds **PTE-Donors** in moderate yields (40%) after purification by column chromatography. The last step is the return to dianhydride functional group by a low-cost reaction. It was performed trough the hydrolysis reaction of the perylenetetraesters (**PTE-Donors**) by an excess of

potassium hydroxide in methanol under reflux. This reaction gives the intermediate perylenetetraacid that can be easily converted into the dianhydride by refluxing in acetic acid to obtain **PDA-Donors** in quantitative yields.
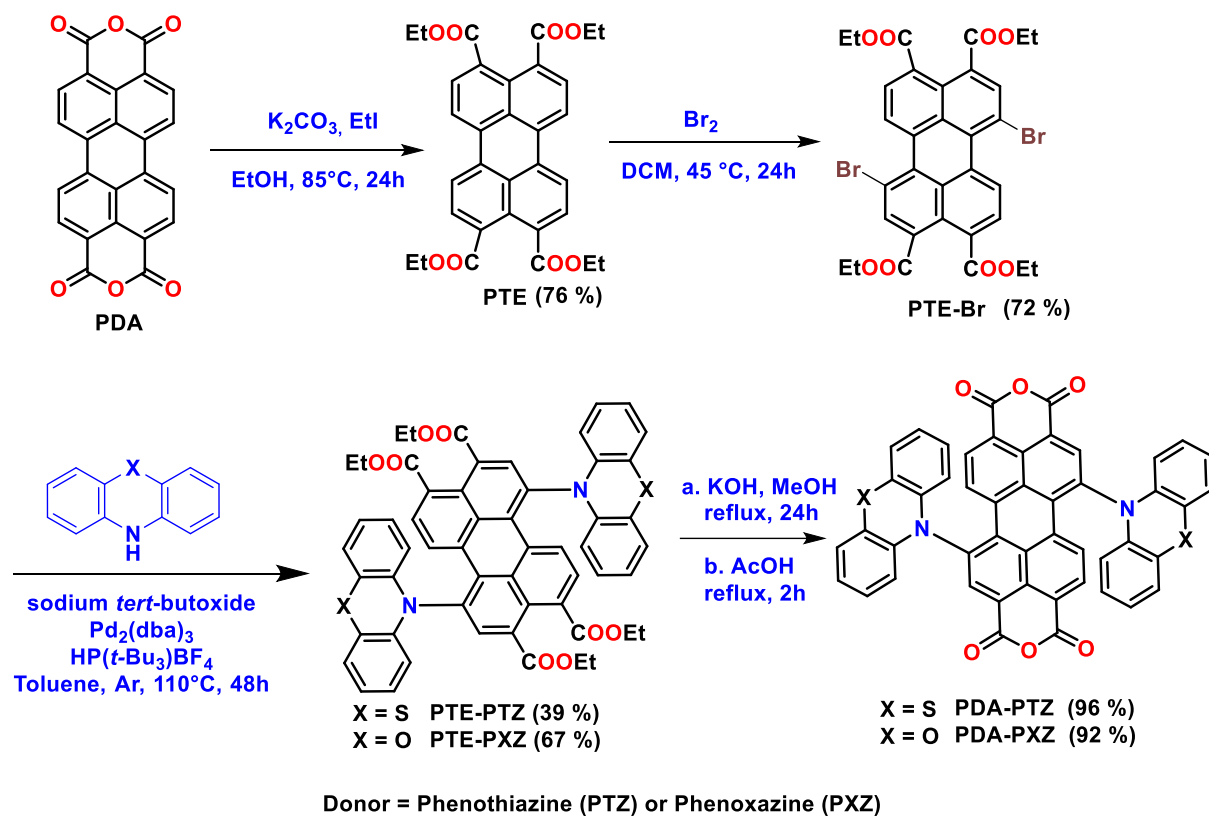
Scheme 4.1. *Synthetic route to obtain the* **PDA-PTZ** *and* **PDA-PXZ.**

All the compounds were fully characterized by Proton (^{1}H) and Carbon (^{13}C) Nuclear Magnetic Resonance (NMR) and by High-Resolution Mass Spectrometry (HRMS) for the final products. All the peaks with attributions are described in the experimental section and as an example, **Figure 4.4** shows the ^{1}H NMR spectrum of **PTE-PTZ** (top).

We can observe the correspondence between the spectra and chemical structure, suggesting the success of the N-C coupling reaction. In 9.2 ppm we observe a doublet (*J*= 8.1 Hz) with integration to 2H, referring to the hydrogen (**Ha**) close to the carbonyl group from the perylene core, which is shifted to the high values of chemical shift due to the high electronegativity of the carbonyl group. The doublet in 8.1 ppm (*J*= 8.1 Hz) is referring to hydrogen **Hb**, also with integration of 2H, with the same coupling constant as **Ha.** The hydrogen signal in 7.98 ppm (2H) appears as a singlet (**Hc**) and is less shifted due to the presence of the phenothiazine nitrogen that has an electron-donor character in the system. Signals from 7-6.1 ppm represent protons from both

phenothiazine moieties connected to the perylene core, indicating the success of the N-C coupling reaction. In the aliphatic part we observe the multiplet in 4.4 ppm (**Hd**) referring to the hydrogens from the ester groups (-COOCH₂-) close to oxygen from the carboxyl group and in 1.4 ppm the multiplet referring the hydrogens from methyl groups (**He**) from tetraester system.
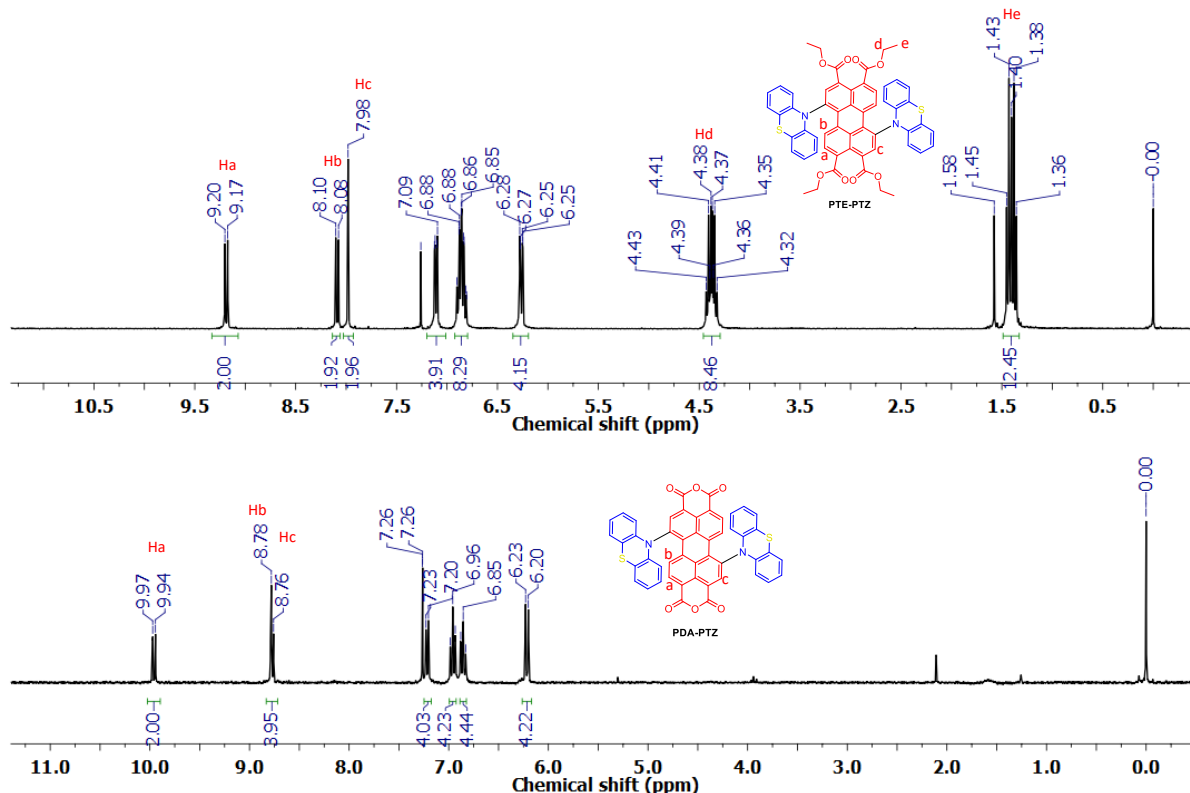
Figure 4.4. ^{1}H NMR spectra of **PTE-PTZ** (top) and **PDA-PTZ** (down) in CDCl₃.

The next reaction was the conversion of the tetraester (**PTE-PTZ**) to dianhydride (**PDA-PTZ**) and we can confirm the structure by the absence of the signals from the aliphatic part and shifting of the signals in the aromatic part as we can see in **Figure 4.4** (down). We observe the influence of the anhydride groups in comparison with the tetraesther system. The first impact is related to the increase of the electronegativity and conjugation degree of the perylene core due to the anhydride system. The Ha proton doublet signal at 9.9 ppm (2H, *J*= 8.3 Hz) is shifted in comparison to the similar proton from **PTE-PTZ** molecule which appears at 9.1 ppm. This behavior is related to the presence of the anhydride system that is more electron withdrawing than the ester. The signals **Hb**-**Hc** appear condensate as multiplet. The compounds **PTE-PXZ** and **PDA-PXZ** were characterized in a similar way.

4.3 Electrochemical characterizations

The electrochemical properties of the **PTE-Donors** and **PDA-Donors** were investigated by cyclic voltammetry (CV) to estimate the HOMO and LUMO energy levels. The estimated ionization potential (IP) and electron affinity (EA) (from onset oxidation (E_{ox}) and reduction (E_{red}) potentials), are correlated with the HOMO (E_{HOMO}) and LUMO (E_{LUMO}) energy levels, respectively, using the following equations: E_{HOMO} = -(E_{ox} + 5.1); E_{LUMO} = -(E_{red} + 5.1).[78] The results are summarized in **Table 4.1** and the voltammograms are compiled in **Figure 4.5**.

Table 4.1. *HOMO and LUMO energy levels estimated from CV measurements and DFT calculations.*

Compounds	Cyclic Voltammetry[a]			Theoretical calculations[b]		
	HOMO (eV)	LUMO (eV)	E_g (eV)	HOMO (eV)	LUMO (eV)	E_g (eV)
PTE-PTZ	-5.42	-3.75	1.67	-5.88	-3.95	1.93
PTE-PXZ	-5.51	-3.81	1.70	-5.83	-4.01	1.82
PDA-PTZ	-5.55	-4.50	1.05	-6.32	-4.89	1.43
PDA-PXZ	-5.69	-4.53	1.16	-6.18	-4.94	1.24

[a] Measurements were performed for 1 mM solutions of investigated compounds in the presence of 100 mM tetrabutylammonium tetrafluoroborate and calibrated using ferrocene/ferrocenium redox couple. [b] theoretical calculations obtained at B3LYP/6-31G** level of theory.

Investigated compounds showed very good stability and reversible electrochemical response in the applied voltage range. All molecules were characterized by a one-step, reversible oxidation process involving phenoxazine (PXZ) or phenothiazine (PTZ) donor unit and a stable, reversible two-step reduction process which is typical for the 1,7 disubstituted PTE and PDA derivatives.[107] The HOMO energy values did not show many differences, presenting slightly higher values for PDA derivatives. On the other hand, the LUMO energy was greatly influenced by the interconversion reaction of **PTE-PTZ** and **PTE-PXZ** (-3.75 eV and -3.81 eV, respectively) to **PDA-PTZ** and **PDA-PXZ** (-4.50eV and -4.53 eV, respectively), showing higher values for PDA-Donors which indicates the easy reduction for these compounds. This behavior leads to lower HOMO-LUMO gaps (E_g) for **PDA-donors** around 1 eV (1.05 eV for **PDA-PTZ** and 1.16 eV for **PDA-PXZ**) in comparison to **PTE-donors** (1.67 for **PDA-PTZ** and 1.70 for **PDA-PXZ**). Other behavior related to donor strength was observed, where the PTZ derivatives showed lower E_g in relation to PXZ derivatives.
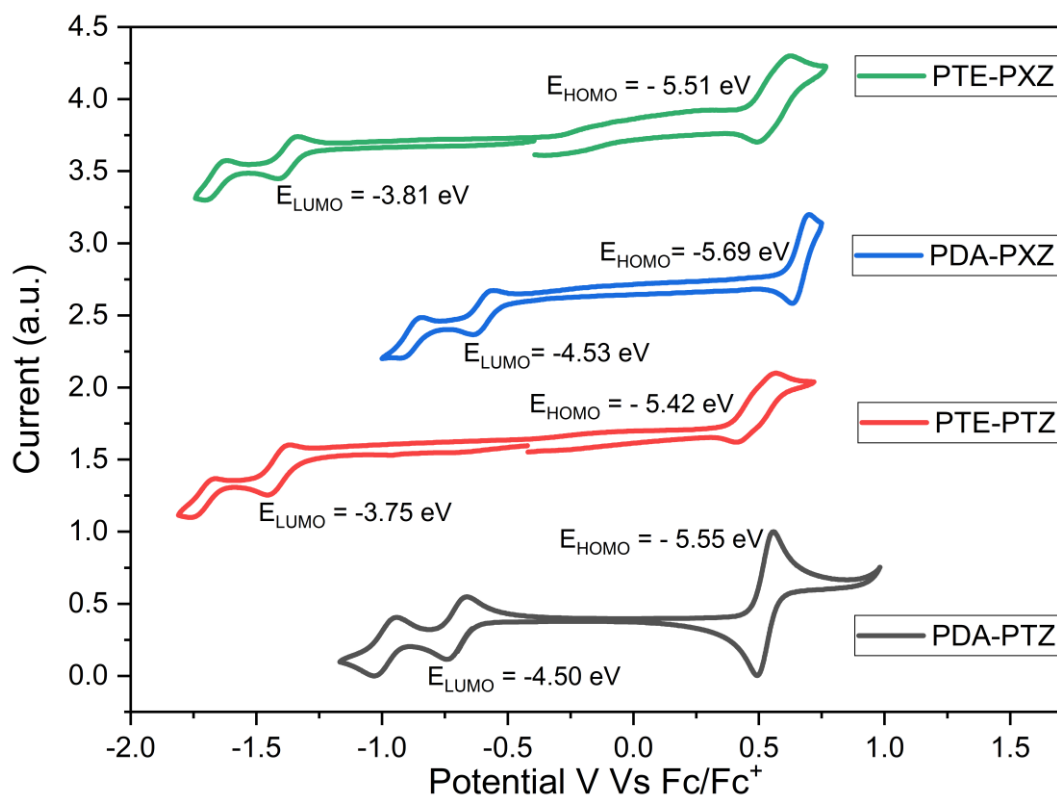
Figure 4.5. *Voltammograms of the 1mM solutions of PTE-donors and PDA-donors in 100mM tetrabutylammonium tetrafluoroborate in DCM at scan rate of 50mV/s.*

4.4 Photophysical analyses

The absorption spectra (UV-Vis) for the compounds **PTE-donors** and **PDA-donors** in dichloromethane (DCM) diluted solutions at room temperature are shown in **Figure 4.6** and the data are summarized in **Table 4.2**.

Table 4.2. *Photophysical properties of PDA-Donor and PTE-donor derivatives in solution.*

Compound	λ_{abs}/nm $[\varepsilon/10^3 M^{-1} cm^{-1}]^a$	λ_{em} (nm)[b]	PLQY (%)[b]
PTE-PTZ	307 [3.98], 397sh [2.97], 425 [6.94], 447 [7.96]	492,573,678	<1
PTE-PXZ	306 [9.9], 424 [12.1], 448 [14.2], 575 [1.4]	486,678	<1
PDA-PTZ	310 [3.94], 372 [2.29], 440 [4.82], 466 [10.7], 499 [15.0]	482, 512, 667	<1
PDA-PXZ	315 [2.45], 366 [1.09], 438 [1.67], 468 [3.71], 500 [4.86]	-	-

[a] Absorption recorded in DCM solutions 1x10⁻⁵ M. [b] Emission recorded in zeonex matrix using 1% of the compounds.

The absorption spectra showed two strong absorption bands around 425 and 450 nm for perylene tetraester derivatives (**PTE-PTZ** and **PTE-PXZ)**, which can be attributed to π-π* transitions characteristic for the perylene system.[98] Broad bands with very low absorptivity can be observed around 575 nm assigned to CT transitions attributed to n-π* transitions from donor to acceptor. The compounds with perylene dianhydride (**PDA-PTZ** and **PDA-PXZ**) had similar profiles but with a red shift. This can be attributed to the ester groups that do not show effective conjugation with the perylene aromatic system due to free rotation around the single bond. On the other hand, the dianhydride is coplanar to the aryl system from perylene resulting in the extension of the π conjugation and consequently the red shift. The two strong absorption bands referring to π-π* transitions appeared around 470 and 500 nm, and CT transitions around 675 nm can be observed with very low absorptivity.
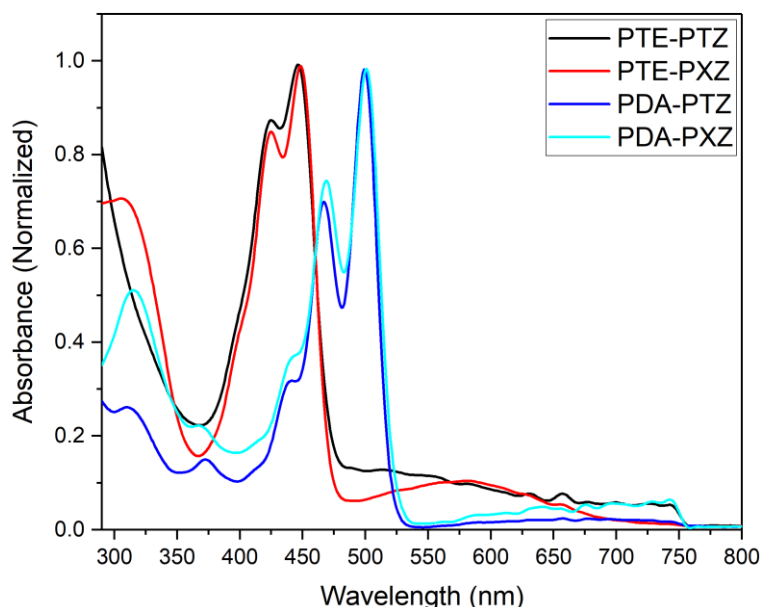
Figure 4.6. *UV-Vis spectra of the compounds PTE-Donors and PDA-Donors in DCM solutions at $1x10^{-5}$ M.*

The compounds were not emissive in DCM solution, indicating a strong aggregation effect, that completely quenched the emission. The emission in solid state, in zeonex matrix, are shown in the **Figure 4.7** showed very small emission with PLQY less than 1. The profile of the emission showed vibronic bands characteristic of perylene derivatives indicating a strong LE character of S_1. The PL spectra (in red line) under vacuum did not show an increase in comparison with air conditions (black line). This behavior can be attributed to the low participation of triplet states in the

mechanism of emissions and consequently no delayed fluorescence is expected for these materials. **PDA-PXZ** did not show emission in the zeonex matrix.
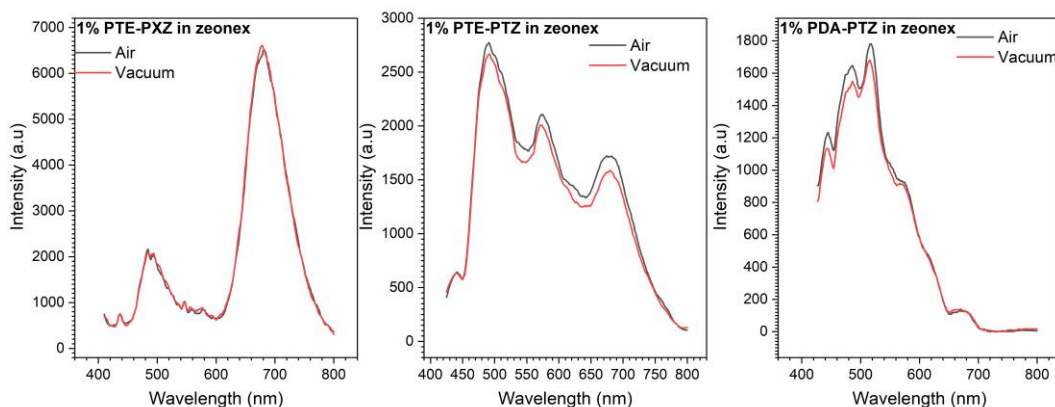
Figure 4.7. *Photoluminescence spectra in Zeonex matrix with 1% **PTE-donors** and **PDA-PTZ**.*

4.5 Conclusions

This chapter describe the design and successful synthesis of a new series of D-A-D molecules based on perylene dianhydride and perylene tetraester as acceptor core, and phenoxazine and phenothiazine as donor moieties attached via N-C palladium catalyzed reactions obtained good to moderate yields (39-67%). The interconversion reaction from perylene tetraester to perylene dianhydride was obtained in very good yields (>92%). All the structural characterization was realized by NMR spectroscopy and by high-resolution mass spectrometry for the final molecules. The electrochemical investigations showed that the materials display good stability in the applied voltage range, with decrease of the electrochemical band gap for the PDA in relation to PTE cores. Which proved as interesting way to control the band gap of materials by a simple and low-cost interconversion reaction. The photophysical properties were also investigated and the materials did not present emission in solution and very low emission in solid state. The electrochemical stability and good range of broad absorption bands in the visible region make these materials good candidates for OPVs applications.

4.6 Synthetic details

Tetraethyl perylene-3,4,9,10-tetracarboxylate (**PTE**)

PTE
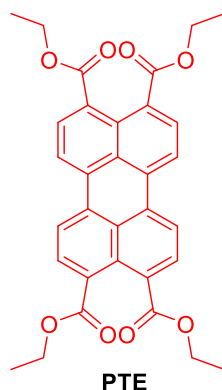
The synthesis was realized according to literature.[95] A mixture of 4.0 g (10.2 mmol) of perylene 3,4,9,10-tetracarboxylicacid dianhydride (PDA), 20 mL (248 mmol) of iodoethane, 10 g of potassium carbonate and 80 mL of ethanol was heated at 85 °C for 24 h. After being cooled down to room temperature, the EtOH and the iodoethane were removed under reduced pressure at 60 °C. The orange-yellow needle residue was collected, and washed with a large amount of water until the filtrate became neutral and was washed with 30 ml of methanol. The solid residue was dried under air to give 4.3 g (76%) of product. The crude product was used directly in the later reaction without further purification. ^{1}H NMR (300 MHz, CDCl$_3$) δ/ppm: 8.20 (d, J = 8.0 Hz, 4H), 8.00 (d, J = 7.9 Hz, 4H), 4.40 (q, J = 7.1 Hz, 8H), 1.43 (t, J = 7.2 Hz, 12H).

*Tetraethyl 1,7-dibromoperylene-3,4,9,10-tetracarboxylate (**PTE-Br**)*

PTE-Br
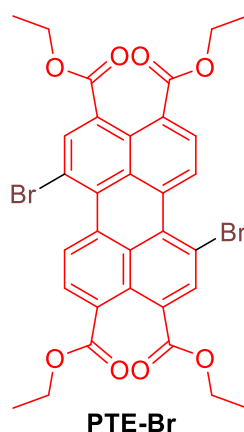
The synthesis was realized according to literature.[95] The mixture of **PTE** (0.65 g, 1.2 mmol), potassium carbonate (0.41 g, 3.0 mmol), and dichloromethane (10 mL) was stirred in 50 mL flask, followed by dropwise addition of bromine (0.92 mL, 18 mmol). The reaction mixture was stirred at room temperature for 24 h, and then 10 mL of 3.0 mol/L sodium sulfite aqueous solution was added. After the solid was removed by filtration, there were two liquid layers formed, one organic and one aqueous. The

organic layer was collected and then chromatographed over hexane/dichloromethane (1:2) using a silica column. The dibrominated compound was collected and the solid was obtained after the solvent was removed under reduced pressure and the sample was dried under vacuum, obtained **PTE-Br** as orange-yellow solid (72 % of yield). ^{1}H NMR (300 MHz, CDCl$_3$) δ/ppm: 8.96 (d, J = 8.0 Hz, 2H), 8.32 (s, 2H), 8.12 (d, J = 8.0 Hz, 2H), 4.40 (qd, J = 7.1, 3.4 Hz, 8H), 0.94 – 0.72 (m, 12H).

*Tetraethyl 1,7-phenotiazine-perylene-3,4,9,10-tetracarboxylate (**PTE-PTZ**)*

PTE-PTZ
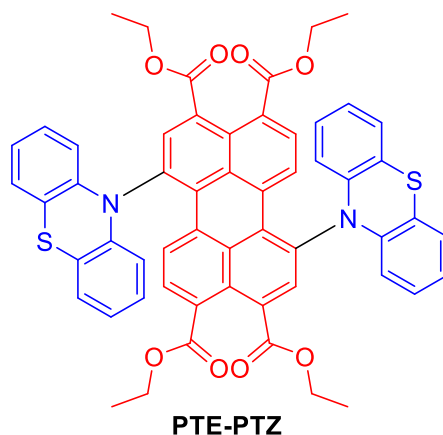
The mixture of **PTE-Br** (0.100 g; 0.143 mmol), phenothiazine (0.069 g; 0.344 mmol), *t*-BuONa (0.055 g, 0.57 mmol), Pd$_2$(dba)$_3$ (7.87 mg; 0.00859 mmol), HP(*t*-Bu)$_3$BF$_4$ (4.98 mg; 0.01718 mmol) and 10 mL of toluene was stirred at 110 °C for 48h under argon atmosphere. After cooling to room temperature, the mixture was filtered through celite and washed with dichloromethane. The combined organic layers were washed with water and brine solution, dried over anhydrous MgSO$_4$ and evaporated to dryness. The residue was purified by column chromatography (hexane/DCM = 4:1 v/v) and crystallized in methanol to give compound **PTE-PTZ** as a brown solid (53 mg; 39.8%). ^{1}H NMR (300 MHz, CDCl$_3$) δ/ppm: 9.19 (d, J = 8.1 Hz, 2H), 8.09 (d, J = 8.2 Hz, 2H), 7.98 (s, 2H), 7.11 (dd, J = 7.1, 2.0 Hz, 4H), 6.92 – 6.80 (m, 8H), 6.26 (dd, J = 7.5, 1.8 Hz, 4H), 4.38 (m, 8H), 1.40 (m, 12H). ^{13}C NMR (75 MHz, CDCl3) δ/ppm: 168.2, 167.6, 142.6, 135.6, 134.8, 132.4, 132.1, 131.9, 131.1, 131.0, 130.5, 127.9, 127.6, 127.42, 127.1, 123.5, 120.5, 115.9, 61.9, 61.7, 29.7, 14.2, 14.1. HRMS: m/z calcd for C$_{56}$H$_{42}$N$_2$O$_8$S$_2$ (M+H)[+]: 934.2383; found: 934.2399.

*Tetraethyl 1,7-phenoxazine-perylene-3,4,9,10-tetracarboxylate (**PTE-PXZ**)*
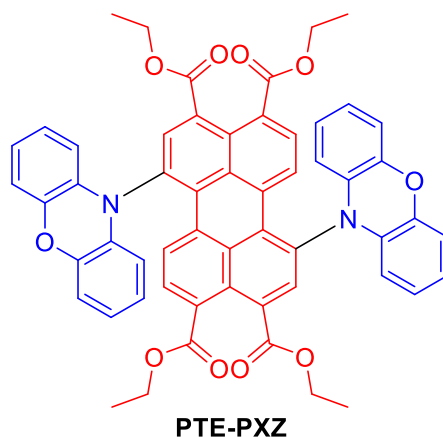
PTE-PXZ

The synthesis procedure is similar to **PTE-PTZ** using phenoxazine (**PXZ**) as donor. The residue was purified by column chromatography (Hexane/CH_2Cl_2 = 3:1 v/v) and recrystallized in methanol to give compound **PTE-PXZ** as a brown solid (200 mg, 67%). ^{1}H NMR (300 MHz, CDCl$_3$) δ/ppm: 9.03 (d, J = 8.2 Hz, 2H), 8.09 (d, J = 8.2 Hz, 2H), 8.03 (s, 2H), 6.81 (m, 16H), 6.69 – 6.60 (m, 4H), 6.08 (dd, J = 8.0, 1.3 Hz, 4H), 4.39 (m, 8H), 1.47 – 1.38 (m, 12H). ^{13}C NMR (75 MHz, CDCl$_3$) δ 168.09, 167.99, 167.42, 167.33, 144.60, 144.52, 134.09, 134.09, 134.06, 133.87, 133.84, 133.76, 133.74, 133.73, 133.68, 133.62, 131.83, 131.79, 131.35, 131.33, 131.15, 131.07, 130.92, 130.84, 127.80, 126.40, 123.95, 122.71, 116.10, 113.86, 61.86, 61.86, 61.76, 61.68, 61.58, 14.17, 14.11, 14.05. HRMS**:** m/z calcd for $C_{56}H_{42}N_2O_{10}$ (M+H)$^+$: 902.2839; found: 902.2837.

*1,7-phenothiazine-perylene-3,4,9,10- tetracarboxylicacid dianhydride (**PDA-PTZ**)*

PDA-PTZ
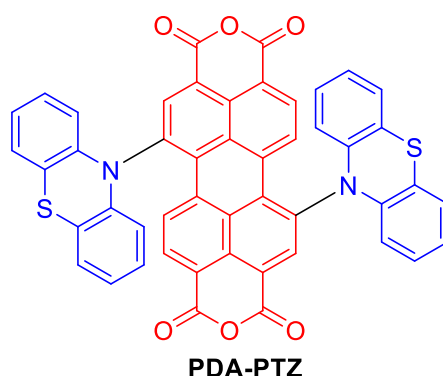
A solution of KOH (0.49g, 8.7 mmol) in 15 ml of methanol was added to **PTE-PTZ** (0.203g, 0.217 mmol) and refluxed for 24h. The consumption of the **PTE-PTZ** was monitored by TLC in dichloromethane. The methanol was evaporated, and water was added to the mixture. Concentrated hydrochloric acid was added until pH=2 and the formed precipitate was collected by filtration. The dark solid was refluxed in acetic acid

(10 mL) for two hours and after cooling, water was added and the precipitate formed was filtrated. The green-dark solid obtained was crystalized in methanol to give the pure compound **PDA-PTZ** in 96% yield. ^{1}H NMR (300 MHz, CDCl$_3$) δ/ppm: 9.96 (d, *J* = 8.3 Hz, 2H), 8.77 (m, 4H), 7.22 (d, *J* = 7.5 Hz, 4H), 6.96 (m, 4H), 6.85 (m, 4H), 6.22 (d, *J* = 8.1 Hz, 4H). ^{13}C NMR (75 MHz, CDCl$_3$) δ/ppm 162.09, 161.92, 144.77, 143.15, 141.45, 137.60, 137.46, 137.08, 133.31, 133.16, 130.85, 130.49, 127.44, 124.60, 124.26, 122.80, 118.67. HRMS: m/z calcd for C$_{48}$H$_{23}$N$_2$O$_6$S$_2$ (M+H)$^+$: 787.0998; found: 787.0990.

*1,7-phenoxazine-perylene-3,4,9,10- tetracarboxylicacid dianhydride (**PDA-PXZ**)*
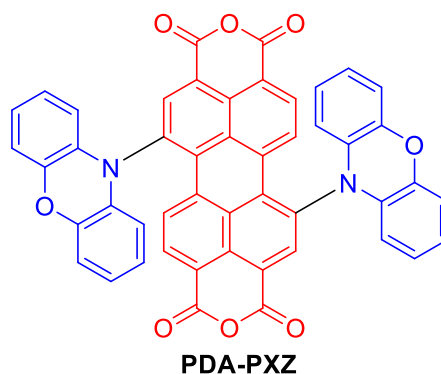
PDA-PXZ

The synthesis procedure is similar to **PDA-PTZ** using **PTE-PXZ**. The green-dark solid was purified by crystallization in methanol to give compound **PDA-PXZ** as a dark-green solid in 92% yield. ^{1}H NMR (300 MHz, CD$_2$Cl$_2$) δ 9.94 (d, J = 8.3 Hz, 2H), 8.79 – 8.69 (m, 4H), 7.21 (dd, *J* = 7.5, 1.6 Hz, 4H), 6.95 (td, *J* = 7.5, 1.0 Hz, 24H), 6.89 – 6.82 (m, 4H), 6.25 (dd, *J* = 8.1, 1.0 Hz, 4H). HRMS: m/z calcd for C$_{48}$H$_{23}$N$_2$O$_8$ (M+H)$^+$: 755.1454; found: 755.1456.

5. Asymmetric D-A-D compounds derived from naphthalene benzimidazole: design, synthesis, photophysical and electrochemical properties

This chapter will demonstrate the design and synthesis of five new compounds derived from naphthalene benzimidazole as acceptor core, and phenothiazine, phenoxazine and diphenylamine as electron donors. These functional materials were synthesized by Pd-catalyzed C−C and C-N cross-coupling reactions aiming optoelectronics applications. In this chapter the author was responsible for all the molecular design, synthesis, structural characterizations (NMRs), and partially for the electrochemical and photophysical investigations.

5.1 Introduction

The development of high-performance organic light-emitting diodes (OLEDs) with purely organic emission materials has been a challenge for researchers in recent years.[4] Small organic molecules based on TADF/RTP properties appear as an excellent strategy to obtain high EQE and easy processability to be applied in OLEDs. Asymmetric D-A-D molecules with spatially separated FMOs can be used as strategy to minimize the ΔE_{ST} and consequently obtain an efficient RISC by charge transfer process from donor to acceptor unit.[22,108,109] The asymmetry in the cores can provide different excited states in the molecule that can relax by different mechanisms. The investigations in these kind of molecular structure can result in materials with dual properties such as TADF and RTP.[29,31,110]

N-rich acceptor cores with good charge transport carriers are useful strategy to optimize the spin-orbit coupling (SOC) that is related with the rate constant of RISC process, which can facilitate the harvest of excited triplet states to singlet states.[111,112] Materials based on benzimidazole core have been largely investigated for application in optoelectronic devices due to the high level of charge transport carriers and intrinsic PLQYs. Naphthalene benzimidazoles can be prepared by the dehydration reaction between *ortho*-diaminobenzene derivatives and naphthalene anhydrides; they have a higher acceptor character due to the presence of the nitrogen and the carbonyl group in the system, which increases the electronegativity in the core.[113]

Welisson de Pontes Silva

The naphthalene benzimidazole is a very interesting N-rich acceptor due to the increase of electronegativity by addition of carbonyl group conjugated with the imidazole system.[95] The naphthalene part is responsible for increment in the π-conjugation degree which contributes to minimization of the HOMO-LUMO gap.[114] The asymmetric core with the bromines in 4,7-positions of the benzimidazole part is a very interesting synthetic strategy allowing for functionalization by addition of different donor moieties. These bromines can be subjected to different types of reactions with emphasis on N-C coupling and C-C coupling.

Therefore, in this part of the work, the design, synthesis, and study of the photophysical and electrochemical behavior of a new series of compounds based on the asymmetric naphthalene benzimidazole as an acceptor core and phenothiazine, phenoxazine, and diphenylamine as donor units are described. Additionally, a phenyl π-spacer group was introduced between the donor and acceptor units to study the relationship between the molecular structure and photophysical and electrochemical properties, which is important for the applications in OLED devices. **Figure 5.1** shows the molecules that were synthesized.

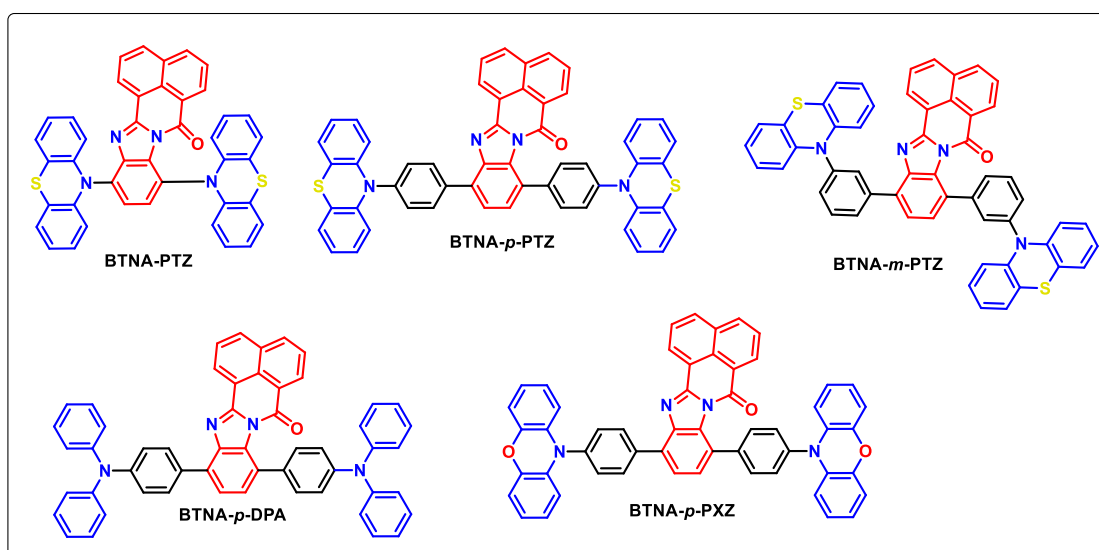**Figure 5.1.** *Molecular structures of the compounds derived from naphthalene benzimidazole (**BTNA-donors**).*

5.2 Design, synthesis, and characterization

The molecular design was based on theoretical calculations to support synthetic choices. The frontier molecular orbitals (MOs) HOMO and LUMO of the **BTNA-donors** were predicted using density functional theory (DFT) calculations. As shown in **Figure**

5.2, the LUMOs of all compounds are especially localized on the naphthalene benzimidazole (**BTNA**) core. On the other hand, their HOMOs are concentrated preferentially on the donor units, showing a clear spatial separation of the frontier MOs. We observe that HOMO is mainly located on the donor unit, which is connected to the core on the carbonyl group side. Only **BTANA-*p*-DPA** showed minimal overlap between HOMO and LUMO orbitals, which is expected for the weaker electron donors such as diphenylamine. The HOMO-LUMO energy gap (E_g) follows the expected behavior determined by the strength of the donor unity, showing the highest value for **BTNA-*p*-DPA**. These theoretical estimates showed a similar trend as the experimental electrochemical data, but they were not well correlated, as will be discussed later in the work. We used time-dependent DFT (TD-DFT) to estimate the energy of the lowest singlet and triplet states. All the compounds showed small and very small ΔE_{ST} values, which is necessary to display TADF properties. The highest value was calculated for **BTNA-*p*-DPA**, in which mentioned earlier overlapping of orbitals was also observed, therefore fluorescence may play a greater role in the emission mechanism of this compound.
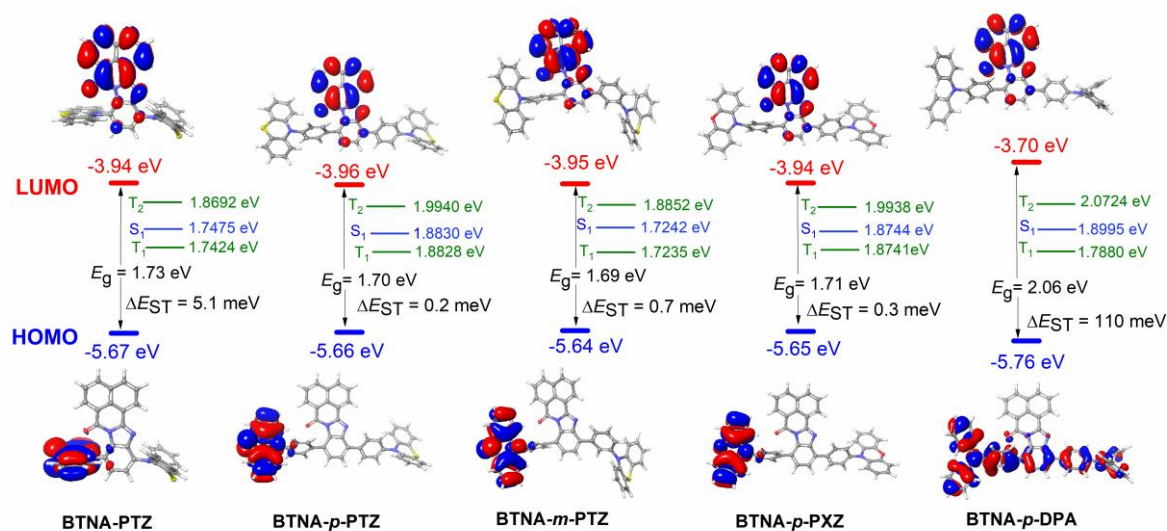

Figure 5.2*. FMOs, singlet-triplet energies gap of the **BTNA-Donors** obtained by DFT and TD-DFT at B3LYP/6-31G level of theory.*

The synthetic route used to obtain the final molecules is shown in **Scheme 5.1.** The strategy used was based on the synthesis of the **BTNA-Br₂** core followed by two types of cross-coupling reaction. The first one was based on the Buchwald-Hartwig

cross-coupling reaction (Nitrogen-Carbon coupling) and the second one was based on the Stille cross-coupling reaction (Carbon-Carbon coupling).

To synthesize the core, several additional steps were necessary in advance. First, brominated benzothiadiazole (**BTZ**) was opened by reduction reaction using sodium borohydride to obtain 3,6-dibromobenzene-1,2-diamine (**BTZ-NH₂)** in good yield. Next, the amine was reacted with 1,8-naphthalic anhydride in boiling acetic acid to give **BTNA-Br₂** as a yellow solid with 70% yield. This important asymmetric core was used in the following steps as a key intermediate.

The Buchwald-Hartwig cross-coupling reaction was performed using two equivalents of phenothiazine as a donor to obtain the compound **BTNA-PTZ**. This synthesis achieved moderate yield (44%) due to the steric hindrance at substitution sites, which are difficult to reach for bulky phenothiazine molecules. To perform the Stille C-C coupling reactions it was necessary to prepare the Stille reagent in advance. The three donors (phenothiazine, phenoxazine, and diphenylamine) were reacted with half equivalent of 1,4-dibromobenzene or 1,3-dibromobenzene via C-N coupling to obtain the compounds (**PTZ-*p*-Br**, **PTZ-*m*-Br, PXZ-*p*-Br** and **DPA-*p*-Br**). The preparation of the Stille reagent was carried out in two steps: lithiation with *n*-butyl lithium at -78 °C, followed by addition of the tributyltin chloride to perform the substitution reaction to obtain the compounds **PTZ-*p*-SnBu₃**, **PTZ-*m*-SnBu₃ PXZ-*p*-SnBu₃** and **DPA-*p*-SnBu₃** in good yields. These compounds require subsequent reaction immediately after preparation due to their low stability. In the following step, they were coupled with **BTNA-Br₂** core in the presence of the tetrakis(triphenylphosphine)palladium(0) as a catalyst to give the final products **BTNA-*p*-PTZ**, **BTNA-*m*-PTZ, BTNA-*p*-PXZ** and **BTNA-*p*-DPA**.
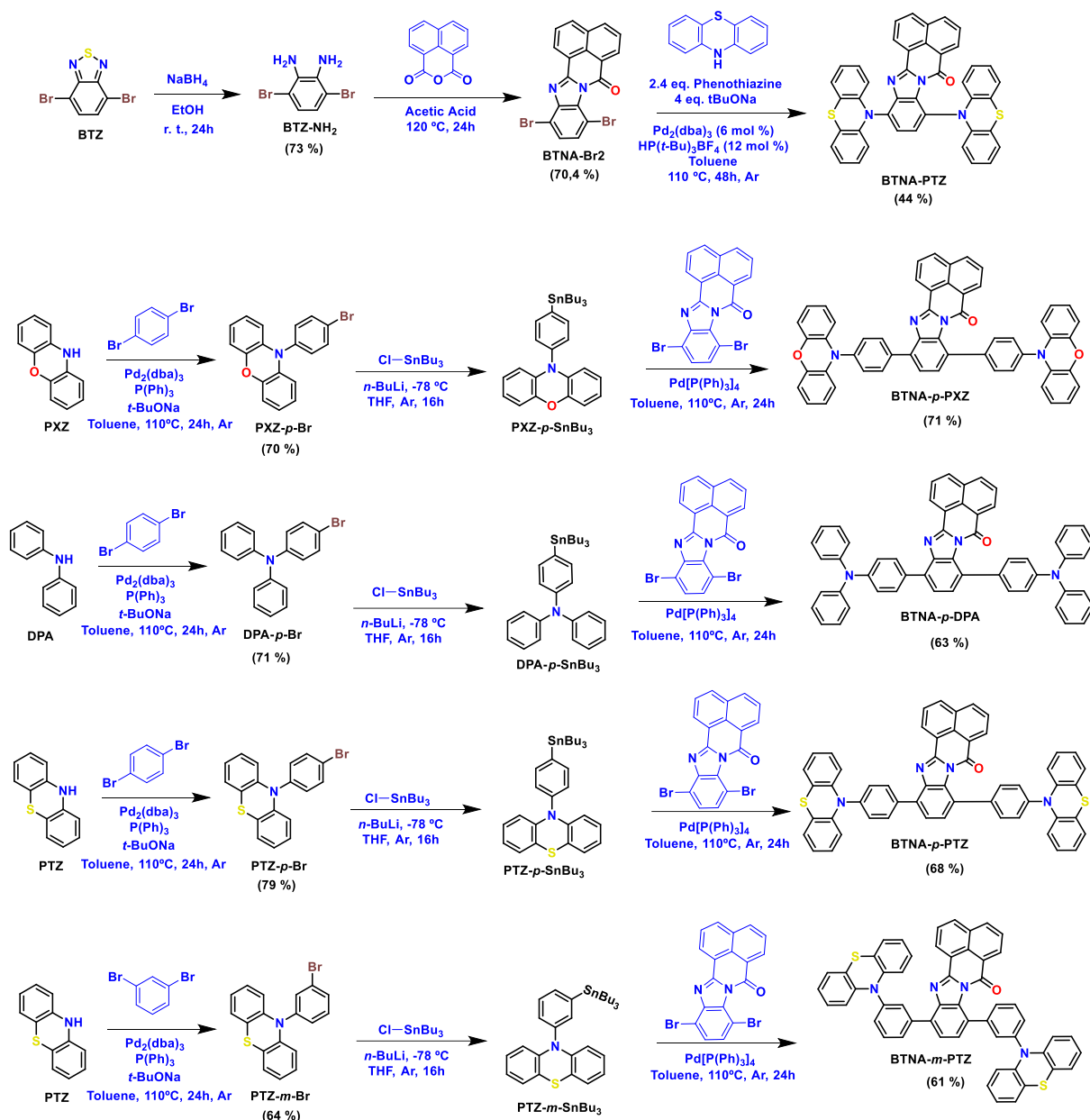
Scheme 5.1. *Synthetic route to obtain* **BTNA-PTZ, BTNA-p-PTZ, BTNA-p-PXZ, BTNA-p-DPA** *and* **BTNA-m-PTZ**.

All newly synthesized compounds were fully characterized by ^{1}H and ^{13}C Nuclear Magnetic Resonance (NMR) and by High-Resolution Mass Spectrometry (HRMS) for the final molecules. The reaction conditions are shown in the synthetic details section. As an example of the characterization of this series of compounds, **Figure 5.3** shows the ^{1}H NMR spectra of **BTNA-PTZ** and **BTNA-p-PTZ**. For both spectra, it is possible to see the signals referring to the acceptor part (naphthalene benzimidazole core) and for donor part (phenothiazine). The asymmetric system in **BTNA-PTZ** is clear and it is possible to recognize by outspread of signals in phenothiazine part due to appearance of the multiplets **m**, **m'** (7.11 ppm, 7.03 ppm)

Welisson de Pontes Silva

and **i**, **i'** (6.31 ppm, 6.05 ppm). The presence of the electron-deficient carbonyl group on only one side of the molecule was sufficient to differentiate these signals which are consistent with the asymmetry of the naphthalene benzimidazole core. The signals assigned also was based in systems containing naphthalene benzimidazole,[114] and phenothiazine derivatives.[88,115]
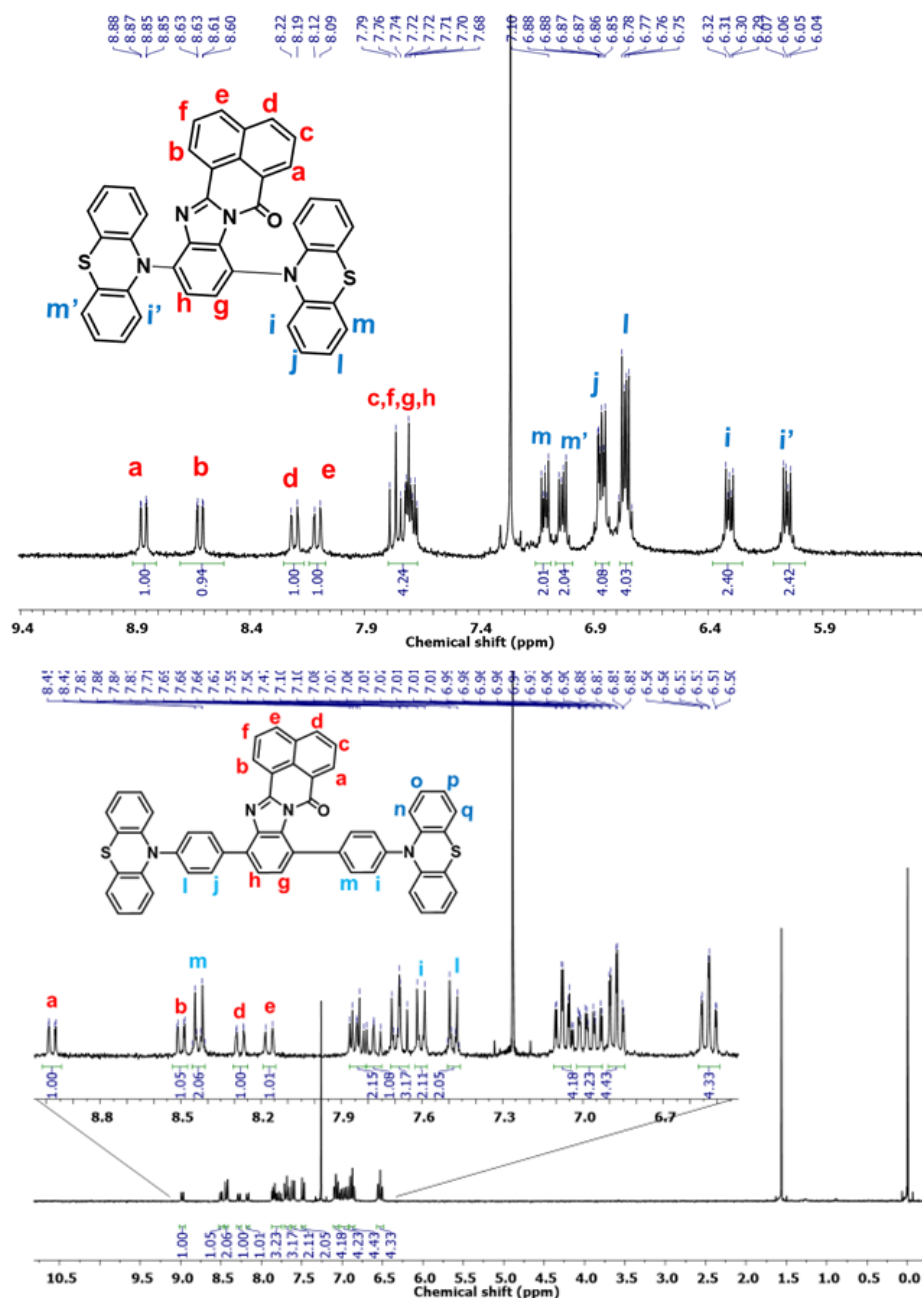
Figure 5.3. [1]*H NMR spectra of* **BTNA-PTZ** *(up) and* **BTNA-p-PTZ** *(down) in CDCl₃ (300 MHz).*

In the case of **BTNA-*p*-PTZ**, the presence of the phenyl spacer between the acceptor and donor units influences the signals of the system due to the extension of the conjugation degree in the molecule (**Figure 5.3** – down). Additionally, the core asymmetry is also reflected in the rest of the molecule which makes the assignment of

the signals more difficult, especially in the region between 7.9-7.4 ppm. Less affected phenothiazine donor parts show multiplets consistent with the spectra of such systems but only a few signals derived from the spacer and core parts have been assigned with certainty.

5.3 Electrochemical properties

The electrochemical properties of the **BTNA-Donors** were investigated by cyclic voltammetry (CV), which allowed for the determination of ionization potential (IP) and electron affinity (EA) of the molecules. The estimated IP and EA are correlated with the HOMO (E_{HOMO}) and LUMO (E_{LUMO}) energy levels, respectively, using the following equations: $E_{HOMO} = -(E_{ox} + 5.1)$; $E_{LUMO} = -(E_{red} + 5.1)$.[78] The results are summarized in **Table 5.1** and the voltammograms are compiled in **Figure 5.4**.

Table 5.1. *HOMO and LUMO energy levels estimated from CV measurements and DFT calculations.*

COMPOUND	Cyclic Voltammetry[a]			Theoretical[b]		
	HOMO (eV)	LUMO (eV)	E_g (eV)	HOMO (eV)	LUMO (eV)	E_g (eV)
BTNA-*p*-DPA	-5.58	-3.48	2.10	-5.76	-3.70	2.06
BTNA-*p*-PXZ	-5.56	-3.63	1.93	-5.65	-3.94	1.71
BTNA-*p*-PTZ	-5.25	-3.25	2.00	-5.66	-3.96	1.70
BTNA-*m*-PTZ	-5.48	-3.59	1.89	-5.64	-3.95	1.69
BTNA-PTZ	-5.51	-3.75	1.76	-5.67	-3.94	1.73

[a] Measurements were performed for 1 mM solutions of investigated compounds in the presence of 100 mM tetrabutylammonium tetrafluoroborate and calibrated using ferrocene/ferrocenium redox couple. [b] obtained by DFT at B3LYP/6-31G level of theory.

The materials showed good stability and reversibility in the applied voltage range with the reduction process occurring on the naphthalene benzimidazole unit (**BTNA** core) and oxidation process occurring on the donor units. The LUMO levels of the investigated compounds presented notable differences in the values, varying from -3.25 eV to -3.75 eV, depending on the donor coupled and by insertion of the phenyl spacer between naphthalene benzimidazole core and donor. The lowest energy of LUMO (-3.75 eV) was found for **BTNA-PTZ**, and the highest (-3.25 eV) for **BTNA-*p*-PTZ**, showing the influence of phenyl spacer in the estimated LUMO energy values. The reversibility in the reduction process is notable for all compounds suggesting the electrochemical stability of the **BTNA** core. The oxidation process also showed reversibility, and appearing at least as two steps oxidation process, which can be

related to the presence of two donor moieties. The first oxidation process was notable reversible for all compounds. The compounds also showed second step oxidation with reversibility for **BTNA-*p*-PTZ**, **BTNA-PTZ** and **BTNA-p-DPA**. On the other hand, it was not reversible for **BTNA-*m*-PTZ** and **BTNA-*p*-PXZ**. **BTNA-*p*-DPA** and **BTNA-PTZ** showed the two oxidation steps very close, being merged together. In the case of **BTNA-*p*-PTZ**, **BTNA-*m*-PTZ** and **BTNA-*p*-PXZ** the second step oxidation appears in higher potentials, in relation to first oxidation process**.** The estimated energies of HOMO showed considerable difference mainly for **BTNA-PTZ**, which can be related to the lack of phenyl spacer between the BTNA core and phenothiazine. Additionally, the variation of the donor position from *par*a to *meta* (in **BTNA-*p*-PTZ** to **BTNA-*m*-PTZ**) decreases the HOMO energy level, indicating the lower potential oxidation for the phenothiazine in *para* position.
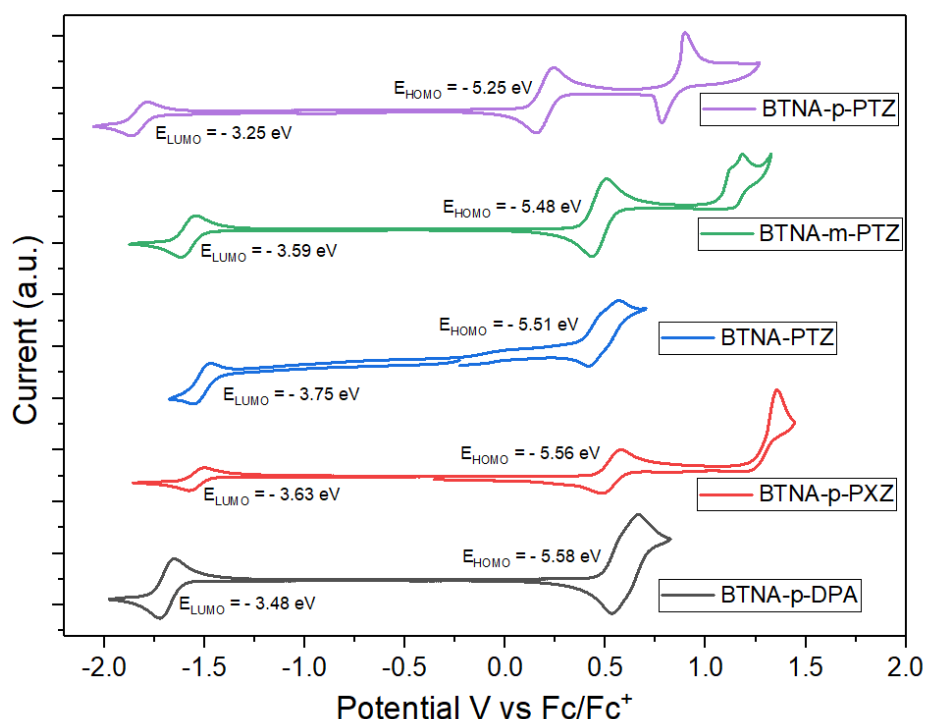
Figure 5.4. *Voltammograms of the 1mM solutions of compounds **BTNA-Donors** in 100mM tetrabutylammonium tetrafluoroborate in DCM. Pt disk as working, Pt wire as counter and Ag/AgCl as reference electrode, at 50 mv s^{-1} scan rate.*

The electrochemical band gap (E_g) showed the lowest value for the compound without the phenyl spacer group (**BTNA-PTZ**, 1.76 eV), indicating the lower π-conjugation degree for this compound. For the compounds with phenyl π-spacer, we observe the higher E_g for **BTNA-*p*-DPA** (2.10 eV), that present the weaker electron-

donor (diphenylamine) attached, and **BTNA-m-PTZ** (1.89 eV) show the lowest value of E_g. The difference in connection position of the donor from **BTNA-*p*-PTZ** to **BTNA-*m*-PTZ** positions also decreases the E_g from 2.00 eV to 1.89 eV. Additionally, the results obtained by DFT calculations showed a moderate correlation with the experimental electrochemical data as we can observe in the **Table 5.1**.

5.4 Photophysical analyses

The absorption spectra (UV‑Vis) in diluted dichloromethane (DCM) solutions are shown in **Figure 5.5** and the data are summarized in **Table 5.2**. We can observe strong absorption bands around 230-270 nm, that can be assigned to the π→π* transitions in the naphthalene core aromatic system. We can observe less intense absorption bands in 290-330 nm, that can be signed to the π→π* transitions in the donor-acceptor structures. Lower intense broad bands can be observed from 380 to 470 nm and can be attributed to a CT transition from the donor units to the acceptor core.

Table 5.2. *Photophysical properties of **BTNA-donors** in solution and in zeonex matrix.*

Compounds	λ_{abs}/nm $[\varepsilon/10^3 M^{-1} cm^{-1}]^a$	λ_{em}/nm[b]	PLQY[c] (%)	Increase	PLQY x Increase (%)
BTNA-*p*-PTZ	258 [33.6], 314 [11.4], 398sh [4.5]	542,577	13.7	1.12	15.3
BTNA-*m*-PTZ	258 [34.7], 294 [11.5], 310 [11.6], 395sh [4.8]	578,595	15.3	1.66	26.0
BTNA-*p*-PXZ	240 [44.7], 270 [10.1], 315 [13.7], 394sh [5.5]	553,583	16.4	1.15	18.9
BTNA-*p*-DPA	232 [24.4], 303 [20.0], 363 [20.4], 465 [2.8]	594	8.3	1.09	9.1
BTNA-PTZ	257 [30.2], 289 [6.6], 301 [7.6], 381 [5.6]	479, 610	<1	1.26	1.1

[a] Absorption measured in DCM 0.01 mM. [b] Obtained in zeonex matrix. [c] obtained in zeonex matrix.

The extension of the π-conjugation in the molecules from **BTNA-PTZ** to **BTNA-*p*-PTZ** can be observed by the more intense absorption band for **BTNA-PTZ** around 380 nm by proximity of the phenothiazine and the naphthalene benzimidazole core

resulting in more intense CT from donor to acceptor. The changes in the donors from phenothiazine to phenoxazine did not show differences in the absorption bands profile. On the other hand, the **BTNA-*p*-DPA** (diphenylamine as a donor) presented very intense absorption bands at 300 and 366 nm referring to $\pi \rightarrow \pi^*$ transitions in the donor/acceptor moieties.
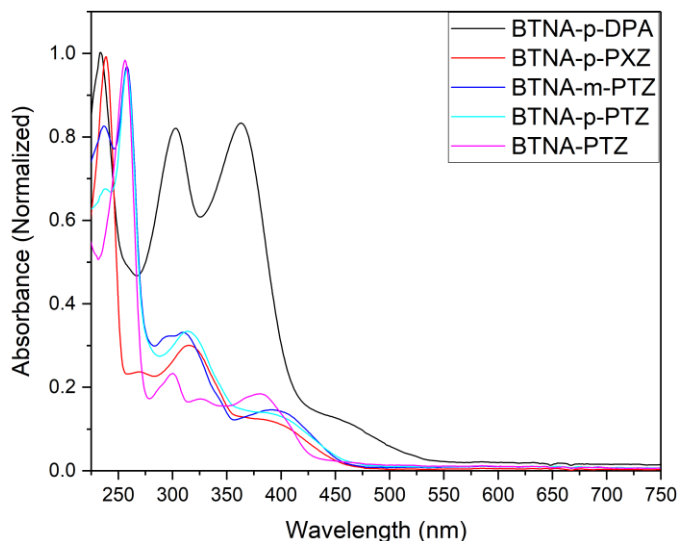

Figure 5.5*. Absorption spectra of **BTNA-Donors** in DCM solutions 0.01 mM.*

The compounds did not show emission in DCM or toluene indicating very strong aggregation effect that totally quenches the emission in solution. It can be attributed to AIE behavior that is usually non-emissive in solution due to non-radiative relaxation pathways such as rotation or vibration. In the solid-state these channels can be blocked upon aggregation and photon excitation results in an increase of efficiency in the radiative decay.[116] **Figure 5.6** shows the photoluminescence (PL) spectra of **BTNA-donors** in zeonex matrix, under air and vacuum conditions. The data are also summarized in **Table 5.2**.
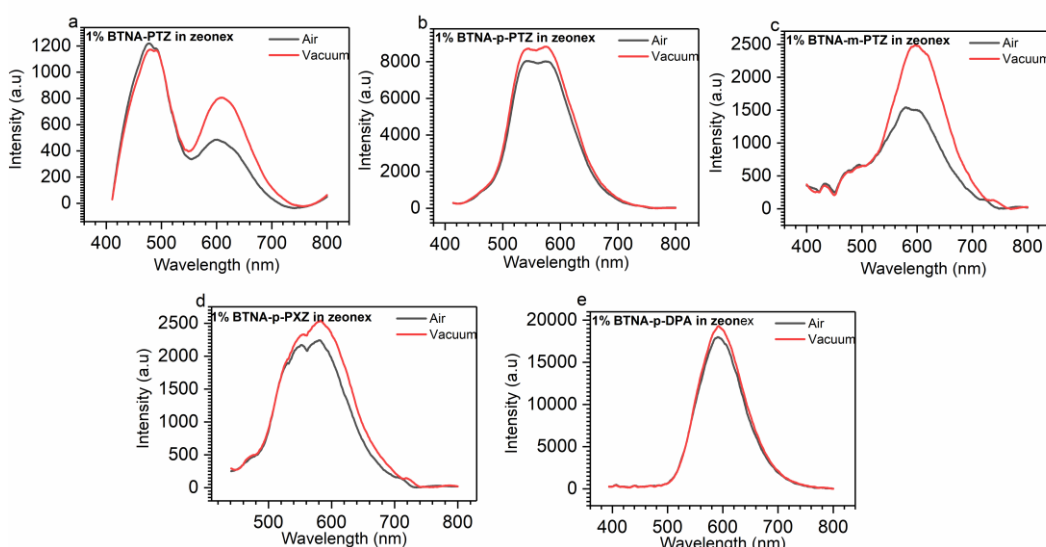
Figure 5.6. *Photoluminescence (PL) spectra of 1% of the compounds **BTNA-donors** in zeonex matrix under air conditions (black line) and under vacuum conditions (red line).*

The PL spectra of **BTNA-PTZ** showed two emission bands centered at λ_{PL}= 479 (more intense) and λ_{PL}= 610 nm (less intense). This behavior can be attributed to the possibility of two ^{1}CT states by the asymmetry of the naphthalene benzimidazole core, with two units of phenothiazine given different CT states.[117] The second explanation may arise from the possibility of the donor units adopting two stable conformations, e.g. *quasi*-axial or *quasi*-equatorial, which will also result in two distinct CT energies. This behavior in phenothiazine D-A derivatives has been previously reported in literature[118] and we also observe similar behavior for other phenothiazine derivatives described in this thesis, such as NQPy-PTZ. The compound **BTNA-*p*-PTZ** (with phenyl π-spacer group) also showed two emission peaks centered at λ_{PL}= 542 and λ_{PL}= 577 nm attributed to the previous explanation. The red shift in the first peak (compared to **BTNA-PTZ**) is related to the increase of the π-conjugation degree by the addition of phenyl spacer group. Comparing the *para* and *meta* positions (**BTNA-*m*-PTZ**) we observe a red shift in the emission due to the character of electron-donation from phenothiazine in meta position being decreased. The compound **BTNA-*p*-PXZ** showed vibronic emission with maximum emission wavelength λ_{PL}= 583 nm. On the other hand, **BTNA-*p*-DPA** clearly showed CT character which can be associated with the gaussian profile of emission with maximum λ_{PL}= 594 nm.

The materials showed moderate PLQYs, where **BTNA-*p*-PXZ** presented the highest value (16.4%). All compounds showed an increase in the emission intensity

under vacuum conditions, which indicates that triplet states are involved in the emission mechanism, which is characteristic of TADF behavior. Considering the increase in the emission intensity (see **Table 5.2**), the highest increase was observed for **BTNA-*m*-PTZ** (1.66x), showing a PLQY of 26.4% under vacuum conditions.

5.5 Conclusions

This chapter described the design and successful synthesis of a new series of D-A-D molecules based on asymmetric naphthalene benzimidazole as acceptor core and different donors attached via N-C Buchwald-Hartwig cross-coupling reaction and C-C Stille cross-coupling reaction. All the structural characterizations were realized by NMR spectroscopy and by high-resolution mass spectrometry for the final molecules. The electrochemical characterization showed that the materials have good stability and reversibility in the applied voltage range, displaying reversible one step reduction concerned in the naphthalene benzimidazole core and reversible oxidation process mainly for the materials with π-spacer aromatic system. The structural changes made by donor variations and additionally the changes in connections from *para* to *meta* positions proved as good alternative to the control of the electrochemical band gap. The photophysical behavior also was directly affected by the structural modifications indicating the versatility of the asymmetric naphthalene benzimidazole core to optoelectronics applications. All materials showed an increase in PL intensity under vacuum conditions indicating the TADF behavior of the materials which lead interesting candidates to application in TADF based OLEDs.

5.6 Synthetic details

*3,6-dibromobenzene-1,2-diamine* (**BTZ-NH₂**)
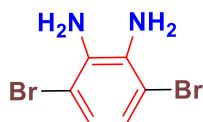
BTZ-NH$_2$

4,7-dibromobenzo[*c*][1,2,5]thiadiazole (1.50 g, 5.10 mmol) was dissolved in EtOH (50 ml) and cooled with an ice/water bath between 0-5 °C. NaBH$_4$ (10.2 mmol, 3.86 g) was added in small portions and the reaction mixture was stirred 14h. The reaction mixture was evaporated at 35 °C to dryness and diluted with water (100 mL). Water and ethyl ether were added, and the aqueous layer was separated and extracted

with dichloromethane. The combined organic layers were washed with brine, dried over MgSO$_4$ and concentrated in vacuo to afford compound **BTZ-NH$_2$** (79%) as yellow pallid solid. The product was used without further purification in the next step. ^{1}H NMR (300 MHz, DMSO-d_6): δ/ppm: 6.62 (s, 2 H), 5.02 (s, 4 H).

9,12-dibromo-7H-benzo[de]benzo[4,5]imidazo[2,1-a]isoquinolin-7-one (**BTNA-Br$_2$**)

BTNA-Br$_2$
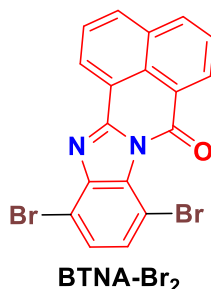
BTZ-NH$_2$ (0.66 g, 2.5 mmol) and 1,8-naphthalic anhydride (0.48 g, 2.5 mmol) were uniformly mixed by grinding in 15 mL of glacial acetic acid. The mixture was heated at 120 °C for 18 h under argon atmosphere with stirring. Then, the solution was poured into distilled water and the yellow precipitate was collected by filtration, washed several times with water, and dried in a vacuum. The crude product was recrystallized in acetone to obtain 0.76 g (71%) of **BTNA-Br$_2$** as a yellow solid.^{1}H NMR (300 MHz, CDCl$_3$): δ (ppm) 8.90 (d, J = 7.3 Hz, 1H), 8.71 (d, J = 7.3 Hz, 1H), 8.24 (d, J = 8.1 Hz, 1H), 8.13 (d, J = 8.2 Hz, 1H), 7.77 (dd, J = 16.5, 8.2 Hz, 2H), 7.49 (dd, J = 22.0, 8.4 Hz, 2H). ^{13}C NMR (75 MHz, CDCl$_3$): δ (ppm) 159.5, 151.6, 145.3, 135.1, 132.7, 132.4, 132.2, 132.1, 132.0, 129.8, 128.3, 127.4, 127.2, 127.1, 123.8, 120.2, 113.4, 106.5.

9,12-di(10H-phenothiazin-10-yl)-7H-benzo[de]benzo[4,5]imidazo[2,1-a]isoquinolin-7-one (**BTNA-PTZ**)


BTNA-PTZ
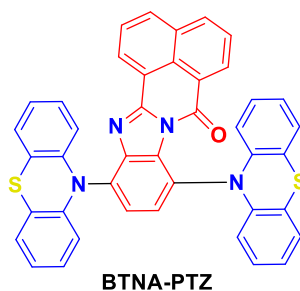
The mixture of **BTNA-Br$_2$** (0.143 mmol), phenothiazine (0.344 mmol), *t*-BuONa (0.57 mmol), Pd$_2$(dba)$_3$ (0.00859 mmol), HP(*t*-Bu)$_3$BF$_4$ (0.01718 mmol) and 10 mL of toluene was stirred at 120 °C for 48h under argon atmosphere. After cooling to room-

temperature the mixture was filtered through celite and washed with dichloromethane. The residue was purified by column chromatography by gradient of hexane/CH_2Cl_2 (6:1) to Hexane/CH_2Cl_2 (3:1) and recrystallized in methanol to give compound **BTNA-PTZ** as a yellow solid (44.8%). ^{1}H NMR (300 MHz, CDCl$_3$) δ/ppm: 8.86 (dd, J = 7.3, 1.0 Hz, 1H), 8.62 (dd, J = 7.4, 1.1 Hz, 1H), 8.21 (d, J = 8.3 Hz, 1H), 8.10 (d, J = 7.4 Hz, 1H), 7.85 – 7.60 (m, 4H), 7.16 – 7.08 (m, 2H), 7.04 (dd, J = 5.9, 3.3 Hz, 2H), 6.91 – 6.82 (m, 4H), 6.80 – 6.71 (m, 4H), 6.38 – 6.25 (m, 2H), 6.06 (dd, J = 6.0, 3.4 Hz, 2H). ^{13}C NMR (75 MHz, CDCl$_3$) δ/ppm: 166.2, 142.3, 136.6, 133.6, 132.6, 132.0, 131.7, 131.1, 130.9, 130.0, 129.7, 128.9, 128.1, 128.0, 127.9, 127.1, 126.9, 126.3, 124.5, 124.5, 123.19, 119.9, 118.1, 117.0. HRMS: m/z calcd for $C_{42}H_{25}N_4OS_2$ (M+H)$^+$: 665.1470; found: 665.1459.

General procedure for N-C coupling reaction of 1,4-dibromobenzene and the donors

The synthesis of these materials followed the procedure described in literature.[119] The mixture of 1,4(or 1,3)-dibromobenzene (12,56 mmol), respective donor (6,28 mmol), t-BuONa (31.4 mmol), Pd$_2$(dba)$_3$ (0.0628 mmol), P(Ph)$_3$ (0.25 mmol) and 30 mL of degassed toluene was stirred at 110 °C for 24h under argon atmosphere. After cooling to room temperature, the mixture was filtered under celite and washed with dichloromethane. The residue was purified by column chromatography using hexane as an eluent. The materials were characterized by ^{1}H NMR.
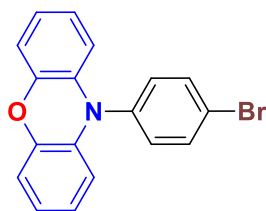
10-(4-bromophenyl)-10H-phenothiazine (**PTZ-*p*-Br**)
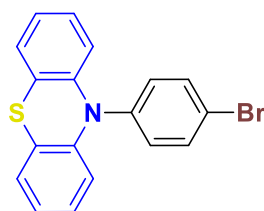
PTZ-*p*-Br

White pallid solid (79% yield). ^{1}H NMR (300 MHz, CDCl$_3$) δ/ppm: 7.71 (d, J = 8.6 Hz, 2H), 7.26 (dd, J = 6.6, 2.0 Hz, 2H), 7.05 (dd, J = 7.2, 1.9 Hz, 2H), 6.95 – 6.79 (m, 4H), 6.32 – 6.15 (m, 2H).

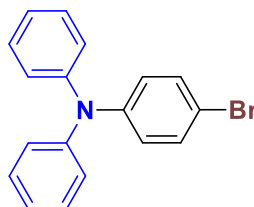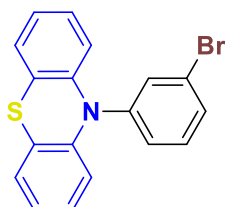*10-(4-bromophenyl)-10H-phenoxazine* (**PXZ-*p*-Br**)

PXZ-*p*-Br

White pallid solid (70% yield). ¹H NMR (300 MHz, CDCl₃) δ/ppm: 7.88 (d, *J* = 8.5 Hz, 2H), 7.31 (dd, *J* = 6.4, 2.0 Hz, 2H), 7.10 (dd, *J* = 7.2, 1.9 Hz, 2H), 6.92 – 6.72 (m, 4H), 6.55 – 6.42 (m, 2H).

4-bromo-N,N-diphenylaniline (**DPA-*p*-Br**)

DPA-*p*-Br

White solid (71% yield). ¹H NMR (300 MHz, CDCl₃) δ/ppm: 7.35 – 7.22 (m, 6H), 7.11 – 6.99 (m, 6H), 6.98 – 6.90 (m, 2H).

10-(3-bromophenyl)-10H-phenothiazine (**PTZ-*m*-Br**)

PTZ-*m*-Br

White pallid solid (64% yield). ¹H NMR (300 MHz, CDCl₃) δ/ppm: 7.56 (s, 1H), 7.32 (m, 3H), 7.03 (dd, *J* = 7.2, 1.9 Hz, 2H), 6.94 – 6.77 (m, 4H), 6.31 – 6.13 (m, 2H).

### *General procedure for preparation of the Stille reagents (Donor-p,m-SnBu₃)*

The respective **Donors-*p,m*-Br** (0.96 mmol) were dissolved in 10 mL of ethyl ether under an argon atmosphere. The system was cooled down to -78 °C, and *n*-BuLi (0.5 mL, 2.5 M in hexanes) was added slowly during 15 min. The mixture was stirred for 45 min, and ClSn(Bu)₃ (0.36 mL) was added slowly and the mixture was heated to room-temperature and stirred for 14h. The mixture was filtered through celite and washed with dichloromethane. The organic solvents were roto-evaporated at 60 °C

and the yellow pallid liquid obtained was used in the next step in sequence without further purification.

### General procedure for Stille Cross-Coupling Reaction in the BTNA-Br₂ core

The mixture of **BTNA-Br₂** (0.363 mmol), **Donor-*p,m*-SnBu₃** (0.797 mmol), Pd[P(Ph)₃]₄ (0.0217 mmol) and 10 mL of degassed toluene was stirred at 110 °C for 48h under argon atmosphere. After cooling to room temperature, the mixture was filtered under celite and washed with chloroform and ethyl acetate. The residue was purified by column chromatography with hexane/DCM (1:1 v/v) mixture. The compounds were crystalized in hexane/DCM (4:1) to give the pure compounds.

9,12-bis(4-(10H-phenothiazin-10-yl)phenyl)-7H-benzo[de]benzo[4,5]imidazo[2,1-a]isoquinolin-7-one (**BTNA-*p*-PTZ**)


BTNA-*p*-PTZ
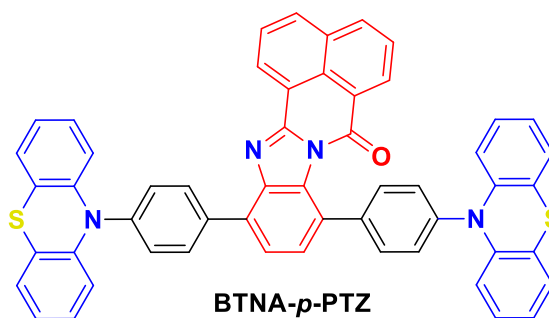
Yellow solid (68.8%). ^{1}H NMR (300 MHz, CDCl₃) δ/ppm: 8.98 (dd, J = 7.3, 1.0 Hz, 1H), 8.50 (dd, J = 7.3, 1.1 Hz, 1H), 8.46 – 8.41 (m, 2H), 8.28 (dd, J = 8.1, 0.6 Hz, 1H), 8.17 (d, J = 7.8 Hz, 1H), 7.84 (dt, J = 8.1, 3.8 Hz, 2H), 7.78 (dd, J = 8.0, 7.5 Hz, 1H), 7.72 – 7.65 (m, 3H), 7.60 (d, J = 8.5 Hz, 2H), 7.51 – 7.46 (m, 2H), 7.08 (td, J = 7.2, 1.6 Hz, 4H), 7.02 – 6.93 (m, 4H), 6.87 (td, J = 7.4, 1.3 Hz, 4H), 6.53 (td, J = 8.0, 1.2 Hz, 4H). ^{13}C NMR (75 MHz, Tetrachloroethane-d₂) δ 158.62, 150.36, 143.91, 143.57, 142.29, 141.34, 141.23, 140.12, 138.78, 136.33, 134.42, 132.29, 131.51, 131.34, 130.85, 130.23, 130.06, 130.00, 129.46, 129.13, 128.87, 127.70, 127.01, 126.62, 126.18, 124.84, 123.25, 122.35, 121.97, 120.62, 120.45, 119.78, 119.00, 116.67, 115.71. HRMS: m/z calcd for C₅₄H₃₃N₄OS₂ (M+H)⁺: 817.2096; found: 817.2092.

9,12-bis(4-(10H-phenoxazin-10-yl)phenyl)-7H-benzo[de]benzo[4,5]imidazo[2,1-a]isoquinolin-7-one (**BTNA-*p*-PXZ**)

BTNA-*p*-PXZ
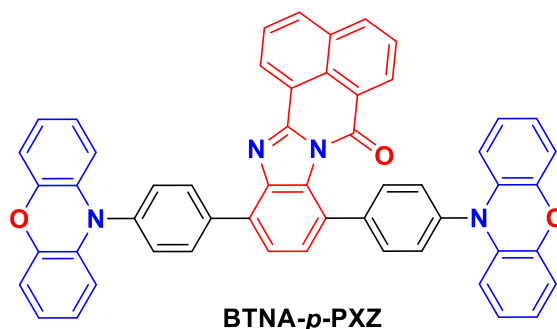
Yellow-orange solid (70.8%). ^{1}H NMR (300 MHz, CDCl$_3$) δ 8.97 (dd, *J* = 7.3, 1.0 Hz, 1H), 8.50 (dd, *J* = 7.3, 1.1 Hz, 1H), 8.46 – 8.40 (m, 2H), 8.27 (dd, *J* = 8.3, 0.9 Hz, 1H), 8.20 – 8.14 (m, 1H), 7.87 – 7.75 (m, 3H), 7.71 – 7.62 (m, 3H), 7.58 – 7.53 (m, 2H), 7.46 – 7.41 (m, 2H), 6.77 – 6.66 (m, 12H), 6.29 – 6.24 (m, 2H), 6.21 – 6.15 (m, 2H). ^{13}C NMR (75 MHz, C$_2$D$_2$Cl$_4$) 160.57, 152.33, 151.91, 144.12, 139.04, 136.44, 136.42, 135.82, 133.68, 133.41, 133.38, 132.84, 132.42, 131.92, 131.11, 130.85, 129.59, 128.98, 128.50, 128.47, 126.89, 125.09, 125.01, 122.31, 122.26, 115.07, 115.06, 115.03, 115.01, 115.00, 114.98, 114.94, 114.88, 109.98. HRMS: m/z calcd for C$_{54}$H$_{32}$N$_4$O$_3$ (M+H)$^+$: 784.2474; found: 784.2470.

9,12-bis(4-(diphenylamine)phenyl)-7H-benzo[de]benzo[4,5]imidazo[2,1-a]isoquinolin-7-one (**BTNA-*p*-DPA**)

BTNA-*p*-DPA
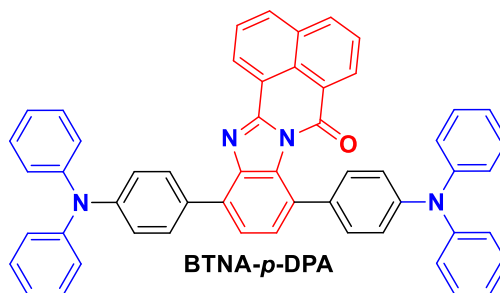
Yellow solid (63.6%). ^{1}H NMR (300 MHz, CDCl$_3$) δ 8.89 (d, *J* = 7.3 Hz, 1H), 8.56 (d, *J* = 7.2 Hz, 1H), 8.24 (d, *J* = 8.1 Hz, 1H), 8.10 (dd, *J* = 12.0, 8.5 Hz, 3H), 7.78 (td, *J* = 7.8, 4.1 Hz, 2H), 7.68 (d, *J* = 7.9 Hz, 1H), 7.51 (d, *J* = 7.9 Hz, 1H), 7.33 (dd, *J* = 8.5, 1.4 Hz, 8H), 7.29 – 7.21 (m, 12H), 7.18 (d, *J* = 8.4 Hz, 2H), 7.06 (dd, *J* = 14.8, 7.4 Hz, 4H). ^{13}C NMR (75 MHz, CDCl$_3$) δ 159.00, 150.42, 148.00, 147.78, 147.41, 146.42, 142.70, 136.72, 134.43, 132.09, 131.63, 131.26, 131.01, 130.38, 129.29, 129.21, 129.10, 128.44, 127.29, 126.85, 124.84, 124.75, 124.25, 123.36, 123.32, 123.00, 122.61, 121.42. HRMS: m/z calcd for C$_{54}$H$_{37}$N$_4$O (M+H)$^+$: 757.2967; found: 757.2966.

9,12-bis(3-(10H-phenothiazin-10-yl)phenyl)-7H-benzo[de]benzo[4,5]imidazo[2,1-a]isoquinolin-7-one (**BTNA-*m*-PTZ**)

BTNA-*m*-PTZ
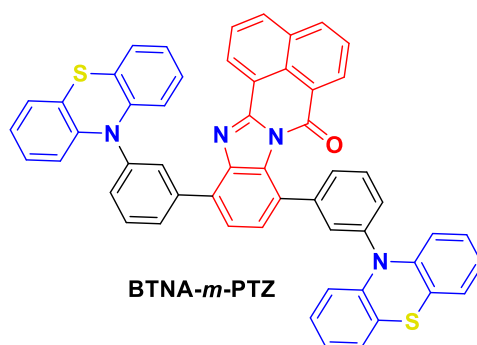
Yellow solid (61.6%). ^{1}H NMR (300 MHz, CDCl$_3$) δ 8.76 (dd, J = 7.3, 1.1 Hz, 1H), 8.45 (dd, J = 7.3, 1.1 Hz, 1H), 8.31 (t, J = 1.8 Hz, 1H), 8.25 – 8.18 (m, 2H), 8.14 – 8.06 (m, 1H), 7.82 – 7.73 (m, 4H), 7.72 – 7.66 (m, 2H), 7.59 (d, J = 7.9 Hz, 1H), 7.50 – 7.43 (m, 2H), 7.34 (t, J = 1.6 Hz, 1H), 7.08 (dd, J = 7.4, 1.6 Hz, 2H), 6.98 – 6.85 (m, 8H), 6.76 (td, J = 7.4, 1.2 Hz, 2H), 6.61 (dd, J = 8.1, 1.2 Hz, 2H), 6.49 (dd, J = 8.2, 1.1 Hz, 2H). HRMS: m/z calcd for C$_{54}$H$_{33}$N$_4$OS$_2$ (M+H)$^+$: 817.2070; found: 817.2096.

6. New D-A-A-D compounds derived from flexible/rigid diquinoxalines/phenazines: design, synthesis, photophysical and electrochemical properties

In this chapter it will be demonstrated the design and synthesis of nine new compounds derived from diquinoxalines and bisphenazines as acceptor cores. The molecules were designed in an unusual D_2-A-A-D_2 structure, where different donor moieties were attached via Pd-catalyzed C−N cross-coupling reactions. These functional materials were synthesized aiming at optoelectronics applications, such as TADF emitters. Additionally, it will be demonstrated the electrochemical and photophysical behavior. In this chapter the author was responsible for all molecular design, synthesis, structural characterizations (NMRs), and partially for the electrochemical and photophysical investigations.

6.1 Introduction

Quinoxalines are important materials that present a high conjugation degree, good charge carriers transport and high electron-acceptor character.[110] Derivatives based on quinoxalines are largely applied in strategies to obtain great photo emissive materials. The presence of the nitrogen atoms in the aromatic system increases the electron-acceptor properties, additionally they can be modulated by the number of quinoxaline rings in the molecular structure. Diquinoxalines are largely investigated as an emissive layer in OLEDs. Quinoxaline derivatives that present TADF and RTP properties were already reported, and OLEDs with a great external quantum efficiency were constructed.[56,71–74]

Quinoxalines can be obtained in very good yields by dehydration reactions between *ortho*-diamino compounds and aromatic dicarbonyl compounds. The presence of two atoms of nitrogen in this core helps in the spin-orbit coupling that is related to the rate of the RISC.[23,55,58] Therewith the design of TADF based materials can be made using different quinoxalines. Diquinoxalines exhibiting TADF properties were already published but not those derived from 3,3'-diaminobenzidine, which opens a new pool of molecules for investigation. The non-planarity in the DQ-Br core induces different behavior in photophysical properties considering the possible conformations in these systems.

Welisson de Pontes Silva

In this way, it was proposed the design and synthesis of a new class of unrealized diquinoxaline derivatives where it is possible to connect four donor units by N-C coupling. The materials are great candidates to present TADF properties due to the large separation between the donor units and the acceptor core. The **Figure 6.1** shows the molecules discussed in this chapter.
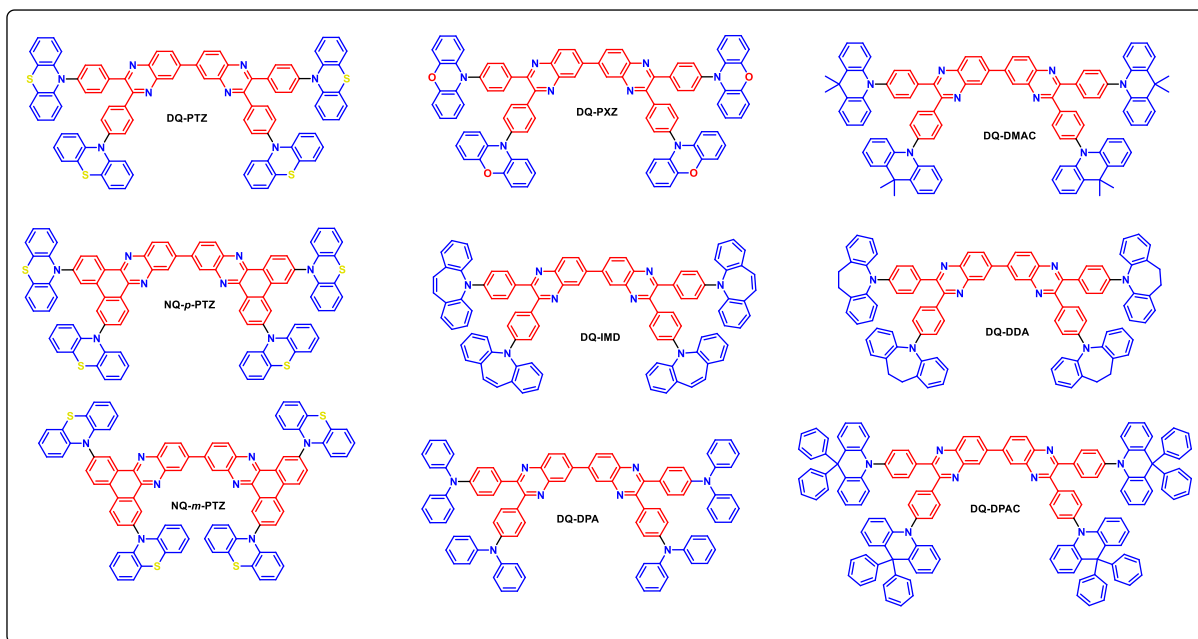

Figure 6.1. *Molecular structures of compounds derived from conjugated diquinoxalines (DQ-donors) and bisphenazines (NQ-p-PTZ and NQ-m-PTZ).*

6.2 Molecular design and synthesis

Herein, we designed and synthesized a new series of compounds based on diquinoxaline (**DQ** core) or bidibenzo[*a,c*]phenazine (**NQ** core) as acceptors and different donor moieties. The flexible diquinoxaline allows the free rotation of the phenyl spacer between the acceptor and the donor moieties. On the other hand, the rigid core bidibenzo[*a,c*]phenazine, did not present a phenyl spacer between the donor and acceptor system. These characteristics make it possible to obtain different photophysical behavior by the control of arrangement in the molecular structures.

The synthetic route to obtain the key intermediate acceptor cores with flexible diquinoxaline (**DQ-Br**) and rigid bisphenazines with bromine in *para* position (**NQ-*p*-Br**) and in *meta* position (**NQ-*m*-Br**) are shown in **Scheme 6.1**. **DQ-Br** was synthesized by condensation reaction of 4,4′-dibromobenzil and 3,3'-diaminobenzidine under reflux in acetic acid in good yield. The rigid bisphenazines with bromine in *para* (**NQ-*p*-Br**) and *meta* (**NQ-*m*-Br**) positions were synthesized in a similar way. The dibrominated

dicarbonyl compounds were synthesized from phenanthrene-9,10-dione using two different bromination procedures already described in the literature. To obtain 3,6-dibromophenanthrene-9,10-dione (**3,6-diBr-ph**) with bromine in *para* position, molecular bromine in nitrotoluene under reflux was used,[120] and for 2,7-dibromophenanthrene-9,10-dione (**2,7-diBr-ph**) with bromine in *meta* position, N-bromosuccinimide (NBS) in sulfuric acid at room-temperature was used.[121] These two procedures are different due to the mechanisms involved. In the first one (3,6-diBr-ph), the bromination mechanism reaction occurs via bromonium ion, which promotes the bromination in the most activated positions of the aromatic ring (*para* positions in relation to the carbonyl group) and in the second one (**2,7-diBr-ph**), the reaction occurs via radical mechanism which promotes bromination in less activated regions in the aromatic ring (*meta* positions in relation to the carbonyl group).
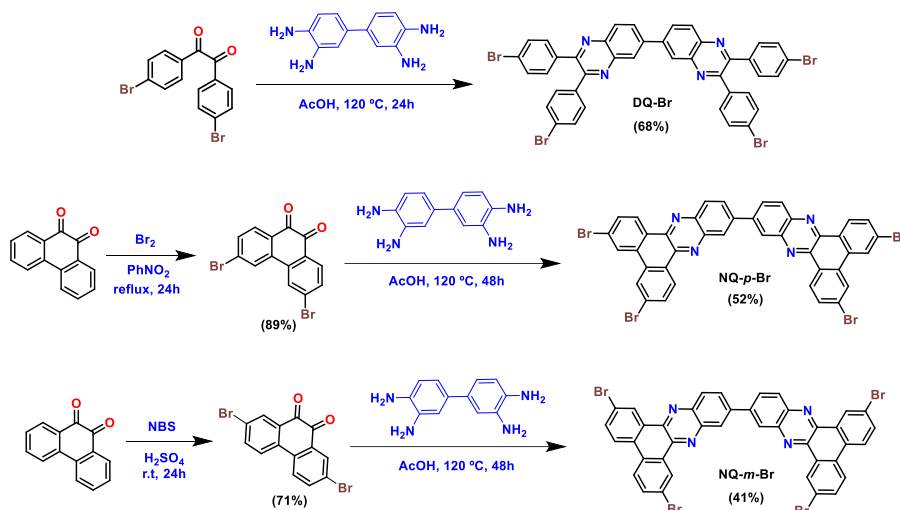
Scheme 6.1. *Synthetic route to obtain the tetrabrominated cores **DQ-Br, NQ-p-Br** and **NQ-m-Br**.*

The next step was based on a nitrogen-carbon coupling reaction catalyzed by palladium as shown in **Scheme 6.2**. The reactions were performed with degassed toluene as a solvent using different donor units (phenothiazine, phenoxazine, diphenylamine, azepine and acridine derivatives) to obtain the final compounds **DQ-PTZ**, **DQ-PXZ**, **DQ-DPA, DQ-DDA, DQ-IMD, DQ-DMAC** and **DQ-DPAC** in moderate to good yields after purification by chromatography column and precipitation in methanol. The donors were used in excess to ensure the N-C coupling in all four positions of the acceptor core. The palladium catalyst (Pd$_2$dba$_3$) was used in a ratio of 8 mol% and the phosphine ligand in 16 mol% following typical procedures of Buchwald-Hartwig cross-coupling reaction. The final molecules were characterized by ^{1}H and ^{13}C

NMR and by High-Resolution Mass Spectrometry and all the characterization details are compiled in the experimental section and the spectra in the appendix section.
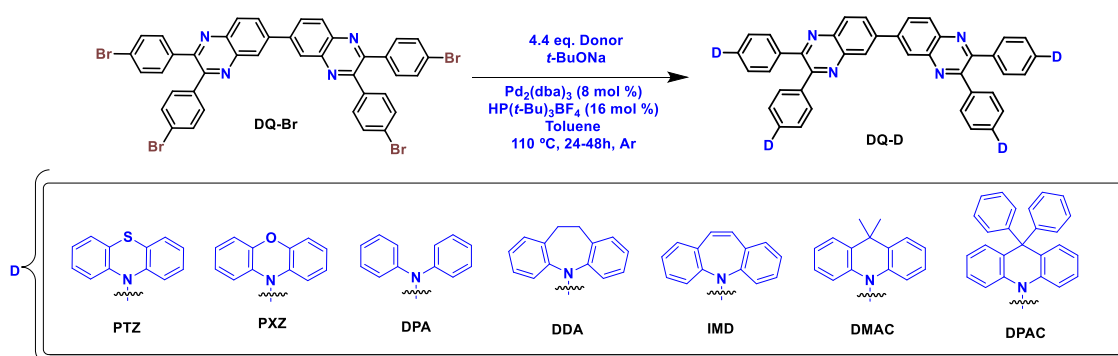
Scheme 6.2. *Synthetic route to obtain the* **DQ-Donors.**

For the bisphenazine acceptors **NQ-*p*-Br** and **NQ-*m*-Br, phenothiazine was** used as donor units with similar to **DQ-Donors** series experimental procedures of the N-C coupling reaction obtaining the final **NQ-*p*-PTZ** and **NQ-*m*-PTZ** in moderate yields after purification by chromatography column (**Scheme 6.3**).
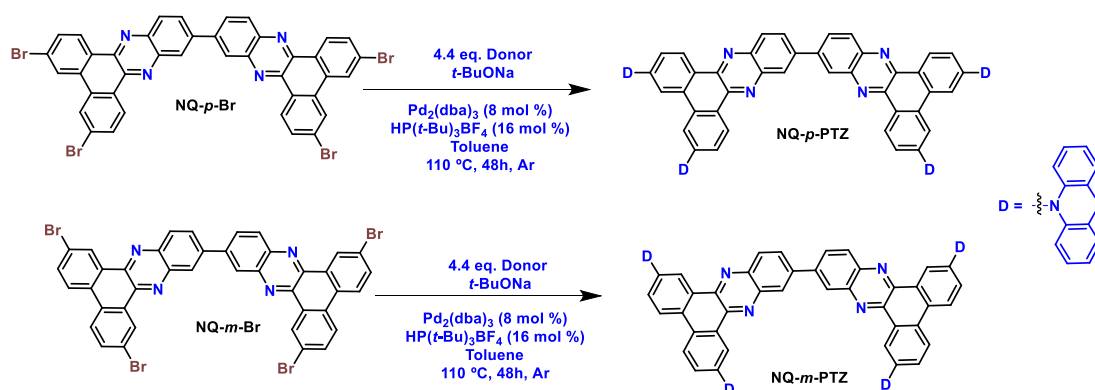
Scheme 6.3. *Synthetic route to obtain the* **NQ-p-PTZ** *and* **NQ-m-PTZ.**

As an example of characterization of this series of materials, the *Figure 6.2* shows the ^{1}H NMR spectrum of the compound **DQ-PTZ**. We can observe around 8.8-8.3 ppm three signals referring to the six hydrogens from diquinoxaline core. The *para* substituted system also can be observed at 7.75 and 7.39 ppm, referring to the hydrogens close to the diquinoxaline and the nitrogen from phenothiazine, respectively. To confirm the success in the reaction we attempted to the characteristics signals from phenothiazine at 7.12, 6.88 and 6.34 ppm. Also, we observe the integral values that are consistent with the four units of phenothiazine coupled.
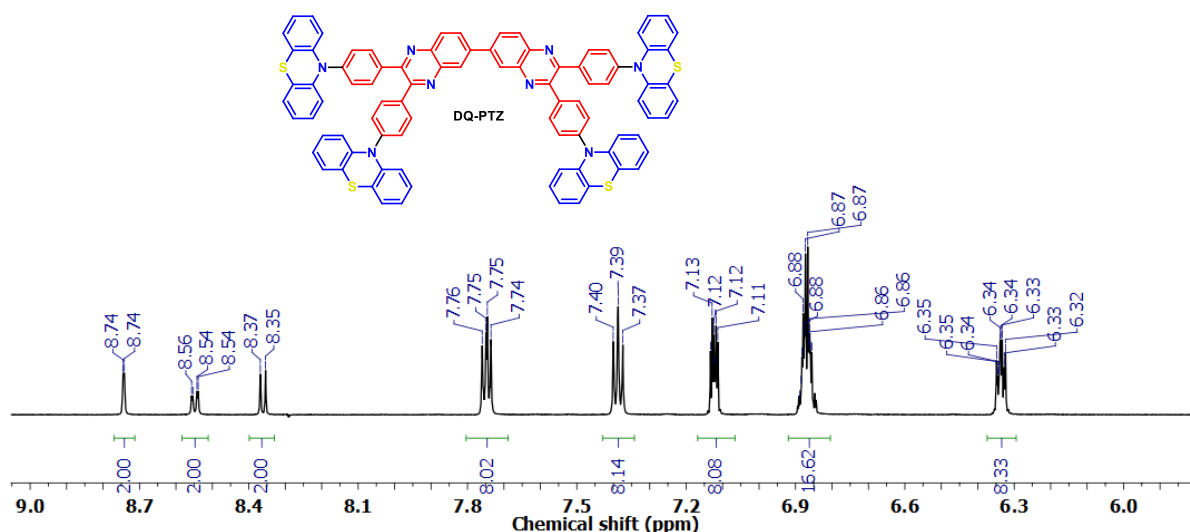
Figure 6.2. ^{1}H NMR (600 MHz) spectrum of the aromatic region for **DQ-PTZ** in DMSO-d_6.

6.3 Electrochemical characterizations

The electrochemical properties of the **DQ-donors** and **NQ-donors** were investigated by cyclic voltammetry (CV) to estimate the HOMO and LUMO energy levels. The estimated ionization potential (IP) and electron affinity (EA) (from onset oxidation (E_{ox}) and reduction (E_{red}) potentials), are correlated with the HOMO (E_{HOMO}) and LUMO (E_{LUMO}) energy levels, respectively, using the following equations: E_{HOMO} = -(E_{ox} + 5.1); E_{LUMO} = -(E_{red} + 5.1).[78] The results are summarized in **Table 6.1** and the voltammograms are compiled in **Figure 6.3** and Figure 6.4**.

Table 6.1. HOMO and LUMO energy levels estimated from CV measurements of **DQ-Donors** and **NQ-Donors**.

Compound	Cyclic Voltammetry[a]		
	HOMO (eV)	LUMO (eV)	E_g (eV)
DQ-PXZ	-5.39	-3.32	2.07
DQ-DPA	-5.40	-3.15	2.25
DQ-IMD	-5.82	-3.34	2.48
DQ-DDA	-5.65	-3.32	2.33
DQ-DMAC	-5.68	-3.54	2.14
DQ-DPAC	-5.91	-3.65	2.26
DQ-PTZ	-5.35	-3.32	2.03
NQ-*p*-PTZ	-5.41	-3.63	1.78
NQ-*m*-PTZ	-5.31	-3.56	1.75

[a] Measurements were performed for 1 mM solutions of investigated compounds in the presence of 100 mM tetrabutylammonium tetrafluoroborate and calibrated using ferrocene/ferrocenium redox couple**.

The electrochemical properties of **DQ-PTZ**, **NQ-*p*-PTZ** and **NQ-*m*-PTZ** were investigated by CV and are shown in **Figure 6.3a**. The compounds exhibited reversible two-step reduction ($^{red1}E_{onset}$ = −1.78 V for **DQ-PTZ**; −1.47 V for **NQ-*p*-PTZ**; -1.54 V for **NQ-*m*-PTZ** vs Fc/Fc$^+$, $^{red2}E_{onset}$ = -1.98 V for **DQ-PTZ**; −1.66 V for **NQ-*p*-PTZ**; -1.74 V for **NQ-*m*-PTZ** vs Fc/Fc$^+$) according to the two quinoxaline or phenazine units and one step oxidation process ($^{ox}E_{onset}$ = +0.26 V for **DQ-PTZ**; +0.30 V for **NQ-*p*-PTZ**; +0.20 V for **NQ-*m*-PTZ** vs Fc/Fc$^+$), indicating their high electrochemical stabilities suitable for carrier injection/transportation in optoelectronic materials. The HOMO and LUMO were estimated by the oxidation potential and the first reduction potential, respectively. The HOMO-LUMO energy gap (E_g) for **DQ-PTZ** (2.03 eV) was higher than for **NQ-*p*-PTZ** (1.78 eV) and **NQ-*m*-PTZ** (1.75 eV). The compound **DQ-PXZ** showed a similar profile in the CV, displaying reversible two-step reduction ($^{red1}E_{onset}$ = −1.78 V; $^{red2}E_{onset}$ = -1.97 V vs Fc/Fc$^+$) and one-step reversible oxidation process ($^{ox}E_{onset}$ = +0.29 V for **DQ-PTZ** vs Fc/Fc$^+$). In **Figure 6.3b**, we observe that **DQ-PXZ** displayed the estimated HOMO energy (-5.39 eV) a little lower than **DQ-PTZ** (-5.35 eV), as expected due to stronger electron-donating character of phenothiazine. The compounds **DQ-DDA** and **DQ-IMD** showed more irreversible character in the reduction and oxidation process. The estimated LUMO energy was very similar for both compounds (-3.32 eV for **DQ-DDA** and -3.34 eV for **DQ-IMD**), while the estimated HOMO energy was higher for **DQ-DDA** (-5.65 eV) than for **DQ-IMD** (-5.82 eV), indicating the higher electro-donation character for DDA.
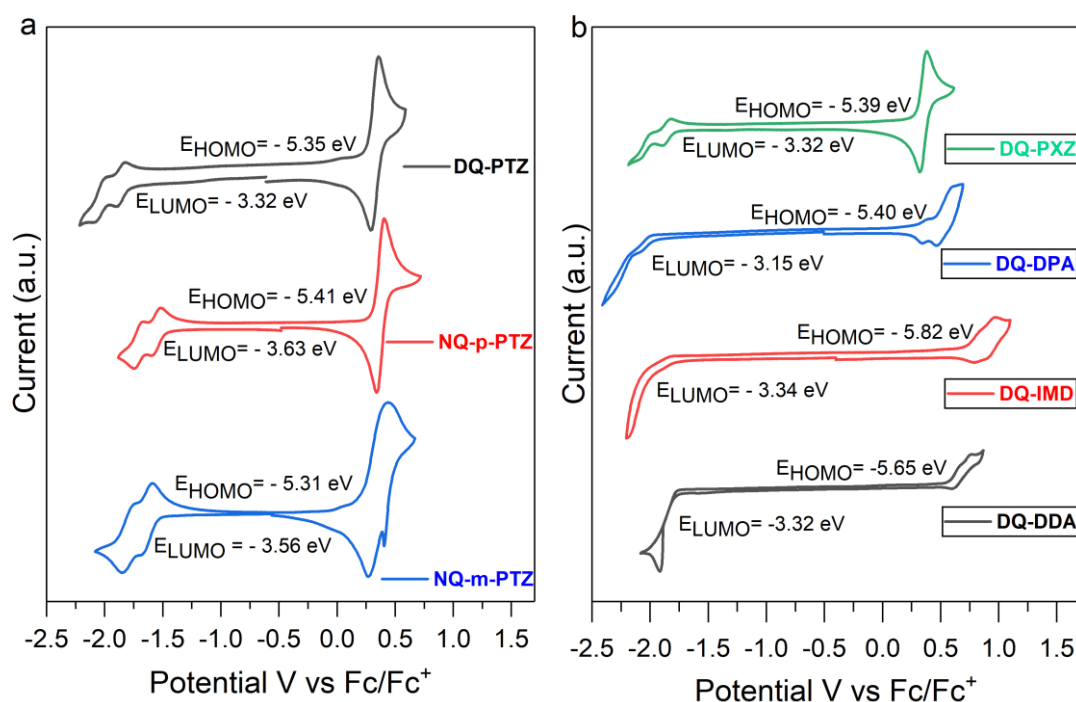
Figure 6.3. *Cyclic voltammograms of a single scan of 1 mM of compounds a)* ***DQ-PTZ, NQ-p-PTZ*** *and* ***NQ-m-PTZ****; b)* ***DQ-PXZ, DQ-DPA, DQ-IMD*** *and* ***DQ-DDA****; in DCM containing 0.1 M Bu₄NBF₄ as electrolyte. Pt disk as working, Pt wire as counter and Ag/AgCl as reference electrode, at 50 mv s⁻¹ scan rate.*

The CV curves for the compounds **DQ-DPA**, **DQ-DMAC** and **DQ-DPAC** are shown in **Figure 6.4**. **DQ-DPA** showed more irreversible character of the reduction process with estimated LUMO energy of -3.15 eV. While the compounds **DQ-DMAC** and **DQ-DPAC**, display more reversible character with estimated LUMO energies of -3.54 eV and -3.65 eV, respectively. For the first oxidation potentials it was possible to estimate the HOMO energies, where DPA showed first oxidation at lower potentials than DMAC and DPAC.
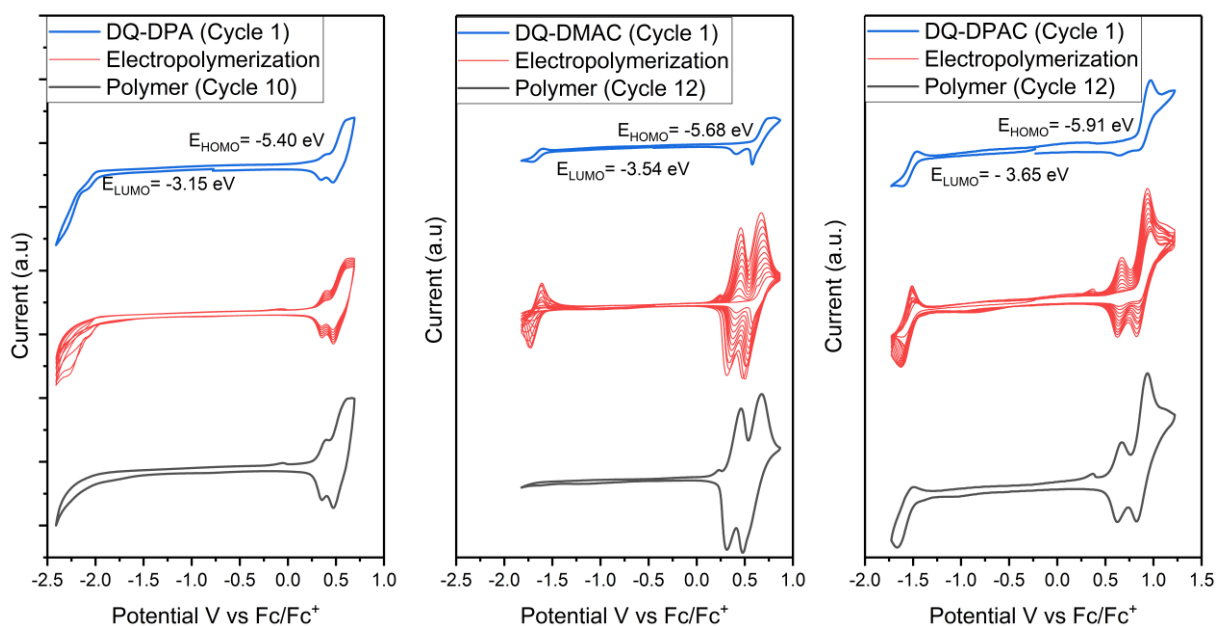
Figure 6.4. *Cyclic voltammetry of 1mM of a) **DQ-DMAC** and b) **DQ-DPAC** in DCM Bu₄NBF₄ (0.1 M) electrolyte with different potential boundaries. First cycle monomer in (blue line); Electropolymerization in red and the electrochemically obtained polymer as last cycle in black.*

These compounds additionally showed electrochemical polymerization process when we increment the number of cycles in CV measurements, where it can be noticed in the second and following scans the emergence of new peaks at lower potentials. The presence of new peaks is an indicative of electrochemical reactions forming new species in the electrochemical cell. If we compare the oxidation potentials of monomer and the formed species, we observe the lower oxidation potential, that indicates a higher conjugation degree of the formed polymer in relation to the monomers. Also, the increases in current during the additional scans suggest the electrodeposition of the materials in the electrode's surface.

6.4 Photophysical analyses

The absorption spectra (UV-Vis) in diluted dichloromethane (DCM) solutions are shown in **Figure 6.5** and the data are summarized in **Table 6.2**. The profile of the absorption spectra differs for the compounds depending on the donor group attached. We can observe strong absorption bands in 260-350 nm, that can be signed to the $\pi \rightarrow \pi^*$ transitions in the donor-acceptor structures.[122,123] Lower intense broad bands can be observed from 360 to 550 nm and can be attributed to a CT transition from the donor units to the acceptor.[70,81] For the molecules with more conjugation degree in the D_2-A-A-D_2 systems (**DQ-DDA**, **DQ-IMD**, **DQ-DPA**) the CT bands are more evident

contributing to a higher HOMO-LUMO overlap. On the other hand, for the compounds **DQ-DMAC**, **DQ-DPAC**, **DQ-PXZ**, **DQ-PTZ**, **NQ-*p*-PTZ** and **NQ-*m*-PTZ** these side CT bands are less intense and attributed to more twisted conformation with minimum HOMO-LUMO overlap. **DQ-DMAC** and **DQ-DPAC** present very similar profiles in the spectra with CT bands around 450 nm. While **NQ-*p*-PTZ** and **NQ-*m*-PTZ** present more intense CT bands around 425 nm.
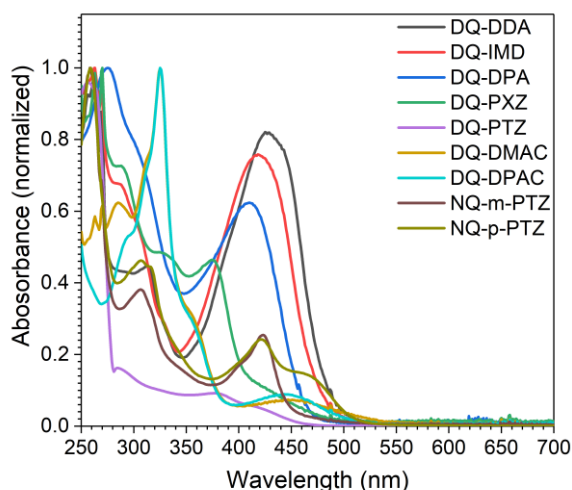

Figure 6.5. *Absorption spectra (left) of **DQ-NQ-donors** compounds in DCM solutions 0.01 mM and photoluminescence spectra (right) of **DQ-NQ-donors** compounds in toluene 0.01 mM.*

Figure 6.6 shows the contribution of photoluminescence (PL) for the compounds **DQ-NQ-donors** in the solvatochromism studies from less polar to more polar solvents: methylcyclohexane (MCH), toluene (TOL), tetrahydrofuran (THF), dichloromethane (DCM) and acetonitrile (ACN). The emitters exhibit a wide range of accessible colors from blue to orange-red bands in PL spectra, depending on the donors attached and the polarities of the solvents.
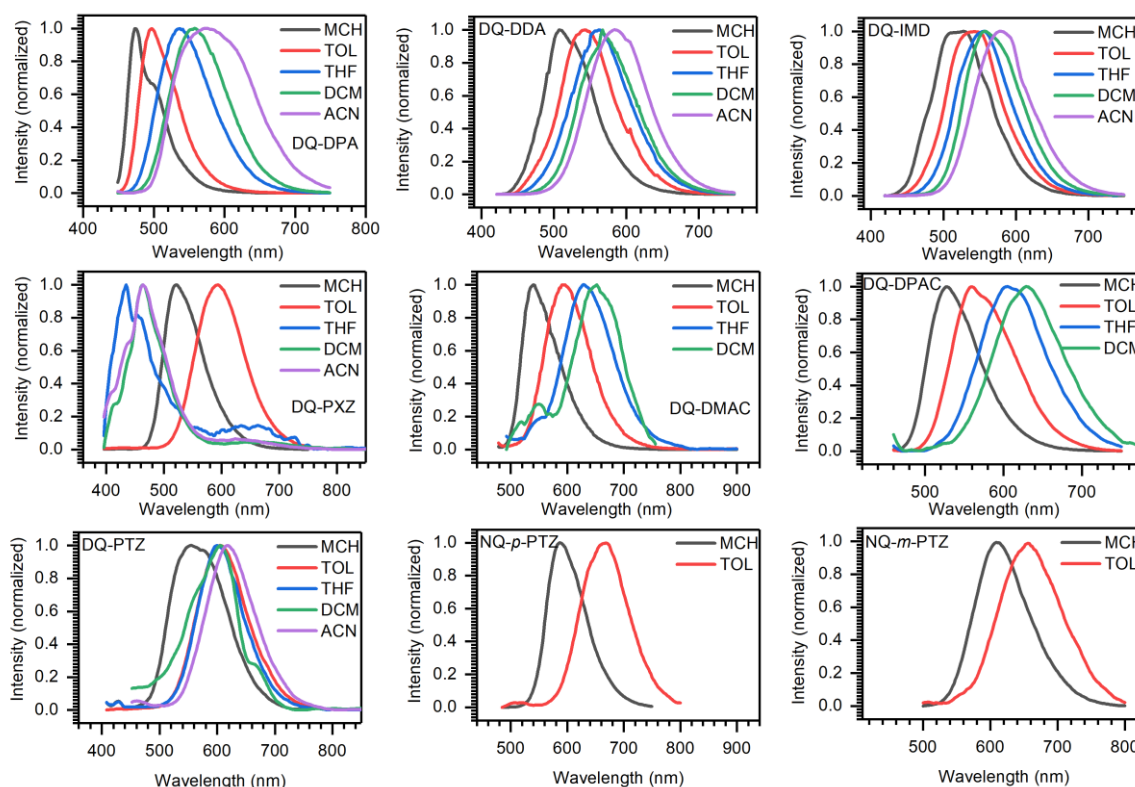
Figure 6.6. *Solvatochromism of **DQ-NQ-donors** in methylcyclohexane (MCH), toluene (TOL), tetrahydrofuran (THF), dichloromethane (DCM) and acetonitrile (ACN) at 0.01 mM concentrations at room-temperature.*

For the compounds **DQ-DPA**, **DQ-DDA** and **DQ-IMD** we observe a clear redshift from MCH to ACN, ranging from green to orange (λ_{PL}= 470-600 nm), indicating the strong ^{1}CT character of S_1 states that are sensible to solvents polarities being stabilized in more polar solvents. **DQ-PXZ** showed different behavior in less polar and more polar solvents. From MCH ($\lambda_{PL(MCH)}$= 521nm) to TOL ($\lambda_{PL(TOL)}$= 594 nm) we observe clear redshift in PL spectra, that is consistent with stabilization of ^{1}CT states. In contrast to the more polar THF ($\lambda_{PL(THF)}$= 434 nm) where we observe a blue shift, that can be attributed to aggregation effects by restriction of intramolecular motion in more polar solvents. **DQ-DMAC** and **DQ-DPAC** showed a redshift from MCH to DCM ranging from green to orange-red (530-650 nm), suggesting the stabilization of ^{1}CT states. These compounds were not emissive in ACN indicating the quenching of ^{1}CT states in very polar solvents. Additionally, we observe a redshift in the solvatochromism for **DQ-PTZ** from MCH ($\lambda_{PL(MCH)}$= 555 nm) to ACN ($\lambda_{PL(ACN)}$= 618 nm). While for the compounds **NQ-*p*-PTZ** and **NQ-*m*-PTZ** the emission was quenched in more polar solvents. But we still can observe a redshift from MCH to TOL. The difference between

diquinoxaline (DQ) and bisphenazine (NQ) can be observed if we compare the emission in toluene, being redshifted from **DQ-PTZ** ($\lambda_{PL(TOL)}$= 606 nm) to **NQ-*p*-PTZ** ($\lambda_{PL(TOL)}$= 667 nm), indicating the more twisted donor attached to the acceptor core.

Table 6.2. *Summary of photophysical characteristics of the studied **DQ-donors** and **NQ-donors**.*

Compounds	λ_{Abs}/nm [ε/10³M⁻¹ cm⁻¹][a]	λ_{Em} [nm] MCH	λ_{Em} [nm] TOL	λ_{Em} [nm] THF	λ_{Em} [nm] DCM	λ_{Em} [nm] ACN	PLQY (%)	Increase[b]	PLQY X Increase
DQ-PTZ	257, [121], 378 [11.6], 421 [6.09]	555	606	600	606	618	7.7[b]; 9.3[c]; 34[d]	1.93	14.9[b]
DQ-PXZ	263 [26.4], 270 [27.1], 289 [19.5], 328 [13.1], 375 [12.4]	521	594	434	463	463	17.7[b]; 9.6[c], 36.5[d]	2.03	35.9[b]
DQ-DPA	263 [23.9], 269 [23.9], 305 [26.4], 334 [20.1], 440 [16.6]	473	497	536	557	575	59.9[b]; 17.6[c]; 32.4[d]	1.09	65.3[b]
DQ-IMD	262 [31.6], 269 [29.0], 287 [21.3], 420 [23.8]	525	543	554	557	579	8.1[b]; 14.3[d]	1.16	9.4[b]
DQ-DDA	262 [33.4], 268 [29.3], 313 [14.7], 429 [27.3]	508	542	561	566	584	24.5[b]	1.28	31.4[b]
DQ-DMAC	262 [22.4], 269 [23.4], 284 [23.8], 325 [37.7], 357 [11.6], 450 [2.97]	539	593	629	651	-	6.1[b]	2.04	12.4[b]
DQ-DPAC	293 [25.8], 326 [49.7], 358 [13.8], 444 [4.35]	527	559	604	630	-	14.7[b]	1.52	22.3[b]
NQ-*p*-PTZ	259 [46.4], 308 [20.8], 422 [11.0], 467 [6.37]	587	667	-	-	-	9.0[b]	2.24	20.1[b]
NQ-*m*-PTZ	258 [75.6], 306 [28.7], 423 [19.0]	610	656	-	-	-	2.4[b]	3.21	7.68[b]

[a] in DCM 0.01 mM; [b] in toluene 0.01 mM; [c] in zeonex matrix; [d] in CBP matrix.

To investigate the possibility of TADF behavior, measurements were realized in air-equilibrated and vacuum conditions in order to observe if oxygen is quenching excited triplet states.[124] **Figure 6.7** shows the PL spectra in the air conditions (black lines) and in vacuum conditions (red lines). We observe an increase in PL intensity in vacuum conditions for all compounds. This behavior indicates that excited triplet states are involved in the mechanism of light emission, and are quenched by oxygen.[125] The remotion of oxygen from the system allows efficient RISC process that support TADF properties. The compounds **DQ-DPA**, **DQ-DDA** and **DQ-IMD** showed smaller PL

increases in comparison with the other compounds, varying from 1.09x, 1.16x and 1.28x, respectively. This suggests that weaker electron donors attached in the diquinoxaline cause small contribution of delayed fluorescence. Otherwise, the compounds with donors with more electron-donating ability implies in the increase of PL intensity in vacuum conditions, up to 3.2x for **NQ-*m*-PTZ**. **NQ-*p*-PTZ** and **DQ-PTZ** display an increase in the PL intensity up to 2.2x and 1.9x, suggesting that the bisphenazine core (NQ) implies more contribution of delayed fluorescence. **DQ-PXZ** and **DQ-DMAC** showed an increment in PL intensity up to 2x, which demonstrates their good usability as electron donors in TADF design.
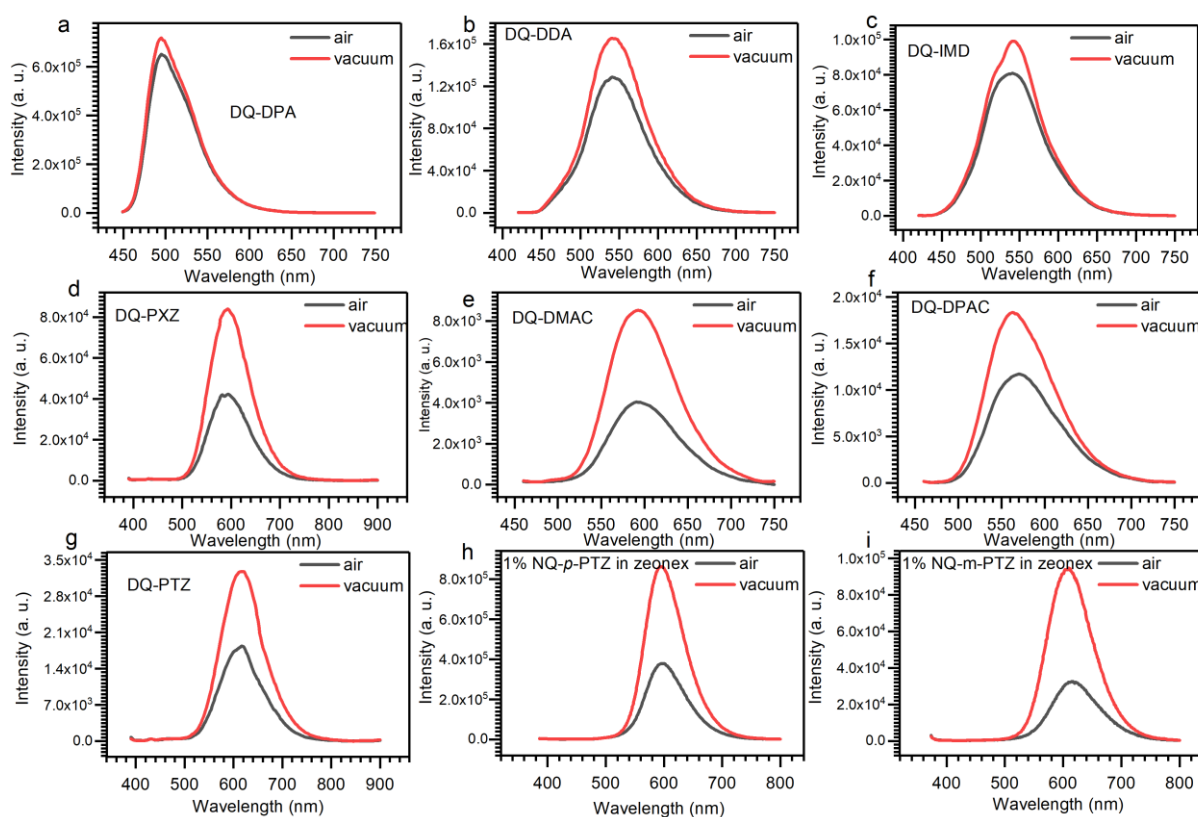
Figure 6.7. *Photoluminescence (PL) spectra of **DQ-donors** in toluene solutions under air conditions (black line) and under vacuum conditions (red line). For **NQ-p-PTZ** and **NQ-m-PTZ**, in 1% of the compounds in zeonex matrix.*

6.5 Conclusions

This chapter described the design and successful synthesis of one new series of D$_2$-A-A-D$_2$ based molecules presenting conjugated diquinoxaline and bisphenazine as acceptor cores. The different donor moieties were attached via N-C Buchwald-Hartwig cross-coupling reactions obtaining good yields varying from 46- 70% depending on the donor attached. All the structural characterizations were realized by

NMR spectroscopy and by high-resolution mass spectrometry for some final molecules. The electrochemical properties were investigated by cyclic voltammetry, displaying good electrochemical stability in the applied voltage range. The compounds DQ-DMAC, DQ-DPAC and DQ-DPA showed electropolymerization properties, which make them interesting candidates to electrochromic windows applications. The photophysical investigations give a good understanding about how the structural modifications influences photophysical properties, leading the control of emission wavelength (473 to 667 nm) by the donor and solvent polarities variation. The materials showed mainly [1]CT emission nature analyzed by solvatochromism measurements. The DQ core proved to be very interesting to be investigated due to versatility in the attachment of different donor moieties by N-C coupling reactions. The NQ and DQ cores were compared using phenothiazine as donors, showing that more rigid bisphenazine core induces more redshifted emission in relation to flexible diquinoxaline core. On the other hand, the DQ derivatives presented more solubility in common organic solvents, being good candidates to solution-processed techniques. All materials showed good to moderate PLQYs, and an increase in the PL intensity under vacuum conditions, suggesting TADF properties. In this way these multifunctional materials are excellent candidates to be applied in the field of optoelectronics, mainly as TADF-based OLEDs devices.

6.6 Synthetic details

2,2',3,3'-Tetrakis(4-bromophenyl)-6,6'-biquinoxaline (**DQ-Br**)
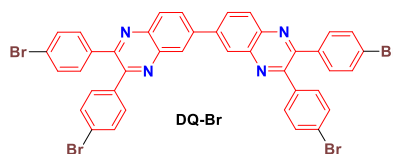
3,3′-diaminobenzidine (0.30 g, 1.3 mmol) and 4,4′-dibromobenzil (1.00 g, 2.72 mmol) were uniformly mixed in 30 mL of glacial acetic acid under argon atmosphere. The mixture was heated at 120 °C for 24h with stirring. Then, the mixed solution was poured into distilled water and the gray precipitate was collected by filtration, washed several times with water, and dried in a vacuum. The solid was dissolved in 200 mL of chloroform and washed two times with sodium hydroxide solution (1 M), brine and distilled water. The organic layer was dried with $MgSO_4$ and evaporated. The solid obtained was crystallized in acetone/methanol to obtain **DQ-Br** in 68% yield as a gray

solid. ¹H NMR (300 MHz, CDCl₃) δ/ppm: 8.57 (d, *J* = 1.9 Hz, 12H), 8.31 (d, *J* = 8.8 Hz, 2H), 8.25 (dd, *J* = 8.8, 2.0 Hz, 2H), 7.54 (d, *J* = 8.6 Hz, 4H), 7.45 (d, *J* = 8.4 Hz, 4H).

### *3,3',6,6'-tetrabromo-11,11'-bidibenzo[a,c]phenazine (NQ-p-Br)*
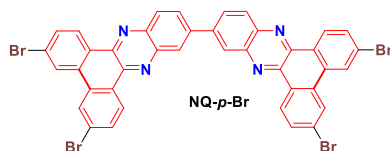
For this compound a similar procedure as for **DQ-Br** was used, but the substrate was changed for 3,6-dibromophenanthrene-9,10-dione. The mixture was reacted for 48h being monitored by TLC. The compound was obtained as pale-yellow solid insoluble in the most common organic solvents in 52% of yield. ¹H NMR (400 MHz, C₂D₂Cl₄) δ 7.64 (d, *J* = 1.2 Hz, 4H), 7.47 (dt, *J* = 7.9, 4.5 Hz, 12H), 7.25 – 7.23 (m, 2H).

3,3',6,6'-tetrabromo-11,11'-bidibenzo[a,c]phenazine (NQ-m-Br)

For this compound a similar procedure as for **DQ-Br** was used, but the substrate was changed for 2,7-dibromophenanthrene-9,10-dione. The mixture was reacted for 48h being checked by TLC and the time reaction was increased to 48h. The compound was obtained as green-yellow solid insoluble in the most common organic solvents in 41% yield.

General procedure for N-C coupling in the DQ-Br or NQ-Br core.

The mixture of **DQ-Br** or **NQ-Br** (0.227 mmol), the respective donor (1.138 mmol), *t*-BuONa (1.57 mmol), Pd₂(dba)₃ (0.027 mmol), HP(*t*-Bu)₃BF₄ (0.054 mmol) and 25 mL of toluene was stirred at 110 °C for 48h under argon atmosphere. The progress of the reaction was monitored by TLC to ensure the total consumption of the core. The hot mixture was filtered through celite and washed with dichloromethane and ethyl acetate. The residue was purified by column chromatography by gradient of pure chloroform and chloroform /ethyl acetate (3:1) as eluent. Compounds were crystallized in methanol to give the pure materials.

Welisson de Pontes Silva

10,10',10'',10'''-([6,6'-biquinoxaline]-2,2',3,3'-tetrayltetrakis(benzene-4,1-diyl))tetrakis(10H-phenothiazine) (**DQ-PTZ**)
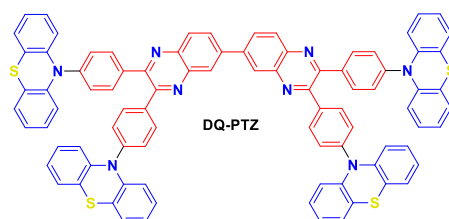
Yellow solid (61% of yield). ^{1}H NMR (600 MHz, DMSO-d_6) δ 8.74 (d, J = 2.0 Hz, 2H), 8.55 (dd, J = 8.8, 2.0 Hz, 2H), 8.36 (d, J = 8.7 Hz, 2H), 7.75 (dd, J = 8.3, 6.1 Hz, 8H), 7.39 (t, J = 7.9 Hz, 8H), 7.17 – 7.07 (m, 8H), 6.92 – 6.80 (m, 16H), 6.34 (ddd, J = 7.7, 4.7, 2.0 Hz, 8H).^{1}H NMR (300 MHz, tetracloroethane-d$_2$ + DMSO-d_6) δ/ppm: 8.71 (s, 2H), 8.51 (dd, J = 8.2, 0.6 Hz, 2H), 8.33 (d, J = 8.8 Hz, 2H), 7.71 (dd, J = 7.9, 2.8 Hz, 8H), 7.36 (dd, J = 8.1, 3.5 Hz, 8H), 7.14 (dd, J = 4.4, 3.8 Hz, 8H), 6.92 – 6.82 (m, 16H), 6.39 – 6.30 (m, 4H). ^{13}C NMR (75 MHz, CDCl$_3$) δ/ppm: 155.4, 153.9, 142.9, 142.7, 141.7, 141.2, 140.2, 137.9, 132.9, 132.6, 130.9, 130.4, 130.1, 126.8, 122.4, 121.7, 113.6, 112.1. HRMS: m/z calcd for $C_{88}H_{55}N_8S_4$ (M+H)$^+$: 1351.4372; found: 1351.4207.

*10,10',10'',10'''-([11,11'-bidibenzo[a,c]phenazine]-3,3',6,6'-tetrayl)tetrakis(10H-phenothiazine) (***NQ-*p*-PTZ***)*
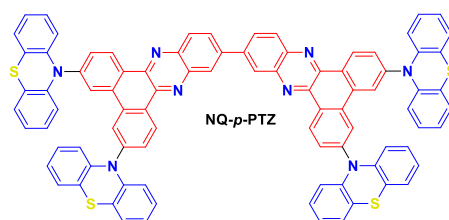
Red solid (48% of yield). ^{1}H NMR (300 MHz, CD$_2$Cl$_2$) δ 9.62 (t, J = 8.4 Hz, 4H), 8.87 (d, J = 1.7 Hz, 2H), 8.54 (d, J = 8.8 Hz, 2H), 8.48 (dd, J = 8.9, 1.9 Hz, 2H), 8.42 (s, 4H), 7.80 (ddd, J = 8.6, 4.6, 1.9 Hz, 4H), 7.16 (dd, J = 6.9, 2.2 Hz, 8H), 6.96 (dq, J = 7.3, 5.6 Hz, 16H), 6.66 – 6.57 (m, 8H). ^{13}C NMR (75 MHz, cdcl$_3$) δ 145.12, 143.92, 143.87, 143.52, 142.45, 140.17, 135.41, 134.38, 133.33, 131.78, 131.29, 130.60, 130.30, 129.14, 128.66, 124.89, 123.84, 121.76, 119.34.

*10,10',10'',10'''-([11,11'-bidibenzo[a,c]phenazine]-2,2',7,7'-tetrayl)tetrakis(10H-phenothiazine) (***NQ-*m*-PTZ***)*

NQ-*m*-PTZ

Red solid (39% of yield). ^{1}H NMR (300 MHz, CDCl$_3$) δ 9.67 (dd, *J* = 8.6, 3.2 Hz, 4H), 8.90 (d, *J* = 1.8 Hz, 2H), 8.60 – 8.54 (m, 2H), 8.52 – 8.44 (m, 6H), 7.85 – 7.79 (m, 4H), 7.19 – 7.09 (m, 8H), 6.97 – 6.87 (m, 16H), 6.51 (dd, *J* = 7.2, 2.1 Hz, 8H).

*10,10',10'',10'''-([6,6'-biquinoxaline]-2,2',3,3'-tetrayltetrakis(benzene-4,1-diyl))tetrakis(10H-phenoxazine)* (**DQ-PXZ**)

DQ-PXZ
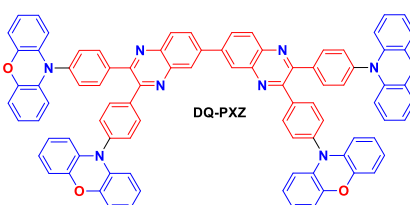
Yellow solid (70% of yield). ^{1}H NMR (300 MHz, CDCl$_3$) δ 8.70 (d, *J* = 1.7 Hz, 1H), 8.43 (d, *J* = 8.7 Hz, 1H), 8.35 (dd, *J* = 8.8, 1.9 Hz, 1H), 7.84 (d, *J* = 8.1 Hz, 4H), 7.47 – 7.38 (m, 4H), 6.73 – 6.61 (m, 8H), 6.53 (td, *J* = 7.7, 1.6 Hz, 4H), 5.98 (d, *J* = 7.7 Hz, 4H). ^{13}C NMR (75 MHz, CDCl$_3$) δ/ppm: 153.4, 152.9, 143.9, 141.7, 141.7, 141.2, 140.2, 138.9, 133.9, 132.6, 130.9, 130.2, 130.1, 127.7, 123.4, 121.7, 115.6, 113.2.

4,4',4'',4'''-([6,6'-biquinoxaline]-2,2',3,3'-tetrayl)tetrakis(N,N-diphenylaniline) (**DQ-DPA**)

DQ-DPA
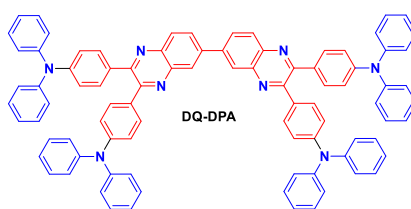
Yellow solid (55% of yield). ^{1}H NMR (300 MHz, CDCl$_3$) δ/ppm: 8.53 (d, *J* = 1.9 Hz, 2H), 8.25 (d, *J* = 8.7 Hz, 2H), 8.17 (dd, *J* = 9.1, 1.5 Hz, 2H), 7.49 (d, *J* = 8.8 Hz, 8H), 7.34 – 7.26 (m, 16H), 7.18 – 7.12 (m, 16H), 7.11 – 7.02 (m, 16H). ^{13}C NMR (75 MHz, CDCl$_3$) δ/ppm: 153.81, 153.37, 148.67, 147.30, 141.32, 140.91, 140.80, 132.42, 130.83, 129.70, 129.39, 129.09, 127.19, 125.05, 123.53, 122.11. HRMS: m/z calcd for C$_{88}$H$_{63}$N$_8$ (M+H)$^+$: 1331.5156; found: 1351.4207.

5,5',5'',5'''-([6,6'-biquinoxaline]-2,2',3,3'-tetrayltetrakis(benzene-4,1-diyl))tetrakis(5H-dibenzo[b,f]azepine) (**DQ-IMD**)
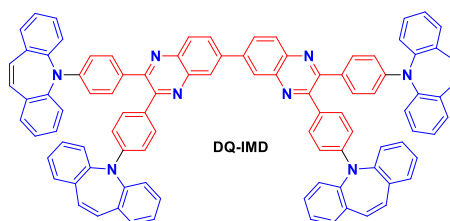

Orange solid (52% of yield). ^{1}H NMR (300 MHz, CDCl$_3$) δ 8.26 (dd, *J* = 7.9, 3.1 Hz, 3H), 8.13 (d, *J* = 7.0 Hz, 1H), 8.08 (d, *J* = 8.2 Hz, 1H), 7.97 (*d*, J = 8.3 Hz, 1H), 7.67 (d, *J* = 7.9 Hz, 4H), 7.63 – 7.38 (m, 36H), 7.19 (dd, *J* = 4.3, 3.1 Hz, 4H), 6.95 (d, *J* = 3.5 Hz, 4H), 6.84 (s, 4H), 6.68 – 6.58 (m, 4H). ^{13}C NMR (75 MHz, CDCl$_3$) δ 154.49, 152.54, 152.30, 148.30, 147.78, 145.06, 144.53, 143.60, 143.42, 141.75, 141.64, 140.72, 139.99, 138.96, 138.84, 136.08, 135.98, 135.92, 135.86, 130.76, 130.74, 130.61, 130.57, 130.39, 130.30, 130.22, 129.70, 129.62, 129.07, 128.98, 128.04, 127.90, 127.70, 127.65, 127.46, 127.41, 125.73, 125.45, 123.89, 123.67, 121.83, 121.70, 121.19, 120.65, 120.44, 115.08, 114.27, 111.77, 111.34.

5,5',5'',5'''-([6,6'-biquinoxaline]-2,2',3,3'-tetrayltetrakis(benzene-4,1-diyl))tetrakis (10,11-dihydro-5H-dibenzo[b,f]azepine) (**DQ-DDA**)
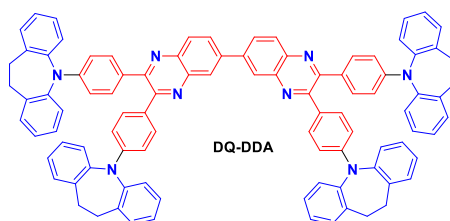
Yellow solid (44% of yield). ^{1}H NMR (300 MHz, CD$_2$Cl$_2$) δ 8.62 (dd, *J* = 9.5, 3.1 Hz, 2H), 8.32 (dd, *J* = 6.0, 1.6 Hz, 1H), 8.26 – 8.16 (m, 2H), 8.08 (d, *J* = 8.1 Hz, 1H), 7.63 – 7.47 (m, 11H), 7.46 – 7.30 (m, 34H), 7.23 (dd, *J* = 17.5, 8.1 Hz, 3H), 3.22 (s, 8H), 3.12 (s, 8H). ^{13}C NMR (75 MHz, CDCl$_3$) δ 152.70, 148.31, 147.70, 145.57, 145.46, 145.33, 144.81, 143.76, 142.20, 142.14, 140.59, 139.28, 137.96, 137.91, 137.27, 136.40, 131.49, 131.37, 131.15, 131.11, 129.25, 129.18, 128.41, 128.38, 128.07, 128.02, 127.81, 127.69, 127.59, 127.54, 127.48, 125.94, 125.72, 124.17, 121.87, 121.40, 121.18, 114.71, 113.98, 30.84, 30.71.

*10,10',10'',10'''-([6,6'-biquinoxaline]-2,2',3,3'-tetrayltetrakis(benzene-4,1-diyl))tetrakis(9,9-dimethyl-9,10-dihydroacridine) (***DQ-DMAC***)*
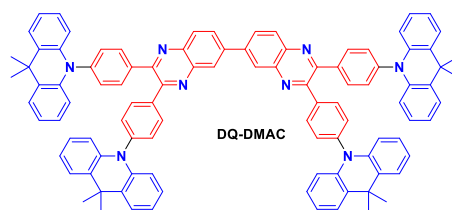
Red solid (48% of yield). ^{1}H NMR (300 MHz, CD$_2$Cl$_2$) δ 9.13 (d, J = 2.6 Hz, 2H), 8.85 (d, J = 7.4 Hz, 1H), 8.77 – 8.65 (m, 4H), 8.52 (d, J = 6.9 Hz, 1H), 8.03 – 7.94 (m, 4H), 7.90 – 7.81 (m, 2H), 7.69 – 7.52 (m, 10H), 7.25 – 6.81 (m, 22H), 6.52 (dd, J = 6.3, 3.1 Hz, 4H), 6.27 – 6.18 (m, 4H), 1.81 (s, 24H). ^{13}C NMR (75 MHz, CD$_2$Cl$_2$) δ 157.61, 156.82, 155.55, 155.52, 155.44, 154.81, 149.82, 141.66, 141.52, 140.79, 140.62, 140.00, 139.97, 139.54, 138.20, 138.16, 137.60, 137.52, 132.80, 132.63, 132.31, 131.95, 131.77, 131.39, 130.06, 129.82, 129.69, 129.48, 128.96, 128.15, 127.23, 127.03, 126.55, 125.77, 125.48, 124.83, 124.13, 123.96, 123.25, 121.72, 121.06, 114.62, 114.19, 109.99, 109.98, 36.19, 36.08, 30.63.

*10,10',10'',10'''-([6,6'-biquinoxaline]-2,2',3,3'-tetrayltetrakis(benzene-4,1-diyl))tetrakis(9,9-diphenyl-9,10-dihydroacridine) (***DQ-DPAC***)*
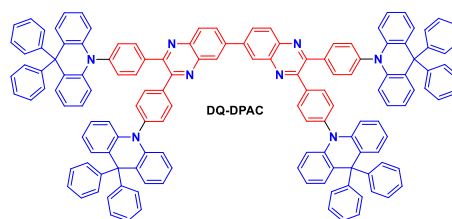
Red solid (46% of yield). ^{1}H NMR (300 MHz, acetone-d_6) δ 8.78 (dd, J = 6.9, 0.8 Hz, 1H), 8.71 (dd, J = 7.0, 0.8 Hz, 1H), 8.60 – 8.48 (m, 4H), 8.44 (d, J = 7.0 Hz, 1H), 8.40 (d, J = 6.9Hz, 1H), 8.12 – 8.02 (m, 2H), 7.50 – 7.32 (m, 28H), 7.24 – 6.92 (m, 46H), 6.80 – 6.68 (m, 6H), 6.60 – 6.50 (m, 4H).

7. D-A compounds derived from asymmetric pyridine benzotriazoles isomers: synthesis, electrochemical and photophysical characterization

This chapter will demonstrate the design and synthesis of six new compounds derived from asymmetric pyridine benzotriazole isomers as acceptor core. The molecules were designed in D-A structure, where two different donor moieties were attached by Pd-catalyzed C−N cross-coupling reactions. These functional materials were synthesized aiming at optoelectronic applications as TADF emitters. Additionally, electrochemical and photophysical behavior will be demonstrated. In this chapter the author was responsible for all the molecular design, synthesis, structural characterizations (NMRs), electrochemical characterizations and partially for the photophysical investigations.

7.1 Introduction

The processability in OLEDs is positively influenced by organic emitters with low molecular mass due to easy thermal evaporation or application in solution processable techniques, which avoids the high costs of device preparation.[126,127] In this way, the development of new low molecular mass organic emitters with a rational synthetic approach is one of the main challenges of the field, due to the market demand focusing on purely organic emitters for TADF/RTP based OLED devices.[128,129] Different acceptors were investigated to be used in TADF/RTP OLEDs such as phenazines,[74,75,111,130] quinoxalines,[131] triazines,[132,133] connected with different donor moieties. These acceptor units presents N-rich systems that can increase the electron-acceptor character and favor the spin-orbit coupling, being an alternative to the use of heavy atoms from phosphorescent emitters.[74,134] Other designs focusing on the increment of the electron-accepting character, with the use of an additional nitrogen-containing pyridinium ring, to increase the electronegativity in the system, have also been developed.[135,136]

Triazole is a five-membered ring with three nitrogen atoms which can promote the higher electron acceptor ability. Due to their versatility in synthesis, the triazole derivatives have been largely explored, mainly in medicinal chemistry because of their biological activity[137–139] but also in materials science with applications in liquid crystals

design.[140,141] On the other hand, their use as an acceptor core in emitters layers of TADF-based OLED devices has not been explored so far, which opens possibilities to be investigated in this field. In this way, this chapter focuses on the use of the triazole ring fused with a pyridine ring aiming to increase the electron acceptor behavior. To understand the relationship between structure and photophysical behavior, three isomers derived from [1,2,3]triazolo[4,5-*b*]pyridine (**PyBTZ**) were investigated (**Figure 7.1**). In these isomers, a methyl group is attached in three different positions of the triazole ring, therefore different dipole moments in the acceptor units are obtained. Thus it is possible to obtain unrealized D-A compounds derived from [1,2,3]triazolo[4,5-*b*]pyridine connected with usual donors, such as dimethyl acridine (DMAC) and diphenyl acridine (DPAC), in position 6 of the pyridine ring. The study of regioisomers of **PyBTZ** can be a great strategy to evaluate the options for different applications, since they provide a wide range of structural and electronic properties.
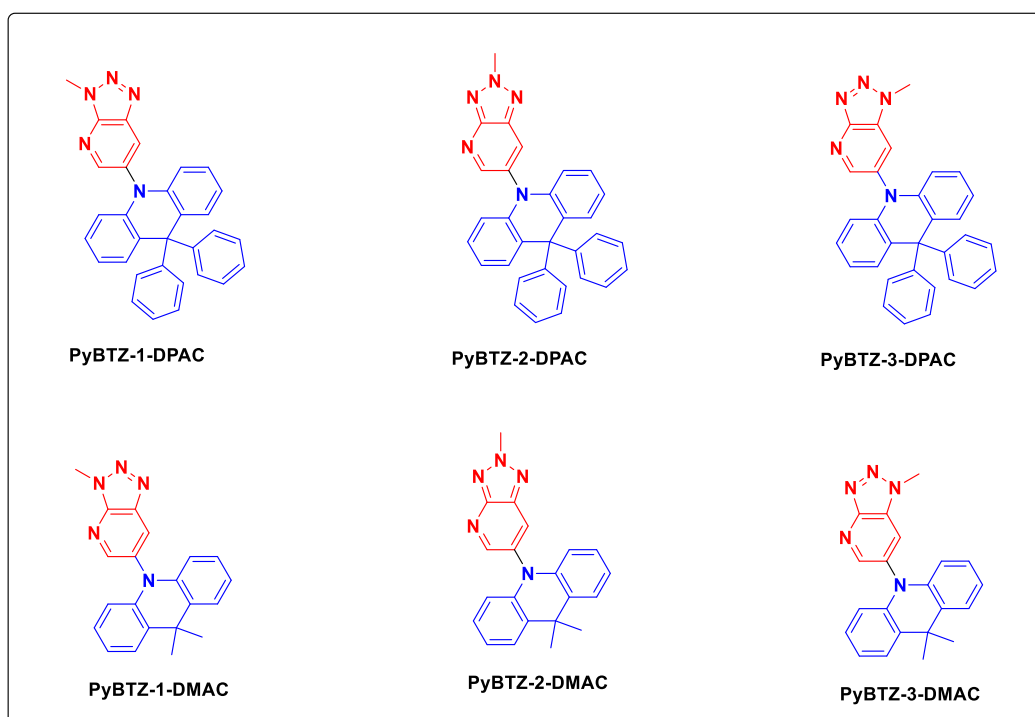
Figure 7.1. *Molecular structures of **PyBTZ-1,2,3-Donors** with the three possible isomers of the PyBTZ with the difference on the methyl group position on the triazole ring.*

7.2 Molecular design, synthesis, and characterization

The target molecules were designed aiming at small molecular mass materials with a D-A system. The choice of [1,2,3]triazolo[4,5-*b*]pyridine for the core was made due to the high number of nitrogens in the molecule. They can provide a good acceptor

structure due to the higher electronegativity of the nitrogen atoms in relation to the carbon atoms. The synthetic route to obtain the **PyBTZ-1,2,3-Br** isomers is shown in **Scheme 7.1**. The first step is based on the diazotization reaction of 5-bromopyridine-2,6-diamine with sodium nitrite to obtain the respective NH-triazolo ring, followed by methylation with methyl iodide to obtain the three isomers of **PyBTZ-1,2,3-Br** in moderate yields after separation by chromatograph column.[142,143]
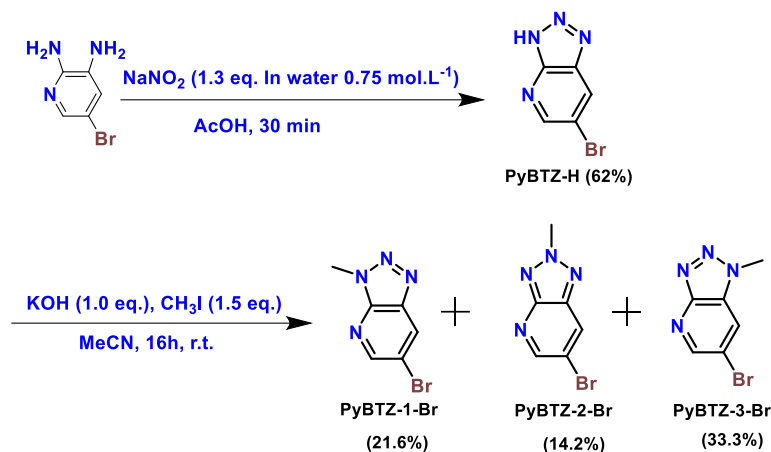
Scheme 7.1. *Synthetic route to obtain the monobromide isomers PyBTZ-1,2,3-Br.*

Figure 7.2 shows the ^{1}H NMR spectra of the **PyBTZ-1,2,3-Br** regioisomers after separation by column chromatography. We can observe the success of the separation of the regioisomers by the split in the signals of the hydrogens signed as Ha and Hb. Which evidence the influence of the position of the methyl group in the triazole ring. Also, we observe a shift in the signal from hydrogens from methyl group linked to the nitrogen atom in the triazole ring. The attribution of the NMR spectra was made based on the order of elution from the chromatographic column and by comparison with literature. [142,143]
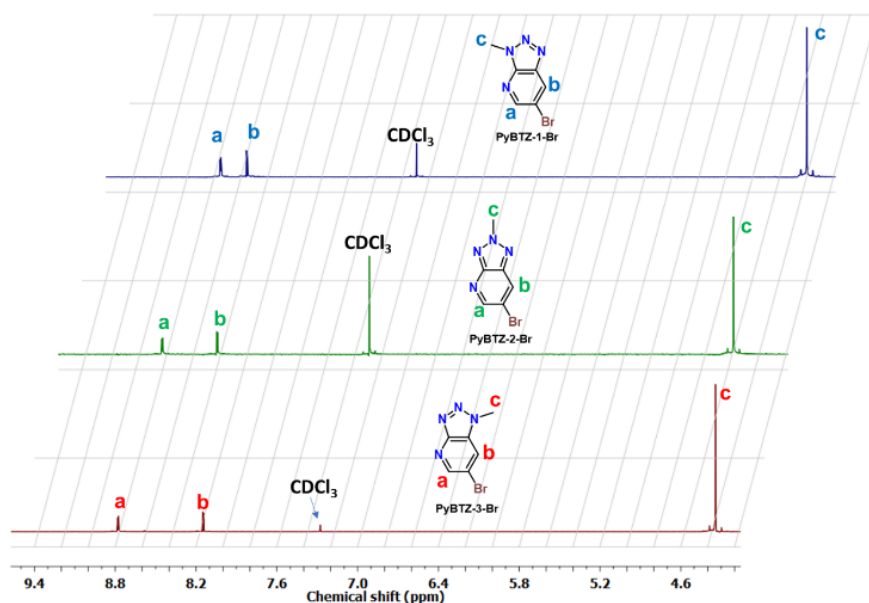
Figure 7.2. ^{1}H NMR (300 MHz) of **PyBTZ-1,2,3-Br** in CDCl$_3$.

       Scheme 7.2 shows the synthetic route to obtain the **PyBTZ-1,2,3-donors** compounds. The donors were attached by Buchwald-Hartwig cross-coupling reaction using dimethyl acridine (**DMAC**) and diphenyl acridine (**DPAC**) as donor moieties. The Pd$_2$dba$_3$ (3 mol%) and [HP(t-Bu)$_3$]BF$_4$ (6 mol%) were used as catalyst and ligand, respectively. The base, sodium *tert*-butoxide was used in excess, and reactions were performed under argon atmosphere, using toluene as a solvent. Obtaining the target compounds in excellent yields (82-96%) after purification by chromatographic column. All the compounds were fully characterized by ^{1}H and ^{13}C NMR and high-resolution mass spectrometry (HRMS). All spectrums are shown in the appendices section, and the experimental data are shown in synthetic details.
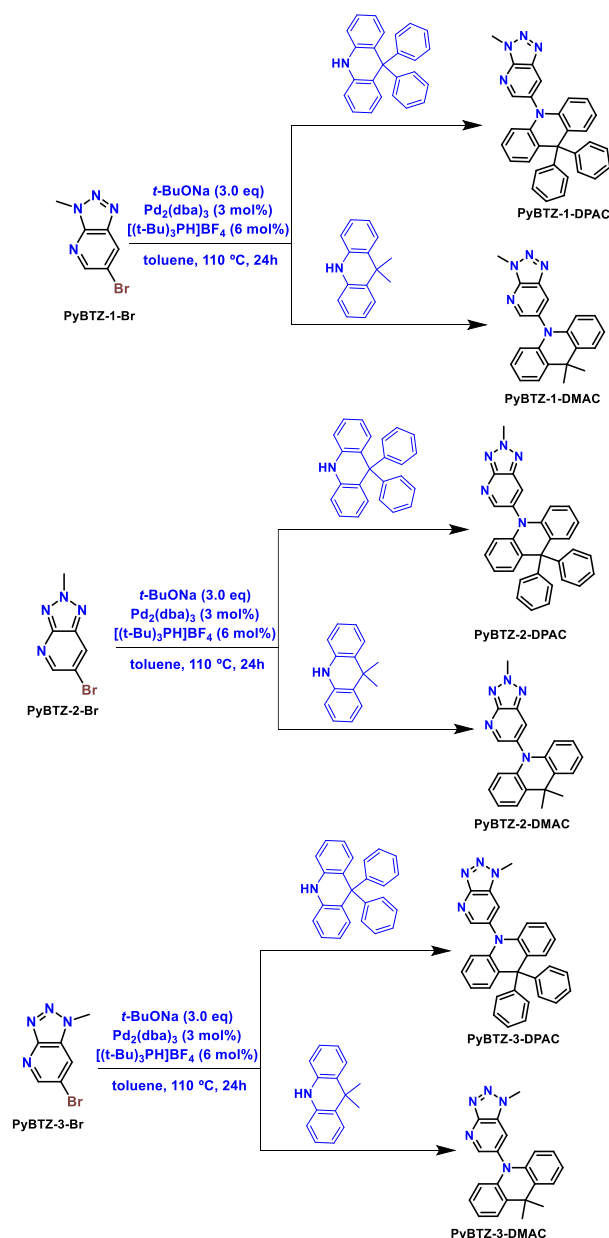
Scheme 7.2. *Synthetic route to obtain D-A compounds derived from the isomers of the [1,2,3]triazolo[4,5-b]pyridine core.*

7.3 Electrochemical characterizations

The electrochemical properties of **PyBTZ-1,2,3-donors** were investigated by cyclic voltammetry (CV) to estimate the HOMO and LUMO energy levels. The estimated ionization potential (IP) and electron affinity (EA) (from onset oxidation (E_{ox}) and reduction (E_{red}) potentials), are correlated with the HOMO (E_{HOMO}) and LUMO (E_{LUMO}) energy levels, respectively, using the following equations: $E_{HOMO} = -(E_{ox} + 5.1)$; $E_{LUMO} = -(E_{red} + 5.1)$.[78] The results are summarized in **Table 7.1** and the voltammograms are compiled in **Figure 7.3**.

Table 7.1. *HOMO and LUMO energy levels obtained from CV measurements of* **PyBTZ-1,2,3-donors***.*

Compound	Cyclic Voltammetry[a]		
	HOMO (eV)	LUMO (eV)	E_g (eV)
PyBTZ-1-DMAC	-5.90	-3.10	2.80
PyBTZ-2-DMAC	-5.83	-3.15	2.68
PyBTZ-3-DMAC	-5.98	-3.23	2.75
PyBTZ-1-DPAC	-5.97	-3.10	2.87
PyBTZ-2-DPAC	-5.97	-3.14	2.83
PyBTZ-3-DPAC	-6.05	-3.23	2.82

[a] Measurements were performed for 1 mM solutions of investigated compounds in the presence of 100 mM tetrabutylammonium tetrafluoroborate and calibrated using ferrocene/ferrocenium redox couple.

All materials showed good stability in the applied voltage range, with non-reversible reduction process taking place on the pyridine benzotriazole ring. The LUMO energy levels are similar in values for all compounds. But appears to be affected by the position of the methyl group in the triazole ring. The oxidation process also appears as irreversible, taking place on the donor moieties (DMAC and DPAC). All compounds showed not reversible reduction and oxidations process. The highest value of energy of LUMO obtained for DMAC derivatives was for **PyBTZ-1-DMAC** (-3.10 eV) and for the compounds with DPAC as donor, the highest energy of LUMO was obtained for the compound **PyBTZ-1-DPAC** (-3.10 eV). Indicating that the isomer 1, implies in the reduction process in lower potentials, following the sequence 1>2>3. The estimated energies of HOMO were more affected by the change from the donor DMAC to DPAC than the variation of the isomer with same donor, which are expected due to difference in the strength of electron-donation. The variations of donor moieties and the position of the methyl group on the triazole ring implies changes in the HOMO-LUMO gap (E_g). Considering the DMAC derivatives, the lowest E_g were observed for the isomer 2 (2.68 eV), while the highest E_g were observed for isomer 1 (2.80 eV), following the sequence 2<3<1. For DPAC derivatives, the E_g follows the sequence 1>2>3. This indicates that the D-A combinations are very important in E_g modulation for which both, the strength of the donor and the variation of the isomer are important.
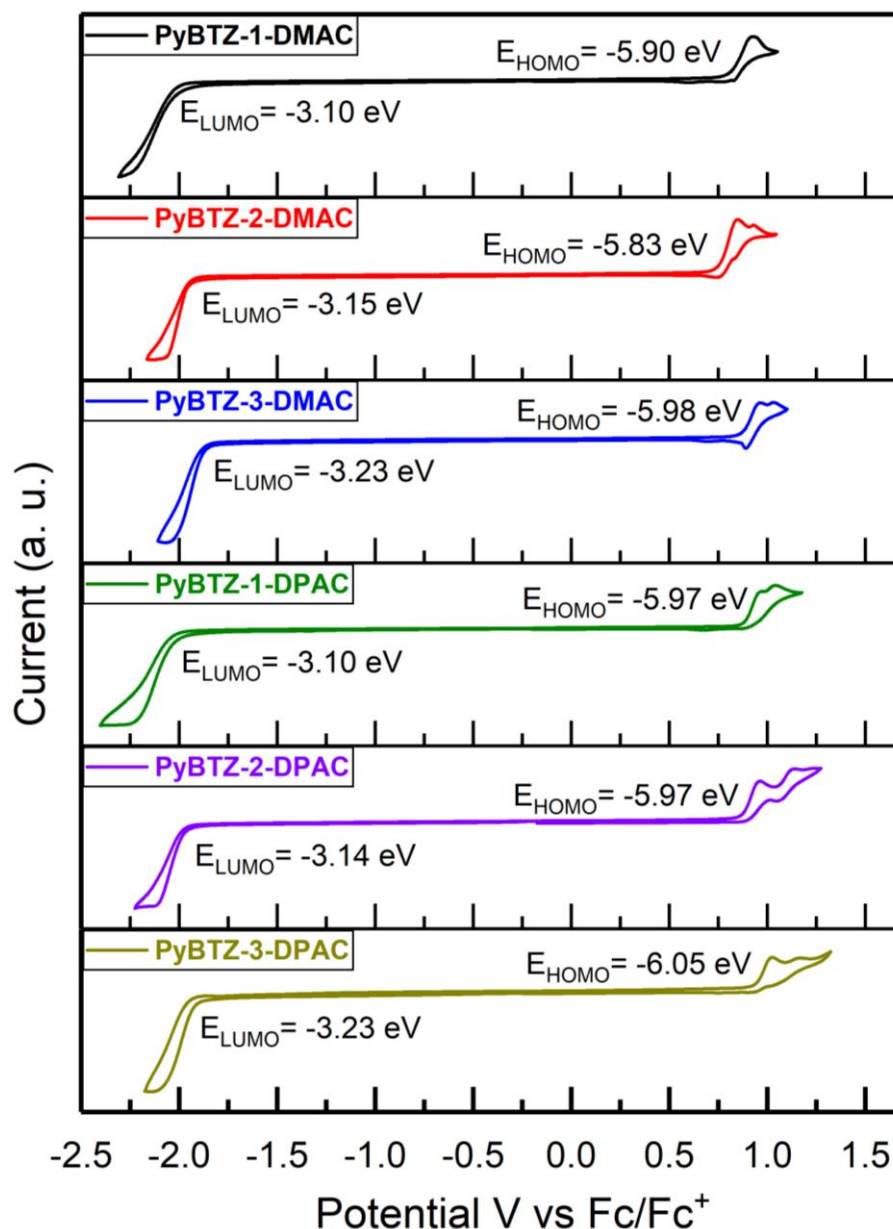
Figure 7.3. *Cyclic voltammograms of a single scan of 1 mM of* **PyBTZ-1,2,3-DMAC,DPAC** *compounds in DCM containing 0.1 M Bu₄NBF₄ as electrolyte. Pt disk as working, Pt wire as counter and Ag/AgCl as reference electrode, at 50 mv s⁻¹ scan rate.*

7.4 Photophysical analyses

The absorption spectra (UV-Vis) in diluted dichloromethane (DCM) solutions are shown in **Figure 7.4** and the data are summarized in **Table 7.2**. The profile of the absorption spectra appears very similar for all compounds. We can observe strong absorption bands around 270-290 nm, that can be signed to the $n\rightarrow\pi^*$ and $\pi\rightarrow\pi^*$ transitions from aromatic systems of pyridine benzotriazole core and the donors moieties.[100,118] We also can observe less intense absorption bands around 380-400

nm, that can be attributed to the CT transitions from the donor units to the acceptor core.[123]
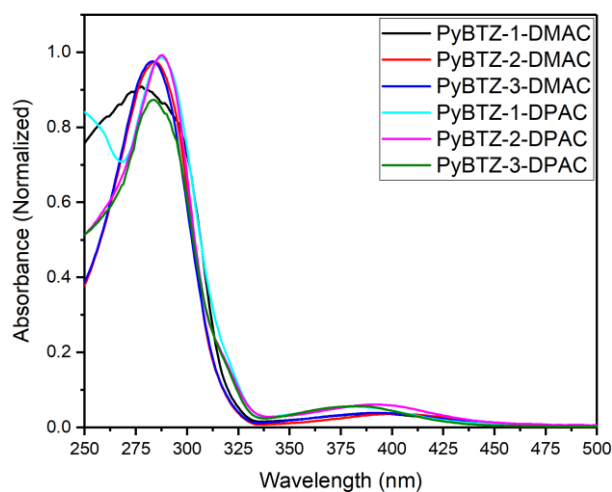
Figure 7.4. *Absorption spectra of **PyBTZ-1,2,3-donors** in DCM solutions 0.1 mM.*

Figure 7.5 shows the contribution of photoluminescence that was observed for the variation of isomers and donors in two different solvents with different polarities: dichloromethane (DCM) and toluene (TOL). Considering the same donor attached, we observe a similar gaussian shape of the emission characteristic of ^{1}CT emission for the isomers 1 and 2. We also observe a red shift from 1 to 2, and additionally a clearly different profile of emission for the isomer 3, displaying two emission bands, more evident in DCM than TOL. This behavior suggests the mixture ^{1}LE+^{1}CT character of the transition $S_1 \rightarrow S_0$ for the isomer 3, with maximum wavelengths in DCM centered at 437 and 556 nm for **PyBTZ-3-DMAC**, and at 421 and 504 nm for **PyBTZ-3-DPAC**. Also, it is possible to observe two emission bands for these compounds in TOL solutions, but with the first less intense, indicating the stabilization of the ^{1}CT emission with the change in the polarities of solvent. The PLQY in air conditions measured in DCM and TOL, showed an increase in less polar solvents, indicating the polarity quenching of ^{1}CT states. The compounds showed moderate PLQY in air conditions up to 9.9%, which can be increased if we consider the removal of oxygen from the solutions.
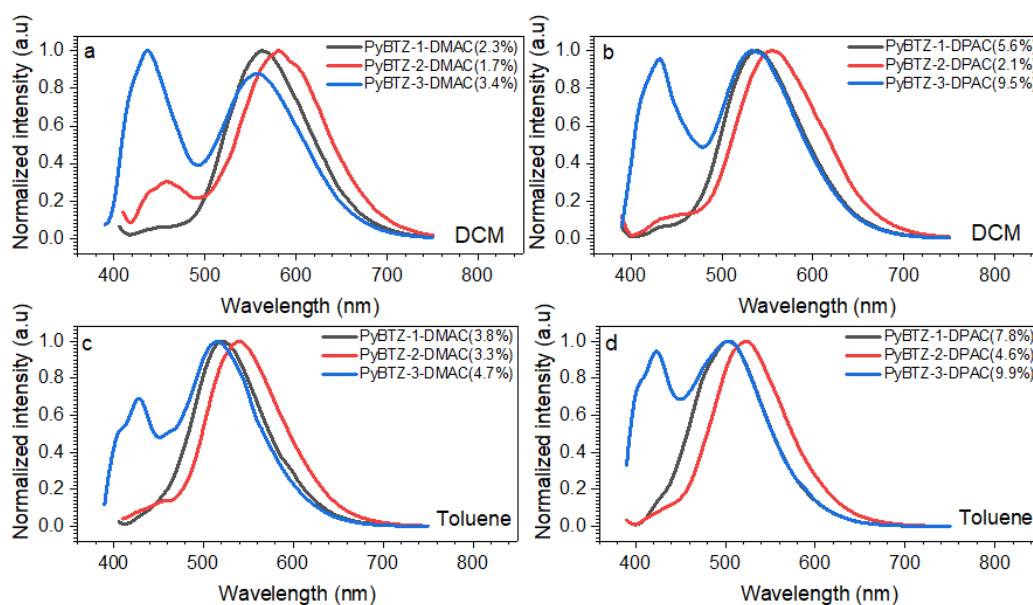
Figure 7.5. *Photoluminescence (PL) spectra of the compounds **PyBTZ-1,2,3-donors** in DCM and TOL solutions 0.1 mM. a) **PyBTZ-1,2,3-DMAC** in DCM; b) **PyBTZ-1,2,3-DPAC** in DCM; c) **PyBTZ-1,2,3-DMAC** in TOL; d) **PyBTZ-1,2,3-DPAC** in TOL. In brackets are the PLQY in DCM or TOL.*

Table 7.2. *Summary of photophysical characteristics of the studied PyBTZ-1,2,3-Donors luminophores.*

Compounds	λ_{Abs}/nm [$\mathcal{E}$/10^3M^{-1} cm^{-1}][a]	λ_{Em} [nm] MCH	λ_{Em} [nm] TOL	λ_{Em} [nm] THF	λ_{Em} [nm] DCM	λ_{Em} [nm] ACN	PLQY [%] DCM/TOL
PyBTZ-1-DMAC	277 [11.0], 391 [0.4]	514	520	534	565	576	2.3/3.8
PyBTZ-2-DMAC	284 [9.15], 400 [0.3]	529	539	555	581	457; 597	1.7/3.3
PyBTZ-3-DMAC	282 [8.9], 392 [0.3]	424; 512	428; 518	431; 541	437; 556	438; 580	3.4/4.7
PyBTZ-1-DPAC	288 [9.7], 381 [0.5]	497	502	516	538	550	5.6/7.8
PyBTZ-2-DPAC	288 [8.2], 391 [0.5]	513	524	538	556	573	2.1/4.6
PyBTZ-3-DPAC	284 [10.8], 382 [0.6]	421; 504	422; 503	424; 516	431; 538	431; 544	9.5/9.9

Figure 7.6 shows the solvatochromism studies from less polar to more polar solvents: methylcyclohexane (MCH), toluene (TOL), tetrahydrofuran (THF), dichloromethane (DCM) and acetonitrile (ACN). For the compounds **PyBTZ-1-DMAC** and **PyBTZ-1-DPAC** we observe a clear redshift from MCH to ACN indicating a strong CT process. With variation of $\lambda_{PL(MCH)}$= 514 nm to $\lambda_{PL(ACN)}$= 576 nm for **PyBTZ-1-DMAC** and variation of $\lambda_{PL(MCH)}$= 497 nm to $\lambda_{PL(ACN)}$= 550 nm for **PyBTZ-1-DPAC**, respectively. Whereas for the compounds **PyBTZ-3-DMAC** and **PyBTZ-3-DPAC** the

behavior showed two emission bands in all solvents. The most intense band differs in less polar solvents (MCH and TOL), while presents blue shift in the maximum emission wavelength according to the polarity of solvents increases from DCM, THF and ACN. For **PyBTZ-3-DMAC** (that behaves in similar way as **PyBTZ-3-DPAC**), we observe two emission peaks for MCH and TOL centered at 424 nm (less intense) and 512 nm (more intense). When we change for more polar solvents, this order is inverted, displaying the more intense emission at $\lambda_{PL(THF)}$= 431 nm and less intense emission at $\lambda_{PL(MCH)}$= 541 nm. In DCM we also observe similar behavior with minimum redshift. However this changes for ACN, with the intensity of emission at $\lambda_{PL(ACN)}$= 580 nm decreasing more and the emission at $\lambda_{PL(ACN)}$= 438 nm became the most intense emission band. These behaviors can be attributed to the quenching of [1]CT states in more polar solvents, while the [1]LE states are not very affected by the solvent polarities, contributing more to the emission profile in more polar solvents.
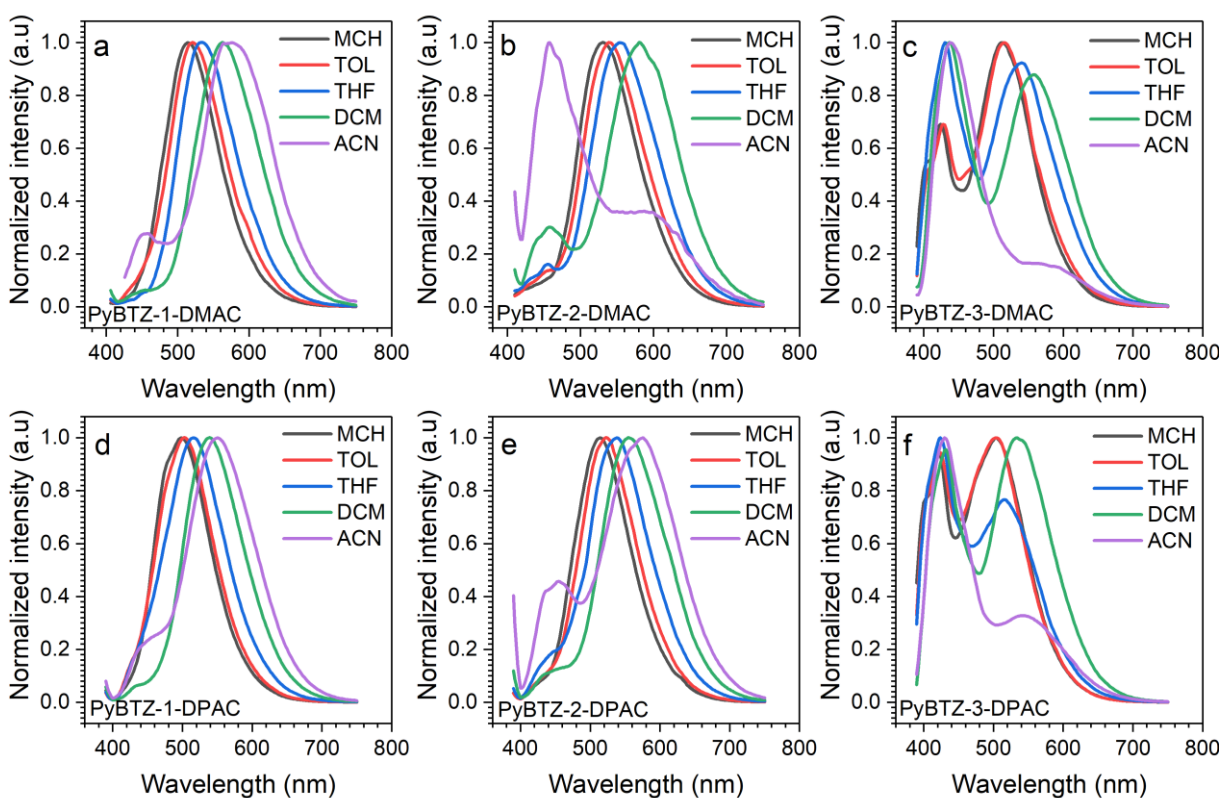
Figure 7.6. *Solvatochromism of **PyBTZ-1,2,3-donors** in methylcyclohexane (MCH), toluene (TOL), tetrahydrofuran (THF), dichloromethane (DCM) and acetonitrile (ACN) at 0.1 mM concentrations.*

The compounds **PyBTZ-2-DMAC** and **PyBTZ-2-DPAC** display redshift in the emission from MCH to THF. While in DCM to THF the presence of two emission bands

becomes more evident. For **PyBTZ-2-DMAC**, the most intense emission in ACN appears at $\lambda_{PL(ACN)}$= 457 nm and less intense at $\lambda_{PL(ACN)}$= 557 nm. While for **PyBTZ-2-DPAC** we also observe the two emission bands, but with inverse in the intensity, less intense at $\lambda_{PL(ACN)}$= 454 nm and more intense at $\lambda_{PL(ACN)}$= 573 nm. Which also can be attributed to the quenching of ^{1}CT states in more polar solvents.

7.5 Conclusions

This chapter described the design and successful synthesis of one new series of D-A compounds using asymmetric pyridine benzotriazole isomers as acceptor core. The regioisomers containing the methyl group in three different positions of the benzotriazole ring were very well separated by chromatography column. The different donor moieties (DMAC and DPAC) were attached by N-C Buchwald-Hartwig coupling reactions with very good yields. All the structural characterizations were realized by NMR spectroscopy and by high-resolution mass spectrometry for final molecules. The electrochemical characterizations showed that the materials present an irreversible reduction process and a semi-reversible oxidation process. The photoluminescence properties was analyzed in different solvents displaying differences in the behavior depending on the methyl group position in the regioisomers and also by the changes of the donor attached. Suggesting that the strategy using different regioisomers is an interesting alternative to modulate the photophysical properties of the materials to be applied as TADF-based OLED devices.

7.6 Synthetic details

*6-bromo-3H-[1,2,3]triazolo[4,5-b]pyridine (**PyBTZ**)*

PyBTZ

To a solution of 5-bromopyridine-2,3-diamine (**PyDA**) (2.00 g, 10.64 mmol) in glacial acetic acid (1.80 mL), was added an aqueous solution of sodium nitrite (0.95 g, 13.83 mmol in 4.8 mL of water). The reaction mixture was stirred at room temperature for 12 h. Then mixture was cooled to 0 °C for 1 h, filtered, washed with water, and dried to

afford 1.31 g (62% of yield) of 6-bromo-3*H*-[1,2,3]triazolo[4,5-*b*]pyridine (PyBTZ-H) as a brown powder. ^{1}H NMR (300 MHz, DMSO): δ = 16.49 (bs, 1H), 8.82 (d, 1H), 8.80 (d, 1H).

6-bromo-3-methyl-3H-[1,2,3]triazolo[4,5-b]pyridine (**PyBTZ-1-Br**), 6-bromo-2-methyl-2H-[1,2,3]triazolo[4,5-b]pyridine (**PyBTZ-2-Br**), *6-bromo-1-methyl-1H-[1,2,3]triazolo[4,5-b]pyridine* (**PyBTZ-3-Br**).

PyBTZ-1-Br   PyBTZ-2-Br   PyBTZ-3-Br
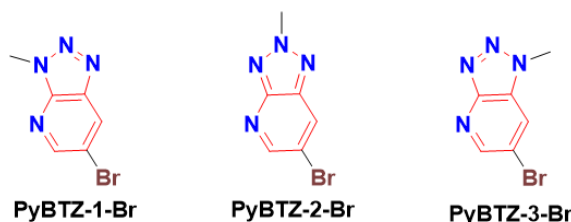
To a solution of 6-bromo-3*H*-[1,2,3]triazolo[4,5-*b*]pyridine (1.40 g, 7.03 mmol) in acetonitrile (40.0 mL) and water (2.0 mL) was added KOH (394.7 mg, 7.03 mmol). The resulting mixture was heated using a heat gun for a few seconds until the base solubilizes. Then iodomethane (1.50 g, 0.66 mL, 10.55 mmol) was added and the resulting solution was stirred overnight at room temperature. The solvent was removed under reduced pressure and the resulting solid was dissolved in DCM, washed with water (3 x 25 mL), brine (1 x 25 mL), dried with $MgSO_4$ filtered, and concentrated under reduced pressure. The crude mixture was purified by silica gel column chromatography eluting with increasing gradient of hexanes:AcOEt providing 0.323 g of **PyBTZ-1-Br** (21.6% of yield, first eluted compound), as a with solid, ^{1}H NMR (300 MHz, $CDCl_3$): δ= 8.72 (d, 1H, *J* = 2.0 Hz), 8.52 (d, 1H, *J* = 2.0 Hz), 0.213 g of **PyBTZ-2-Br** (14.2% of yield, second eluted compound) as a with solid, ^{1}H NMR (300 MHz, $CDCl_3$): δ= 8.80 (d, *J* = 2.2 Hz, 1H), 8.40 (d, *J* = 2.2 Hz, 1H), 4.56 (s, 3H), and 0.499 g of **PyBTZ-3-Br** (33.3% of yield, third eluted compound), as a pale yellow solid, ^{1}H NMR (300 MHz,$CDCl_3$) δ 8.78 (d, *J* = 2.0 Hz, 1H), 8.15 (d, *J* = 2.0 Hz, 1H), 4.34 (s, 3H). The structure of these three obtained isomers was confirmed by comparing with the literature. [142,143]

General procedure for C-N coupling of PyBTZ-1,2,3-Br with DMAC or DPAC

A flame dried 100 mL Schlenk tube equipped with a rubber septum was charged with **PyBTZ-1-Br** or **PyBTZ-2-Br** or **PyBTZ-3-Br** (1.0 eq.); DMAC or DPAC (1.2 eq.), sodium *tert*-butoxide (2.0 eq), $Pd_2(dba)_3$ (3 mol%) and [(t-Bu)₃PH]BF₄ (6 mol%). The

atmosphere of the system was changed by argon and degassed toluene (30 mL/mmol) was added and the resulting mixture was heated to 110 °C with stirring for 24h under argon atmosphere. The solution was filtered over celite bed and the solvent removed under reduced pressure. The crude mixture was purified by silica gel column chromatography eluting with DCM:hexane (2:3 v/v).

*9,9-dimethyl-10-(3-methyl-1H-[1,2,3]triazolo[4,5-b]pyridin-6-yl)-9,10-dihydroacridine*
(PyBTZ-1-DMAC)
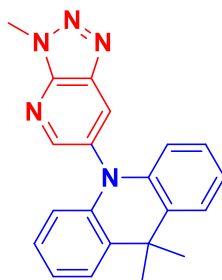
PyBTZ-1-DMAC

Obtained as yellow solid with 90% of yield. ^{1}H NMR (300 MHz, CDCl$_3$) δ 8.62 (d, *J* = 2.1 Hz, 1H), 8.44 (d, *J* = 2.1 Hz, 1H), 7.56 – 7.49 (m, 2H), 6.98 (dt, *J* = 5.9, 2.1 Hz, 4H), 6.18 – 6.11 (m, 2H), 4.47 (s, 3H), 1.73 (s, 6H). ^{13}C NMR (75 MHz, CDCl$_3$) δ 154.24, 145.47, 140.85, 138.07, 134.14, 131.92, 130.57, 126.58, 125.61, 121.47, 113.84, 109.98, 36.08, 33.31, 31.19. HRMS: m/z calcd for C$_{21}$H$_{20}$N$_5$ (M+H)$^+$: 342.1719; found: 342.1711.

9,9-dimethyl-10-(2-methyl-1H-[1,2,3]triazolo[4,5-b]pyridin-6-yl)-9,10-dihydroacridine
(PyBTZ-2-DMAC)
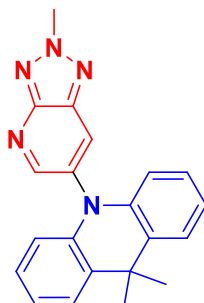
PyBTZ-2-DMAC

Obtained as yellow solid with 96% of yield. ^{1}H NMR (300 MHz, CDCl$_3$) δ 8.69 (d, *J* = 2.3 Hz, 1H), 8.31 (d, *J* = 2.3 Hz, 1H), 7.53 – 7.47 (m, 2H), 7.01 – 6.96 (m, 4H), 6.24 – 6.19 (m, 2H), 4.65 (s, 3H), 1.73 (s, 6H). ^{13}C NMR (75 MHz, CDCl$_3$) δ 155.81, 155.30,

140.74, 137.51, 135.81, 130.65, 129.85, 126.68, 125.65, 121.56, 113.97, 44.36, 36.17, 31.23. HRMS: m/z calcd for $C_{21}H_{20}N_5$ (M+H)$^+$: 342.1719; found: 342.1716.

9,9-dimethyl-10-(1-methyl-1H-[1,2,3]triazolo[4,5-b]pyridin-6-yl)-9,10-dihydroacridine **(PyBTZ-3-DMAC)**
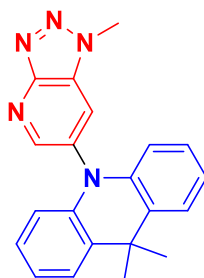
PyBTZ-3-DMAC

Obtained as yellow solid with 91% of yield. ^{1}H NMR (300 MHz, CDCl$_3$) δ 8.71 (d, *J* = 2.1 Hz, 1H), 8.01 (d, *J* = 2.1 Hz, 1H), 7.54 – 7.50 (m, 2H), 7.02 – 6.96 (m, 4H), 6.17 – 6.11 (m, 2H), 4.38 (s, 3H), 1.73 (s, 6H). ^{13}C NMR (75 MHz, CDCl$_3$) δ 151.98, 148.66, 140.62, 136.60, 130.64, 126.89, 126.63, 125.70, 121.67, 121.05, 113.91, 36.09, 35.10, 31.27. HRMS: m/z calcd for $C_{21}H_{20}N_5$ (M+H)$^+$: 342.1719; found: 342.1717.

10-(3-methyl-3H-[1,2,3]triazolo[4,5-b]pyridin-6-yl)-9,9-diphenyl-9,10-dihydroacridine (**PyBTZ-1-DPAC**)
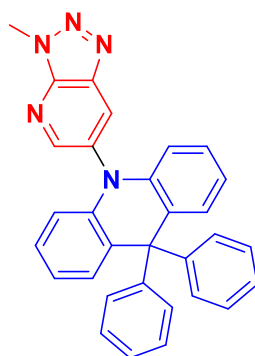
PyBTZ-1-DPAC

Obtained as yellow solid with 86% of yield. ^{1}H NMR (300 MHz, cd2cl2) δ 8.22 (d, *J* = 2.1 Hz, 1H), 8.18 (d, *J* = 2.1 Hz, 1H), 7.32 – 7.27 (m, 6H), 7.08 – 7.03 (m, 2H), 7.00 (dd, *J* = 5.9, 3.9 Hz, 4H), 6.93 (dd, *J* = 4.8, 0.9 Hz, 4H), 6.36 (d, *J* = 7.6 Hz, 2H), 4.39 (s, 3H). ^{13}C NMR (75 MHz, CD$_2$Cl$_2$) δ 153.72, 146.10, 145.50, 142.13, 137.65,

133.49, 131.41, 130.53, 130.33, 130.16, 127.72, 127.02, 126.50, 120.92, 114.12, 56.82, 33.09, 29.68. HRMS: m/z calcd for $C_{31}H_{24}N_5$ (M+H)$^+$: 466.2032; found: 466.2036.

10-(2-methyl-3H-[1,2,3]triazolo[4,5-b]pyridin-6-yl)-9,9-diphenyl-9,10-dihydroacridine (**PyBTZ-2-DPAC**)
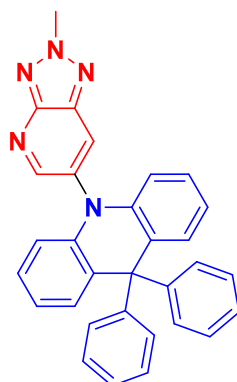
PyBTZ-2-DPAC

Obtained as yellow solid with 88% of yield. ^{1}H NMR (300 MHz, CD$_2$Cl$_2$) δ 8.27 (d, J = 2.3 Hz, 1H), 8.07 (d, J = 2.3 Hz, 1H), 7.29 (dd, J = 5.2, 1.9 Hz, 6H), 7.10 – 7.04 (m, 2H), 7.00 (dt, J = 5.3, 2.1 Hz, 4H), 6.95 – 6.90 (m, 4H), 6.41 (d, J = 8.1 Hz, 2H), 4.59 (s, 3H). ^{13}C NMR (75 MHz, CD$_2$Cl$_2$) δ 155.19, 146.19, 142.01, 137.18, 135.15, 130.53, 130.41, 130.28, 129.55, 127.80, 127.13, 126.57, 121.03, 114.20, 56.89, 44.32. HRMS: m/z calcd for $C_{31}H_{24}N_5$ (M+H)$^+$: 466.2032; found: 466.2049.

10-(1-methyl-3H-[1,2,3]triazolo[4,5-b]pyridin-6-yl)-9,9-diphenyl-9,10-dihydroacridine (**PyBTZ-3-DPAC**)
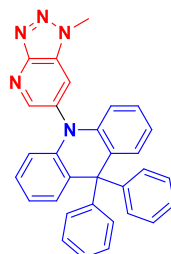
PyBTZ-3-DPAC

Obtained as yellow solid with 82% of yield. ^{1}H NMR (300 MHz, CD$_2$Cl$_2$) δ 8.35 (d, J = 2.2 Hz, 1H), 7.64 (d, J = 2.1 Hz, 1H), 7.26 (dt, J = 5.7, 2.8 Hz, 6H), 7.07 – 7.01 (m, 2H), 6.99 – 6.94 (m, 4H), 6.90 (dd, J = 6.1, 2.7 Hz, 4H), 6.32 (d, J = 8.2 Hz, 2H), 4.28 – 4.22 (m, 3H). ^{13}C NMR (75 MHz, CD$_2$Cl$_2$) δ 156.75, 151.45, 146.22, 142.08,

136.10, 130.42, 130.36, 127.85, 127.16, 126.74, 126.61, 121.23, 114.34, 60.30, 35.11.
HRMS: m/z calcd for $C_{31}H_{24}N_5$ (M+H)$^+$: 466.2032; found: 466.2035.

8. D-A regioisomers derived from benzopyridoimidazoisoquinolinone and phosphanimine cores: design, synthesis and photophysical/electrochemical properties

This chapter will demonstrate the design and synthesis of new compounds derived from benzopyridoimidazoquinolinone and triphenyl-phosphanimine isomers as acceptor core. The molecules were designed in D-A structure, where phenothiazine was attached by Pd-catalyzed C−N cross-coupling reactions. These functional materials were synthesized aiming optoelectronics applications as TADF emitters. Additionally, electrochemical and photophysical behavior will be demonstrated. In this chapter the author was responsible for all the molecular design, synthesis, structural characterizations (NMRs), electrochemical characterizations and partially for the photophysical investigations.

8.1 Introduction

Materials based on N-rich acceptors cores based on imidazoquinolinones have been largely investigated for application in optoelectronic devices due to their high level of charge transport carriers.[145] Imidazoisoquinolinone can be prepared by the dehydration reaction between *ortho*-diamino compounds and anhydrides. They have a high acceptor character due to the presence of the nitrogen atom and the carbonyl group in the system, which increase the electronegativity in the core. The electron-accepting character can also be increased by the addition of a pyridine moiety to the system.[146]

The condensation with the use of asymmetric aromatic diamines leads to isomers in different ratios. These results are due to the electron-donating/withdrawing behavior of the functional groups in the aromatic part of diamine, which affects the nucleophilicity of the amino group. Thus, electron-donating groups (EDG) in *ortho* or *para* positions in the diamine lead to strong nucleophilicity of the diamine helping to increase the reaction yield. On the other hand, electron-withdrawing groups (EWG) in *ortho* or *para* positions decrease the reactivity and promote the formation of isomers with carbonyl group and EWG on opposite sides of the molecule, as demonstrated by Anzenbacher and co-authors.[147] In this way, EWG in position 9 and EDG in position

10 improve the yield of the isomer with the group on the opposite side of the carbonyl group (**Figure 8.1**).[147] This is very useful to perform reactions controlling the ratio of the regio-isomers formed. Generally, the reactions give very good yields, but the separation of the isomers is a challenge. Due to that, the compounds are generally used as a mixture of isomers.
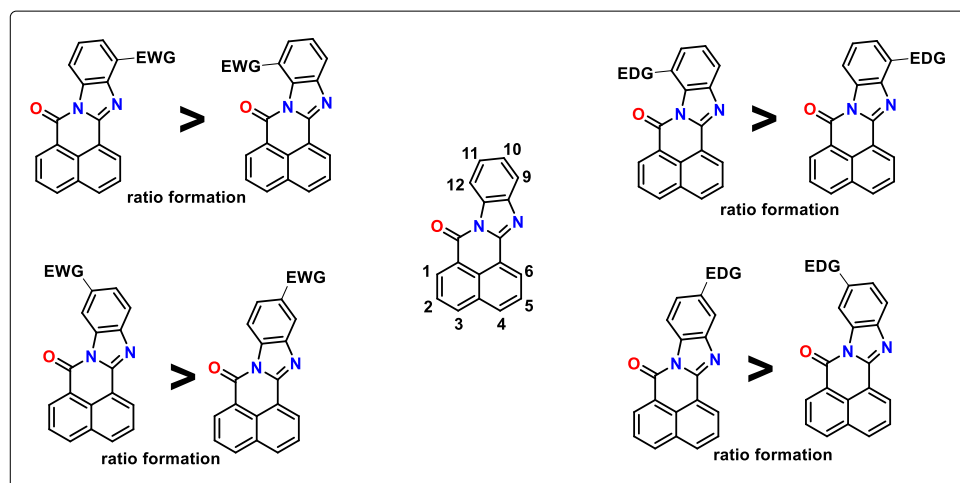
Figure 8.1. *The yield of the isomers differs with the position of the substituent as well as electronic nature of the substituent.*

The chemistry of organophosphorus has been largely studied in different areas. Related to materials science the application of these materials is not very explored mainly due to the poor stability of the C=P and P=P bonds.[148] Just some classes of organophosphorus, such as triaryl phosphines, phospholes, and phosphazenes, have good stability that allows for use in optoelectronics devices. Large part of these applications were based on the use of organophosphorus transition metal ligands, for example.[149] Other studies indicate that the lone electron pair of the P atom is involved in the delocalization around the conjugated system and the lone pair can induce luminescence quenching. This make them more investigated as electron transport layers (ETLs) and host materials in optoelectronic devices due to chemical stability and electron affinity. The polarity of P=O bond was investigated in the applications using the electron transport ability in π-extended phosphine oxides that present electron-withdrawing properties.[150] Combinations of P=O with pyrenes, for example, give an increase in the electron transport ability as reported by Oyamada et al., other applications include matrices of phosphorescent complexes, where The P=O moiety is used as an electron-withdrawing group combined with an electron rich group, such

as amines. In this way, P=O based hosts can also contain carbazole and other π-extended units in their structure, due to good holes transport behavior.[150]

Other classes of P-based compounds, such as phosphazenes (or phosphanimines) are organic compounds where P and N atoms are linked through a double bond (P=N).[151] Due to the high polarity of the bond, there is no evidence of conjugation in phosphazenes because they behave as ylides. These materials present good thermal and hydrolytic stability. Which makes them investigated in applications as emitters for OLEDS and as electrolytes for dye-sensitized solar cells (DSSCs). Similarly to P=O systems, applications as hosts were also explored. In literature, research focusing in the use of triphenyl-phosphanimine are not very explored.[150] The presence of the triphenyl group connected with P=N can enhance the conjugation degree in the molecular structure. In this way the connection of the triphenyl-phosphanimine (Ph$_3$P=N) with common electron-donors used in TADF systems was not explored so far. The design of new Ph$_3$P=N based compounds can be an excellent strategy to obtaining multifunctional materials for optoelectronic applications.

Based on that, this chapter will show the design and synthesis of two different regioisomers cores, both connected with a common donor used in TADF systems (**Figure 8.2**). One core based on triphenyl-phosphanimine (**Ph$_3$PN**) with phenothiazine connected in *para* and *meta* positions, to evaluate the electrochemical and photophysical properties for suitability in optoelectronics applications. The other system based on benzopyridoimidazoisoquinolinone (**PyNA**) as acceptor core, also connected with phenothiazine, to investigate the electrochemical and photophysical behavior.

Phenothiazine derivarives

phosphanimine

F1-PyNA-PTZ   F2-PyNA-PTZ   Ph$_3$PN-*p*-PTZ   Ph$_3$PN-*m*-PTZ

benzopyridoimidazoisoquinolinone   Phenothiazine derivarives
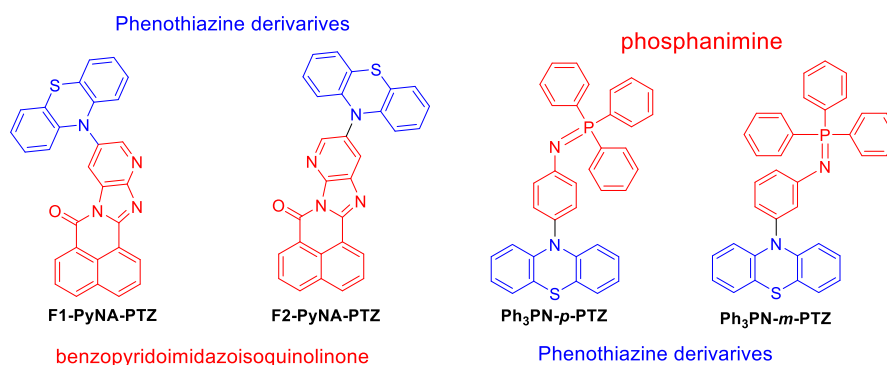
Figure 8.2. *Molecular structures of the regioisomers of triphenyl-phosphanimine and benzopyridoimidazoisoquinolinone acceptor cores with phenothiazine donor.*

8.2 Design, synthesis, and characterization

8.2.1 Synthesis of PyNA-Br isomers

The benzimidazole isomers **PyNA-Br** were synthesized based on the condensation reaction of naphthalic anhydride and 2,3-diamino-5-bromopyridine using the classic method under reflux in acetic acid (**Scheme 8.1**). As an asymmetric diamine was used, the reaction gave two isomers in a ratio of 7:3, with 72% yield for the mixture of isomers. The isomers were separated by chromatography column using a gradient chloroform/hexane (6:1) to pure chloroform as eluent. The **F1-PyNA-Br** and **F2-PyNA-Br** were the first and second fraction, respectively, eluted from the column with a majority of **F2-PyNA-Br.** The isomers were isolated in 17% and 47% yield for F1 and F2, respectively. As for 2,3-diamino-5-bromopyridine, the pyridine nitrogen is *ortho* to diamine, the majority product from the condensation reaction presents the carbonyl group and pyridine nitrogen to the same side and consequently the bromine to opposite side to carbonyl group (F2-PyNa-Br), which was consistent with the yields of the regio-isomers.
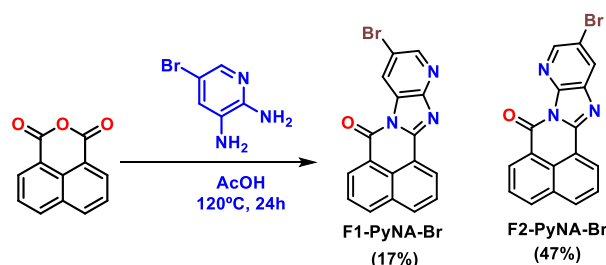
Scheme 8.1. *Synthesis of bromo-benzopyridoimidazoisoquinolinone isomers* **F1,F2-PyNA-Br**.

The compounds were fully characterized by ^{1}H and ^{13}C NMR, all related data are shown in the synthetic section and the appendix. **Figure 8.3** shows the ^{1}H NMR spectra of each isomer after separation by chromatography column. We can observe the differences in the chemical shifts of the protons which shows the success in the separation of the two compounds. If we compare the chemical shifts of the protons signed Ha and Hb for both regioisomers, we note that for the **F2-PyNA-Br** the signals for the hydrogens are more shifted to high chemical shifts in relation to **F1-PyNA-Br**, suggesting more electron density in the hydrogens close to pyridine system. The hydrogens signed as Hc and Hd, also appear with differences in chemical shifts, and are more separated for the isomer **F2-PyNA-Br**. The hydrogens signed as He and Hf, are not very affected by the regioisomers due to distance from benzimidazole system.
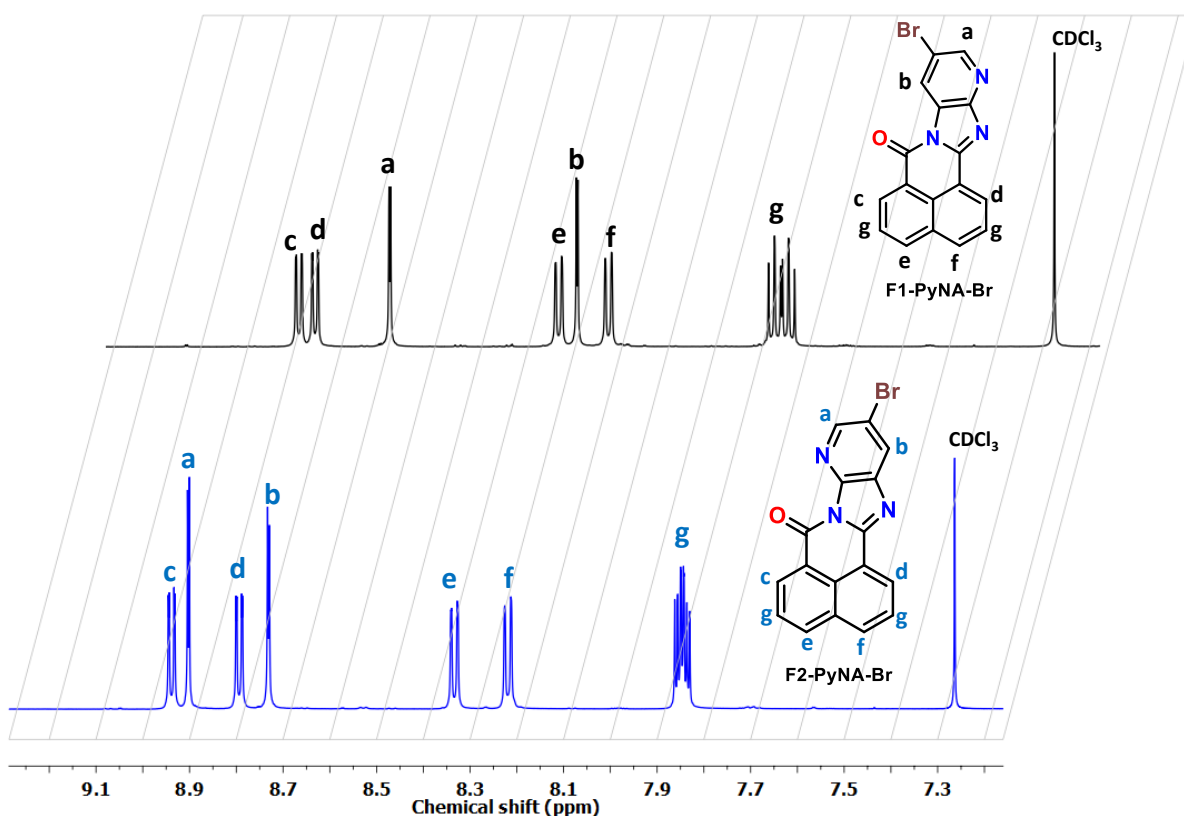
Figure 8.3. ^{1}H NMR (600 MHz) spectrum in CDCl₃ of the aromatic region for **F1-PyNA-Br** and **F2-PyNA-Br**.

8.2.2 Synthesis of phosphanimine brominated cores Ph₃PN-Br

The synthesis of the phosphanimine cores follows typical procedures from literature.[152] The first step involved the formation of aryl azides via diazonium salts, which resulted in obtaining *para-* and *meta*-substituted products (**N3-*p*-Br** and **N3-*m*-Br**) in good yields. The second step was based on the reaction aryl azide with triphenylphosphine to obtain triphenylphosphanimine cores (**Ph₃PN-*p,m*-Br**) in excellent yields. The compounds were characterized by NMR and the related data are shown in synthetic details and appendix sections.
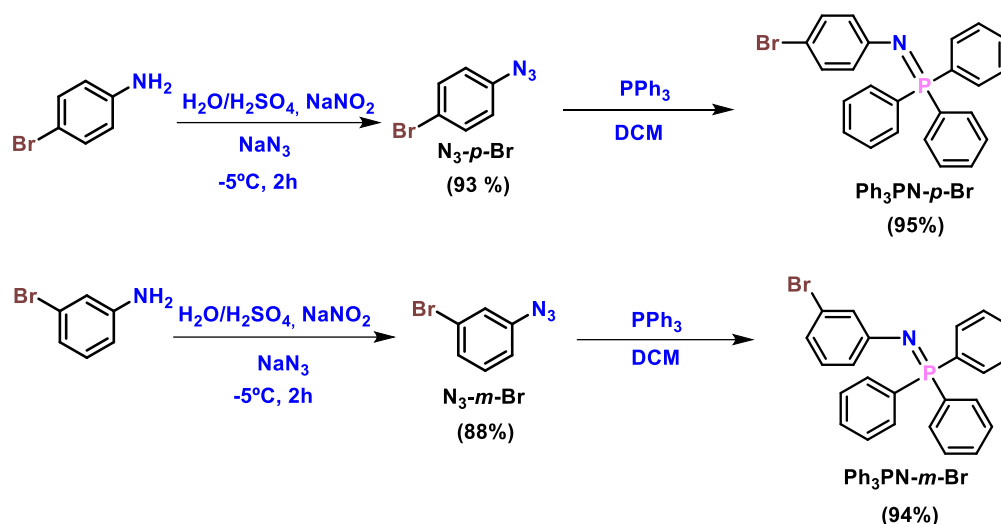
Scheme 8.1. *Synthetic route used to obtain the brominated cores **Ph₃PN-p,m-Br**.*

8.2.3 Buchwald-Hartwig reactions in triphenylphosphanimine and benzopyridoimidazoisoquinolinone cores

The brominated cores were used as substrate in the N-C Buchwald-Hartwig cross-coupling reactions using phenothiazine as donor moieties. The conditions are shown in **Scheme 8.2**. Similar procedures were used for both cores, employing Pd₂dba₃ (3 mol%) and [(*t*-Bu₃)PH]BF₄ (6 mol%) as catalyst and ligand, respectively. The compounds were obtained in moderate yields after purification by chromatography column. **Ph₃PN-*p*-PTZ** and **Ph₃PN-*m*-PTZ** were obtained in 53% and 78% of yield, respectively, indicating that the bromine in *meta* position presents more reactivity in the phosphanimine core. Related with **PyNA-Br** isomers, we try to perform the N-C cross-coupling reaction with the two isomers in same conditions, but **F1-PyNA-Br** did not show reactivity with phenothiazine. The lack of reaction in **F1-PyNA-Br** suggests that the carbonyl and bromine on the same side in the molecule makes the connection of phenothiazine difficult due to steric hindrance. From the other side, **F2-PyNA-PTZ** was obtained in moderate yield (36 %) after purification by chromatography column, indicating that the bromine and carbonyl groups on opposite sides increase the reactivity. All the compounds were fully characterized by NMR and HRMS, and the data related are shown in the synthetic details and appendix sections.

Welisson de Pontes Silva
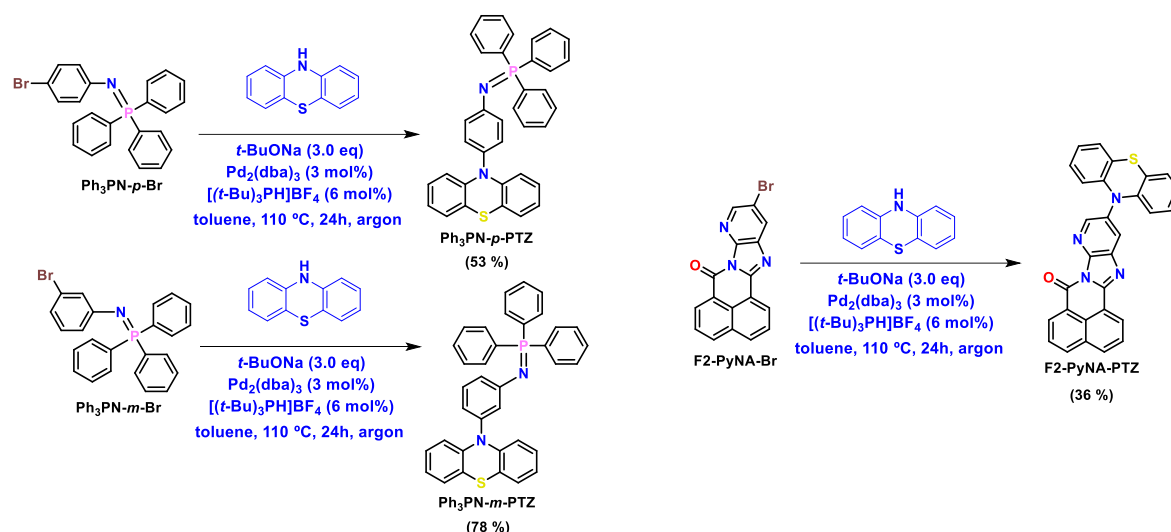
Scheme 8.2. *Synthetic route used to obtain the regioisomers derived from triphenylphosphanimine and benzopyridoimidazoisoquinolinone cores.*

As an example of the characterization of these series of compounds, **Figure 8.4** shows the ^{1}H NMR spectra of **Ph₃PN-*p*-PTZ** and **F2-PyNA-PTZ**. We can observe the success in N-C coupling reactions by the group of hydrogen signals from phenothiazine and the respective cores. For **F2-PyNA-PTZ** we observe hydrogen signals from 9.0-8.3 ppm, referring to hydrogens from benzopyridoimidazoisoquinolinone core. Additionally, the signals referring from the coupled phenothiazine from 7.1-6.3 ppm, show the success in the N-C coupling reaction. Related to **Ph₃PN-*p*-PTZ**, we observe the signals referring to triphenylphosphine system signed as Ha and Hb appearing as multiplets. The signal of hydrogens Hc at 6.95 ppm appears as singlet due to the hydrogens being close to two nitrogen atoms. Also here, all signals referring to the phenothiazine ring are observed, which shows the success of the N-C coupling reaction.
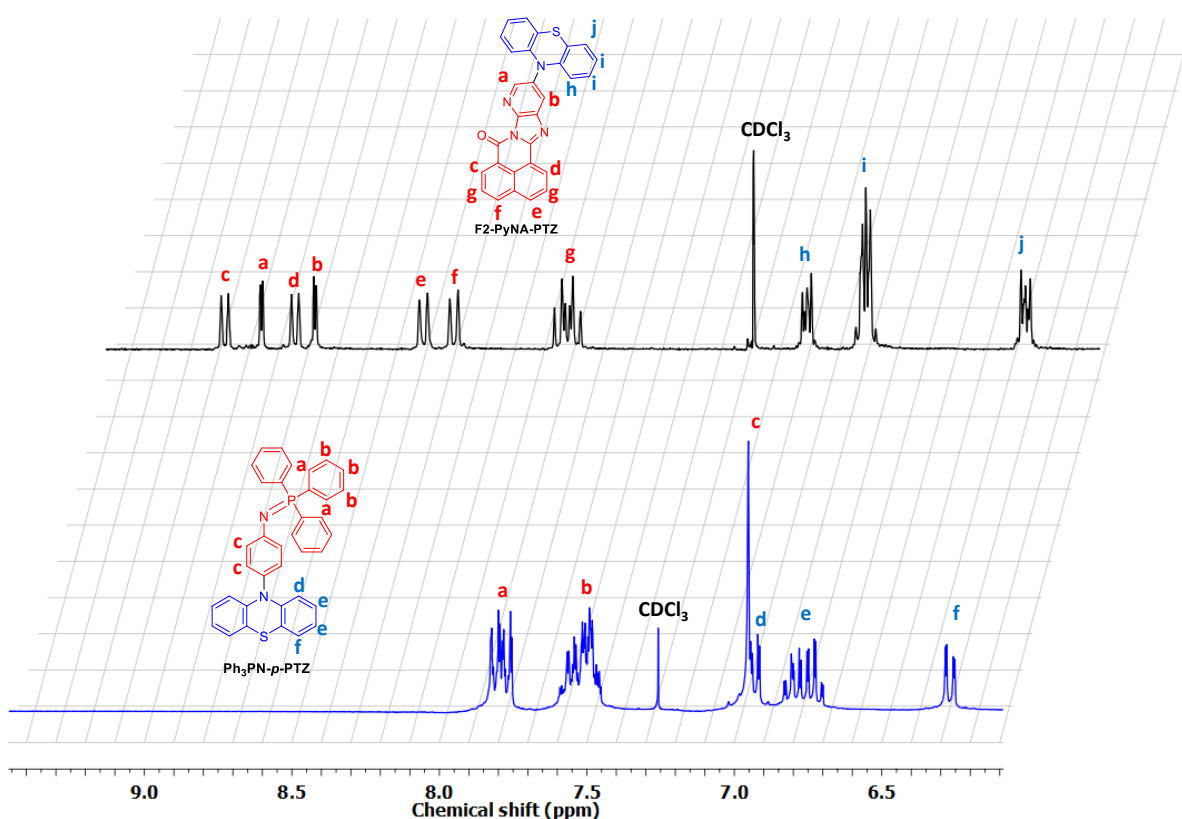
Figure 8.4. ^{1}H NMR (300 MHz) spectrum in CDCl$_3$ of the aromatic region for **F2-PyNA-PTZ** (top) and **Ph$_3$PN-p-PTZ** (down).

8.3 Electrochemical characterizations

The electrochemical properties of **Ph$_3$PN-p,m-PTZ** and **F2-PyNA-PTZ** were investigated by cyclic voltammetry (CV) to estimate the HOMO and LUMO energy levels from ionization potentials (IP) and electron affinity (EA). The estimated IP and EA (from onset oxidation (E$_{ox}$) and reduction (E$_{red}$) potentials), are correlated with the HOMO (E_{HOMO}) and LUMO (E_{LUMO}) energy levels, respectively, using the following equations: E_{HOMO} = -(E$_{ox}$ + 5.1); E_{LUMO} = -(E$_{red}$ + 5.1).[78] The results are summarized in **Table 8.1** and the voltammograms are compiled in **Figure 8.5**.

Table 8.1. HOMO and LUMO energy levels estimated from CV measurements.

Compound	Cyclic Voltammetry[a]		
	HOMO (eV)	LUMO (eV)	E_g (eV)
Ph$_3$PN-p-PTZ	-5.26	-	-
Ph$_3$PN-m-PTZ	-5.36	-	-
F2-PyNA-PTZ	-5.72	-3.95	1.77

[a] Measurements were performed for 1 mM solutions of investigated compounds in the presence of 100 mM tetrabutylammonium tetrafluoroborate and calibrated using ferrocene/ferrocenium redox couple.

The materials showed good stability in the applied voltage range, with reversible oxidation process centered on the phenothiazine unit. The reduction process **Ph₃PN-p-PTZ** and **Ph₃PN-m-PTZ** were not observed in the electrochemical window of the used electrolyte, making it difficult to estimate LUMO energy levels. In the oxidation process we observe differences in the isomers in *para* and *meta* positions. For **Ph₃PN-p-PTZ** we observed two step reversible oxidation process at +0.17 V and +0.51 V. On the other side, for **Ph₃PN-m-PTZ** we observe non-reversible two step oxidation process, with first oxidation process at +0.26 V and second at 0.44 V. In this way the HOMO energy level was highest for the isomer in *para* position. For the compound **F2-PyNA-PTZ** we observe both, reversible reduction in the benzopyridoimidazoisoquinolinone core and oxidation process in the phenothiazine unit.
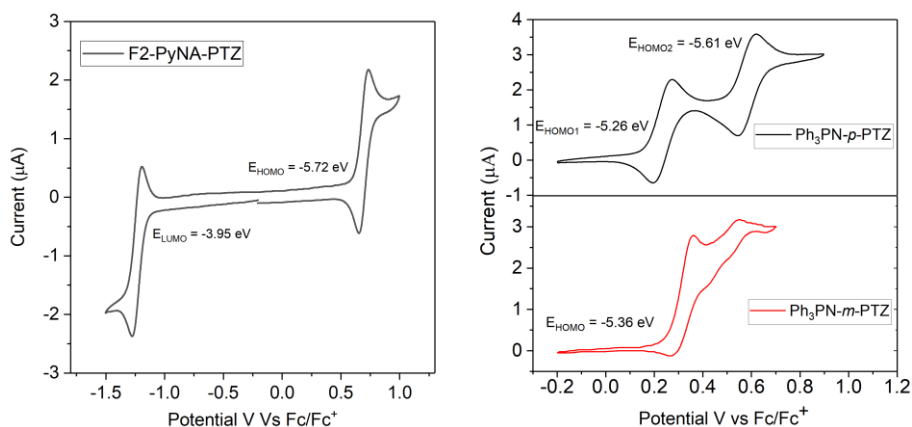
Figure 8.5. *Cyclic voltammograms of a single scan of 1 mM of compounds **Ph3PN-p,m-PTZ** and **F2-PyNA-PTZ** in DCM containing 0.1 M Bu₄NBF₄ as electrolyte. Pt disk as working, Pt wire as counter and Ag/AgCl as reference electrode, at 50 mVs⁻¹ scan rate.*

8.4 Photophysical characterizations

The absorption spectra (UV-Vis) in diluted dichloromethane (DCM) solutions for **Ph₃PN-p,m-PTZ** are shown in **Figure 8.6**, and the data are summarized in **Table 8.2**.

Table 8.2. *Summary of photophysical characteristics of **Ph₃PN-p,m-PTZ** and **F2-PyNA-PTZ**.*

Compounds	λ_{Abs}/nm $[\epsilon/10^3 M^{-1} cm^{-1}]^a$	λ_{Em} [nm] TOL	λ_{Em} [nm] DCM	λ_{Em} [nm] ACN
Ph₃PN-p-PTZ	260 [24.6], 323 [4.7]	453	455	455
Ph₃PN-m-PTZ	259 [21.3], 312 [2.6]	463, 509	458, 513	460, 510
F2-PyNA-PTZ	257 [20.0], 300 [7.8], 379 [7.0]	468, 499, 540, 600 [b]	-	-

[a] results obtained in DCM solutions 0.01 mM. [b] obtained in 1% of F2-PyNA-PTZ in zeonex matrix.

The profile of the absorption spectra appears very similar for the both isomers. We can observe strong absorption bands around 260 nm, that can be signed to the $\pi \to \pi^*$ transitions from aromatic systems of triphenylphosphanimine (Ph₃PN) core and the donor moieties.[153] We can note less intense shoulders in the absorption bands around 320 nm, that can be attributed to the CT transitions from the donor units to the acceptor core.
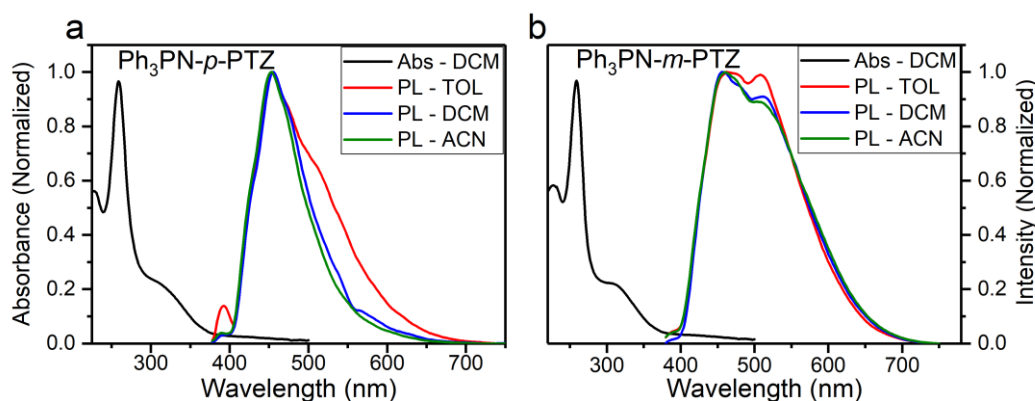
Figure 8.6. *Absorption spectra in DCM solutions 0.01 mM and PL spectra in TOL, DCM and ACN solutions 0.01 mM of **Ph₃PN-p,m-PTZ**.*

Figure 8.6 shows the contribution of photoluminescence that was observed for the variation of the isomers in three different solvents with different polarities: toluene (TOL), dichloromethane (DCM) and acetonitrile (ACN). We can note a different profile of emission considering the isomers. For **Ph₃PN-*p*-PTZ** we observe a minimum vibronic profile of emission with maximum at 453 nm, which suggests contribution of ^{1}LE states and ^{1}CT states in the emission for the *para*-substituted isomer. From the other side, **Ph₃PN-*m*-PTZ** displays two peaks centered at 463 and 509 nm, indicating more contribution of ^{1}LE character of the emission, and being better described as mixture of ^{1}LE+^{1}CT states. With the increase of solvent polarity, we observe the decrease of the peak at 509 nm, suggesting the polarity-related quenching of ^{1}CT states. For both isomers we did not observe a redshift due to less sensitivity of ^{1}LE excited states to changes in solvent polarities.

To further understand the optical properties of the **Ph₃PN-*p,m*-PTZ** in the aggregation state, we investigated the photoluminescent behavior in THF/water mixtures with different water fractions (f_w) at 0.1 mM concentration. The experimental results and photographs (**Figure 8.7**) show that the emission spectra of the compounds show similar behavior in THF/water mixtures. **Ph₃PN-*p*-PTZ** and **Ph₃PN-*m*-PTZ** display very low emission in THF solutions, while the emission is increased

upon addition of water (f_w = 80-90%) indicating evident aggregation induced emission enhancement (AIEE) behavior.
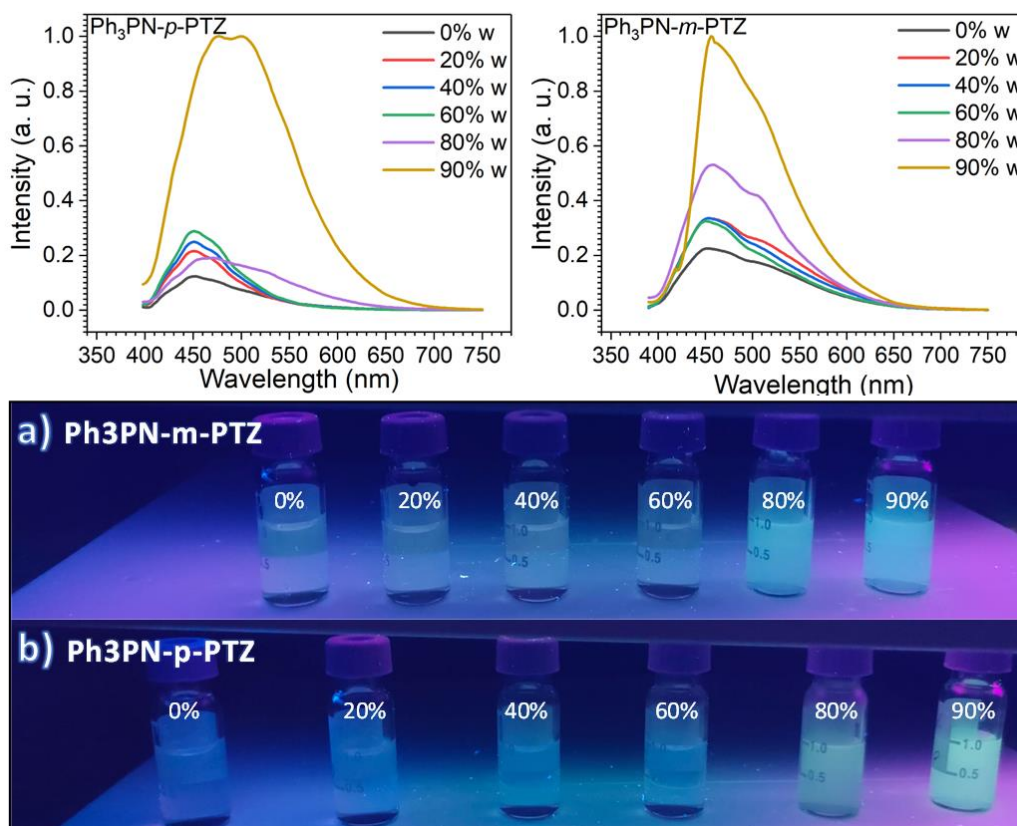
Figure 8.7. *Aggregation studies of **Ph₃PN-p-PTZ** and **Ph₃PN-m-PTZ** in different water fractions (fw) in THF solution 0.1 mM.*

For **Ph₃PN-*p*-PTZ** we observe interesting behavior, where the emission increase is not linear with the increase of water. For 0-60%, we can note a linear increase of the PL intensity, while it decreases at 80%, indicating a plateau where the increase of the polarity of the solution by addition of water stabilizes the CT states until 60% of water and the aggregates starts to be formed at f_w = 80%. For f_w= 90%, where we have more aggregates formed, we observe a great increase of the PL intensity, typical of AIEE behavior. Additionally, we observe differences in the profile of the PL spectra if we compare pure THF PL at f_w = 90%, where we can note two peaks of emission centered at 474 and 503 nm. For **Ph₃PN-*m*-PTZ**, we observe a linear dependence of increased amount of water with the PL intensity. This can be attributed to the linear formation of aggregates with increasing solution polarity.
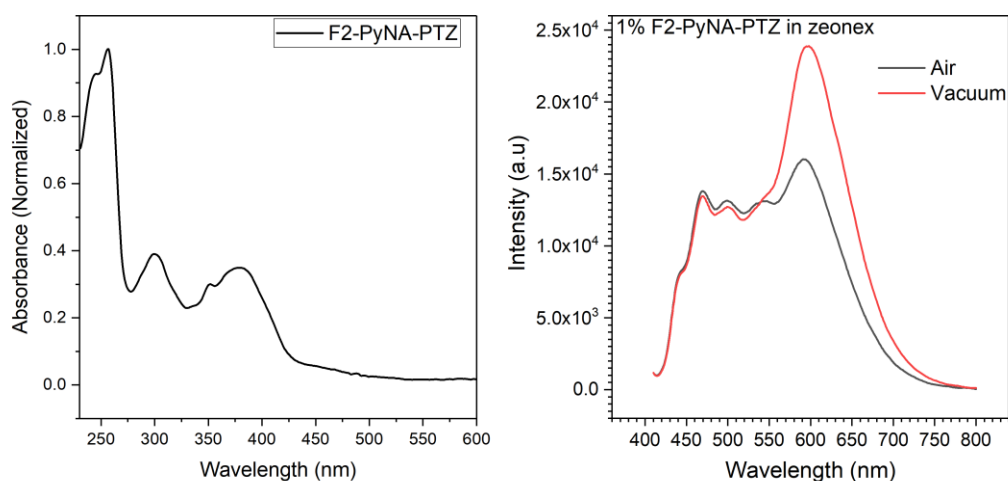
Figure 8.8*. Absorption spectra in DCM solution 0.01 mM and PL spectra in air equilibrated and under vacuum of 1% of **F2-PyNA-PTZ** in Zeonex matrix.*

Figure 8.8 shows the UV-Vis absorption in DCM and PL spectra in zeonex matrix at air equilibrated and vacuum conditions for **F2-PyNA-PTZ**. We can observe strong absorption band around 250 nm, that can be signed to the π→π* transitions from aromatic systems related to benzopyridoimidazoisoquinolinone core (PyNA). [145] We can note less intense broad absorption band around 380 nm, that can be attributed to the CT transitions from the donor unit to the acceptor core. [154] The contribution of photoluminescence was investigated under air and vacuum conditions and we can note the increase of PL intensity under vacuum, indicating that triplet excited states are involved in the emission mechanism. Also, we can note that the PL emission displays very large broad band with maximum wavelengths varying from 468 to 600 nm. This behavior leads to emission to near-white, which is an interesting photophysical behavior.

8.5 Conclusions

This chapter described the design and successful synthesis of one new series of D-A compounds using different regioisomers as acceptor cores, such as triphenylphosphanimine with attached phenothiazine in *para* and *meta* positions. Additionally, a regioisomer derived from benzopyridoimidazoisoquinolinone, was successfully separated by column chromatography, and in sequence, connected to phenothiazine donor. In both cases, the donor was connected by N-C Buchwald-Hartwig cross-coupling reactions obtaining the products in good to moderate yields.

The electrochemical characterization of the triphenylphosphanimine derivatives showed no reduction process in the applied voltage range and displaying different behavior in the oxidation process for the regioisomers of triphenylphosphanimine cores. In turn, the benzopyridoimidazoisoquinolinone derivative showed reversible reduction and oxidation process. The photophysical properties showed AIEE behavior for the compounds derived from phosphanimine system, indicating the versatility of the materials for optoelectronic applications. From the other side, the naphthalene benzopyridoimidazoisoquinolinone showed a very large range of emission in zeonex matrix, indicating the versatility to be applied white emitter as candidate to OLEDs.

8.6 Synthetic details

General procedure to synthesis of Ph$_3$PN-p,m-Br following the literature.[152]

To a round-bottom flask equipped with a condenser 40 mL of water and 6 mL of 98% H$_2$SO$_4$ were added. After the system reached the room-temperature the respective *para* or *ortho* aniline (30 mmol) was added. The system was cooled down to -5ºC and dissolved in water (20mL) sodium nitrite (36 mmol) was added dropwise for 20 minutes. The mixture was stirred for 1h and sodium azide (45 mmol) dissolved in water (25 mL) was added dropwise for 20 minutes. The mixture was stirred for additional 1h, and then neutralized by sodium carbonate. The resulting mixture was extracted with ethyl acetate (3 x 50 mL). The organic layer was dried over sodium sulfate and concentrated in the roto-evaporator to give the respective *para* or *meta* bromo-azidobenzene as a pale-yellow oil, that solidifies in the fridge. The compounds were used in next steps without further purifications (**N$_3$-p-Br** and **N$_3$-m-Br** in 94% and 88% of yield).

The resulting materials were then dissolved in 20 mL of dichloromethane and triphenylphosphine (30 mmol) dissolved in dichloromethane (20 mL) was added dropwise during 15 minutes. After that, the mixture was stirred for 12 h. Then the solvent was removed in the roto-evaporator and hexane was added. The precipitate was filtered under vacuum and washed with hexane to give the target materials.

N-(4-bromophenyl)-1,1,1-triphenyl-λ^5-phosphanimine (**Ph$_3$PN-p-Br**)

Ph₃PN-*p*-Br
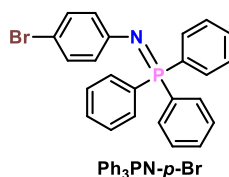
Pale-yellow solid. 95% of yield. ^{1}H NMR (300 MHz, CDCl$_3$) δ 7.82 – 7.67 (m, 6H), 7.58 – 7.41 (m, 9H), 7.08 (dd, J = 8.7, 1.1 Hz, 2H), 6.66 (dd, J = 8.7, 0.8 Hz, 2H).

N-(3-bromophenyl)-1,1,1-triphenyl- λ^5-phosphanimine (**Ph₃PN-*m*-Br**)

Ph₃PN-*m*-Br
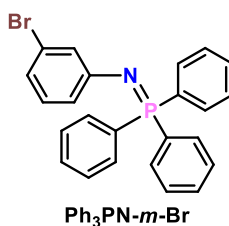
Pale-yellow solid. 94% of yield. ^{1}H NMR (300 MHz, CDCl$_3$) δ 7.78 – 7.69 (m, 6H), 7.57 – 7.42 (m, 9H), 7.06 – 6.91 (m, 1H), 6.86 – 6.72 (m, 2H), 6.64 (m, 1H).

N-(4-(10H-phenothiazin-10-yl)phenyl)-1,1,1-triphenyl-λ^5-phosphanimine (**Ph₃PN-*p*-PTZ)**

Ph₃PN-*p*-PTZ
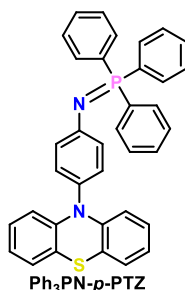
A flame dried 100 mL Schlenk tube equipped with a rubber septum was charged with Ph₃PN-*p*-Br (1.0 eq.); phenothiazine (1.2 eq.), sodium *tert*-butoxide (2.0 eq), Pd$_2$(dba)$_3$ (3 mol%) and [(^{t}-Bu)$_3$PH]BF$_4$ (6 mol%). The atmosphere of the system was changed by argon and degassed toluene (30 mL/mmol) was added and the resulting mixture was heated at 110 °C with stirring under argon atmosphere for 24h. The solution was filtered over celite bed and the solvent removed under reduced pressure. The crude mixture was purified by silica gel column chromatography eluting with DCM:hexane (1:3 v/v). Off-white solid. 53 % of yield. ^{1}H NMR (300 MHz, Acetone-*d$_6$*) δ 7.95 – 7.85 (m, 6H), 7.69 – 7.55 (m, 9H), 7.00 – 6.92 (m, 6H), 6.86 (ddd, J = 8.2, 7.4, 1.7 Hz, 2H), 6.77 (td, J = 7.4, 1.4 Hz, 2H), 6.26 (dd, J = 8.2, 1.3 Hz, 2H). ^{1}H NMR (300 MHz, CDCl$_3$) δ 7.79 (m, 6H), 7.59 – 7.45 (m, 9H), 7.00 – 6.89 (m, 6H), 6.80 (ddd, *J* =

8.1, 7.4, 1.8 Hz, 2H), 6.73 (td, J = 7.3, 1.4 Hz, 2H), 6.27 (dd, J = 8.1, 1.3 Hz, 2H). ^{13}C NMR (75 MHz, CDCl$_3$) δ 151.31, 145.09, 132.72, 132.59, 131.85, 131.81, 131.62, 131.06, 130.30, 130.19, 128.77, 128.61, 126.68, 126.34, 125.24, 125.01, 121.85, 121.78, 119.35, 115.83. HRMS: m/z calcd for C$_{36}$H$_{28}$N$_2$PS (M+H)$^+$: 551.1711; found: 551.1708.

N-(3-(10H-phenothiazin-10-yl)phenyl)-1,1,1-triphenyl-λ^5-phosphanimine (Ph$_3$PN-*m*-PTZ)

Ph$_3$PN-*m*-PTZ
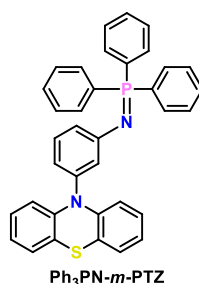
Similar procedure as for **Ph₃PN-*p*-PTZ**. Using **Ph₃PN-*m*-Br**. Off-White solid. 78 % of yield. ^{1}H NMR (300 MHz, CDCl$_3$) δ 7.79 – 7.69 (m, 6H), 7.55 – 7.40 (m, 9H), 7.25 – 7.18 (m, 1H), 7.00 (d, J = 7.9 Hz, 1H), 6.96 – 6.87 (m, 2H), 6.77 – 6.69 (m, 4H), 6.68 – 6.61 (m, 2H), 6.21 – 6.14 (m, 2H). ^{1}H NMR (300 MHz, CD$_2$Cl$_2$) δ 7.81 – 7.69 (m, 6H), 7.58 – 7.43 (m, 9H), 7.22 (td, J = 7.9, 1.1 Hz, 1H), 6.99 – 6.87 (m, 3H), 6.80 – 6.71 (m, 4H), 6.58 (dd, J = 5.3, 4.5 Hz, 2H), 6.21 – 6.09 (m, 2H). ^{13}C NMR (75 MHz, CDCl$_3$) δ 144.38, 140.91, 132.73, 132.60, 132.18, 132.05, 132.01, 131.96, 131.93, 130.87, 128.85, 128.69, 128.60, 128.44, 126.81, 126.73, 126.56, 126.29, 125.54, 125.34, 124.35, 124.11, 122.32, 121.86, 120.27, 119.58, 119.14, 116.13. HRMS: m/z calcd for C$_{36}$H$_{28}$N$_2$PS (M+H)$^+$: 551.1711; found: 551.1716.

*Synthesis of the Isomers **F1,F2-PyNA-Br***

2,3-diamino-5-bromopyridine (2.5 mmol) and 1,8-naphthalic anhydride (2.5 mmol) were uniformly mixed by grinding in 15 mL of glacial acetic acid. The mixture was heated at 120 °C for 24 h under argon with stirring. Then, the mixed solution was poured into distilled water and the yellow precipitate was collected by filtration, washed several times with water, and dried in a vacuum, obtaining 72% yield for mixtures of isomers after chromatography column using CHCl$_3$ as eluent. Then, it was separated by chromatography column using a gradient CHCl$_3$/hexane (6:1) to pure chloroform as eluent. The **F1-PyNA-Br** and **F2-PyNA-Br** were the first and second fraction,

respectively, eluted from the column with majority of **F2-PyNA-Br.** The isomers were isolated as yellow solid in 17% and 47% of yield for F1 and F2, respectively.

10-bromo-7H-benzo[de]pyrido[2',3':4,5]imidazo[2,1-a]isoquinolin-7-one (**F1-PyNA-Br**)

F1-PyNA-Br
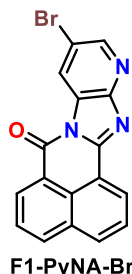
^{1}H NMR (600 MHz, CDCl$_3$) δ 8.88 (dd, J = 7.3, 1.0 Hz, 1H), 8.84 (dd, J = 7.3, 0.9 Hz, 1H), 8.68 (d, J = 2.1 Hz, 1H), 8.32 (d, J = 7.6 Hz, 1H), 8.28 (d, J = 2.1 Hz, 1H), 8.22 (d, J = 8.0 Hz, 1H), 7.88 – 7.81 (m, 2H). ^{13}C NMR (151 MHz, CDCl$_3$) δ 159.15, 151.28, 146.60, 145.23, 137.60, 135.67, 132.96, 132.67, 132.18, 130.10, 127.77, 127.38, 127.32, 127.22, 122.87, 119.85, 117.10.

11-bromo-7H-benzo[de]pyrido[3',2':4,5]imidazo[2,1-a]isoquinolin-7-one (**F2-PyNA-Br**)

F2-PyNA-Br

^{1}H NMR (600 MHz, cdcl$_3$) δ 8.94 (dd, J = 7.3, 1.0 Hz, 1H), 8.90 (d, J = 2.2 Hz, 1H), 8.79 (dd, J = 7.3, 1.1 Hz, 1H), 8.73 (d, J = 2.2 Hz, 1H), 8.33 (dd, J = 8.1, 0.7 Hz, 1H), 8.22 (d, J = 7.7 Hz, 1H), 7.87 – 7.83 (m, 2H). ^{13}C NMR (151 MHz, CDCl3) δ 160.16, 155.01, 151.93, 148.73, 136.14, 133.21, 132.50, 132.18, 129.14, 127.63, 127.14, 127.05, 126.04, 125.20, 122.17, 119.54, 116.05.

11-phenothiazine-7H-benzo[de]pyrido[3',2':4,5]imidazo[2,1-a]isoquinolin-7-one **(F2-PyNA-PTZ)**

F2-PyNA-PTZ
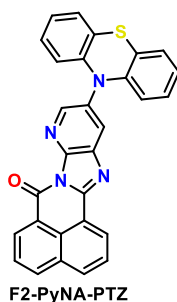
A flame dried 100 mL Schlenk tube equipped with a rubber septum was charged with **F2-PyNA-Br** (1.0 eq.); phenothiazine (1.2 eq.), sodium tert-butoxide (2.0 eq), $Pd_2(dba)_3$ (3 mol%) and $[(t\text{-Bu})_3PH]BF_4$ (6 mol%). The atmosphere of the system was changed by argon and degassed toluene (30 mL/mmol) was added and the resulting mixture was heated at 110 °C with stirring for 24h. The solution was filtered over celite bed and the solvent removed under reduced pressure. The crude mixture was purified by silica gel column chromatography eluting with chloroform/hexane (2:1 v/v), followed by precipitation in methanol/hexane (3:1).Yellow solid. 36 % yield. ^{1}H NMR (300 MHz, $CDCl_3$) δ 9.06 (d, J = 7.3 Hz, 1H), 8.97 – 8.90 (m, 1H), 8.82 (d, J = 7.3 Hz, 1H), 8.75 (dd, J = 2.4, 0.6 Hz, 1H), 8.38 (d, J = 8.3 Hz, 1H), 8.28 (d, J = 8.3 Hz, 1H), 7.94 – 7.85 (m, 2H), 7.08 (dd, J = 5.7, 3.3 Hz, 2H), 6.91 – 6.86 (m, 4H), 6.36 – 6.32 (m, 2H). HRMS: m/z calcd for $C_{29}H_{17}N_4OS$ $(M+H)^+$: 469.1123; found: 469.1121.

Welisson de Pontes Silva

9. *General Conclusions*

This thesis describes the design and synthesis of several series of multifunctional compounds belonging to distinct classes of compounds. In total, 35 unprecedented molecules were designed and synthesized, with full structure characterization by NMR and HRMS. The Pd-catalyzed reactions, such as N-C and C-C cross-coupling, were the base reactions to connect electron-donors and electron-acceptors in different arrangements, such as D-A, D-A-D and D-A-A-D. The electron acceptors covered a wide range of chemical reactions. The chemistry of quinoxalines, perylene, benzotriazoles, phosphanimine, and benzimidazoles was used to obtain functional materials.

Additionally, electrochemical and photophysical behavior were investigated in order to check the suitability of the new materials for optoelectronics applications. The electrochemical and photophysical properties were controlled by different molecular designs, where common electron-donors were connected to new acceptors to be investigated. The materials present different behaviors, depending on the core, regioisomers, and donors attached. It was observed that N-rich electron acceptors such as quinoxaline are attractive candidates to be connected with strong to moderate electron donors, such as phenothiazine, phenoxazine, and acridine derivatives to have the possibility of TADF properties, due to a strong CT character. On the other side, weaker donors such as diphenylamine, azepine derivatives, and carbazoles imply in a more substantial HOMO-LUMO overlap, which decreases the TADF behavior.

The acenaphtopyridopyrazine (NQPy) core in a D-A structure proves to be an excellent strategy to obtain materials that can present TADF properties and control the emission wavelength covering a wide range of colors, from green to red, depending on the strength of the donor connected. Additionally, AIE/AIEE properties were observed, emphasizing the multifunctional properties of the materials. Related to perylene D-A-D derivatives (PTE and PDA), new functional materials were obtained where the low-cost hydrolysis reaction controlled the HOMO-LUMO gap from perylene tetraester to perylene dianhydride. The electrochemical stability and the absorption spectra in the visible region suggest interesting candidates for OPV applications. The asymmetric naphthalenebenzimidazole (BTNA) was connected with different donor units with the addition of the π-spacer aromatic between the donor and acceptor (D-π-A-π-D), which proved as a good strategy to maximize the PL emission in comparison with the

compound with direct connection between the donor and acceptor. Also, the isomer with the phenothiazine in *meta* position shows that the design of the TADF molecules can be affected by the position of the donor on the regioisomers. Other regioisomers derived from pyridinebenzotriazole, presenting a methyl group in three different positions and connected with acridine derivatives in D-A structure, show that the different regioisomers are an interesting alternative to modulate the photophysical properties of the materials to be applied as TADF based OLEDs devices.

Additionally, diquinoxaline and diphenazine in a D_2-A-A-D_2 structure with different donors connected show that these acceptors cores are interesting candidates to obtain TADF properties since a great increment in the PL intensity was observed in degassed conditions, mainly for the compounds with more strong electron-donors, such as phenothiazine, phenoxazine, and acridine derivatives. For the benzopyridoimidazoisoquinolinone (PyNA), where one of the regioisomers was connected with phenothiazine, it showed a wide range of PL emission in the zeonex matrix, indicating the versatility to be applied as a candidate to white emitter in OLEDs. For the compounds derived from the triphenylphosphanimine (Ph3PN) system, the photophysical properties showed AIEE behavior, indicating the versatility of the materials for optoelectronics applications.

Welisson de Pontes Silva

10.   *Experimental part*

10.1 Materials *and equipment*

All the reagents were obtained from commercial sources and used without further purification. The N-C and C-C coupling reactions were performed under Ar atmosphere. The organic solvents were of commercial grade quality. In general, all the compounds were purified by column chromatography on silica gel (60–200 mesh), and recrystallized/crystallized from analytical grade solvents. The purity of the sample was checked by thin-layer chromatography (TLC) (Merck Kieselgel 60F254). ^{1}H and ^{13}C NMR spectra were majority recorded on a Varian Unity Inova spectrometer (^{1}H NMR: 300 MHz, ^{13}C NMR: 75MHz) using tetramethylsilane (δ = 0 ppm) as an internal. High resolution mass spectrometry analyses were performed on a Waters Xevo G2 Q-TOF mass spectrometer (Waters Corporation) equipped with an ESI source operating in positive- ion modes. Full-scan MS data were collected from 100 to 5000 Da in positive ion mode with scan time of 0.1 s. To ensure accurate mass measurements, data were collected in centroid mode and mass was corrected during acquisition using leucine enkephalin solution as an external reference (Lock-Spray TM), which generated reference ion at m/z 556.2771 Da ([M+H]+) in positive ESI mode. The accurate mass and composition for the molecular ion adducts were calculated using the MassLynx software (Waters) incorporated with the instrument. Parameters: Polarity: ES⁺; Analyser: Resolution Mode; Capillary (kV): 4.0000; Sampling Cone: 40.0000-120.0000; Extraction Cone: 4.0000; Source Temperature (°C): 120; Desolvation Temperature (°C): 200; Cone Gas Flow (L/Hr): 100.0; Desolvation Gas Flow (L/Hr): 400.0.

10.2 Photophysical analyses

Steady-state UV-vis absorption and photoluminescence (PL) spectra of the compounds were acquired on a Shimadzu UV-2550 UV-VIS spectrometer and HAMAMATSU C11347-01 spectrometer with an integrating sphere, respectively. The measurements of PL were carried out in solution or in zeonex matrix in a glass sapphire.

10.3 Electrochemical Analyses

The electrochemical characterization of the all compounds were carry out by cyclic voltammetry (CV) in a potentiostat PGSTAT100 AUTOLAB or CHI620 (CH Instruments) and a system of three electrodes, reference electrode (RE) was silver/silver chloride (Ag/AgCl calibrated against ferrocene), working electrode (WE) (platinum disc with 1 mm of diameter) and counter electrode (CE) (platinum wire) in solution of tetrabutylammonium tetrafluoroborate (Bu_4NBF_4) as electrolyte at 100 mM concentration in dichloromethane (DCM) as a solvent. Cyclic voltametric measurements were conducted at room temperature at a scan rate of 50 mV/s and under Argon (Ar) inert atmosphere. The concentration of each compound in solution was 1 mM in the electrochemical cell.

Ionization potential (IP) and electron affinity (EA) were estimated from onset oxidation (E_{ox}) and reduction (E_{red}) potentials, respectively. Where IP and EA are associated with the energy levels of frontier molecular orbitals, HOMO (E_{HOMO}) and LUMO (E_{LUMO}) using the following equations: $E_{HOMO} = -(E_{ox} + 5.1)$; $E_{LUMO} = -(E_{red} + 5.1)$.[78]

10.4 Theoretical details

All theoretical calculations were performed using Schrodinger® software release 2018-1. Density functional theory (DFT) calculations were used to obtain the optimized molecular geometries of all compounds. To calculate the frontier molecular orbitals (FMOs) with HOMO-LUMO spatial distributions were used the hybrid functional B3LYP along the 6-31G** basis set. To excited states calculations to estimate the energies of S_1, T_1 and T_2 were employed the Tamm-Dancoff Approximation (TDA) by time-dependent (TD) DFT at B3LYP/6-31G** level.

11.   References

1.   Huang, Y., Hsiang, E. L., Deng, M. Y. & Wu, S. T. Mini-LED, Micro-LED and OLED displays: present status and future perspectives. *Light Sci. Appl.* **9**, (2020).

2.   Qiu, X. *et al.* Novel 12,12-Dimethyl-7,12-dihydrobenzo[a]acridine as a Deep-Blue Emitting Chromophore for OLEDs with Narrow-Band Emission and Suppressed Efficiency Roll-Off. *J. Mater. Chem. C* (2021) doi:10.1039/d1tc03898b.

3.   Yao, J. *et al.* High efficiency blue/green/yellow/red fluorescent organic light-emitting diodes sensitized by phosphors: General design rules and electroluminescence performance analysis. *J. Mater. Chem. C* **7**, 11293–11302 (2019).

4.   Chaudhry, M. U. *et al.* Organic Light-Emitting Transistors: Advances and Perspectives. *Adv. Funct. Mater.* **30**, 1–15 (2020).

5.   Data, P., Okazaki, M., Minakata, S. & Takeda, Y. Thermally activated delayed fluorescence: Vs. room temperature phosphorescence by conformation control of organic single molecules. *J. Mater. Chem. C* **7**, 6616–6621 (2019).

6.   Lichtman, J. W. & Conchello, J. A. Fluorescence microscopy. *Nat. Methods* **2**, 910–919 (2005).

7.   Mitschke, U. & Bäuerle, P. The electroluminescence of organic materials. *J. Mater. Chem.* **10**, 1471–1507 (2000).

8.   Adachi, C., Tsutsui, T. & Saito, S. Organic electroluminescent device having a hole conductor as an emitting layer. *Appl. Phys. Lett.* **55**, 1489–1491 (1989).

9.   Data, P. & Takeda, Y. Recent Advancements in and the Future of Organic Emitters: TADF- and RTP-Active Multifunctional Organic Materials. *Chemistry - An Asian Journal* vol. 14 1613–1636 (2019).

10.   Sahl, S. J., Hell, S. W. & Jakobs, S. Fluorescence nanoscopy in cell biology. *Nat. Rev. Mol. Cell Biol.* **18**, 685–701 (2017).

11.   SKOOG, D. A., HOLLER, F. J. & CROUCH, S. R. *Principles of Instrumental Analyses. Journal of the Spectroscopical Society of Japan* vol. 9 (1961).

12.   Li, H. Z., Xie, F. M., Li, Y. Q. & Tang, J. X. Recent progress and prospects of fluorescent materials based on narrow emission. *J. Mater. Chem. C* 6471–6511 (2023) doi:10.1039/d3tc00676j.

13. Sahl, S. J., Hell, S. W. & Jakobs, S. Fluorescence nanoscopy in cell biology. *Nat. Rev. Mol. Cell Biol.* **18**, 685–701 (2017).

14. An, Z. *et al.* Stabilizing triplet excited states for ultralong organic phosphorescence. *Nat. Mater.* **14**, 685–690 (2015).

15. Hong, G. *et al.* A Brief History of OLEDs—Emitter Development and Industry Milestones. *Adv. Mater.* **33**, (2021).

16. Yadav, R. A. K., Dubey, D. K., Chen, S. Z., Liang, T. W. & Jou, J. H. Role of Molecular Orbital Energy Levels in OLED Performance. *Sci. Rep.* **10**, 1–15 (2020).

17. C., A., Pahlevani, M. & Welch, G. C. Organic light emitting diodes (OLEDs) with slot-die coated functional layers. *Mater. Adv.* **2**, 628–645 (2021).

18. Sun, N. *et al.* Performance of OLED under mechanical strain: a review. *J. Mater. Sci. Mater. Electron.* **31**, 20688–20729 (2020).

19. Chen, J., Zhao, F. & Ma, D. Hybrid white OLEDs with fluorophors and phosphors. *Mater. Today* **17**, 175–183 (2014).

20. Bauri, J., Choudhary, R. B. & Mandal, G. Recent advances in efficient emissive materials-based OLED applications: a review. *J. Mater. Sci.* **56**, 18837–18866 (2021).

21. *Highly Efficient OLEDs. Highly Efficient OLEDs* (2018). doi:10.1002/9783527691722.

22. Reddy, S. S. *et al.* Highly Efficient Bipolar Deep-Blue Fluorescent Emitters for Solution-Processed Non-Doped Organic Light-Emitting Diodes Based on 9,9-Dimethyl-9,10-dihydroacridine/Phenanthroimadazole Derivatives. *Adv. Opt. Mater.* **4**, 1236–1246 (2016).

23. Data, P. & Takeda, Y. Recent Advancements in and the Future of Organic Emitters: TADF- and RTP-Active Multifunctional Organic Materials. *Chem. - An Asian J.* **14**, 1613–1636 (2019).

24. Maria Angela, V., Anjali, A., Harshini, D. & Nagarajan, S. Organic Light-Emitting Transistors: From Understanding to Molecular Design and Architecture. *ACS Appl. Electron. Mater.* **3**, 550–573 (2021).

25. Xue, Q. & Xie, G. Thermally Activated Delayed Fluorescence beyond Through-Bond Charge Transfer for High-Performance OLEDs. *Adv. Opt. Mater.* **2002204**, 1–23 (2021).

26. Nobuyasu, R. S. Photophysics of TADF Emitters and their application in OLEDs

Photophysics of TADF Emitters and their application in OLEDs. **0**, (2018).

27. Valeur, B. & Berberan-santos, N. A Brief History of Fluorescence and Phosphorescence before the Emergence of Quantum Theory. *J. Chem. Educ.* 731–738 (2011).

28. Mahoro, G. U. *et al.* Recent Advances in Solid-State Lighting Devices Using Transition Metal Complexes Exhibiting Thermally Activated Delayed Fluorescent Emission Mechanism. *Adv. Opt. Mater.* **8**, 1–36 (2020).

29. Chapran, M. *et al.* Realizing 20% External Quantum Efficiency in Electroluminescence with Efficient Thermally Activated Delayed Fluorescence from an Exciplex. *ACS Appl. Mater. Interfaces* **11**, 13460–13471 (2019).

30. Lustig, W. P. *et al.* Chromophore-Based Luminescent Metal-Organic Frameworks as Lighting Phosphors. *Inorg. Chem.* **55**, 7250–7256 (2016).

31. Dias, F. B., Penfold, T. J. & Monkman, A. P. Photophysics of thermally activated delayed fluorescence molecules. *Methods Appl. Fluoresc.* **5**, (2017).

32. Zhang, T. *et al.* Highly Twisted TADF Molecules and Their Applications in OLEDs. *Angew. Chemie Int. Ed.* **17**, 955 (2023).

33. Xu, X. & Yan, B. Recent advances in room temperature phosphorescence materials: design strategies, internal mechanisms and intelligent optical applications. *Phys. Chem. Chem. Phys.* **25**, 1457–1475 (2022).

34. Kenry, Chen, C. & Liu, B. Enhancing the performance of pure organic room-temperature phosphorescent luminophores. *Nat. Commun.* **10**, 1–15 (2019).

35. Yang, J. *et al.* The influence of the molecular packing on the room temperature phosphorescence of purely organic luminogens. *Nat. Commun.* **9**, 1–10 (2018).

36. Pander, P., Data, P. & Dias, F. B. Time-resolved photophysical characterization of triplet-harvesting organic compounds at an oxygen-free environment using an iCCD camera. *J. Vis. Exp.* **2018**, 0–9 (2018).

37. Luo, J. *et al.* Aggregation-induced emission of 1-methyl-1,2,3,4,5-pentaphenylsilole. *Chem. Commun.* **18**, 1740–1741 (2001).

38. Zhao, Z., Zhang, H., Lam, J. W. Y. & Tang, B. Z. Aggregation-Induced Emission: New Vistas at the Aggregate Level. *Angew. Chemie - Int. Ed.* **59**, 9888–9907 (2020).

39. Wang, H. *et al.* Novel thermally activated delayed fluorescence materials-thioxanthone derivatives and their applications for highly efficient OLEDs. *Adv. Mater.* **26**, 5198–5204 (2014).

40. Huang, J. *et al.* Highly Efficient Nondoped OLEDs with Negligible Efficiency Roll-Off Fabricated from Aggregation-Induced Delayed Fluorescence Luminogens. *Angew. Chemie - Int. Ed.* **56**, 12971–12976 (2017).

41. Liu, H. *et al.* High-Performance Non-doped OLEDs with Nearly 100 % Exciton Use and Negligible Efficiency Roll-Off. *Angew. Chemie Int. Ed.* **57**, 9290–9294 (2018).

42. Huang, B. *et al.* Manipulation of Molecular Aggregation States to Realize Polymorphism, AIE, MCL, and TADF in a Single Molecule. *Angew. Chemie - Int. Ed.* **57**, 12473–12477 (2018).

43. Suman, G. R., Pandey, M. & Chakravarthy, A. S. J. Review on new horizons of aggregation induced emission: From design to development. *Mater. Chem. Front.* **5**, 1541–1584 (2021).

44. Mei, J. *et al.* Aggregation-induced emission: The whole is more brilliant than the parts. *Adv. Mater.* **26**, 5429–5479 (2014).

45. Sun, Y., Lei, Z. & Ma, H. Twisted Aggregation-induced Emission Luminogens（AIEgens） Contribute to Mechanochromism Materials : A Review. *J. Mater. Chem. C* (2022) doi:10.1039/d2tc02512d.

46. Liang, X., Tu, Z. L. & Zheng, Y. X. Thermally Activated Delayed Fluorescence Materials: Towards Realization of High Efficiency through Strategic Small Molecular Design. *Chem. - A Eur. J.* **25**, 5623–5642 (2019).

47. Yang, Z. *et al.* Recent advances in organic thermally activated delayed fluorescence materials. *Chem. Soc. Rev.* **46**, 915–1016 (2017).

48. Im, Y. *et al.* Molecular Design Strategy of Organic Thermally Activated Delayed Fluorescence Emitters. *Chem. Mater.* **29**, 1946–1963 (2017).

49. Jiang, T., Liu, Y., Ren, Z. & Yan, S. The design, synthesis and performance of thermally activated delayed fluorescence macromolecules. *Polym. Chem.* **11**, 1555–1571 (2020).

50. Dos Santos, P. L., Etherington, M. K. & Monkman, A. P. Chemical and conformational control of the energy gaps involved in the thermally activated delayed fluorescence mechanism. *J. Mater. Chem. C* **6**, 4842–4853 (2018).

51. Che, W., Xie, Y. & Li, Z. Structural Design of Blue-to-Red Thermally-Activated Delayed Fluorescence Molecules by Adjusting the Strength between Donor and Acceptor. *Asian J. Org. Chem.* **9**, 1262–1276 (2020).

52. Godumala, M., Choi, S., Cho, M. J. & Choi, D. H. Recent breakthroughs in thermally activated delayed fluorescence organic light emitting diodes containing non-doped emitting layers. *J. Mater. Chem. C* **7**, 2172–2198 (2019).

53. Rayappa Naveen, K., Prabhu CP, K., Braveenth, R. & Hyuk Kwon, J. Molecular Design Strategy for Orange Red Thermally Activated Delayed Fluorescence Emitters in Organic Light-Emitting Diodes (OLEDs). *Chem. - A Eur. J.* **28**, (2022).

54. Braveenth, R., Raagulan, K., Kim, Y. J. & Kim, B. M. Recent advances in green thermally activated delayed fluorescence emitters towards high colour purity and good electroluminescence performance. *Mater. Adv.* 374–388 (2022) doi:10.1039/d2ma00967f.

55. Zhan, L. *et al.* A Simple Organic Molecule Realizing Simultaneous TADF, RTP, AIE, and Mechanoluminescence: Understanding the Mechanism Behind the Multifunctional Emitter. *Angew. Chemie - Int. Ed.* **58**, 17651–17655 (2019).

56. Xu, Z., Hean, D., Climent, C., Casanova, D. & Wolf, M. O. Switching between TADF and RTP: anion-regulated photoluminescence in organic salts and co-crystals. *Mater. Adv.* **2**, 5777–5784 (2021).

57. Hall, D. *et al.* Diindolocarbazole - achieving multiresonant thermally activated delayed fluorescence without the need for acceptor units. *Mater. horizons* **9**, 1068–1080 (2022).

58. Kukhta, N. A., Huang, R., Batsanov, A. S., Bryce, M. R. & Dias, F. B. Achieving conformational control in room-temperature phosphorescence and thermally activated delayed fluorescence emitters by functionalization of the central core. *J. Phys. Chem. C* **123**, 26536–26546 (2019).

59. Hall, D. *et al.* Benchmarking DFT Functionals for Excited-State Calculations of Donor-Acceptor TADF Emitters: Insights on the Key Parameters Determining Reverse Inter-System Crossing. *J. Phys. Chem. A* (2022) doi:10.1021/acs.jpca.2c08201.

60. Lv, L. L., Yuan, K., Zhao, T. Y., Li, H. X. & Wang, Y. C. Theoretical Studies on the Photophysical Properties of the Ag(I) Complex for Thermally Activated Delayed Fluorescence Based on TD-DFT and Path Integral Dynamic Approaches. *ACS Omega* **7**, 7380–7392 (2022).

61. Li, F. *et al.* Theoretical Study on Thermally Activated Delayed Fluorescence Emitters in White Organic Light-Emitting Diodes: Emission Mechanism and Molecular Design. *J. Phys. Chem. A* **124**, 7526–7537 (2020).

62. Zhang, K. *et al.* Theoretical Study on the Light-Emitting Mechanism of Multifunctional Thermally Activated Delayed Fluorescence Molecules. *J. Phys. Chem. C* **126**, 2437–2446 (2022).

63. Goya, T. *et al.* A New Entry to Purely Organic Thermally Activated Delayed Fluorescence Emitters Based on Pyrido[2,3-b]pyrazine-Dihydrophenazasilines Donor-Acceptor Dyad. *Asian J. Org. Chem.* **11**, 1–7 (2022).

64. Izumi, S. *et al.* Thermally Activated Delayed Fluorescent Donor–Acceptor–Donor–Acceptor π-Conjugated Macrocycle for Organic Light-Emitting Diodes. *J. Am. Chem. Soc.* **142**, 1482–1491 (2020).

65. Sonar, P., Ng, G. M., Lin, T. T., Dodabalapur, A. & Chen, Z. K. Solution processable low bandgap diketopyrrolopyrrole (DPP) based derivatives: Novel acceptors for organic solar cells. *J. Mater. Chem.* **20**, 3626–3636 (2010).

66. Noguchi, Y. & Sugino, O. High-Lying Triplet Excitons of Thermally Activated Delayed Fluorescence Molecules. *J. Phys. Chem. C* **121**, 20687–20695 (2017).

67. Sun, J. W. *et al.* Thermally Activated Delayed Fluorescence from Azasiline Based Intramolecular Charge-Transfer Emitter (DTPDDA) and a Highly Efficient Blue Light Emitting Diode. *Chem. Mater.* **27**, 6675–6681 (2015).

68. Goushi, K., Yoshida, K., Sato, K. & Adachi, C. Organic light-emitting diodes employing efficient reverse intersystem crossing for triplet-to-singlet state conversion. *Nat. Photonics* **6**, 253–258 (2012).

69. Mane, S. K. B. *et al.* Tuning the organic persistent roomerature phosphorescence through aggregated states. *J. Mater. Chem. C* **7**, 15219–15224 (2019).

70. Data, P. *et al.* Dibenzo[a,j]phenazine-Cored Donor-Acceptor-Donor Compounds as Green-to-Red/NIR Thermally Activated Delayed Fluorescence Organic Light Emitters. *Angew. Chemie - Int. Ed.* **55**, 5739–5744 (2016).

71. Li, H. *et al.* Highly Efficient Orange-Red Thermally Activated Delayed Fluorescence Compounds Comprising Dual Dicyano-Substituted Pyrazine/Quinoxaline Acceptors. *Chempluschem* **86**, 95–102 (2021).

72. Huang, T., Liu, D., Jiang, J. & Jiang, W. Quinoxaline and Pyrido[x,y-b]pyrazine-Based Emitters: Tuning Normal Fluorescence to Thermally Activated Delayed Fluorescence and Emitting Color over the Entire Visible-Light Range. *Chem. - A Eur. J.* **25**, 10926–10937 (2019).

73. Yu, L. *et al.* Molecular design to regulate the photophysical properties of

multifunctional TADF emitters towards high-performance TADF-based OLEDs with EQEs up to 22.4% and small efficiency roll-offs. *Chem. Sci.* **9**, 1385–1391 (2018).

74. Sk, B., Sharma, S., James, A., Kundu, S. & Patra, A. N-Rich electron acceptors: triplet harvesting in multichromophoric pyridoquinoxaline and pyridopyrazine-based organic emitters. *J. Mater. Chem. C* **8**, 12943–12950 (2020).

75. Xie, F. M. *et al.* Rational Molecular Design of Dibenzo[a, c]phenazine-Based Thermally Activated Delayed Fluorescence Emitters for Orange-Red OLEDs with EQE up to 22.0%. *ACS Appl. Mater. Interfaces* **11**, 26144–26151 (2019).

76. Yu, L. & Yang, C. Multipath exciton harvesting in diazine-based luminescent materials and their applications for organic light-emitting diodes. *J. Mater. Chem. C* **9**, 17265–17286 (2021).

77. Kim, G. H. *et al.* Controlling the exciton lifetime of blue thermally activated delayed fluorescence emitters using a heteroatom-containing pyridoindole donor moiety. *Mater. Horizons* **4**, 619–624 (2017).

78. Cardona, C. M., Li, W., Kaifer, A. E., Stockdale, D. & Bazan, G. C. Electrochemical considerations for determining absolute frontier orbital energy levels of conjugated polymers for solar cell applications. *Adv. Mater.* **23**, 2367–2371 (2011).

79. Kothavale, S., Chung, W. J. & Lee, J. Y. Color tuning of dibenzo[a,c]phenazine-2,7-dicarbonitrile-derived thermally activated delayed fluorescence emitters from yellow to deep-red. *J. Mater. Chem. C* **8**, 7059–7066 (2020).

80. Chen, J.-X. *et al.* Red Organic Light-Emitting Diode with External Quantum Efficiency beyond 20% Based on a Novel Thermally Activated Delayed Fluorescence Emitter. *Adv. Sci.* **5**, 1800436 (2018).

81. Hong, G. *et al.* Fluorinated dibenzo[a , c]-phenazine-based green to red thermally activated delayed fluorescent OLED emitters . *J. Mater. Chem. C* **10**, 4757–4766 (2022).

82. Chen, J. X. *et al.* Efficient Orange-Red Thermally Activated Delayed Fluorescence Emitters Feasible for Both Thermal Evaporation and Solution Process. *ACS Appl. Mater. Interfaces* **11**, 29086–29093 (2019).

83. Urban, M. *et al.* TADF Invariant of Host Polarity and Ultralong Fluorescence Lifetimes in a Donor-Acceptor Emitter Featuring a Hybrid Sulfone-Triarylboron Acceptor**. *Angew. Chemie Int. Ed.* **62**, (2023).

84. Klimash, A. *et al.* Intermolecular interactions in molecular crystals and their effect on thermally activated delayed fluorescence of helicene-based emitters. *J. Mater. Chem. C* **6**, 10557–10568 (2018).

85. Maggiore, A. *et al.* Novel Easy to Synthesize Benzonitrile Compounds with Mixed Carbazole and Phenoxazine Substituents Exhibiting Dual Emission and TADF Properties. *J. Phys. Chem. B* **126**, 2740–2753 (2022).

86. Okazaki, M. *et al.* Thermally activated delayed fluorescent phenothiazine–dibenzo[a,j]phenazine–phenothiazine triads exhibiting tricolor-changing mechanochromic luminescence. *Chem. Sci.* **8**, 2677–2686 (2017).

87. Etherington, M. K. *et al.* Regio- and conformational isomerization critical to design of efficient thermally-activated delayed fluorescence emitters. *Nat. Commun.* **8**, 14987 (2017).

88. Zhang, J. *et al.* Design of Stimuli-Responsive Phenothiazine Derivatives with Triplet-Related Dual Emission and High-Contrast Mechanochromism Guided by Polymorph Prediction. *Chem. – A Eur. J.* **28**, (2022).

89. Xiang, S. *et al.* Highly efficient yellow nondoped thermally activated delayed fluorescence OLEDs by utilizing energy transfer between dual conformations based on phenothiazine derivatives. *Dye. Pigment.* **170**, 107636 (2019).

90. Marghad, I. *et al.* Control of the dual emission from a thermally activated delayed fluorescence emitter containing phenothiazine units in organic light-emitting diodes. *RSC Adv.* **9**, 4336–4343 (2019).

91. Hong, Y., Lam, J. W. Y. & Tang, B. Z. Aggregation-induced emission: phenomenon, mechanism and applications. *Chem. Commun.* 4332 (2009) doi:10.1039/b904665h.

92. Liu, Y. *et al.* Tuning the electronic nature of aggregation-induced emission chromophores with enhanced electron-transporting properties. *J. Mater. Chem.* **22**, 5184–5189 (2012).

93. Yang, Z. *et al.* High-Tg carbazole derivatives as a new class of aggregation-induced emission enhancement materials. *J. Mater. Chem.* **20**, 7352–7359 (2010).

94. Cekaviciute, M. *et al.* Towards blue AIE/AIEE: Synthesis and applications in OLEDs of tetra-/triphenylethenyl substituted 9,9-dimethylacridine derivatives. *Molecules* **25**, (2020).

95. Li, C. & Wonneberger, H. Perylene imides for organic photovoltaics: Yesterday,

today, and tomorrow. *Adv. Mater.* **24**, 613–636 (2012).

96. Zhu, M., Chen, Y., Guo, H., Yang, F. & Song, X. Perylene liquid crystals with multiple alkyl chains: Investigation of the influence of peripheral alkyl chain number on mesomorphic and photophysical properties. *New J. Chem.* **42**, 8998–9005 (2018).

97. Huang, C., Barlow, S. & Marder, S. R. Perylene-3,4,9,10-tetracarboxylic acid diimides: Synthesis, physical properties, and use in organic electronics. *J. Org. Chem.* **76**, 2386–2407 (2011).

98. Dubey, R. K. *et al.* Tunable and highly efficient light-harvesting antenna systems based on 1,7-perylene-3,4,9,10-tetracarboxylic acid derivatives. *Chem. Sci.* **7**, 3517–3532 (2016).

99. Reghu, R. R. *et al.* Air stable electron-transporting and ambipolar bay substituted perylene bisimides. *J. Mater. Chem.* **21**, 7811–7819 (2011).

100. Imran, M. *et al.* Intersystem crossing: via charge recombination in a perylene-naphthalimide compact electron donor/acceptor dyad. *J. Mater. Chem. C* **8**, 8305–8319 (2020).

101. Macedo, A. G. *et al.* Perylene derivatives for solar cells and energy harvesting: a review of materials, challenges and advances. *J. Mater. Sci. Mater. Electron.* **30**, 15803–15824 (2019).

102. Nowak-Król, A. & Würthner, F. Progress in the synthesis of perylene bisimide dyes. *Org. Chem. Front.* **6**, 1272–1318 (2019).

103. Würthner, F. Perylene bisimide dyes as versatile building blocks for functional supramolecular architectures. *Chem. Commun.* **4**, 1564–1579 (2004).

104. Qiu, W., Chen, S., Sun, X., Liu, Y. & Zhu, D. Suzuki coupling reaction of 1,6,7,12-tetrabromoperylene bisimide. *Org. Lett.* **8**, 867–870 (2006).

105. Huo, L., Zhou, Y. & Li, Y. Synthesis and absorption spectra of n-type conjugated polymers based on perylene diimide. *Macromol. Rapid Commun.* **29**, 1444–1448 (2008).

106. Sharma, V., Chandra, F., Sahoo, D. & Koner, A. L. Efficient Microwave-Assisted Synthesis of Sonogashira-Coupled Perylene Monoimide Derivatives: Impact of Electron-Donating Groups on Optoelectronic Properties. *European J. Org. Chem.* **2017**, 6901–6905 (2017).

107. Pearce, N., Davies, E. S. & Champness, N. R. Electrochemical and spectroelectrochemical investigations of perylene peri-tetracarbonyl species.

Dye. Pigment. **183**, 108735 (2020).

108. Xia, G. *et al.* A TADF Emitter Featuring Linearly Arranged Spiro-Donor and Spiro-Acceptor Groups: Efficient Nondoped and Doped Deep-Blue OLEDs with CIEy <0.1. *Angew. Chemie - Int. Ed.* (2021) doi:10.1002/anie.202100423.

109. Xiao, P. *et al.* Emergence of white organic light-emitting diodes based on thermally activated delayed fluorescence. *Appl. Sci.* **8**, (2018).

110. Chen, J. X. *et al.* Origin of thermally activated delayed fluorescence in a donor-acceptor type emitter with an optimized nearly planar geometry. *J. Mater. Chem. C* **8**, 13263–13269 (2020).

111. Yu, L. *et al.* Pyrido[2,3-b]pyrazine-based full-color fluoresent materials for high-performance OLEDs. *J. Mater. Chem. C* **8**, 12445–12449 (2020).

112. Yoon, J. *et al.* Asymmetric Host Molecule Bearing Pyridine Core for Highly Efficient Blue Thermally Activated Delayed Fluorescence OLEDs. *Chem. - A Eur. J.* **26**, 16383–16391 (2020).

113. Rajakannu, P. *et al.* Naphthalene Benzimidazole Based Neutral Ir(III) Emitters for Deep Red Organic Light-Emitting Diodes. *Inorg. Chem.* **59**, 12461–12470 (2020).

114. Gao, M. *et al.* Nonvolatile Ternary Memristor Based on Fluorene-Benzimidazole Copolymer/Au NP Composites. *Nanomaterials* **12**, (2022).

115. Baraket, F. *et al.* Novel phenoxazine-benzonitrile and phenothiazine-benzonitrile donor-acceptor molecules with thermally activated delayed fluorescence (TADF). *Dye. Pigment.* **175**, 1–5 (2020).

116. Schillmöller, T., Ruth, P. N., Herbst-Irmer, R. & Stalke, D. Analysis of Solid-State Luminescence Emission Amplification at Substituted Anthracenes by Host–Guest Complex Formation. *Chem. – A Eur. J.* **26**, 17390–17398 (2020).

117. Okazaki, M. *et al.* Thermally activated delayed fluorescent phenothiazine-dibenzo[a,j]phenazine-phenothiazine triads exhibiting tricolor-changing mechanochromic luminescence. *Chem. Sci.* **8**, 2677–2686 (2017).

118. Data, P. & Takeda, Y. Recent Advancements in and the Future of Organic Emitters: TADF- and RTP-Active Multifunctional Organic Materials. *Chem. - An Asian J.* **14**, 1613–1636 (2019).

119. Yang, X. *et al.* Thieno[3,2-b]thiophene-DPP based near-infrared nanotheranostic agent for dual imaging-guided photothermal/photodynamic synergistic therapy. *J. Mater. Chem. B* **7**, 2454–2462 (2019).

120. Wang, W. *et al.* Type-I organic photosensitizers with two complementary reactive oxygen species based on donor-acceptor (D-A) molecules. *Dye. Pigment.* **218**, 111444 (2023).

121. Chatir, E. *et al.* Synthesis of Redox-Active Photochromic Phenanthrene Derivatives. *Chem. - A Eur. J.* **28**, (2022).

122. de Oliveira, A. H. *et al.* Non-symmetrical three and two-core ring mesogens based on quinoxaline and benzimidazole derivatives: Supramolecular layers through amphoteric donating/accepting H-bonds. *J. Mol. Struct.* **1180**, 399–405 (2019).

123. Liu, Y. *et al.* Quinoxaline-Based Semiconducting Polymer Dots for in Vivo NIR-II Fluorescence Imaging. *Macromolecules* **52**, acs.macromol.9b01142 (2019).

124. Kumar, S. *et al.* Investigation of Intramolecular Through-Space Charge-Transfer States in Donor-Acceptor Charge-Transfer Systems. *J. Phys. Chem. Lett.* **12**, 2820–2830 (2021).

125. Woon, K. L. *et al.* Intramolecular Dimerization Quenching of Delayed Emission in Asymmetric D-D'-A TADF Emitters. *J. Phys. Chem. C* **123**, 12400–12410 (2019).

126. Huang, T., Jiang, W. & Duan, L. Recent progress in solution processable TADF materials for organic light-emitting diodes. *J. Mater. Chem. C* **6**, 5577–5596 (2018).

127. Zou, Y., Gong, S., Xie, G. & Yang, C. Design Strategy for Solution-Processable Thermally Activated Delayed Fluorescence Emitters and Their Applications in Organic Light-Emitting Diodes. *Adv. Opt. Mater.* **6**, 1800568 (2018).

128. Wong, M. Y. & Zysman-Colman, E. Purely Organic Thermally Activated Delayed Fluorescence Materials for Organic Light-Emitting Diodes. *Adv. Mater.* **29**, (2017).

129. Chen, Z. *et al.* Highly Efficient Purely Organic Phosphorescence Light-Emitting Diodes Employing a Donor–Acceptor Skeleton with a Phenoxaselenine Donor. *Adv. Sci.* 2207003 (2023) doi:10.1002/advs.202207003.

130. Hosono, T. *et al.* The regioisomeric effect on the excited-state fate leading to room-temperature phosphorescence or thermally activated delayed fluorescence in a dibenzophenazine-cored donor-acceptor-donor system. *J. Mater. Chem. C* **10**, 4905–4913 (2022).

131. Wang, X. Y. *et al.* A 2-phenylfuro[2,3-b]quinoxaline-triphenylamine-based

emitter: photophysical properties and application in TADF-sensitized fluorescence OLEDs. *New J. Chem.* 18854–18864 (2022) doi:10.1039/d2nj03508a.

132. Braveenth, R. *et al.* High efficiency green TADF emitters of acridine donor and triazine acceptor D-A-D structures. *J. Mater. Chem. C* **7**, 7672–7680 (2019).

133. Matulaitis, T. *et al.* Impact of Donor Substitution Pattern on the TADF Properties in the Carbazolyl-Substituted Triazine Derivatives. *J. Phys. Chem. C* **121**, 23618–23625 (2017).

134. Rayappa Naveen, K., Prabhu CP, K., Braveenth, R. & Hyuk Kwon, J. Molecular Design Strategy for Orange Red Thermally Activated Delayed Fluorescence Emitters in Organic Light-Emitting Diodes (OLEDs). *Chem. – A Eur. J.* **28**, (2022).

135. Hempe, M. *et al.* Intramolecular Hydrogen Bonding in Thermally Activated Delayed Fluorescence Emitters: Is There Evidence beyond Reasonable Doubt? *J. Phys. Chem. Lett.* **13**, 8221–8227 (2022).

136. Huang, T., Liu, D., Jiang, J. & Jiang, W. Quinoxaline and Pyrido[x , y - b]pyrazine-Based Emitters: Tuning Normal Fluorescence to Thermally Activated Delayed Fluorescence and Emitting Color over the Entire Visible-Light Range. *Chem. – A Eur. J.* **25**, 10926–10937 (2019).

137. Zoidis, G. *et al.* The Triazole Ring as a Privileged Scaffold for Putative Antifungals: Synthesis and Evaluation of a Series of New Analogues. *ChemMedChem* **16**, 134–144 (2021).

138. Vala, D. P., Vala, R. M. & Patel, H. M. Versatile Synthetic Platform for 1,2,3-Triazole Chemistry. *ACS Omega* **7**, 36945–36987 (2022).

139. Lauria, A. *et al.* 1,2,3-Triazole in Heterocyclic Compounds, Endowed with Biological Activity, through 1,3-Dipolar Cycloadditions. *European J. Org. Chem.* **2014**, 3289–3306 (2014).

140. Yeap, G. Y., Balamurugan, S., Srinivasan, M. V. & Kannan, P. Synthesis and comparative study on phase transition behavior of triazole-cored liquid crystals armed with cholesterol and double or triple aromatic rings systems. *New J. Chem.* **37**, 1906–1911 (2013).

141. Gimeno, N. *et al.* 'Click chemistry' as a versatile route to synthesize and modulate bent-core liquid crystalline materials. *J. Mater. Chem.* **22**, 16791–16800 (2012).

142. Bookser, B. C. *et al.* Solvent-Controlled, Site-Selective N -Alkylation Reactions of Azolo-Fused Ring Heterocycles at N1-, N2-, and N3-Positions, Including Pyrazolo[3,4- d]pyrimidines, Purines, [1,2,3]Triazolo[4,5]pyridines, and Related Deaza-Compounds. *J. Org. Chem.* **83**, 6334–6353 (2018).

143. Kozlova, A. *et al.* Rational Design of Original Fused-Cycle Selective Inhibitors of Tryptophan 2,3-Dioxygenase. *J. Med. Chem.* **64**, 10967–10980 (2021).

144. Sk, B., Sharma, S., James, A., Kundu, S. & Patra, A. N-Rich electron acceptors: triplet harvesting in multichromophoric pyridoquinoxaline and pyridopyrazine-based organic emitters. *J. Mater. Chem. C* **8**, 12943–12950 (2020).

145. Nayak, S. R., Girase, J. D., Nagar, M. R., Jou, J. H. & Vaidyanathan, S. Solution Processable Deep-Blue OLEDs Based on Benzimidazole-TPA Conjugated through 9,9-Diethyl Fluorene (D-π-A) Luminophore with a Hybridized Local and Charge Transfer Excited State. *Journal of Physical Chemistry C* vol. 127 10291–10302 (2023).

146. Yildiz, U., Kandemir, I., Cömert, F., Akkoç, S. & Coban, B. Synthesis of naphthalimide derivatives with potential anticancer activity, their comparative ds- and G-quadruplex-DNA binding studies and related biological activities. *Mol. Biol. Rep.* **47**, 1563–1572 (2020).

147. Mamada, M. *et al.* Benzimidazole derivatives: Synthesis, physical properties, and n-type semiconducting properties. *Chem. - A Eur. J.* **20**, 11835–11846 (2014).

148. Smith, D. A. *et al.* From Cyclic Iminophosphoranes to π-Conjugated Materials. *Angew. Chemie Int. Ed.* **48**, 9109–9113 (2009).

149. Ullrich, S., Kovačević, B., Xie, X. & Sundermeyer, J. Phosphazenyl Phosphines: The Most Electron-Rich Uncharged Phosphorus Brønsted and Lewis Bases. *Angew. Chemie Int. Ed.* **58**, 10335–10339 (2019).

150. Joly, D., Bouit, P. A. & Hissler, M. Organophosphorus derivatives for electronic devices. *J. Mater. Chem. C* **4**, 3686–3698 (2016).

151. Rotering, P., Wilm, L. F. B., Werra, J. A. & Dielmann, F. Pyridinylidenaminophosphines: Facile Access to Highly Electron-Rich Phosphines. *Chem. - A Eur. J.* **26**, 406–411 (2020).

152. Savva, A. C. *et al.* Preparation of Blatter Radicals via Aza-Wittig Chemistry: The Reaction of N-Aryliminophosphoranes with 1-(Het)aroyl-2-aryldiazenes. *J. Org. Chem.* **82**, 7564–7575 (2017).

153. Buß, F. *et al.* Tris(tetramethylguanidinyl)phosphine: The Simplest Non-ionic Phosphorus Superbase and Strongly Donating Phosphine Ligand. *Chem. - A Eur. J.* **28**, 1–7 (2022).

154. Zhang, H. *et al.* Ternary Memory Devices Based on Bipolar Copolymers with Naphthalene Benzimidazole Acceptors and Fluorene/Carbazole Donors. *Macromolecules* **52**, 9364–9375 (2019).

12.   Appendices

12.1 NQPy-Donor compounds
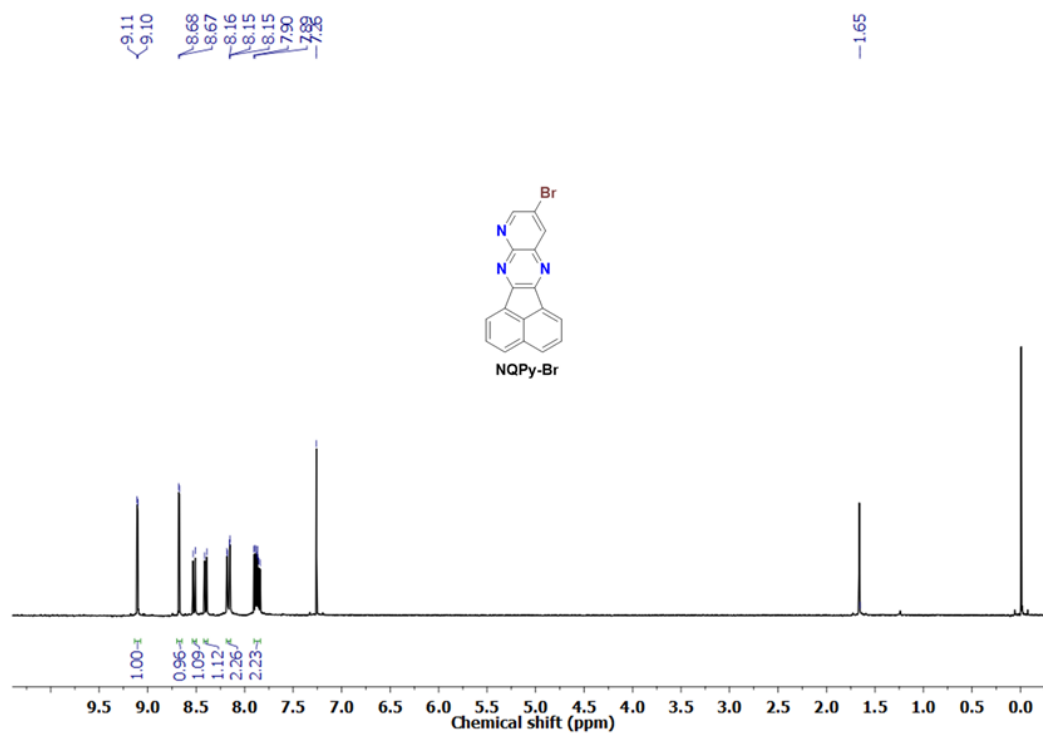
^{1}H NMR (300 MHz) in CDCl$_3$ of the compound **NQPy-Br**.
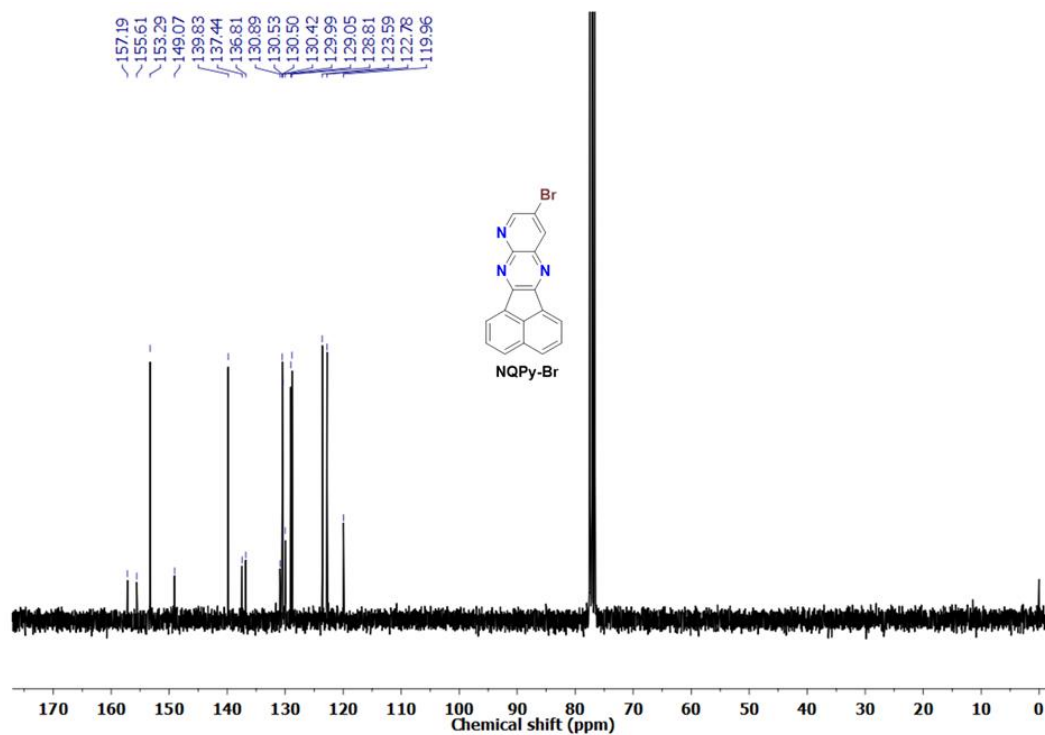
^{13}C NMR (75 MHz) in CDCl$_3$ of the compound **NQPy-Br**.
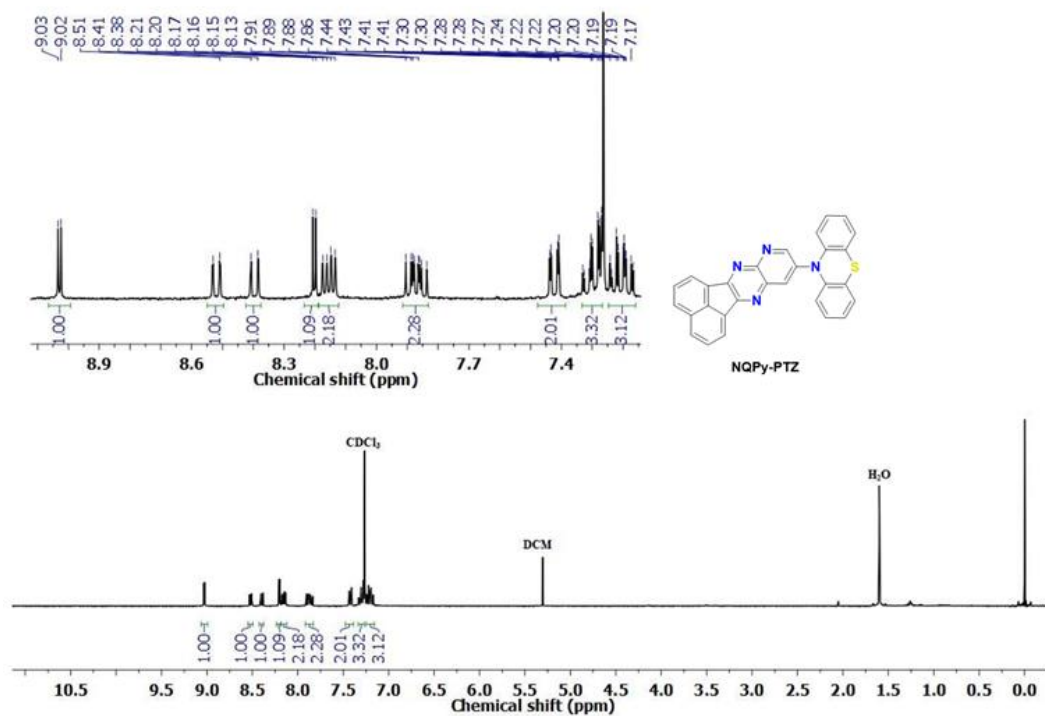
^{1}H NMR (300 MHz) in CDCl$_3$ of the compound **NQPy-PTZ**.
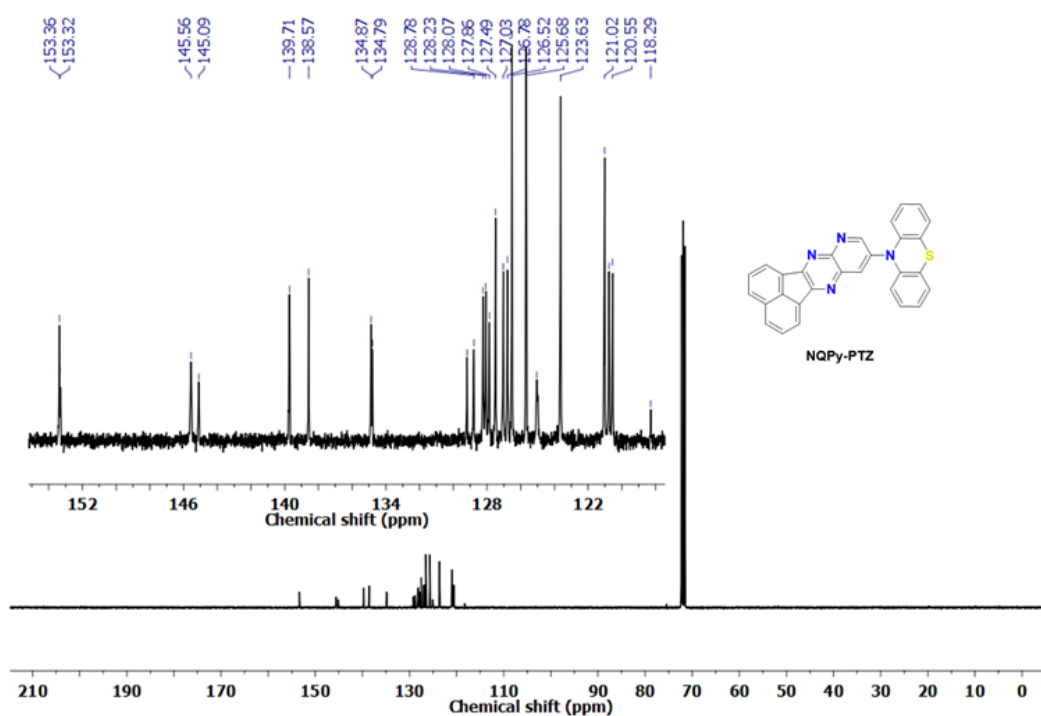
^{13}C NMR (75 MHz) in 1,1,2,2-Tetrachloroethane-d$_2$ of the compound **NQPy-PTZ**

HRMS (TOF MS ES$^+$) of the compound **NQPy-PTZ.**

Welisson de Pontes Silva
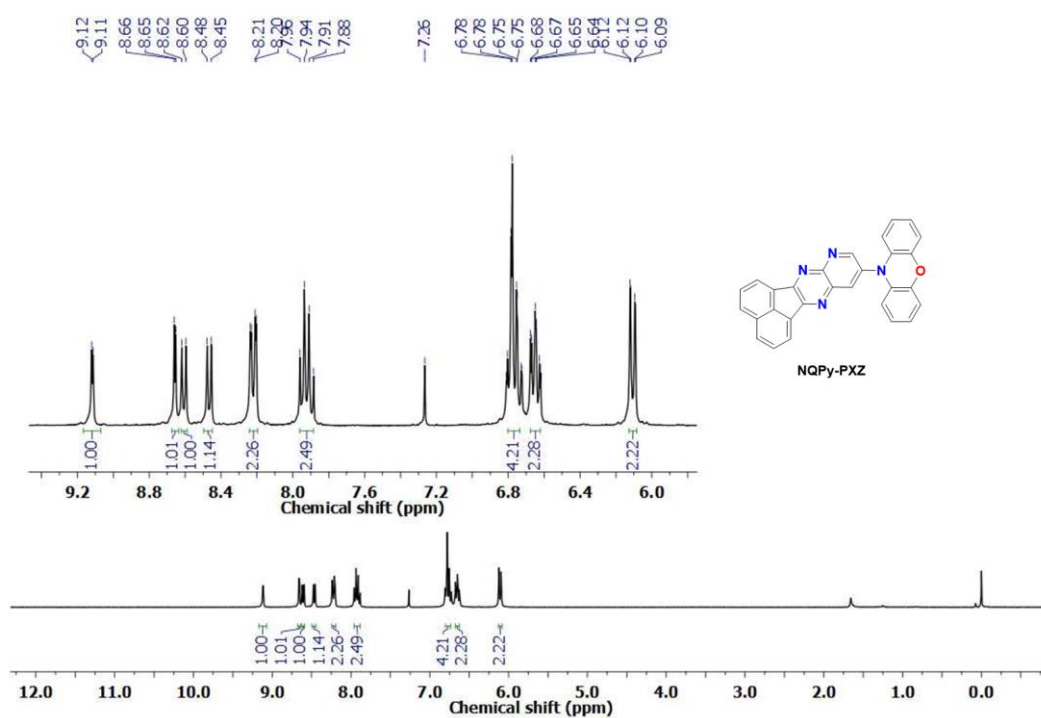
*1H NMR (300 MHz) in CDCl₃ of the compound **NQPy-PXZ.***
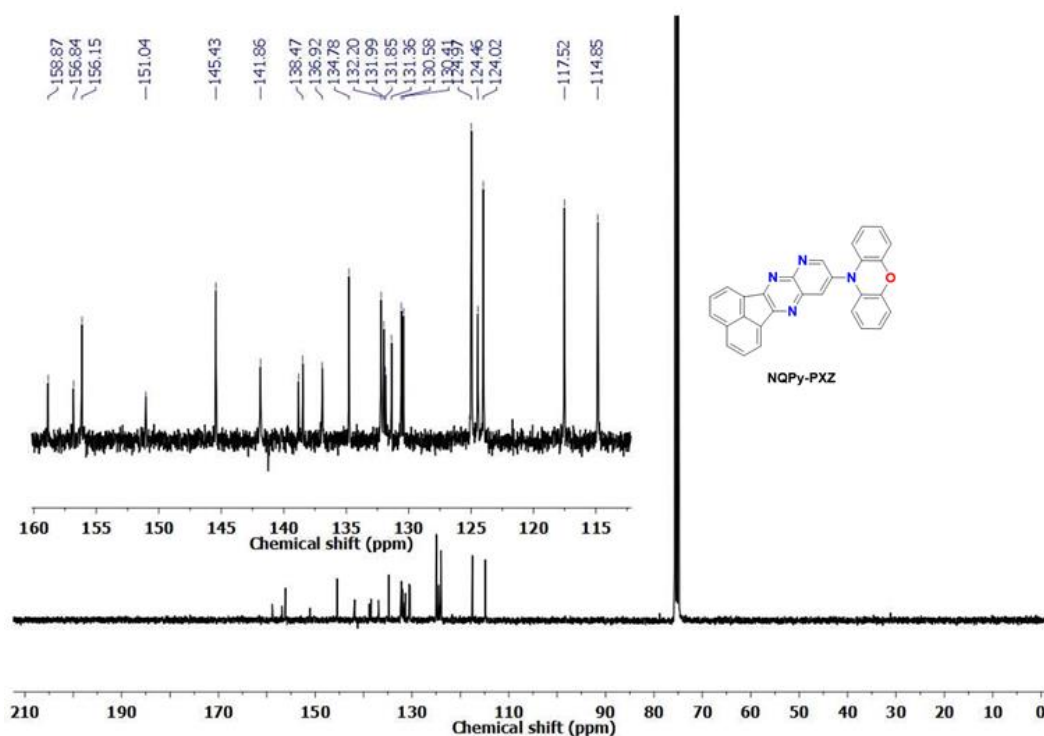
*13C NMR (75 MHz) in 1,1,2,2-Tetrachloroethane-d₂ of the compound **NQPy-PXZ***
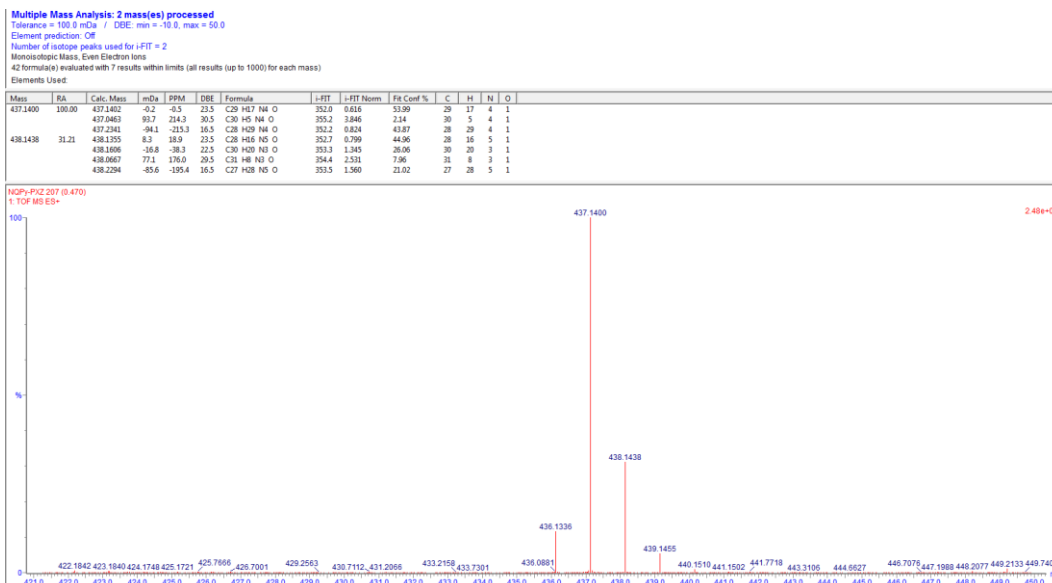
HRMS (TOF MS ES⁺) of the compound **NQPy-PXZ.**
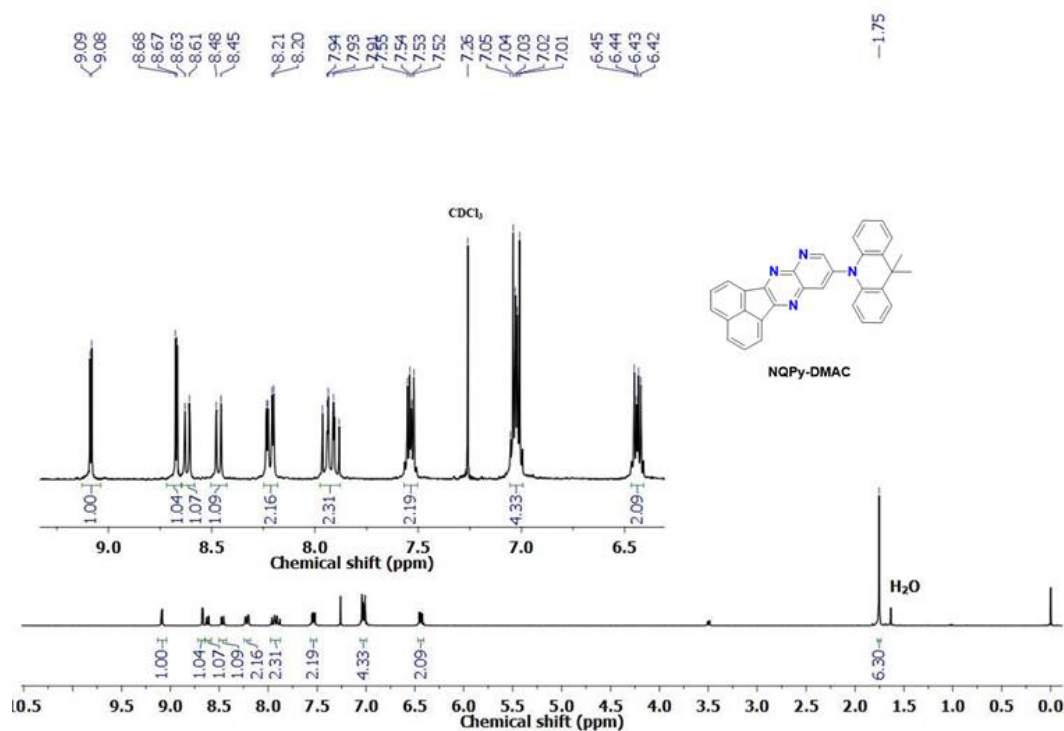
^{1}H NMR (300 MHz) in CDCl$_3$ of the compound **NQPy-DMAC**
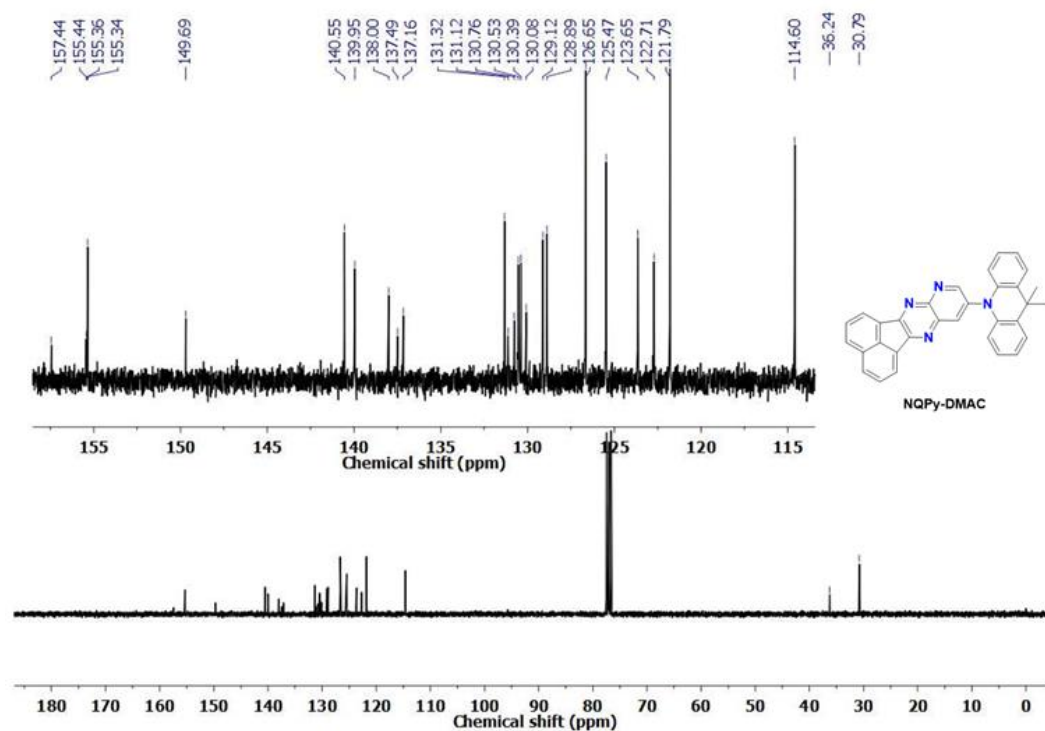
^{13}C NMR (75 MHz) in CDCl$_3$ of the compound **NQPy-DMAC**
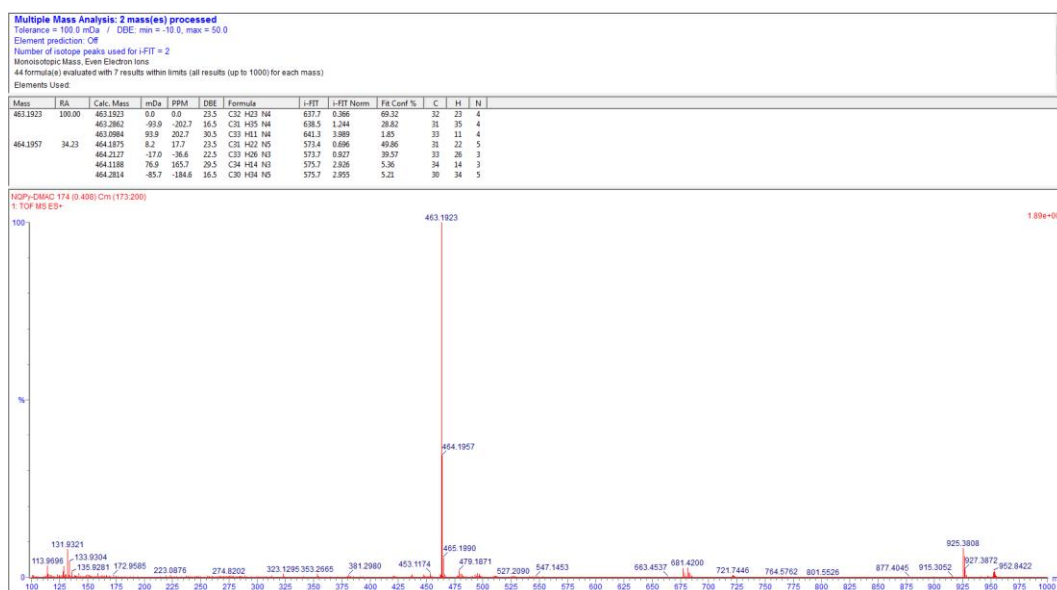
HRMS (TOF MS ES$^+$) of the compound **NQPy-DMAC.**
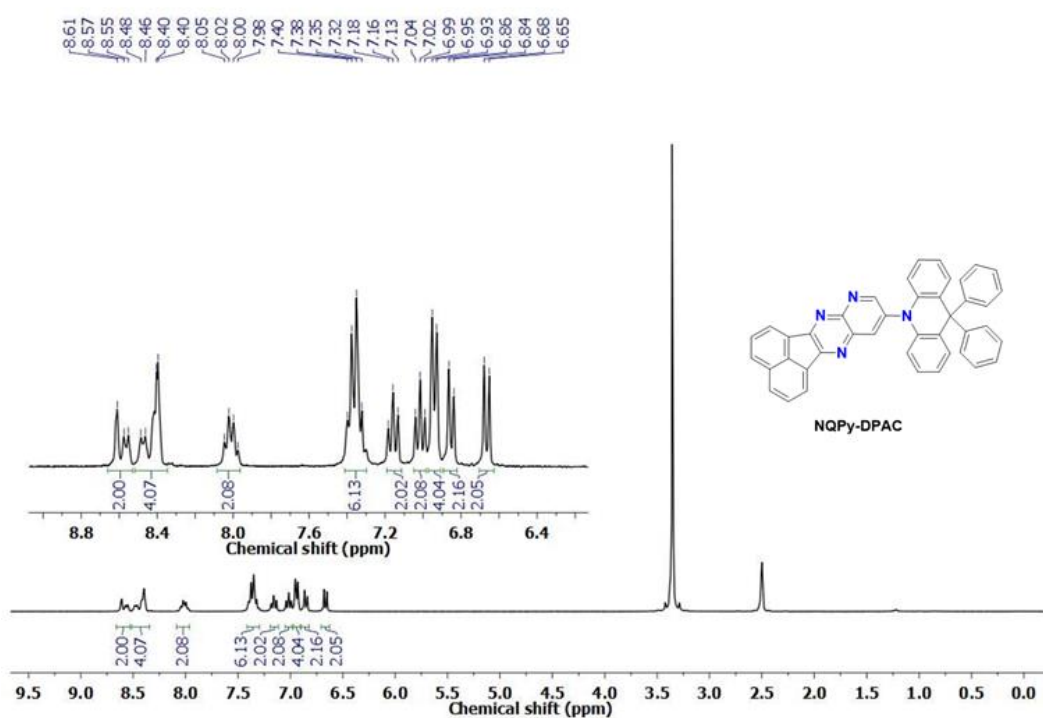
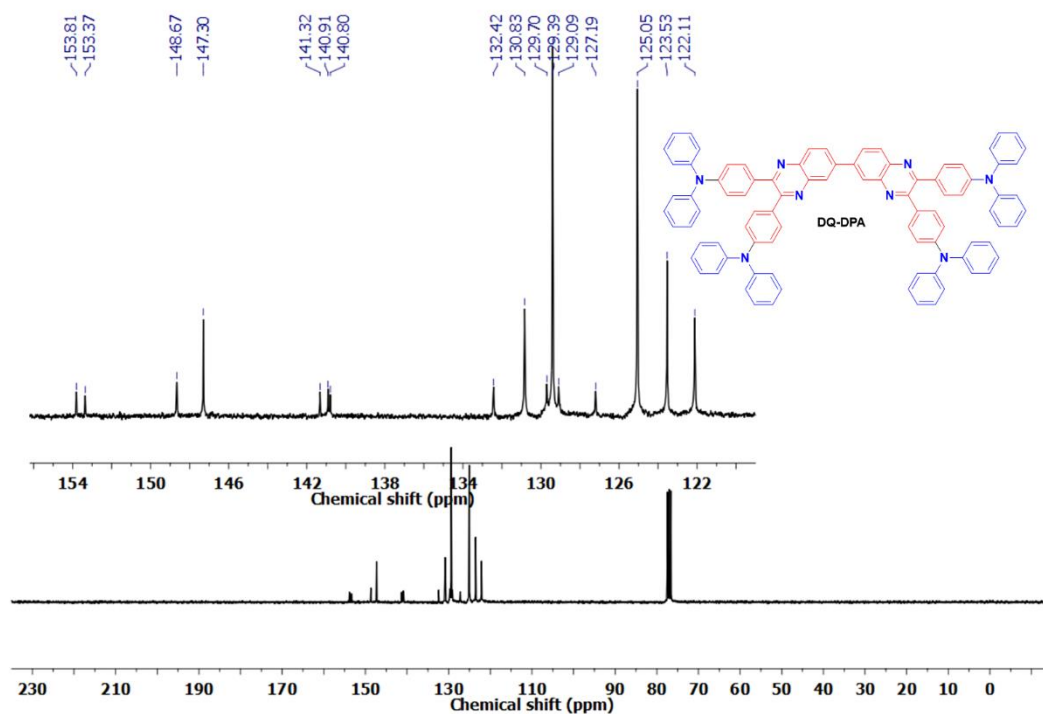*1H NMR (300 MHz) in DMSO-d6 of the compound **NQPy-DPAC.***
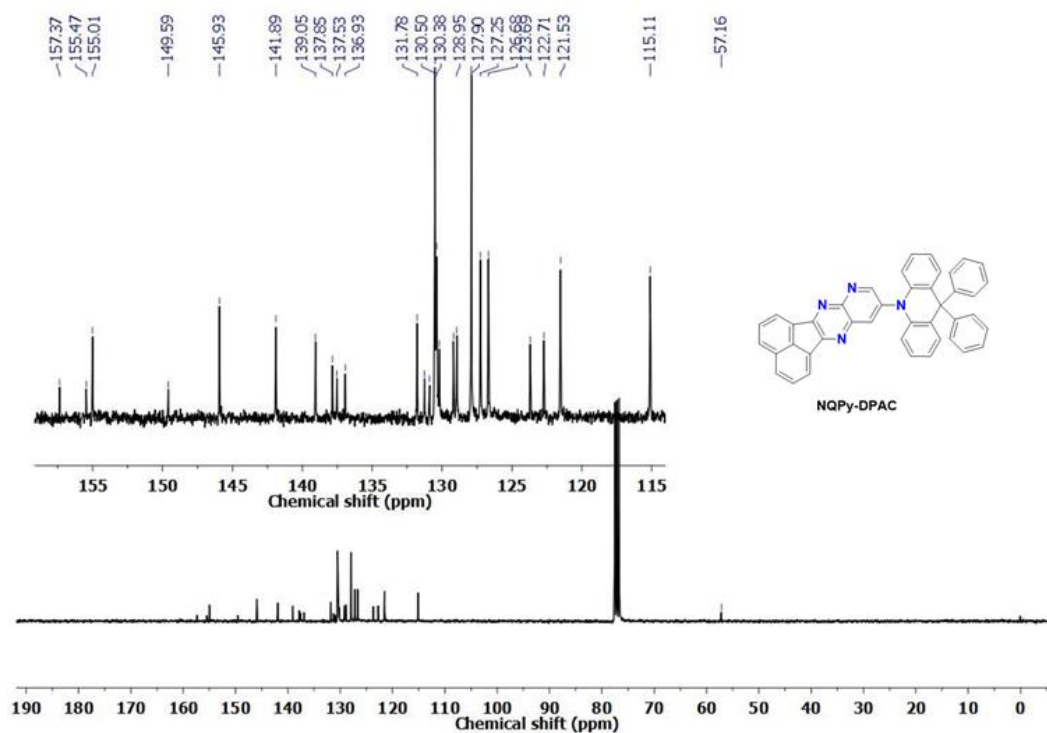
*13C NMR (75 MHz) in CDCl3 of the compound **NQPy-DPAC.***

*HRMS (TOF MS ES⁺) of the compound **NQPy-DPAC***.
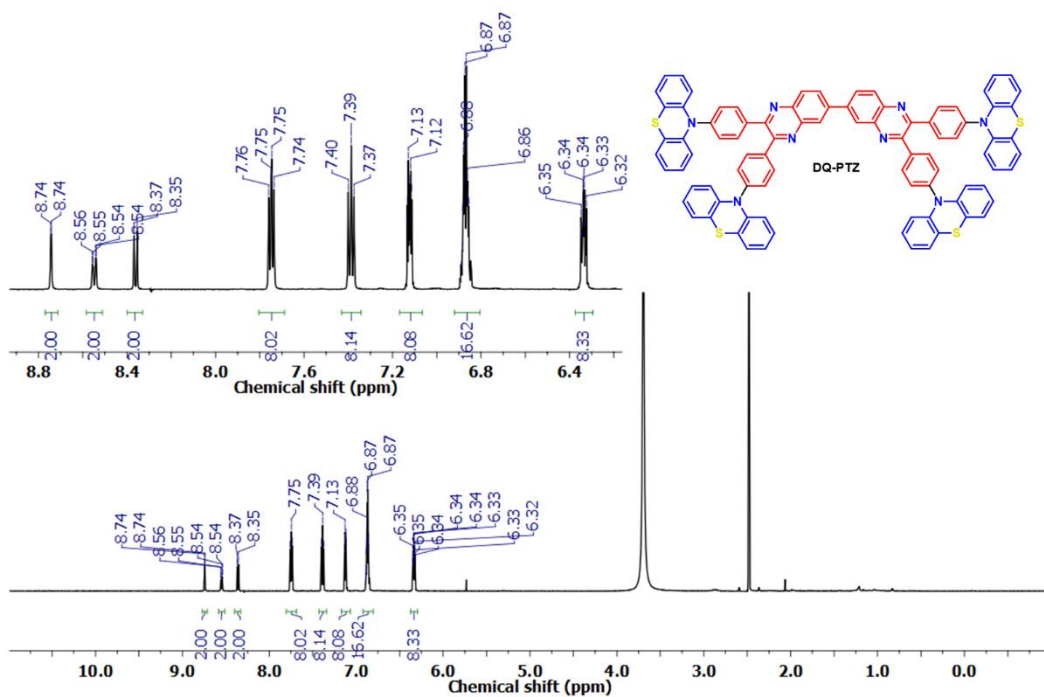

*¹H NMR (300 MHz) in CDCl₃ of the compound **NQPy-CBZ***.

Welisson de Pontes Silva
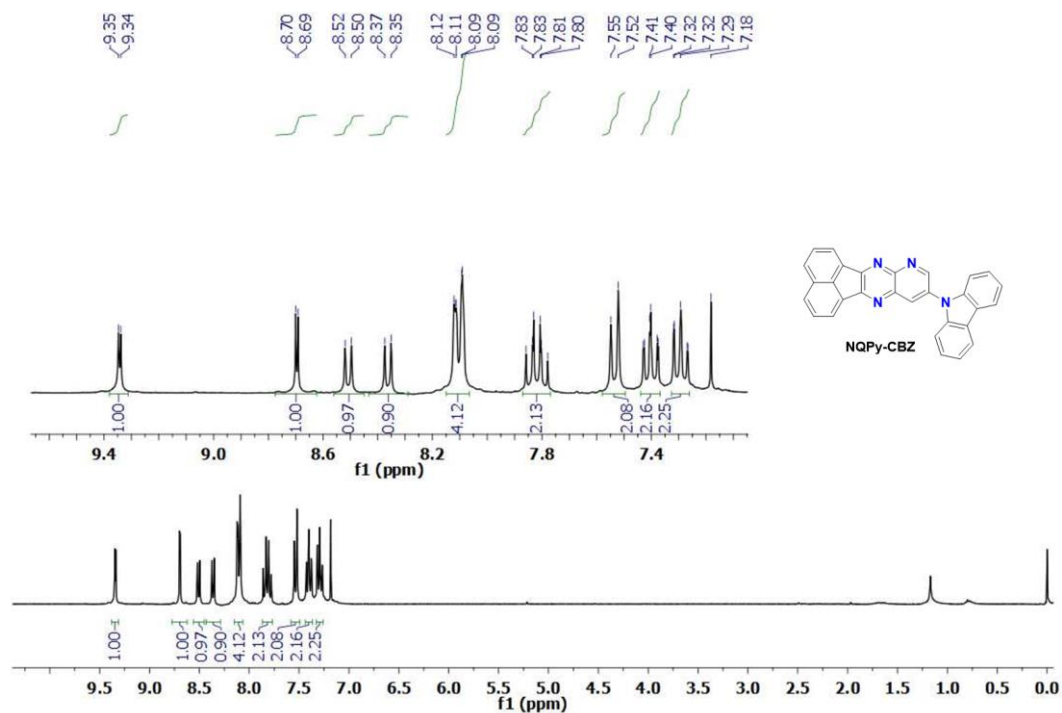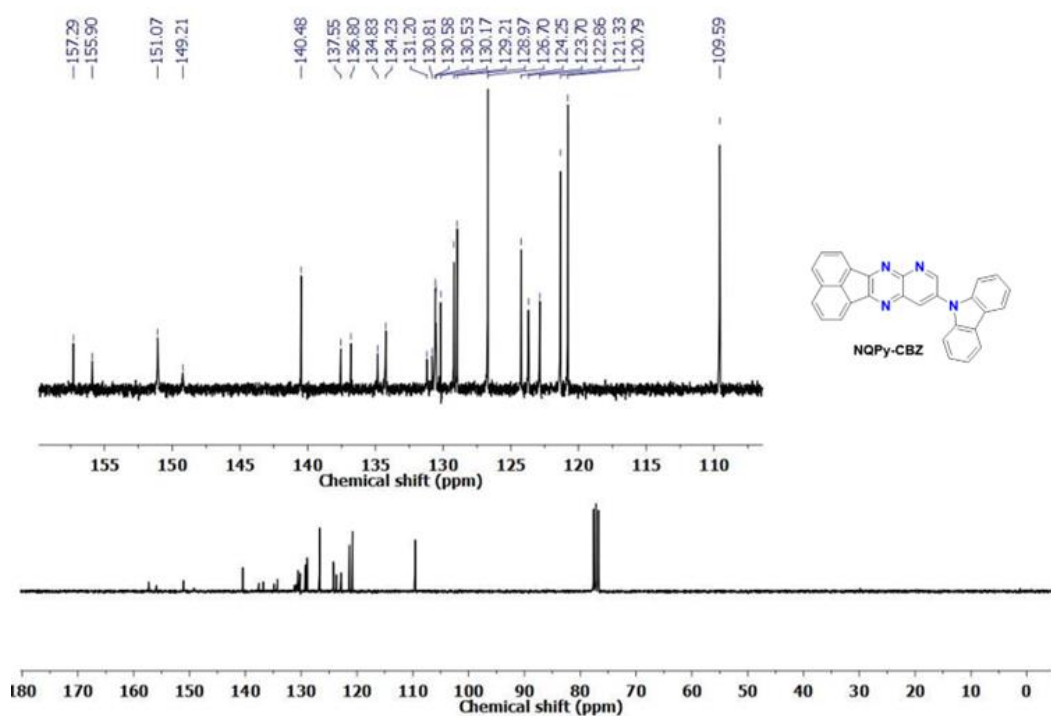
^{13}C NMR (75 MHz) in CDCl$_3$ of the compound **NQPy-CBZ.**

HRMS (TOF MS ES$^+$) of the compound **NQPy-CBZ.**
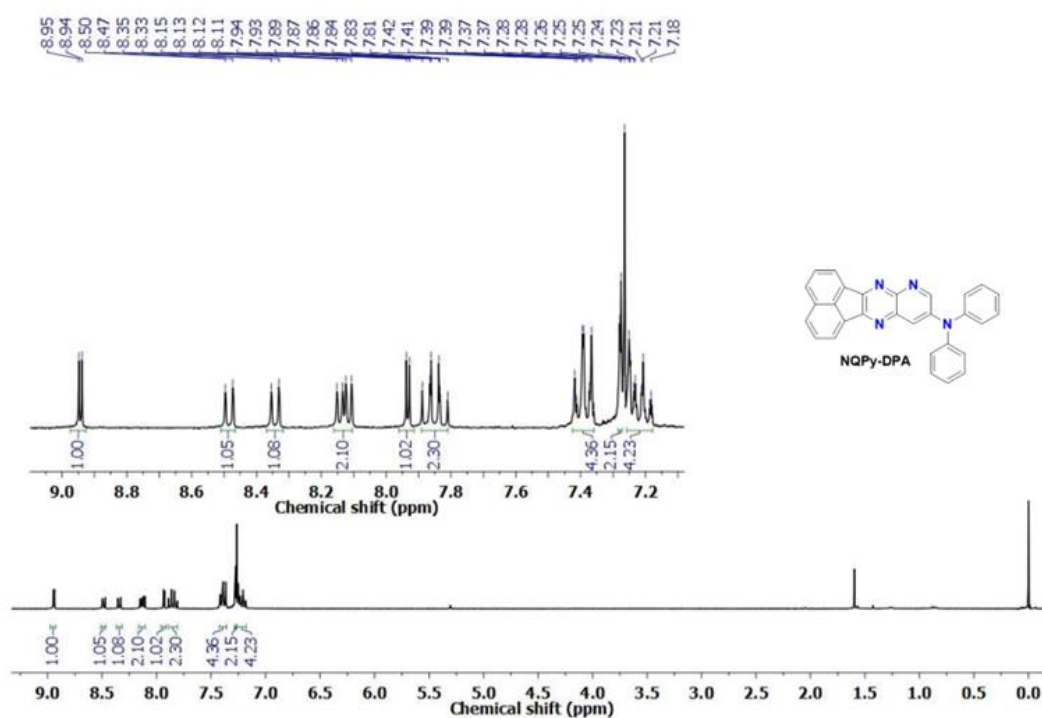
8.95 8.94 8.50 8.47 8.35 8.33 8.15 8.13 8.12 8.11 7.94 7.93 7.89 7.87 7.86 7.84 7.83 7.81 7.42 7.41 7.39 7.37 7.37 7.28 7.28 7.26 7.25 7.25 7.24 7.23 7.21 7.21 7.18

*¹H NMR (300 MHz) in CDCl₃ of the compound **NQPy-DPA***

155.36 154.42 148.55 146.19 145.13 137.45 136.71 130.13 130.01 129.58 129.04 128.70 128.62 125.22 124.47 122.71 122.12
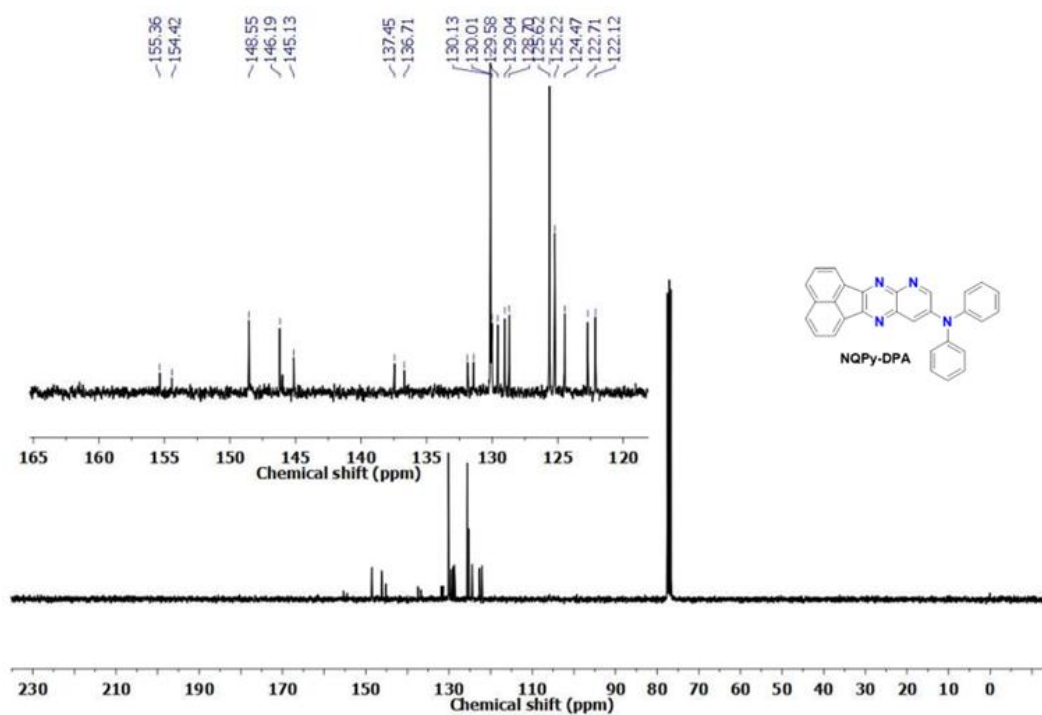
*¹³C NMR (75 MHz) in CDCl₃ of the compound **NQPy-DPA**.*

HRMS (TOF MS ES⁺) of the compound **NQPy-DPA.**
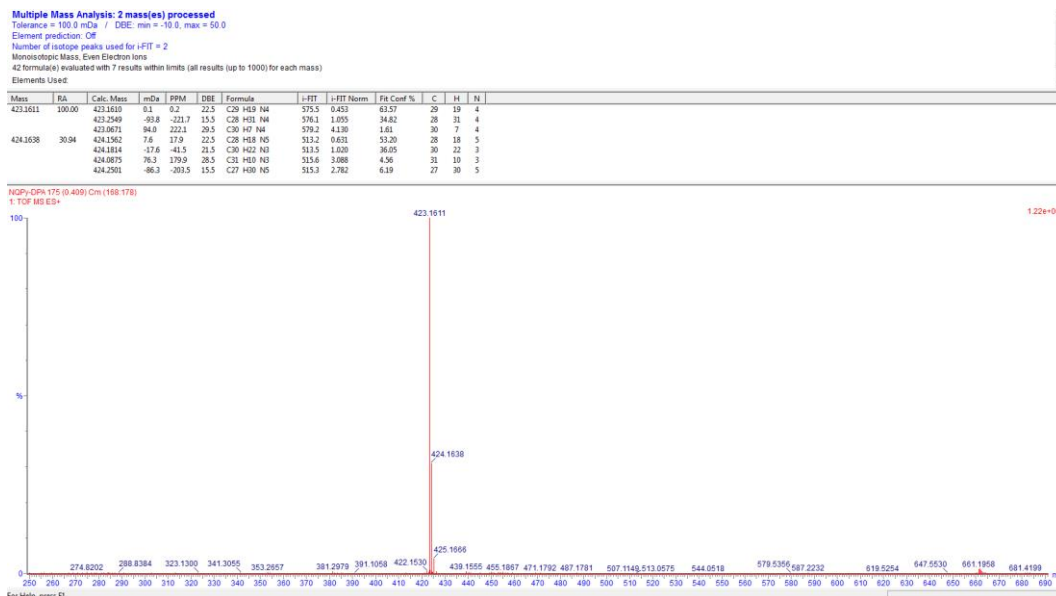
^{1}H NMR (300 MHz) in CDCl$_3$ of the compound **NQPy-DDA**
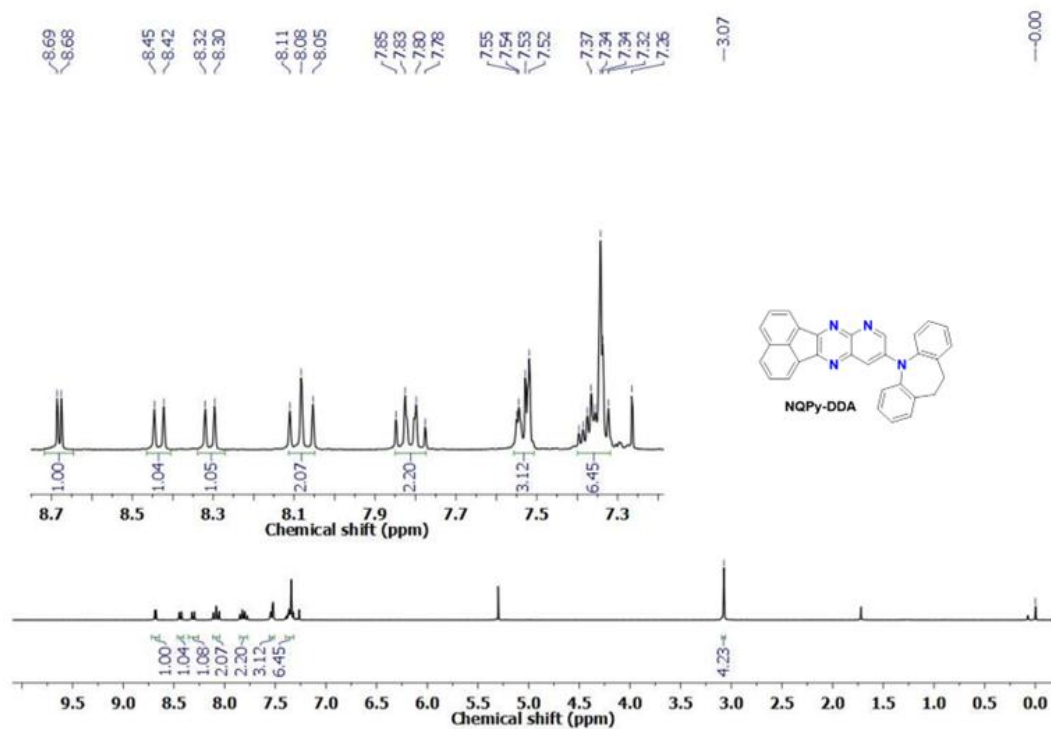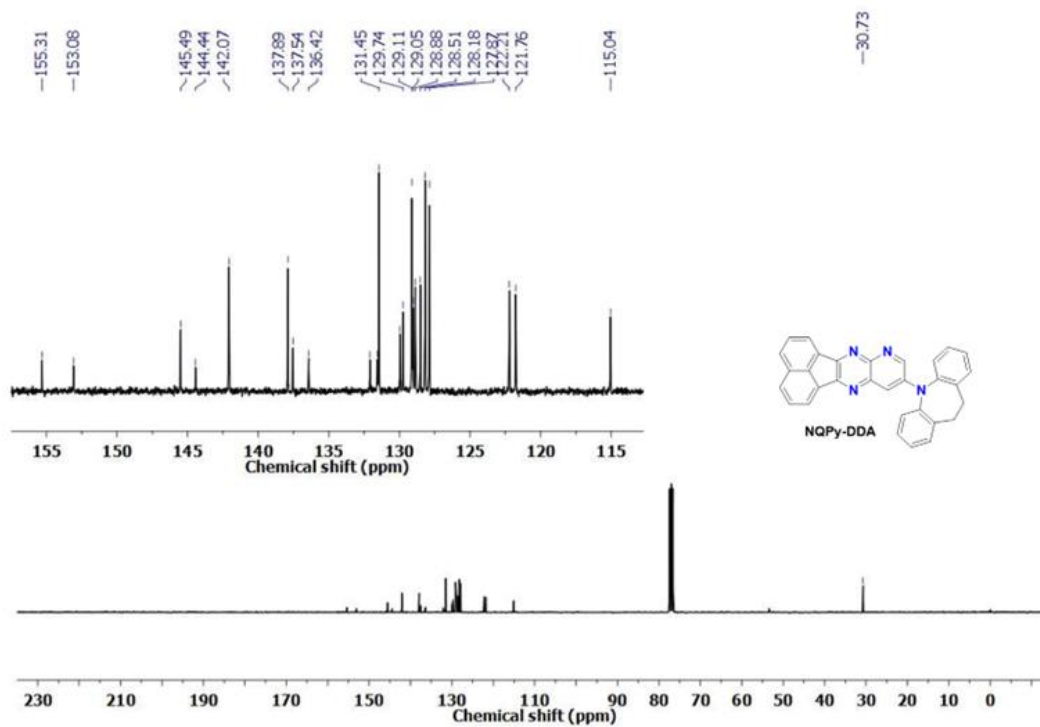
^{13}C NMR (75 MHz) in CDCl$_3$ of the compound **NQPy-DDA**

HRMS (TOF MS ES$^+$) of the compound **NQPy-DDA.**

Welisson de Pontes Silva
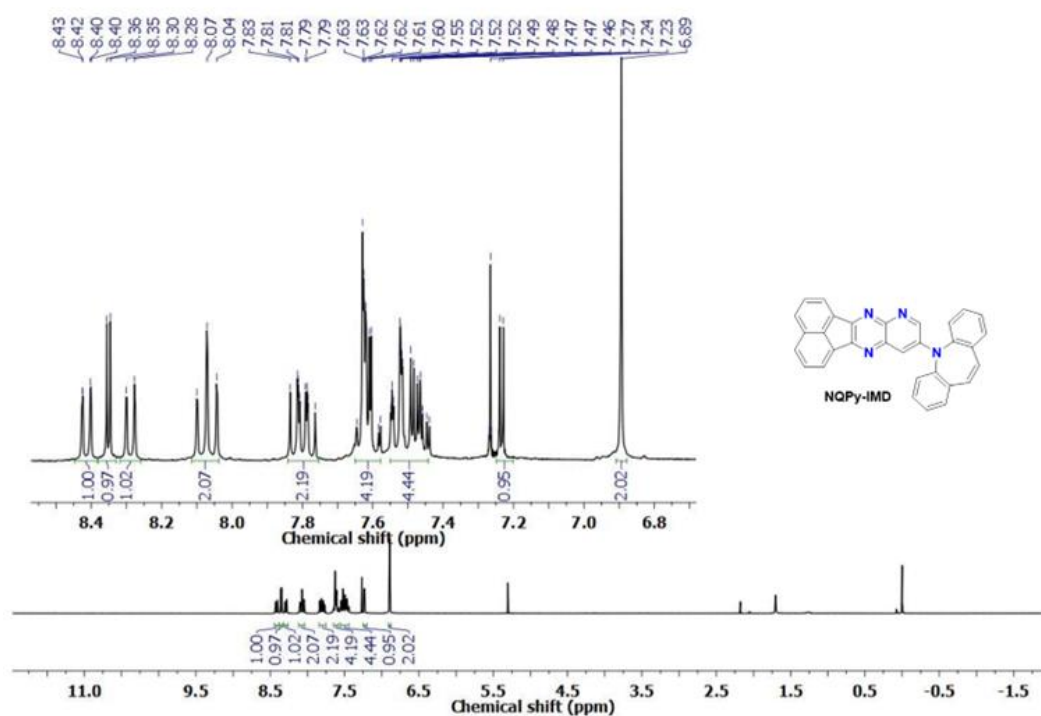
^{1}H NMR (300 MHz) in CDCl$_3$ of the compound **NQPy-IMD**
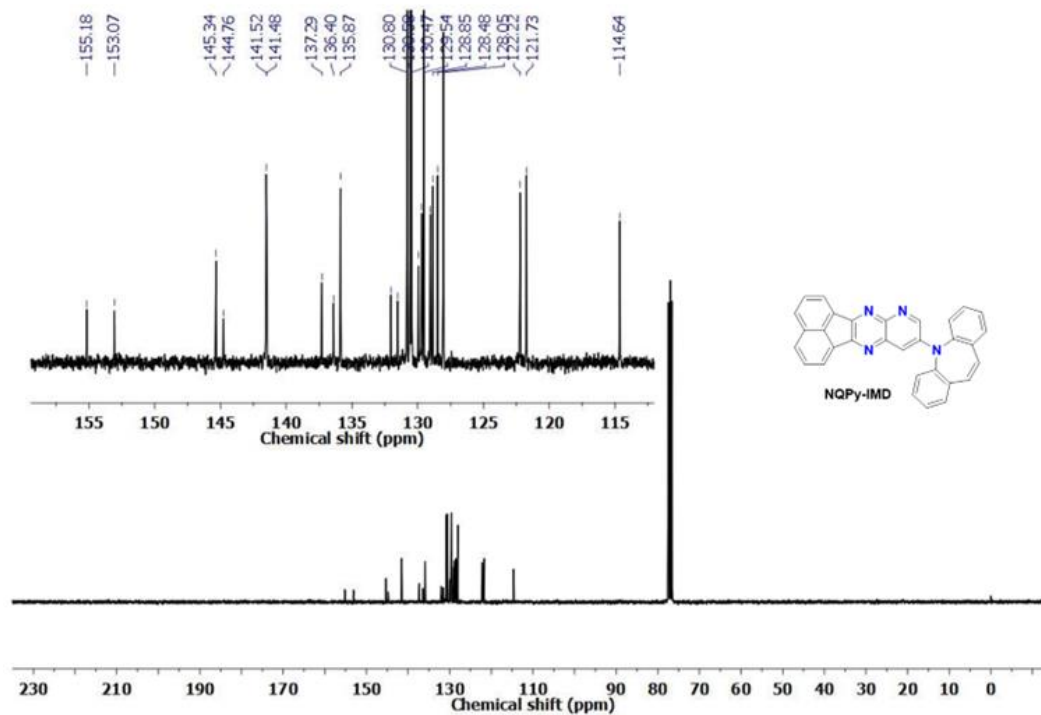
^{13}C NMR (75 MHz) in CDCl$_3$ of the compound **NQPy-IMD.**

HRMS (TOF MS ES⁺) of the compound **NQPy-IMD.**

12.2 PTE-Donor and PDA-Donor compounds
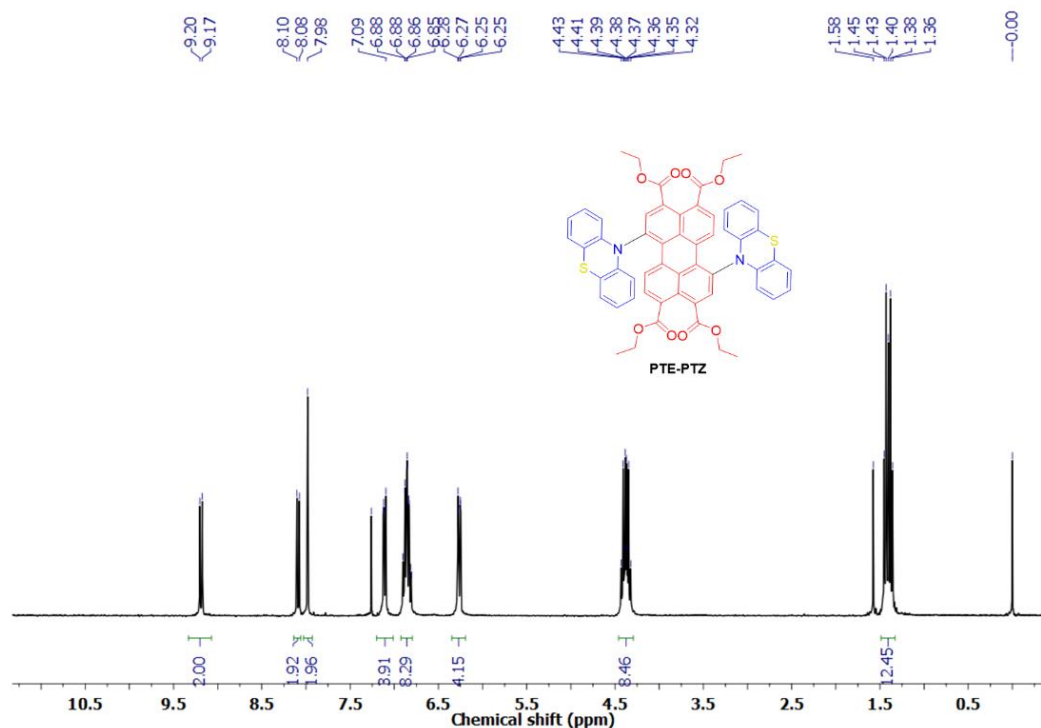
^{1}*H NMR (300 MHz) in CDCl$_3$ of the compound* **PTE-PTZ**.
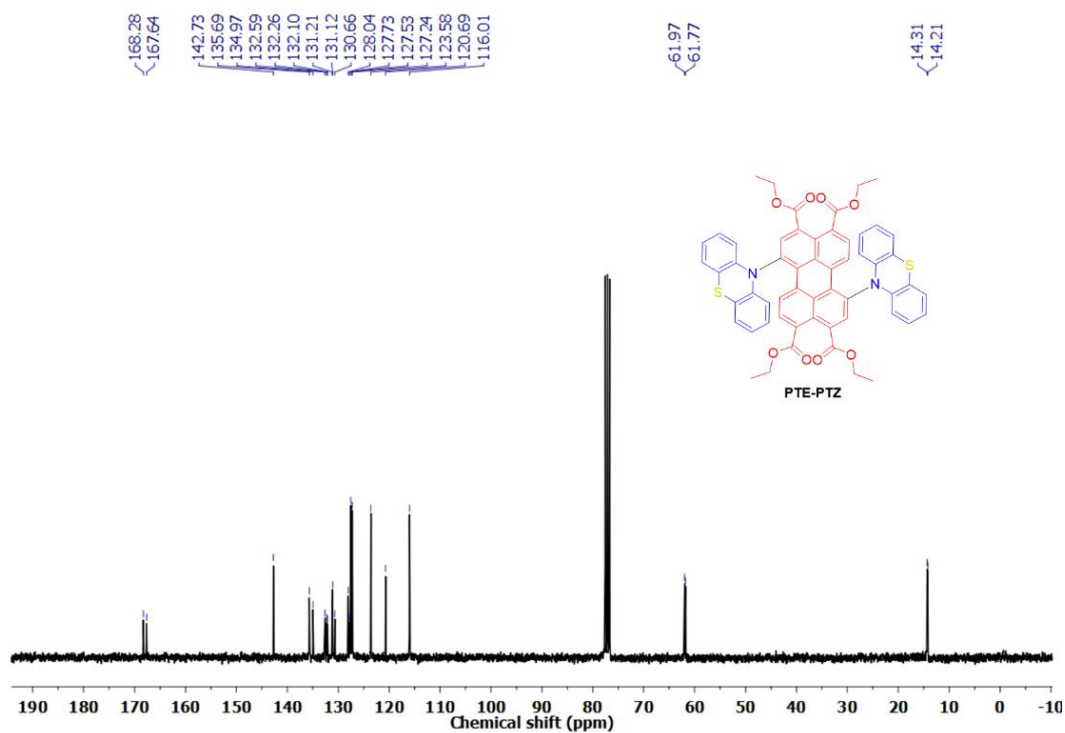
^{13}C NMR (75 MHz) in CDCl$_3$ of the compound **PTE-PTZ**.
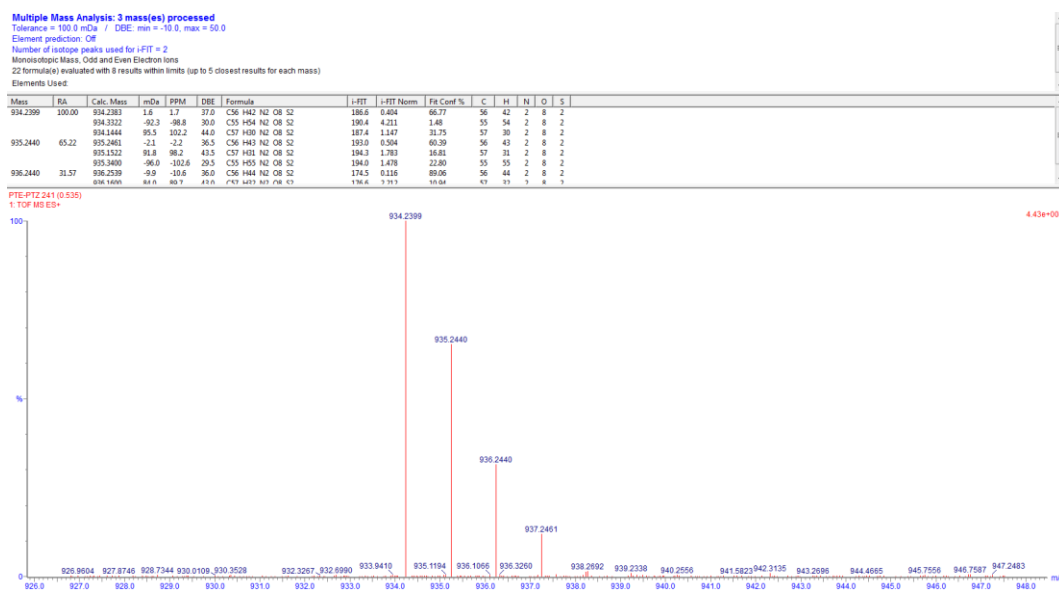
HRMS (TOF MS ES$^+$) of the compound **PTE-PTZ**.
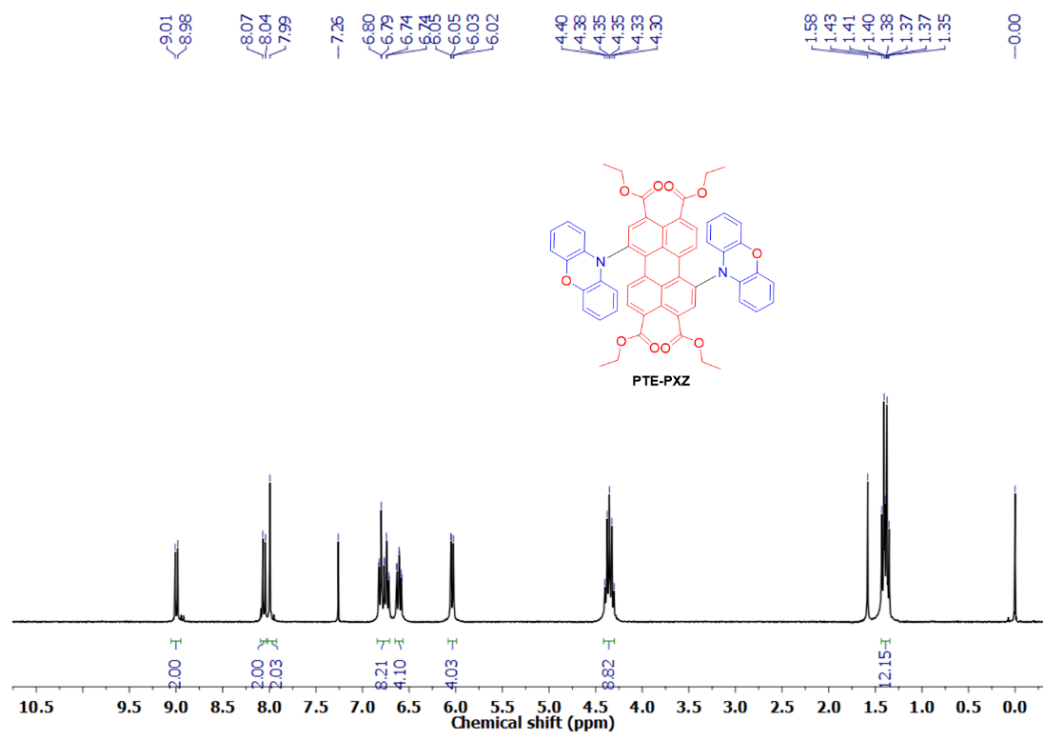
^{1}H NMR (300 MHz) in CDCl$_3$ of the compound **PTE-PXZ**.
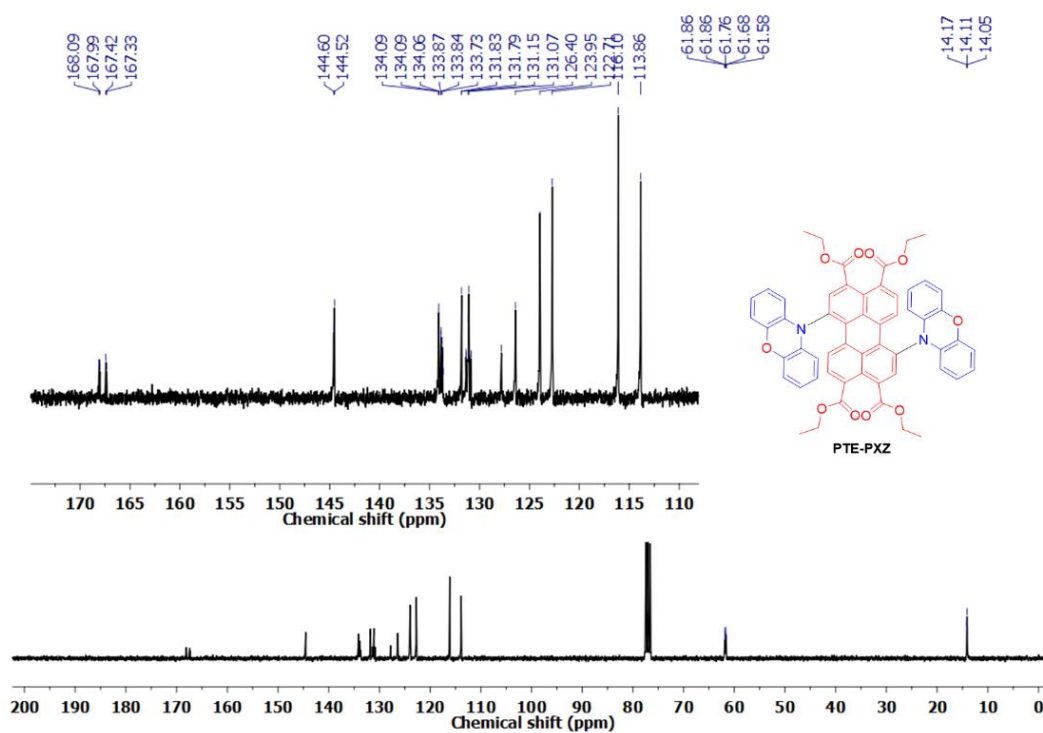
^{13}C NMR (75 MHz) in CDCl$_3$ of the compound **PTE-PXZ**.

HRMS (TOF MS ES⁺) of the compound **PTE-PXZ**.
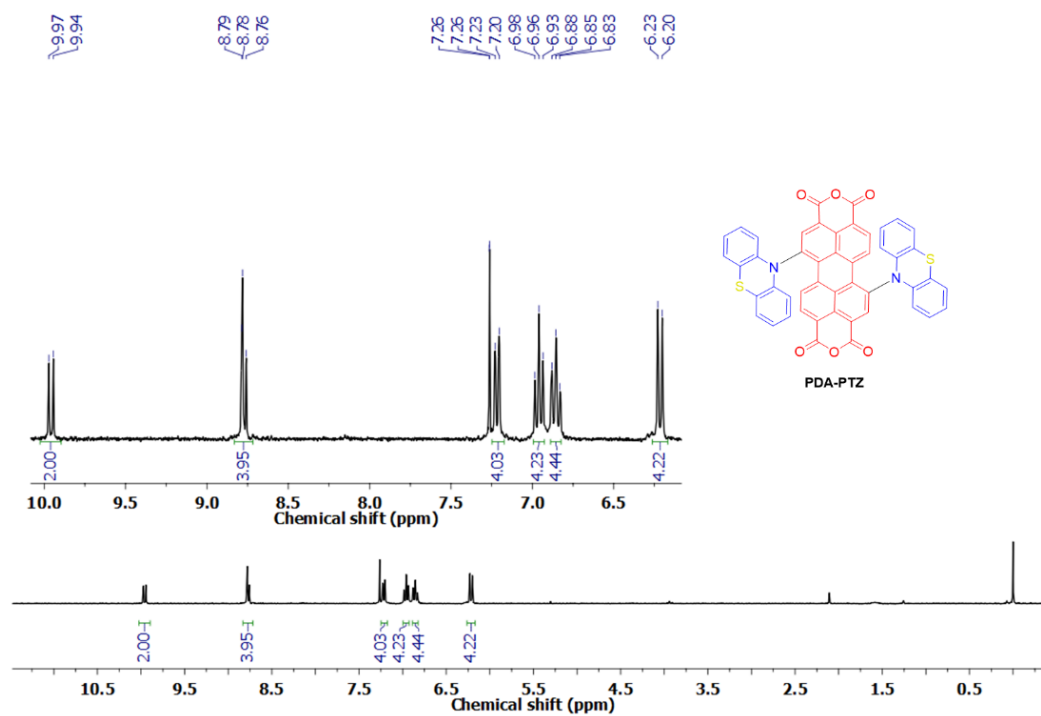
^1H NMR (300 MHz) in CDCl$_3$ of the compound **PDA-PTZ**.
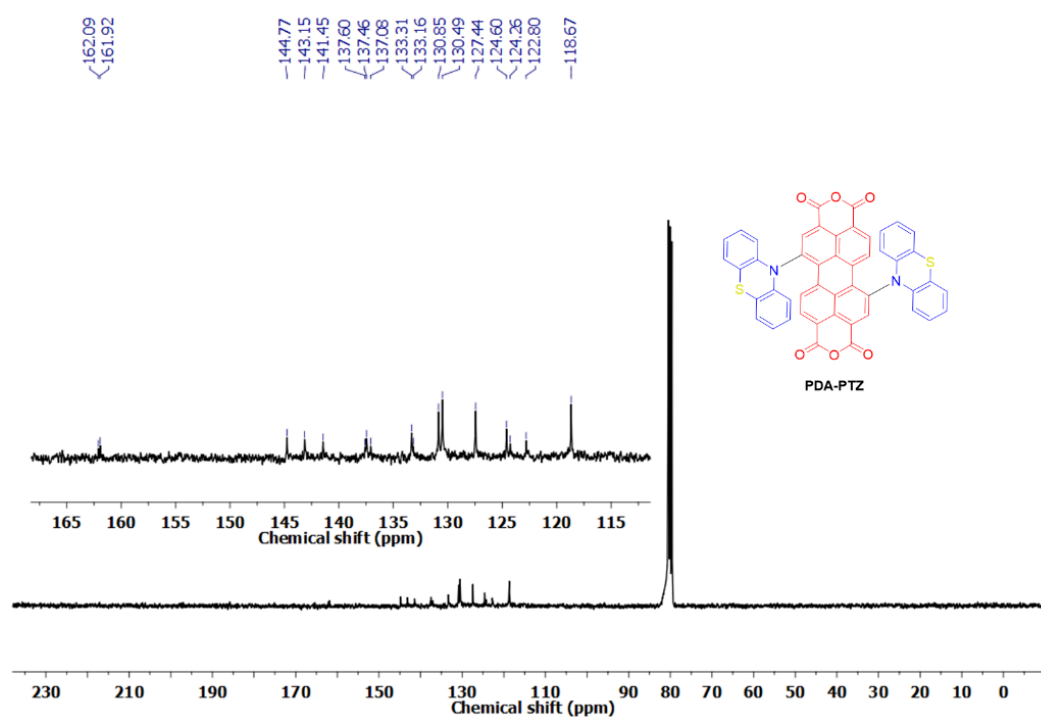
^{13}C NMR (75 MHz) in CDCl$_3$ of the compound **PDA-PTZ**.

HRMS (TOF MS ES$^+$) of the compound **PDA-PTZ.**

*^{1}H NMR (300 MHz) in CDCl$_3$ of the compound **PDA-PXZ**.*
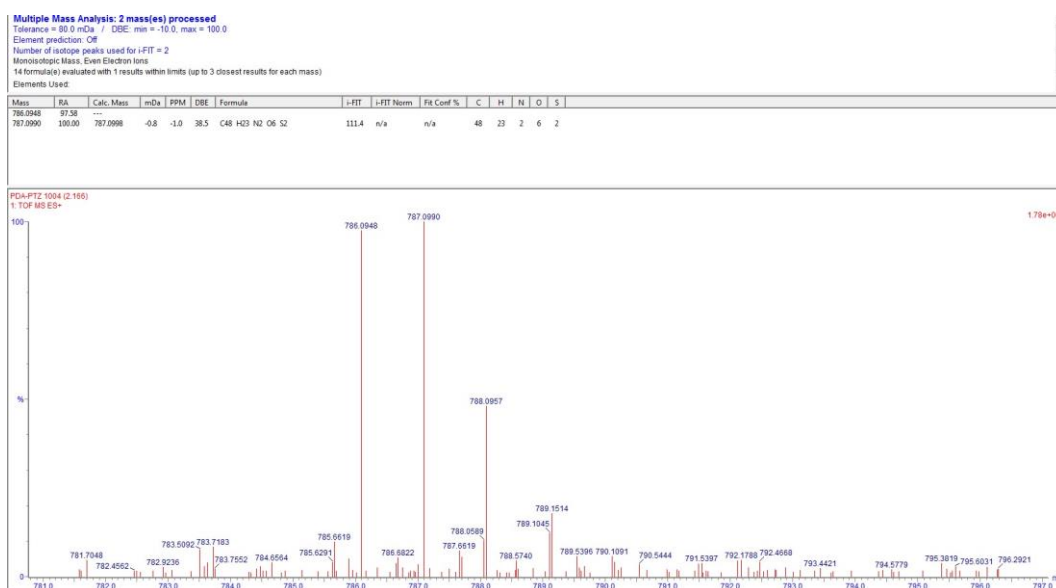
*HRMS (TOF MS ES$^+$) of the compound **PDA-PXZ**.*
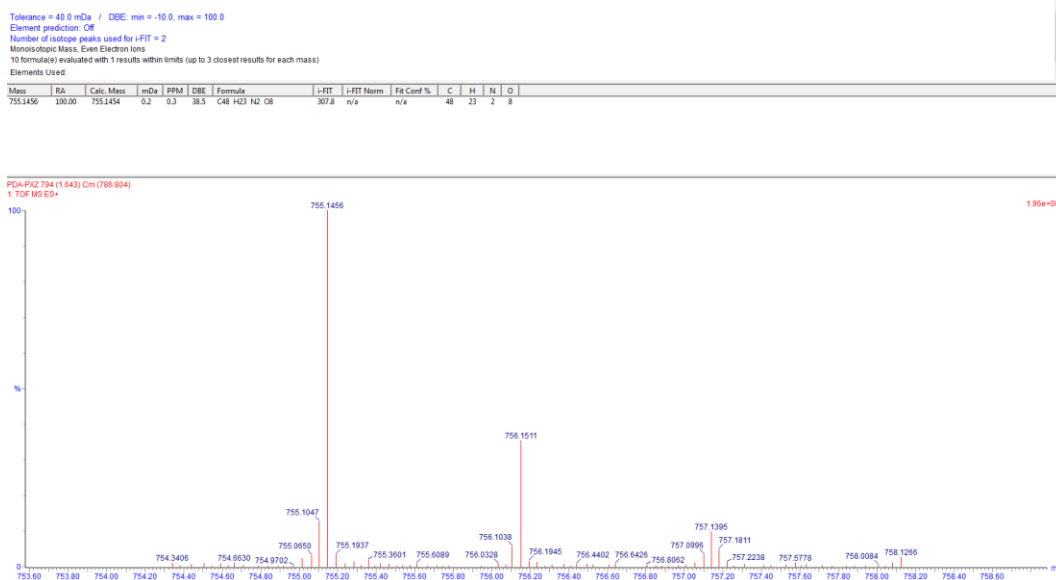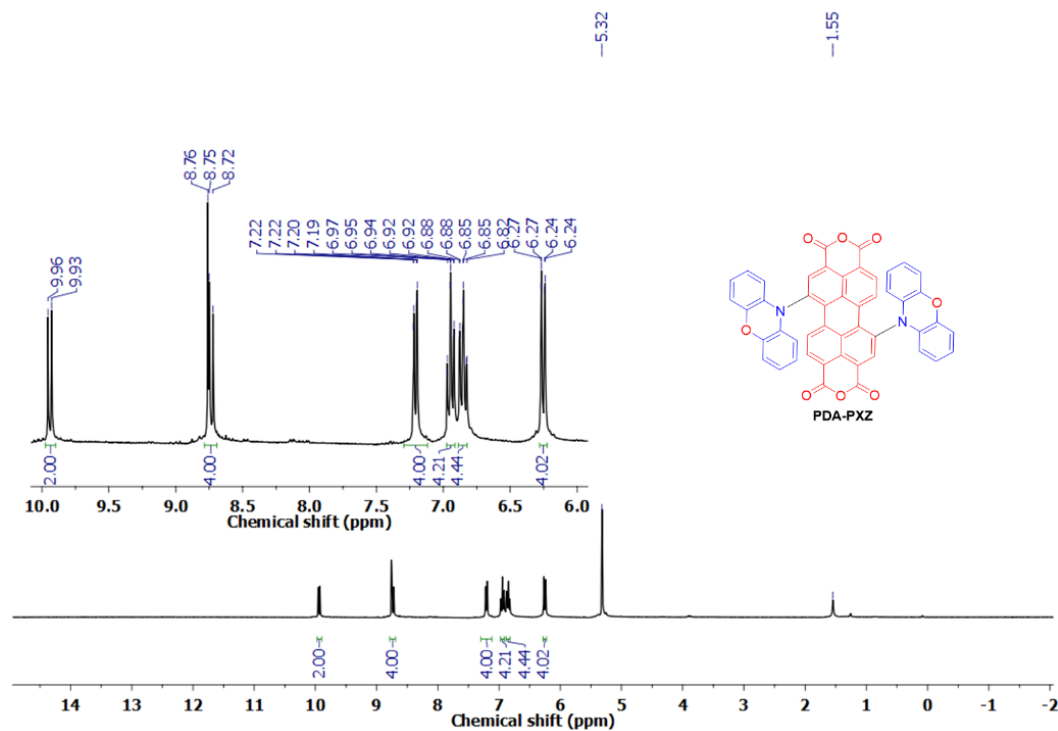
12.3 BTNA-Donor compounds
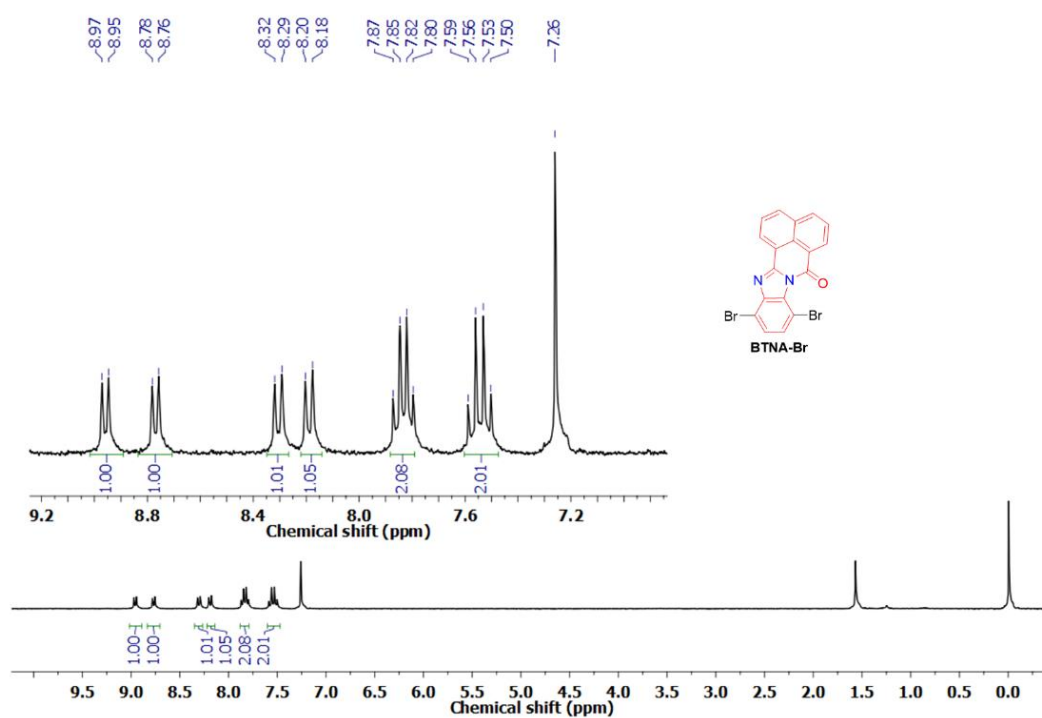
^{1}H NMR (300 MHz) in CDCl$_3$ of the compound **BTNA-Br.**
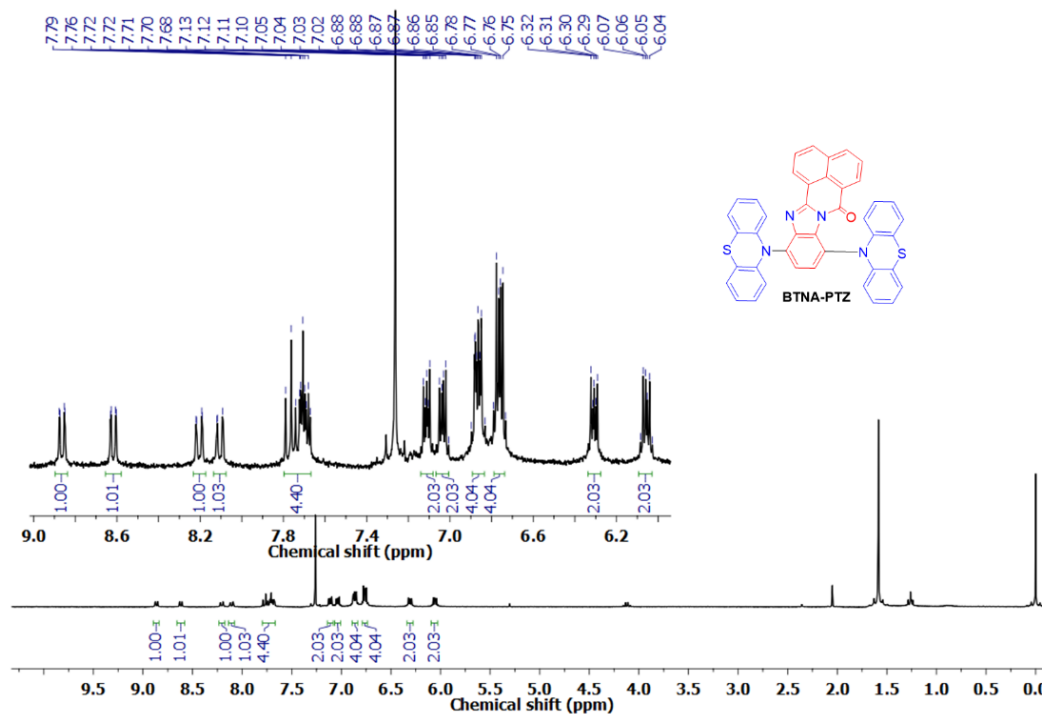
^{1}H NMR (300 MHz) in CDCl$_3$ of the compound **BTNA-PTZ.**
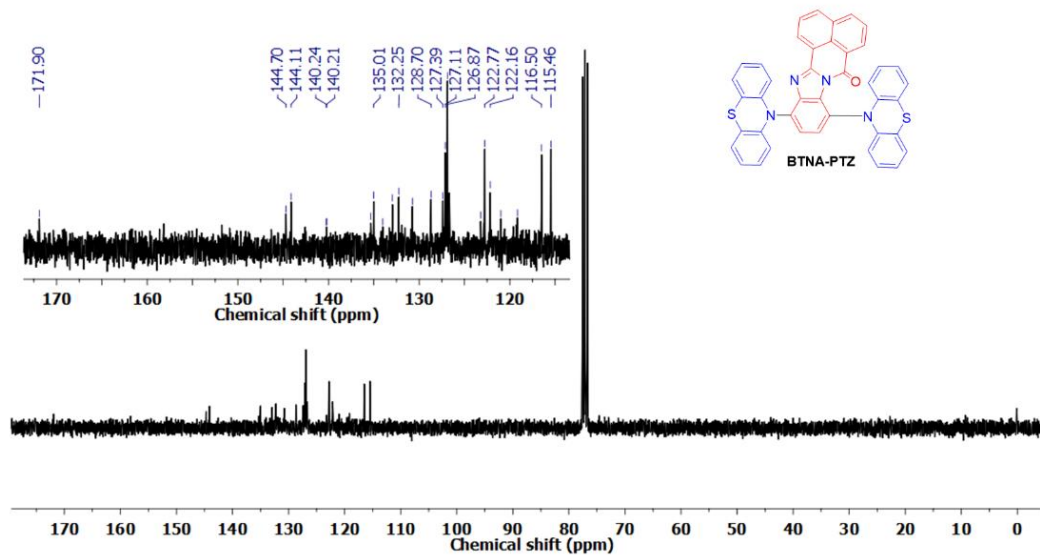
^{13}C NMR (75 MHz) in CDCl$_3$ of the compound **BTNA-PTZ.**
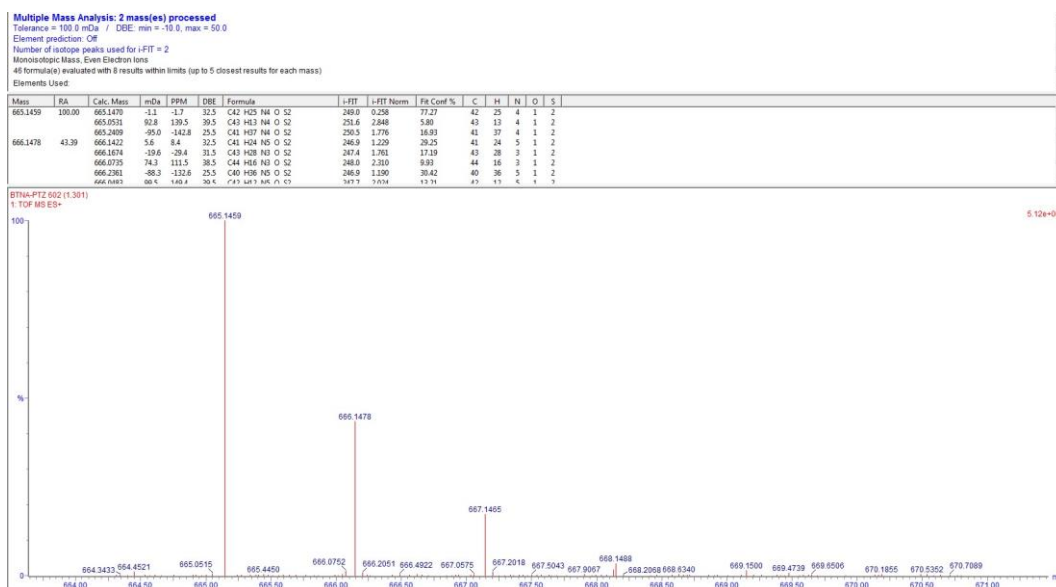
HRMS (TOF MS ES$^+$) of the compound **BTNA-PTZ.**
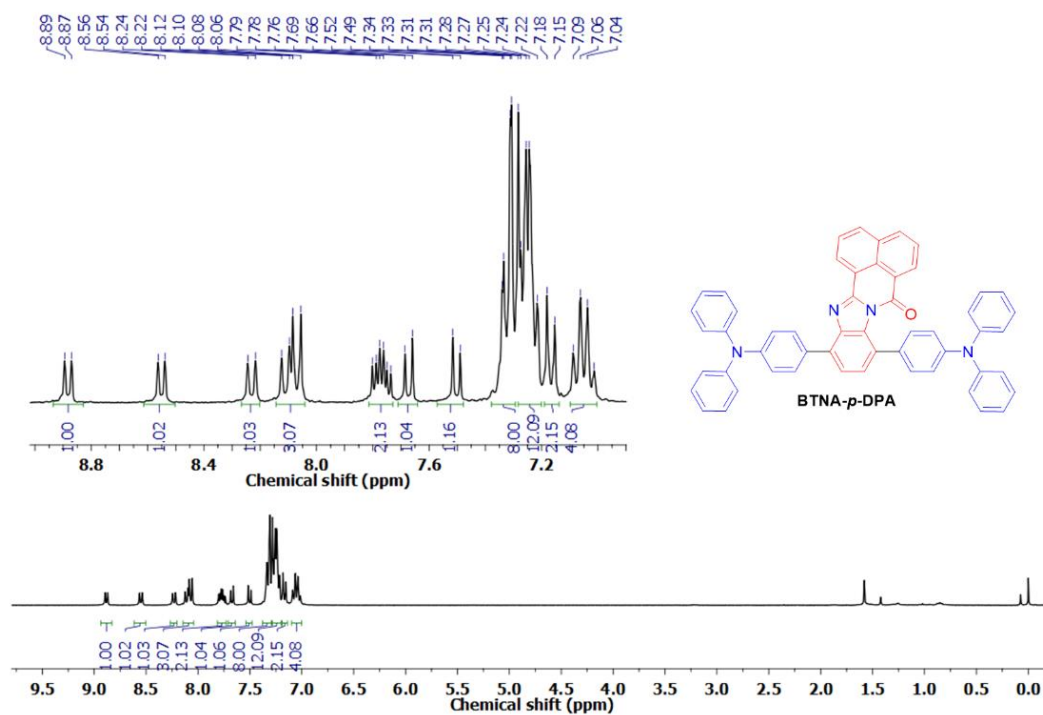
^{1}H NMR (300 MHz) in CDCl$_3$ of the compound **BTNA-p-DPA.**
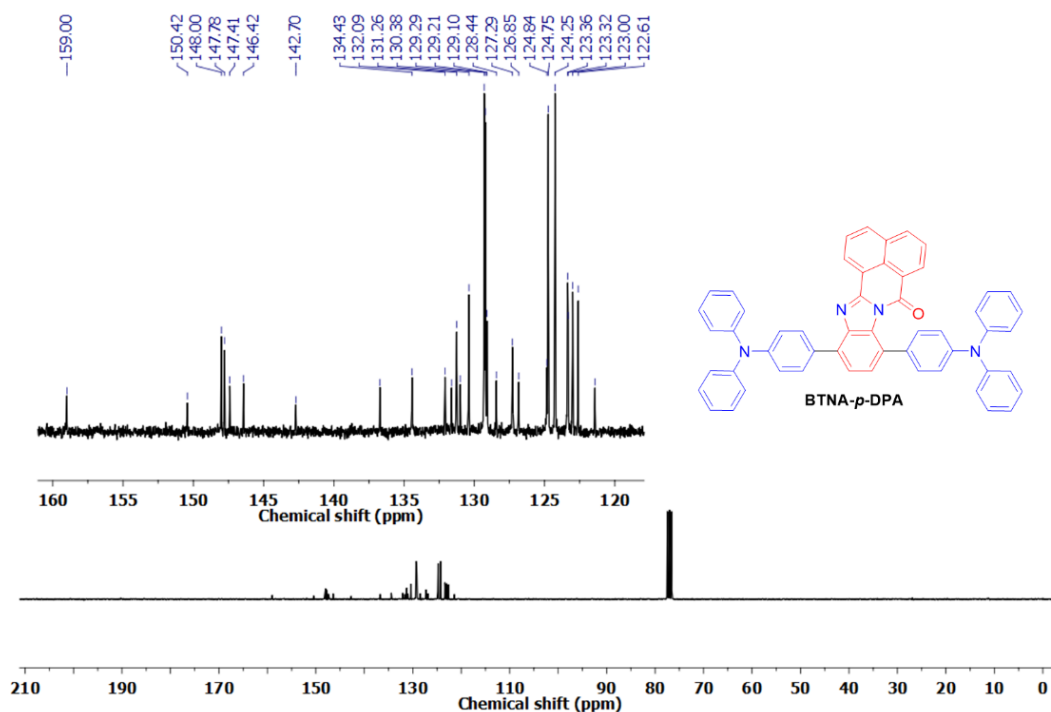
^{13}C NMR (75 MHz) in CDCl$_3$ of the compound **BTNA-p-DPA.**
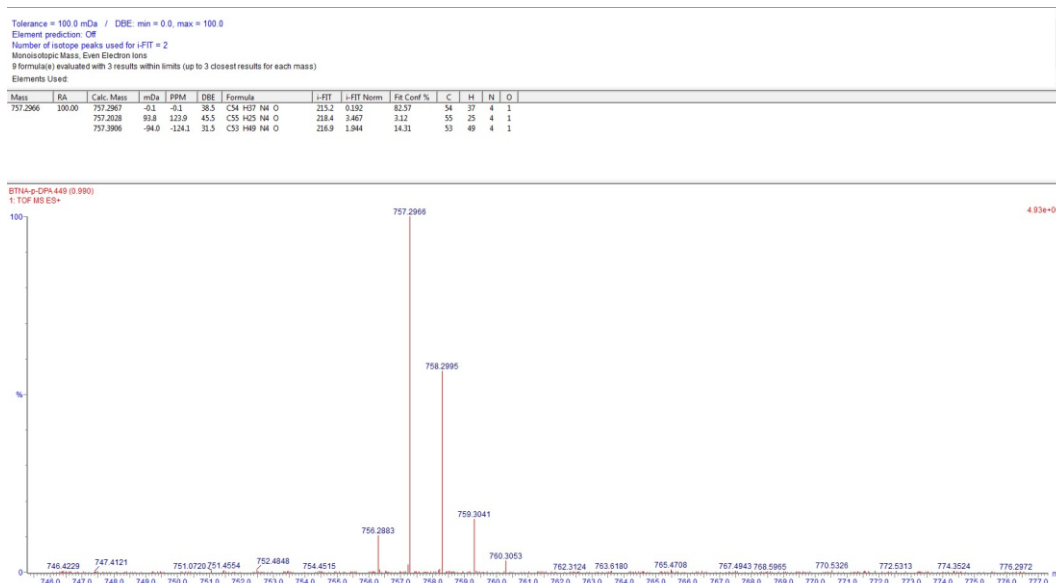
HRMS (TOF MS ES⁺) of the compound **BTNA-p-DPA.**
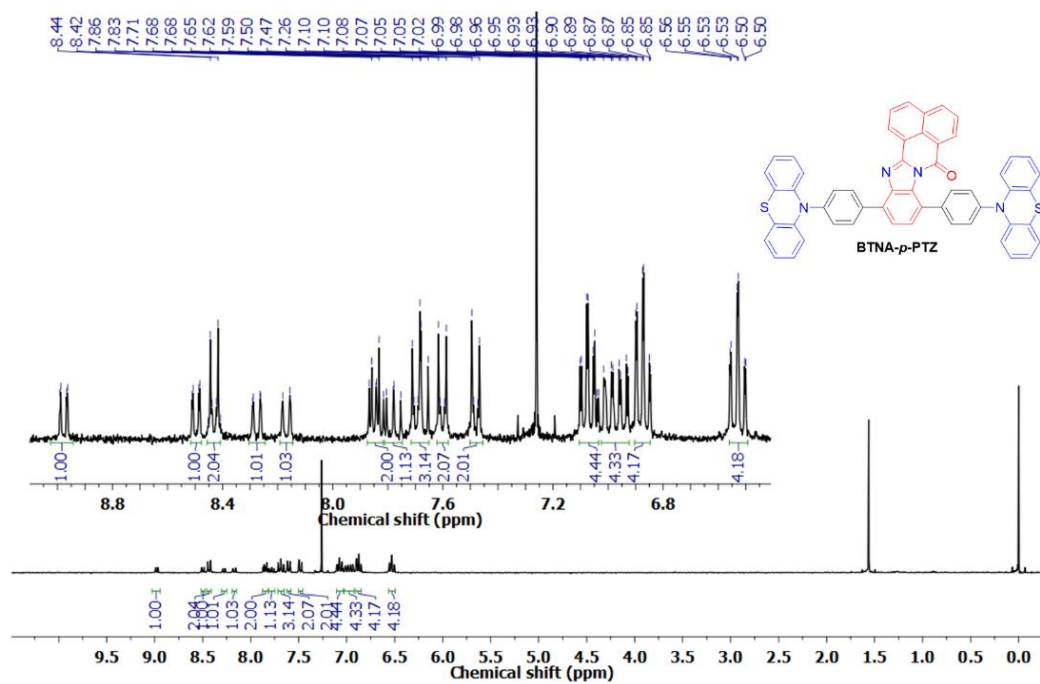
¹H NMR (300 MHz) in CDCl₃ of the compound **BTNA-p-PTZ.**
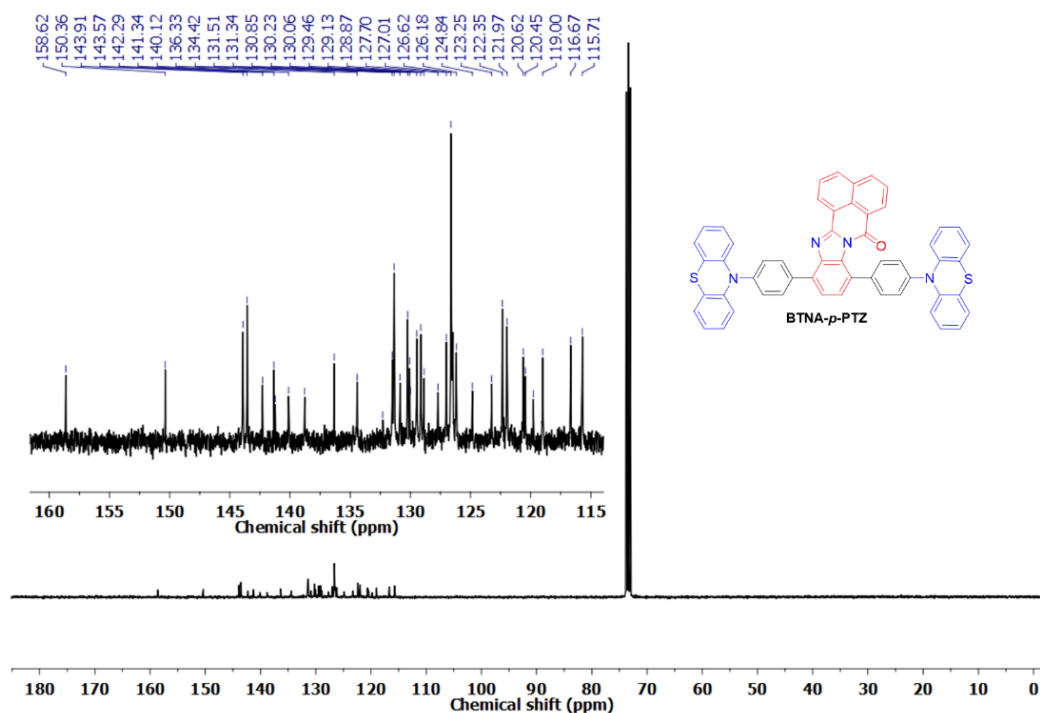
*13C NMR (75 MHz) in Tetraclhoroethane-d₂ of the compound **BTNA-p-PTZ.***
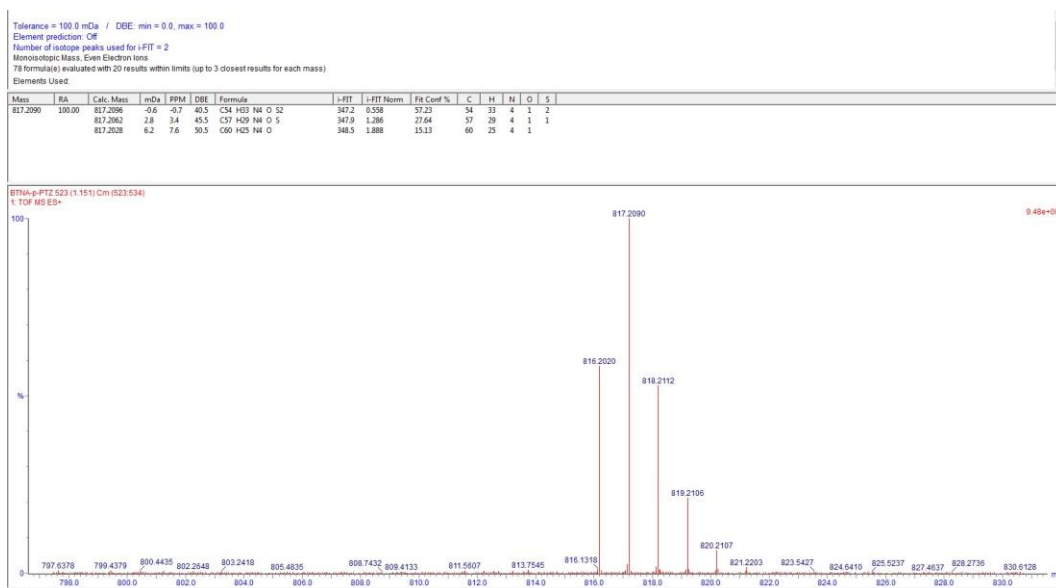
*HRMS (TOF MS ES⁺) of the compound **BTNA-p-PTZ.***

*¹H NMR (300 MHz) in CDCl₃ of the compound **BTNA-p-PXZ.***
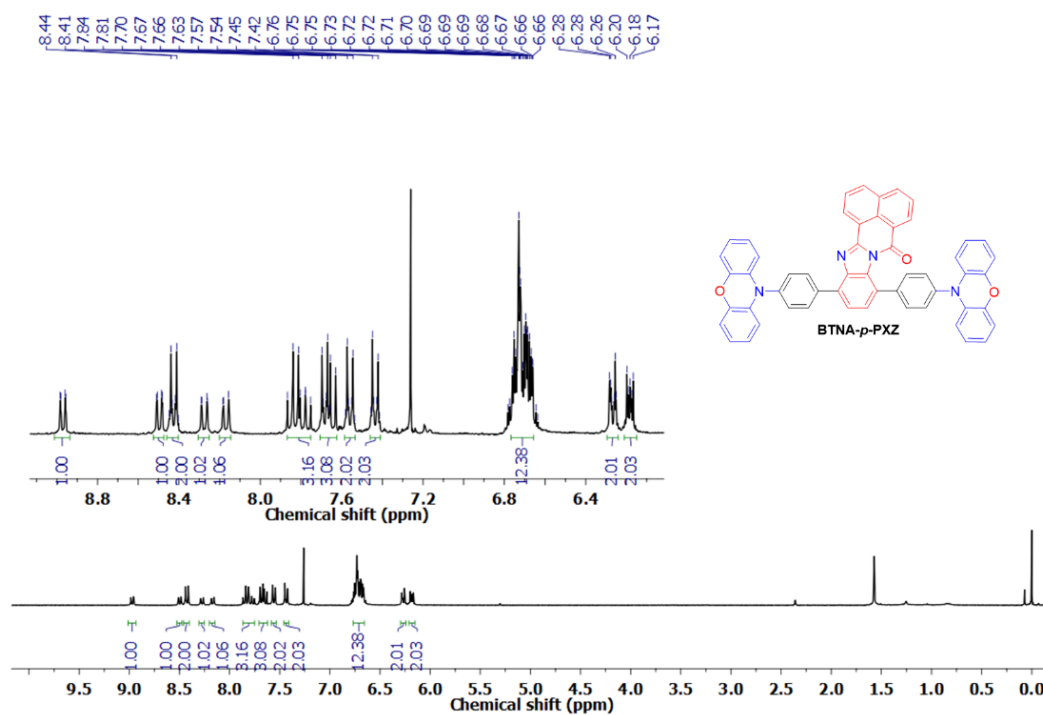
¹H NMR (300 MHz) in CDCl₃ of the compound **BTNA-p-PXZ.**
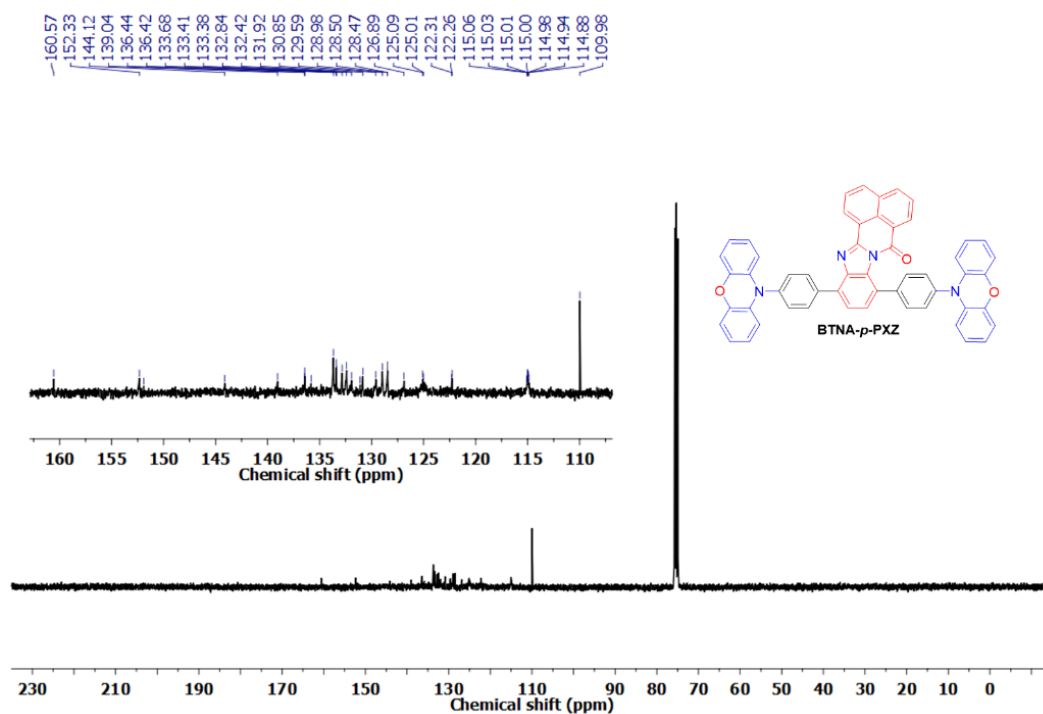
*¹³C NMR (75 MHz) in Tetraclhoroethane-d₂ of the compound **BTNA-p-PXZ**. (Due very small solubility in common deuterated solvents, the ¹³C NMR operating at 75 MHz was very hard to get the spectra in good resolution).*
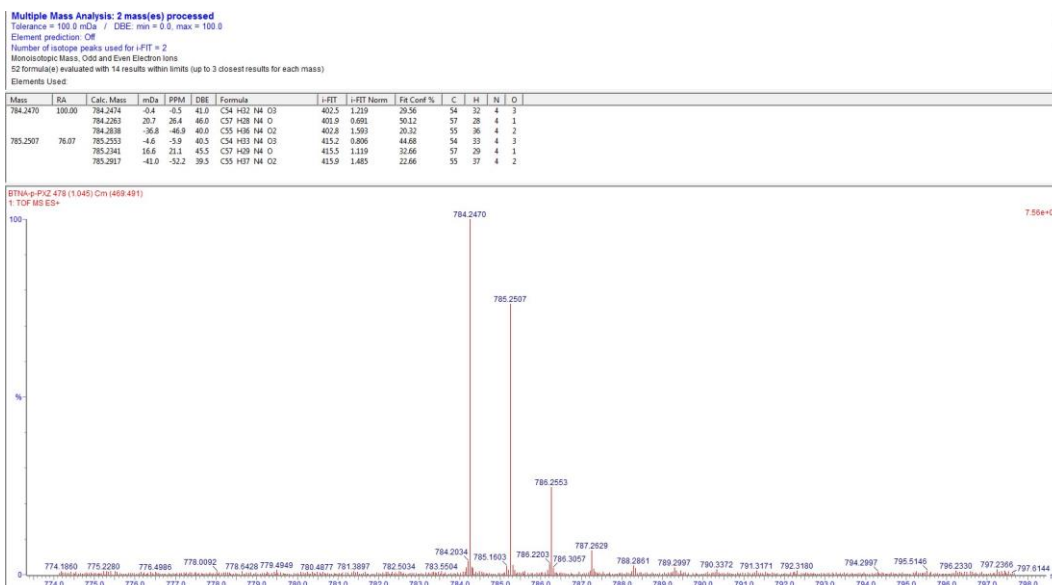
HRMS (TOF MS ES⁺) of the compound **BTNA-*p*-PXZ.**
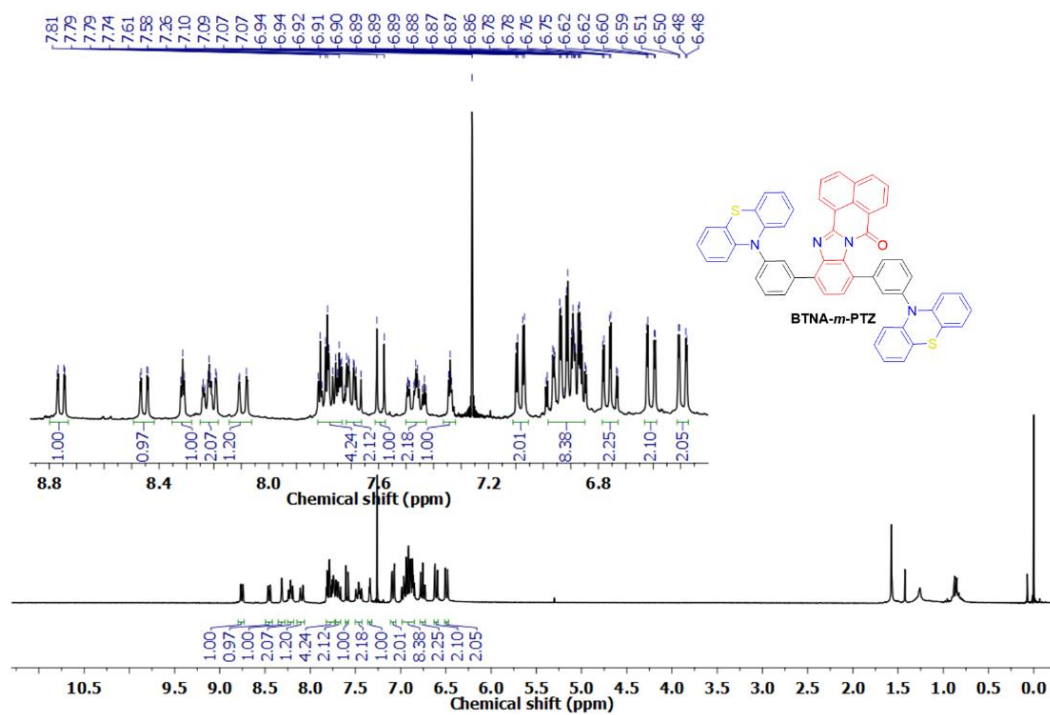
¹H NMR (300 MHz) in CDCl₃ of the compound **BTNA-*m*-PTZ.**
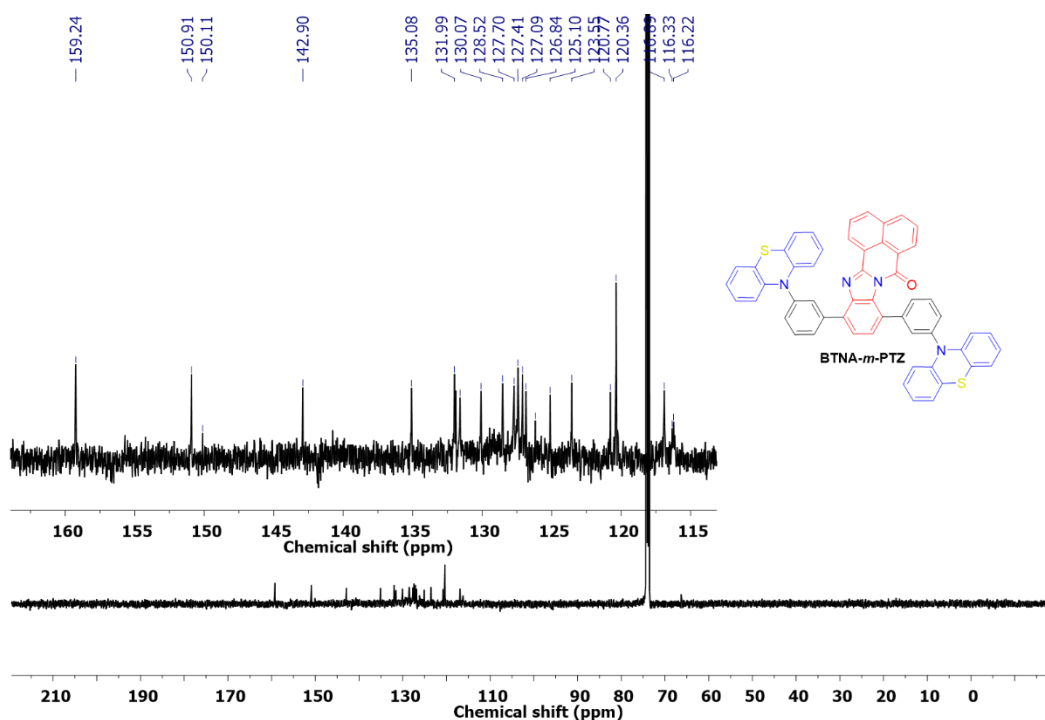
^{13}C NMR (100 MHz) in Tetraclhoroethane-d_2 of the compound **BTNA-m-PTZ**. The low solubility in common deuterated solvents makes it difficult to get a good ^{13}C NMR spectra**.
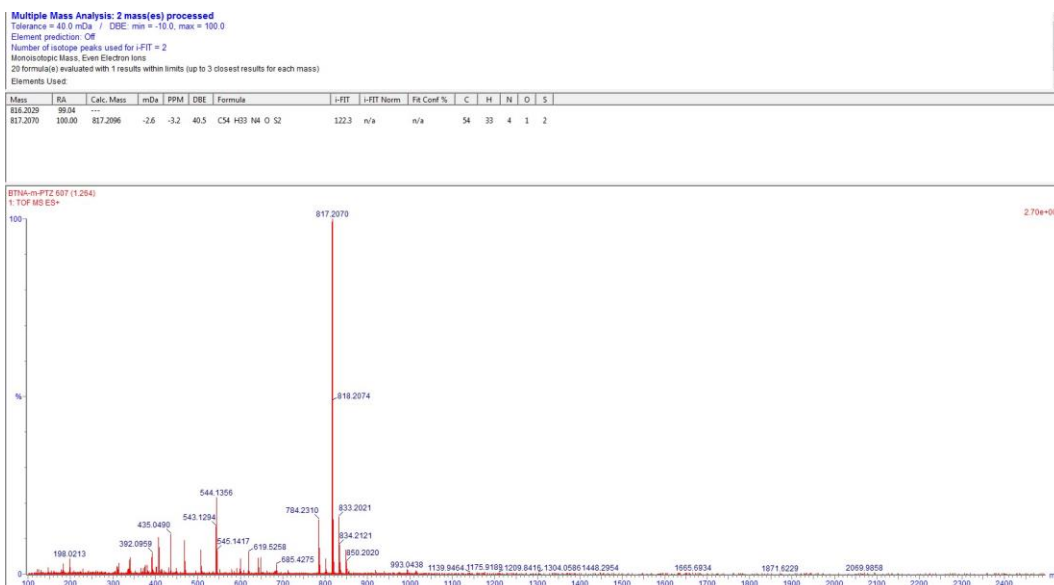
HRMS (TOF MS ES$^+$) of the compound **BTNA-m-PTZ.**

12.4 DQ-Donor and NQ-Donor compounds
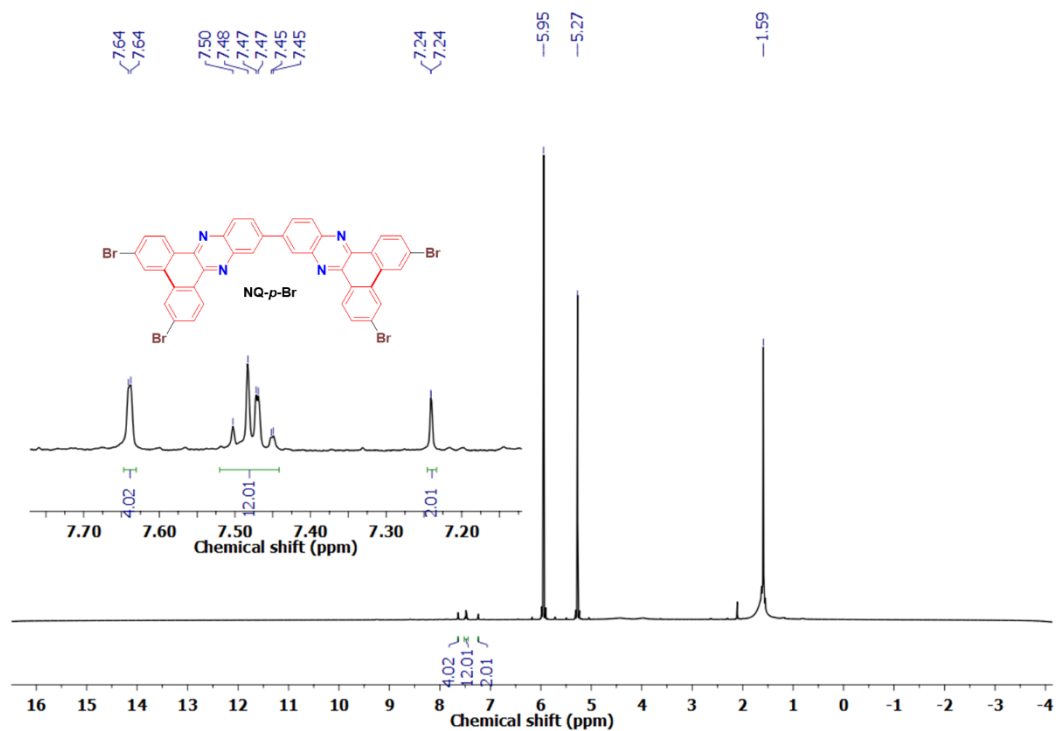
*¹H NMR (400 MHz) in C₂D₂Cl₄ of the compound **NQ-p-Br.** The low solubility in common deuterated solvents difficulties the ¹³C NMR analyses.*
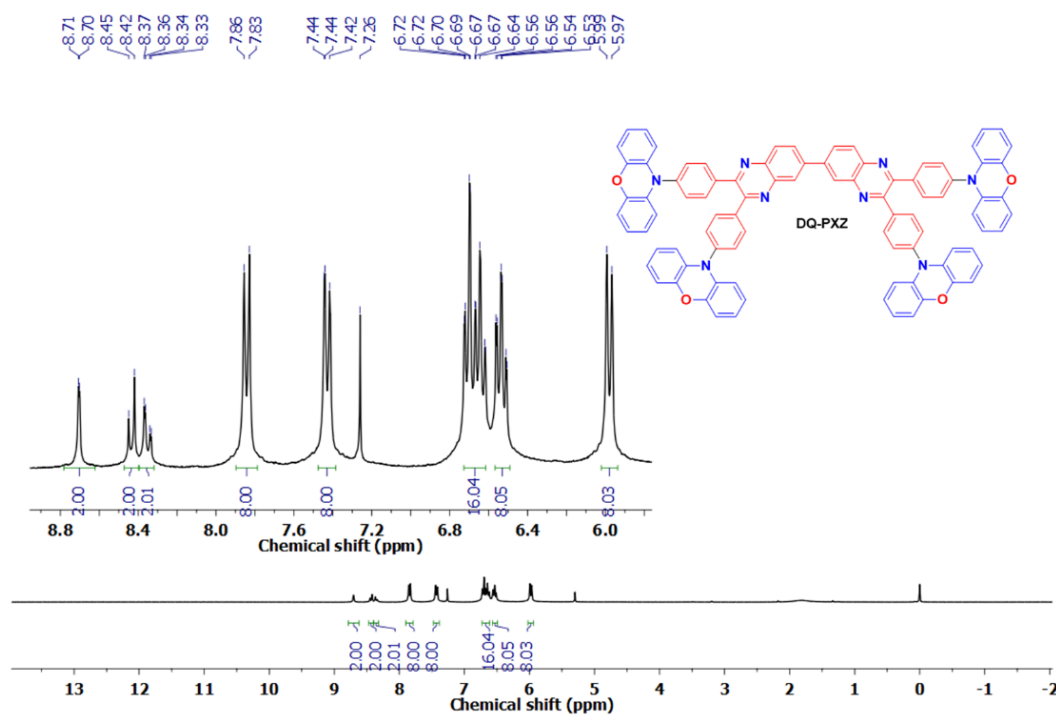
*¹H NMR (300 MHz) in CDCl₃ of the compound **DQ-PXZ.***
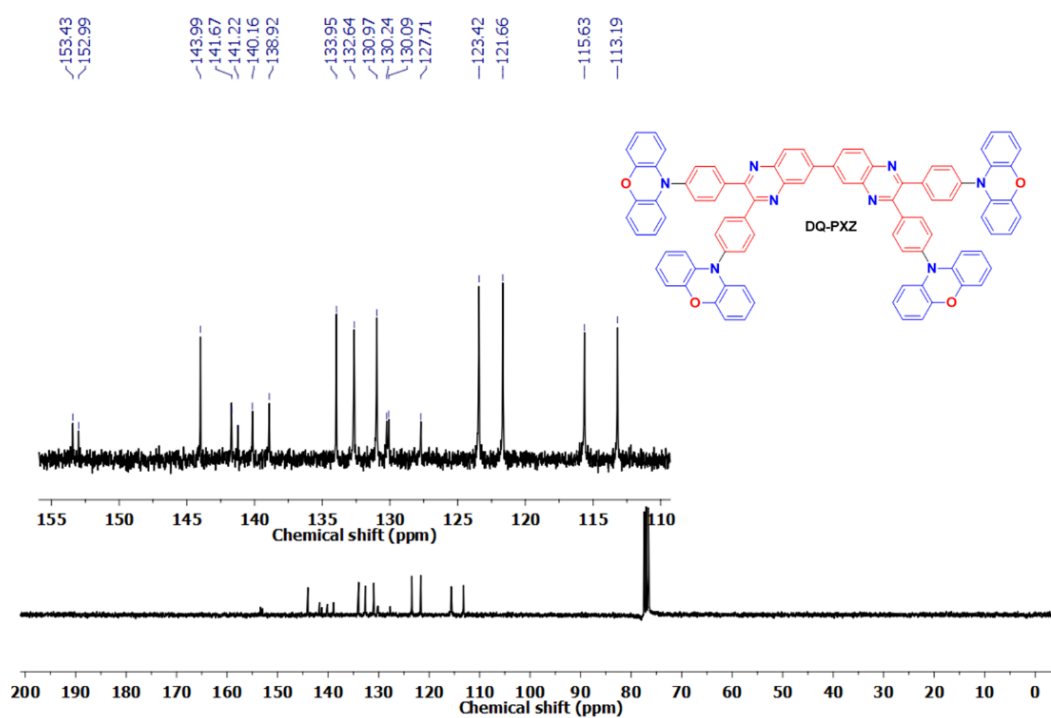
^{13}C NMR (75 MHz) in CDCl$_3$ of the compound **DQ-PXZ.**
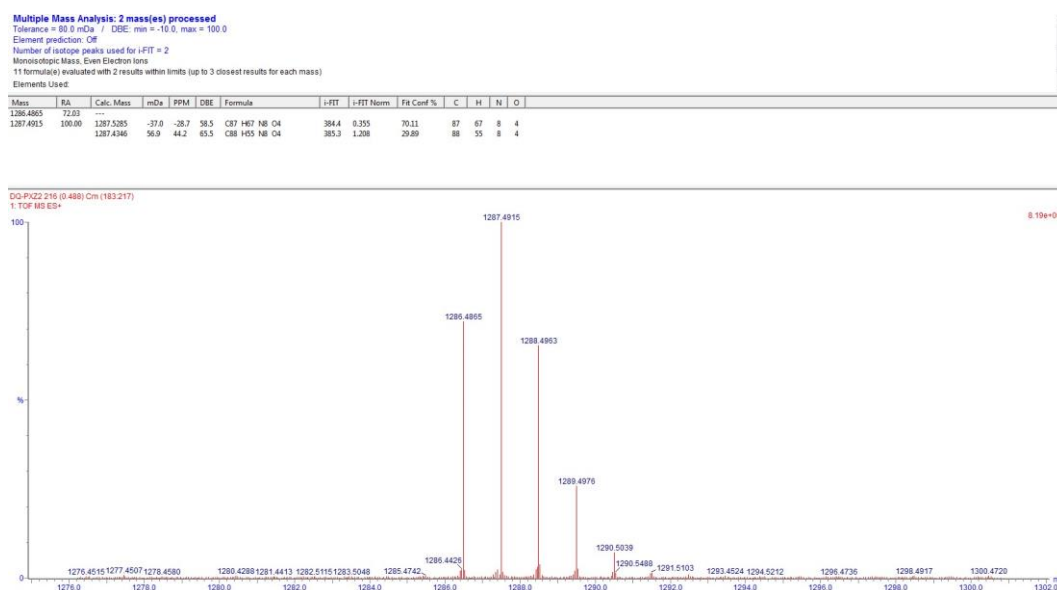
HRMS (TOF MS ES$^+$) of the compound **DQ-PXZ.**
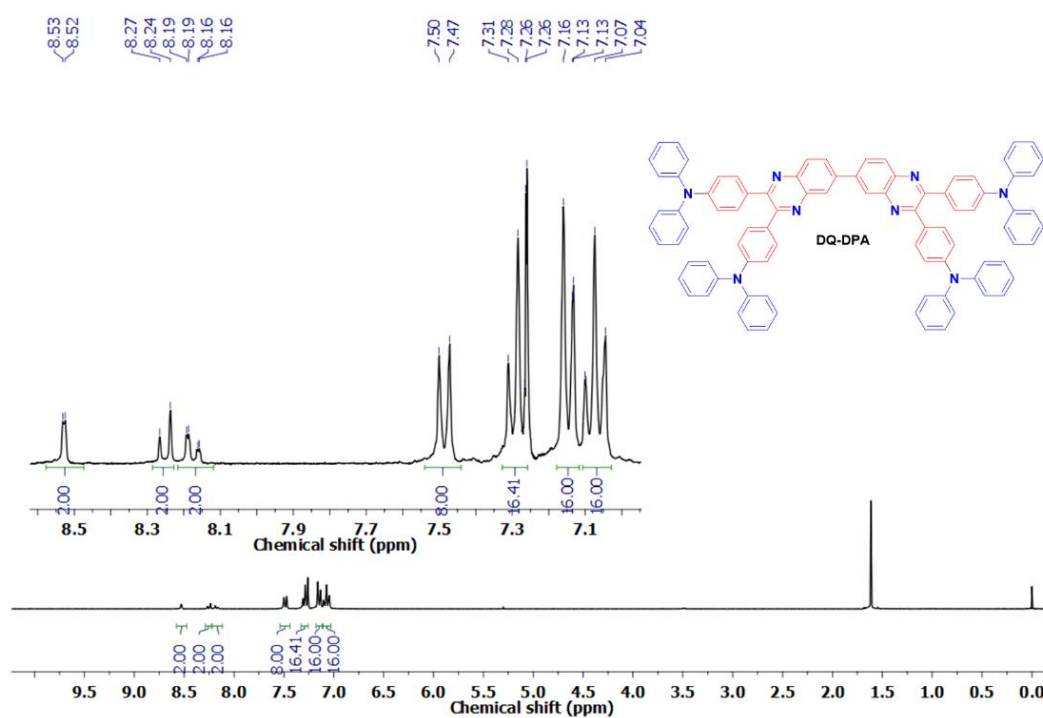
*1H NMR (300 MHz) in CDCl₃ of the compound **DQ-DPA.***
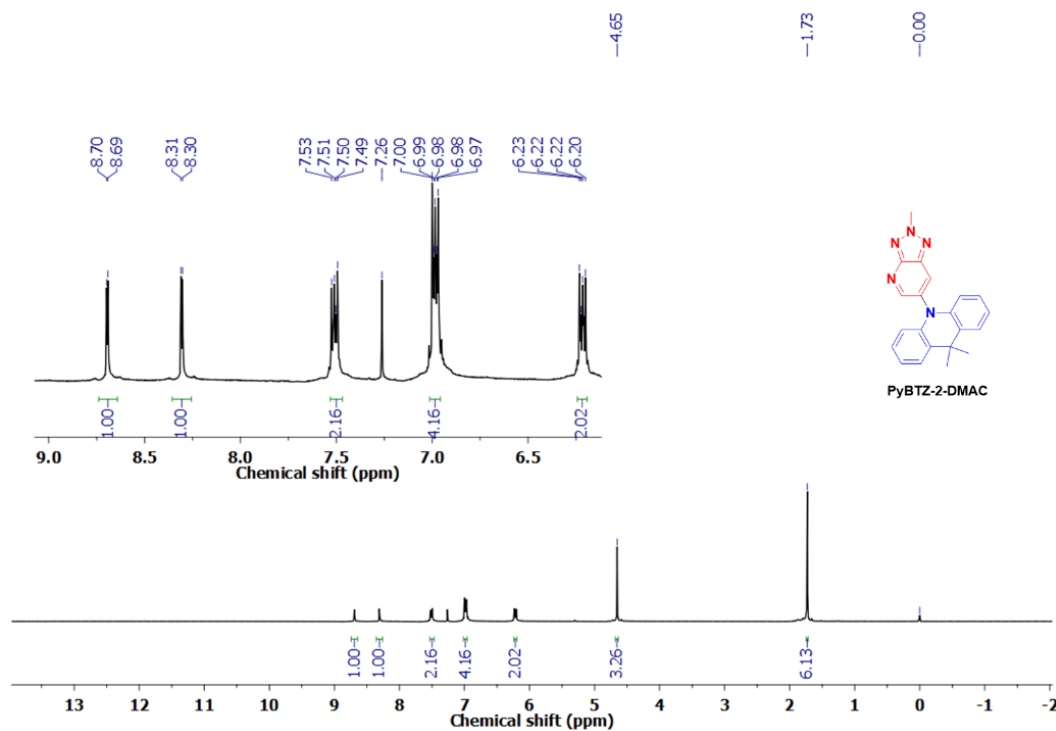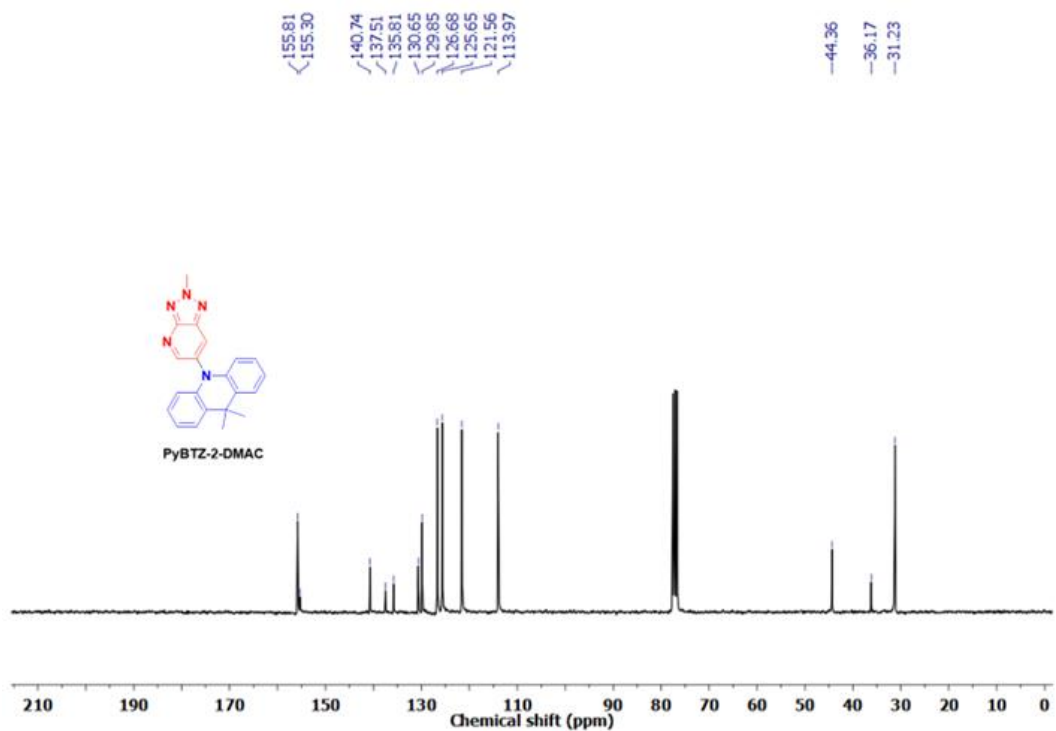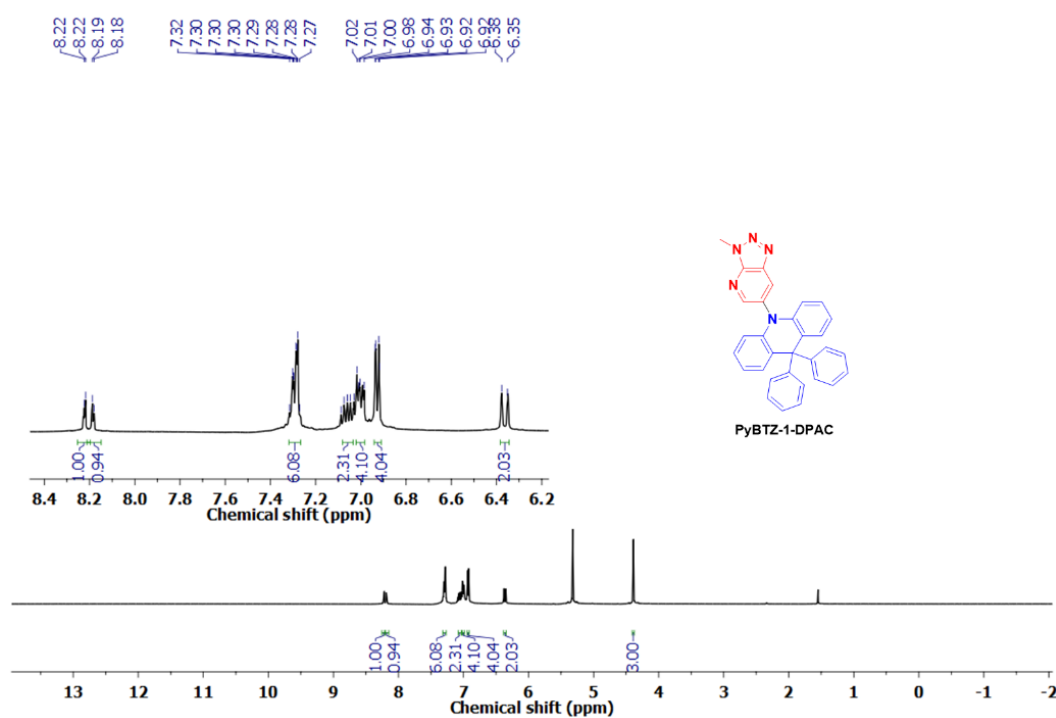

*13C NMR (75 MHz) in CDCl₃ of the compound **DQ-DPA.***

Multiple Mass Analysis: 2 mass(es) processed
Tolerance = 100.0 mDa / DBE: min = 0.0, max = 100.0
Element prediction: Off
Number of isotope peaks used for i-FIT = 2
Monoisotopic Mass, Odd and Even Electron Ions
18 formula(e) evaluated with 4 results within limits (up to 3 closest results for each mass)
Elements Used:

Mass	RA	Calc. Mass	mDa	PPM	DBE	Formula	i-FIT	i-FIT Norm	Fit Conf %	C	H	N
1231.5632	100.00	1231.5176	45.6	37.0	61.5	C88 H63 N8	240.4	0.837	43.28	88	63	8
		1231.6115	-48.3	-39.2	54.5	C87 H75 N8	240.1	0.567	56.72	87	75	8
1232.5652	90.85	1232.5254	39.8	32.3	61.0	C88 H64 N8	259.9	0.489	61.31	88	64	8
		1232.6193	-54.1	-43.9	54.0	C87 H76 N8	260.3	0.950	38.69	87	76	8

HRMS (TOF MS ES⁺) of the compound **DQ-DPA.**

^{1}H NMR (300 MHz) in $C_2D_2Cl_4$/DMSO-d_6 (2:1) of the compound **DQ-PTZ**.

^{1}H NMR (600 MHz) in DMSO-d$_6$ of the compound **DQ-PTZ**.
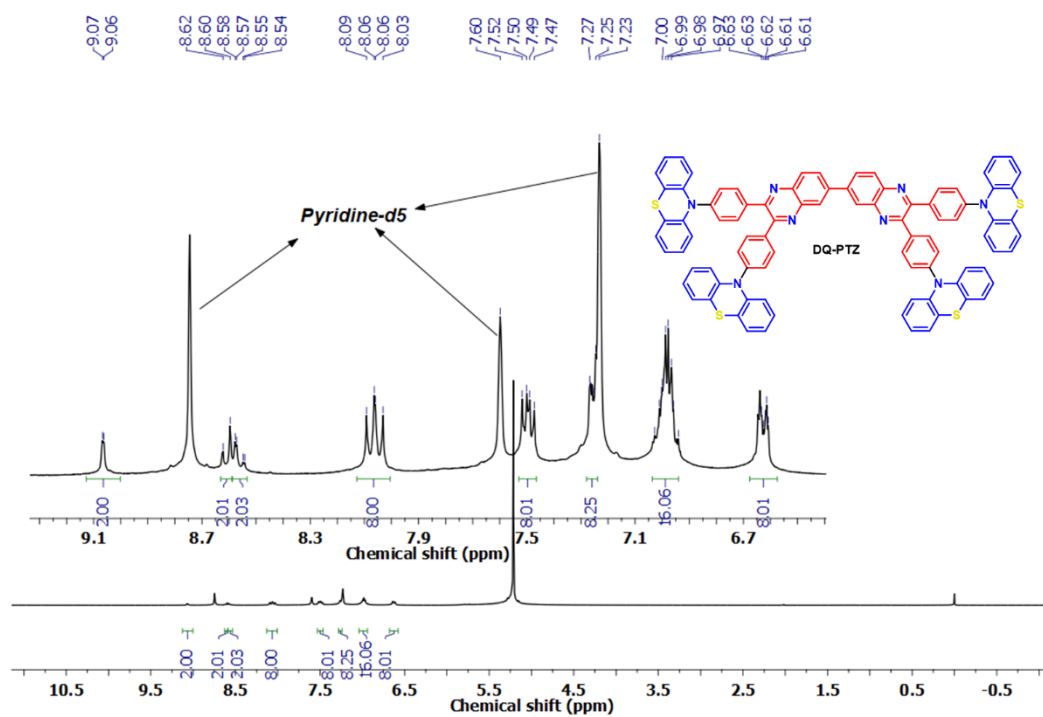
^{1}H NMR (300 MHz) in pyridine-d$_5$ of the compound **DQ-PTZ**.
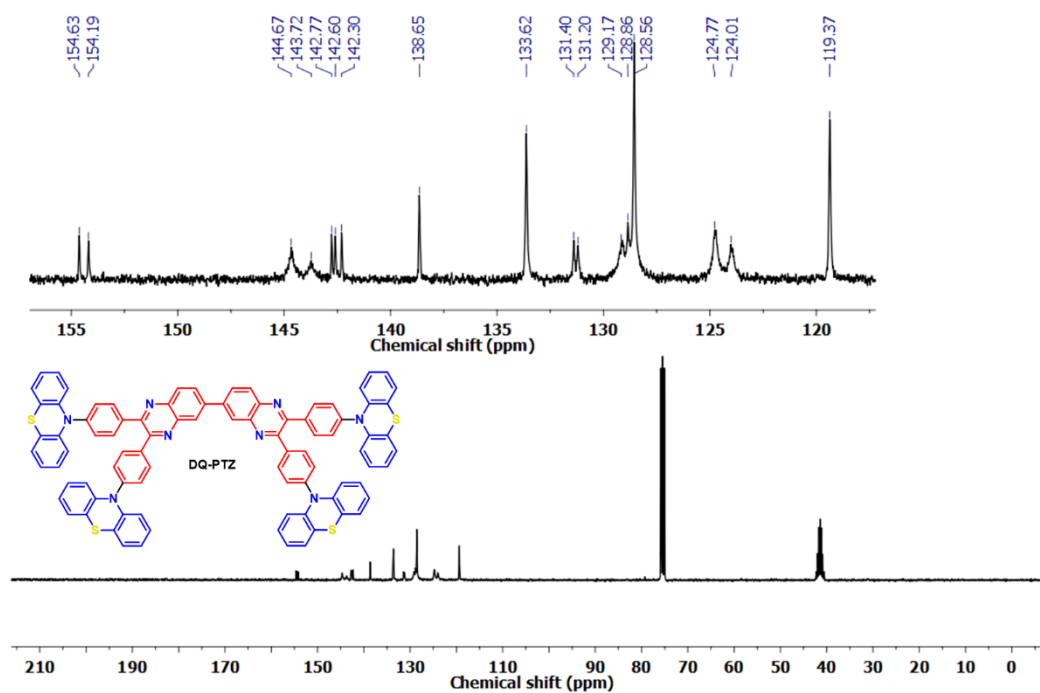
^{13}C NMR (75 MHz) in $C_2D_2Cl_4$/DMSO-d_6 (2:1) of the compound **DQ-PTZ**.
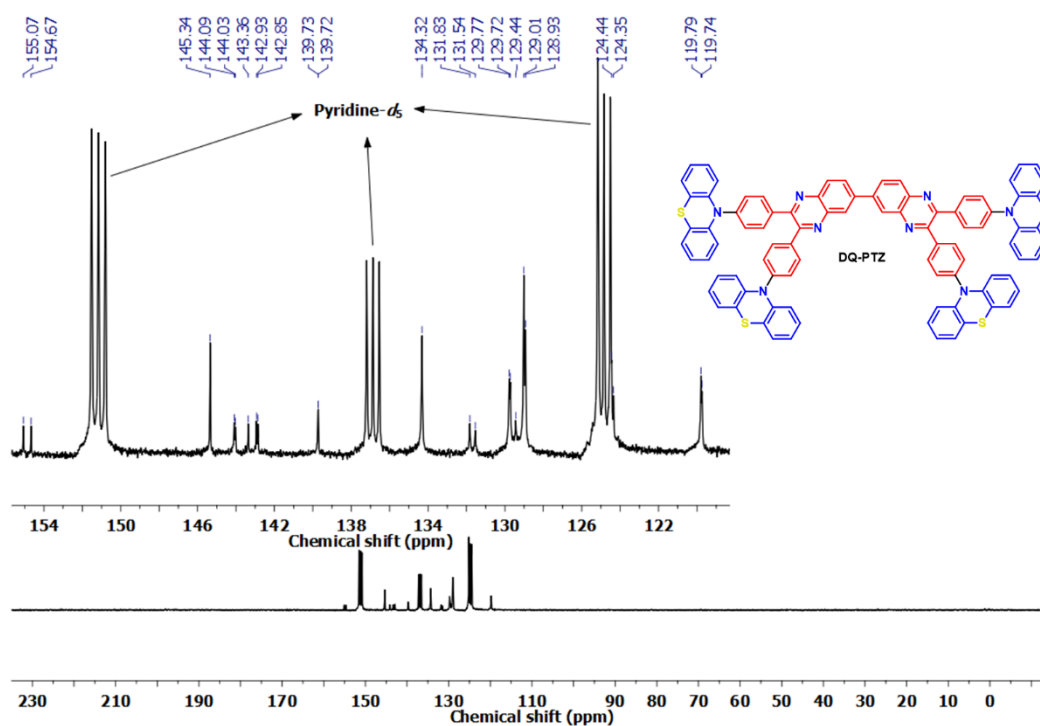
^{13}C NMR (75 MHz) in pyridine-d_5 of the compound **DQ-PTZ**.
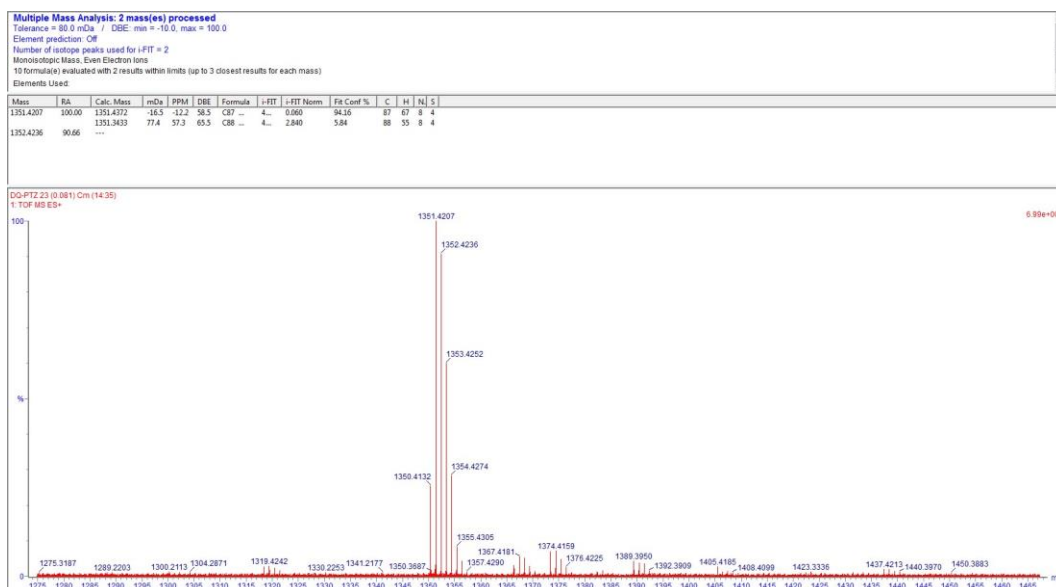
*HRMS (TOF MS ES⁺) of the compound **DQ-PTZ**.*
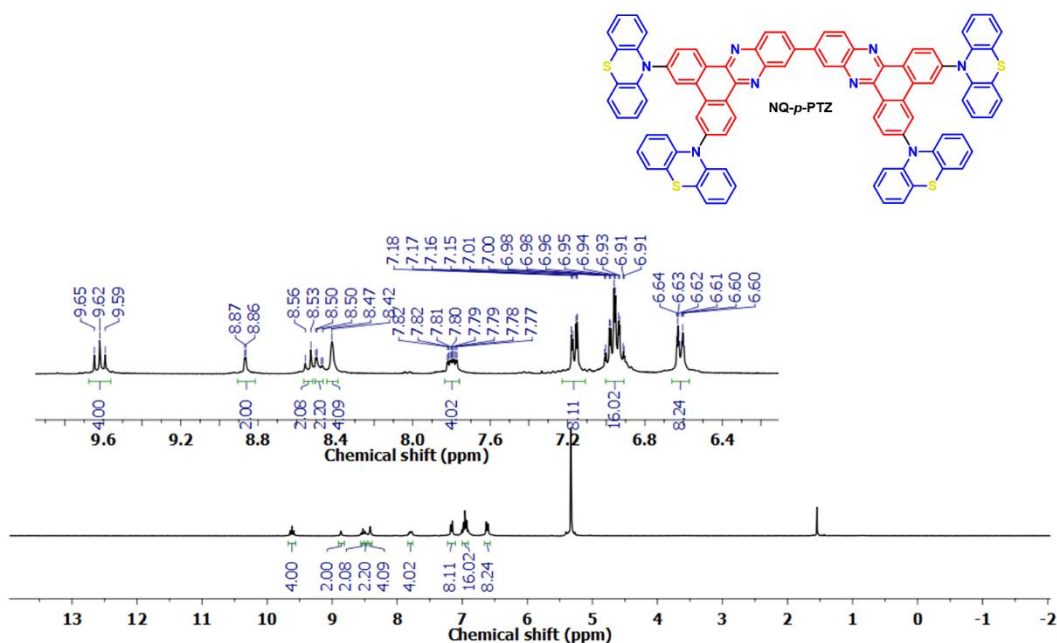
*¹H NMR (300 MHz) in CD₂Cl₂ of the compound **NQ-p-PTZ**.*

184
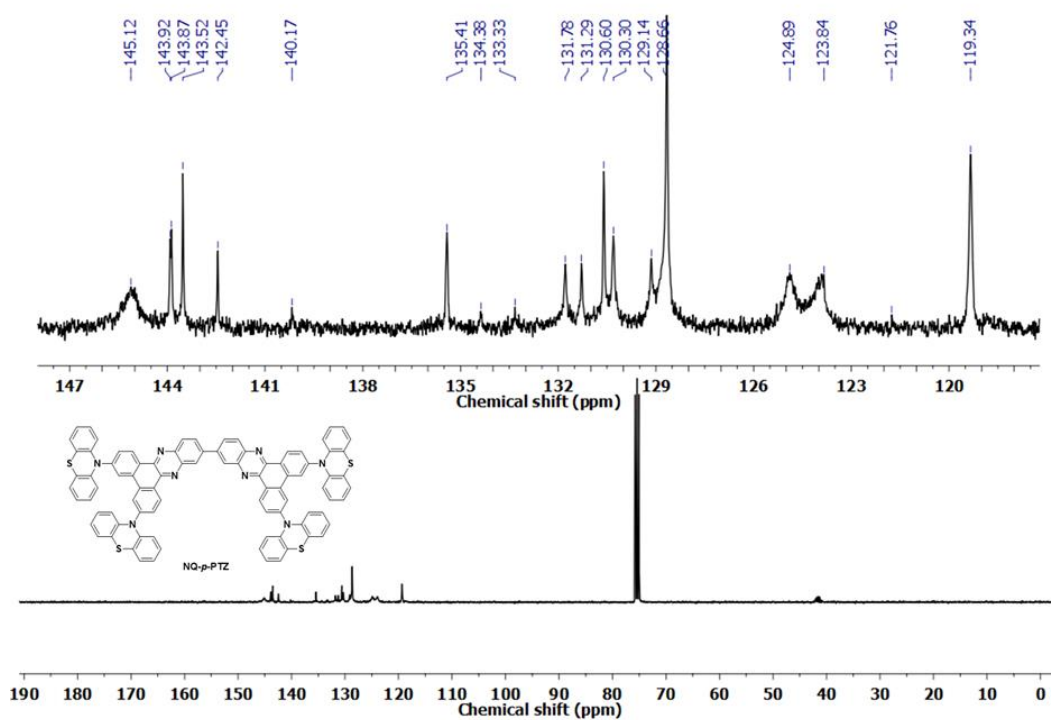
13C NMR (75 MHz) in C₂D₂Cl₄/DMSO-d₆ of the compound NQ-p-PTZ. Due to low solubility in common deuterated solvents was difficult to get a good 13C NMR spectra.

1H NMR (300 MHz) in CDCl₃ of the compound NQ-m-PTZ.

Welisson de Pontes Silva
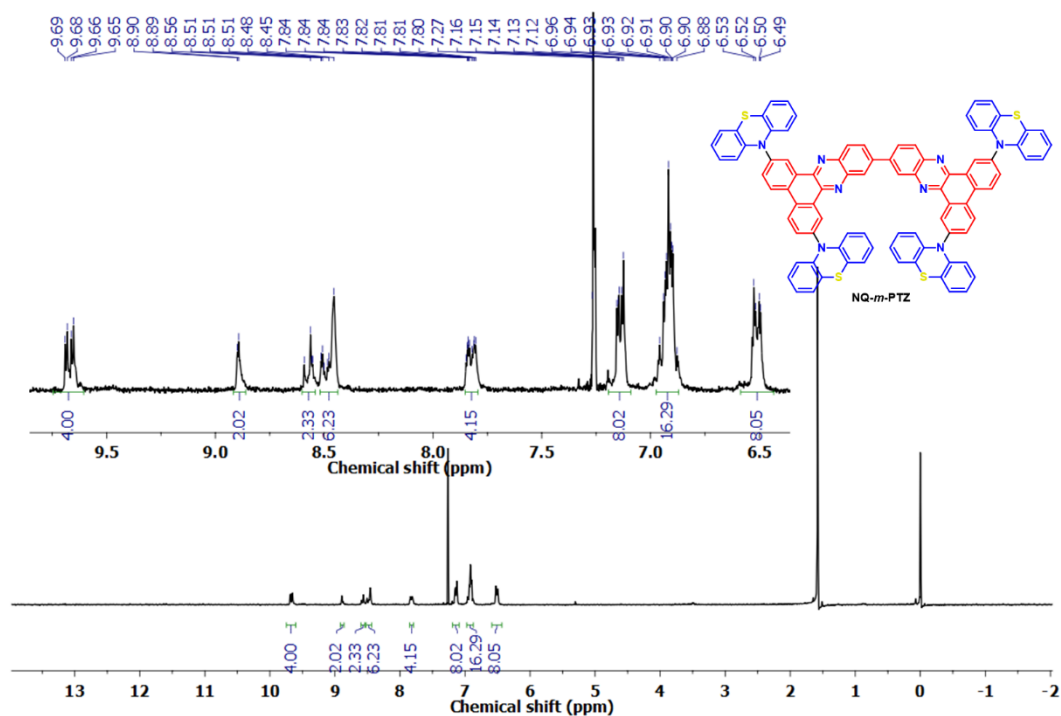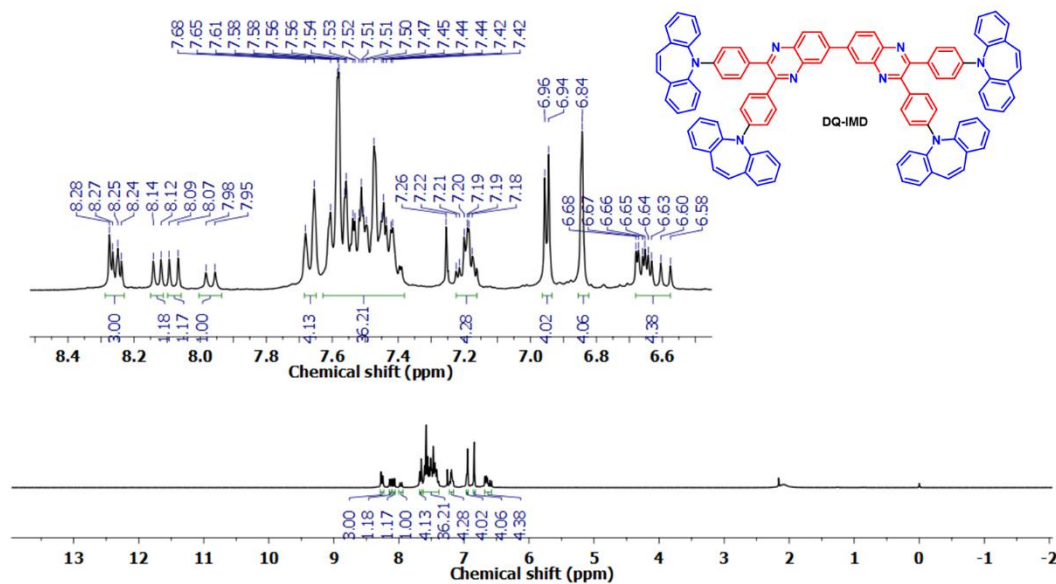
^{1}H NMR (300 MHz) in CDCl$_3$ of the compound **DQ-IMD.**
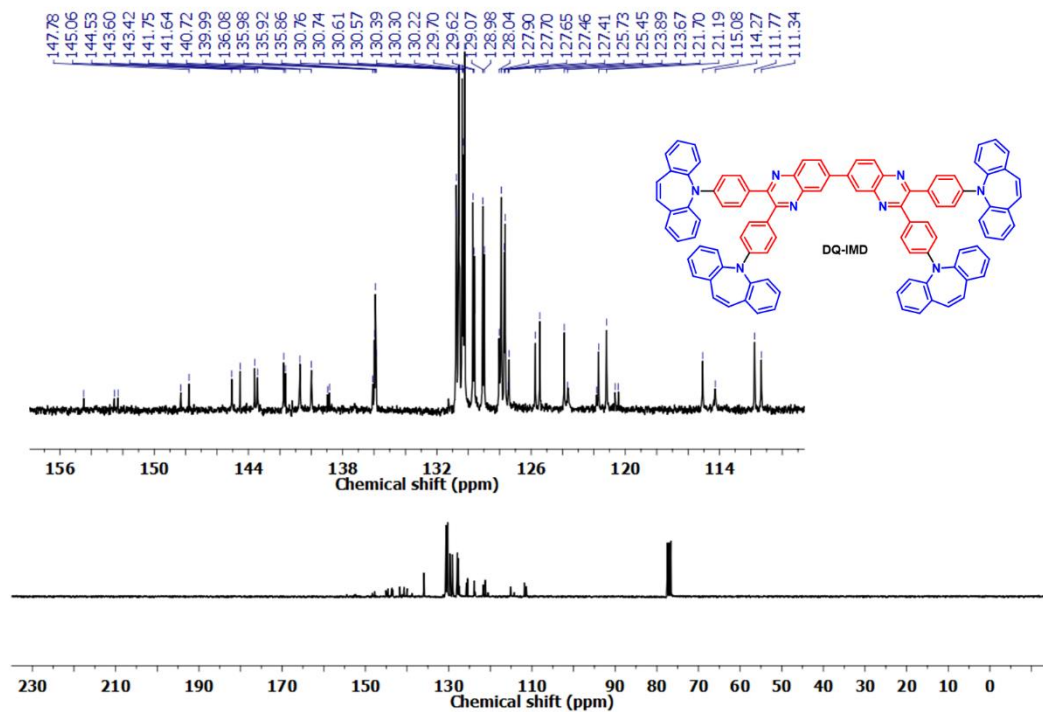
^{13}C NMR (75 MHz) in CDCl$_3$ of the compound **DQ-IMD.**
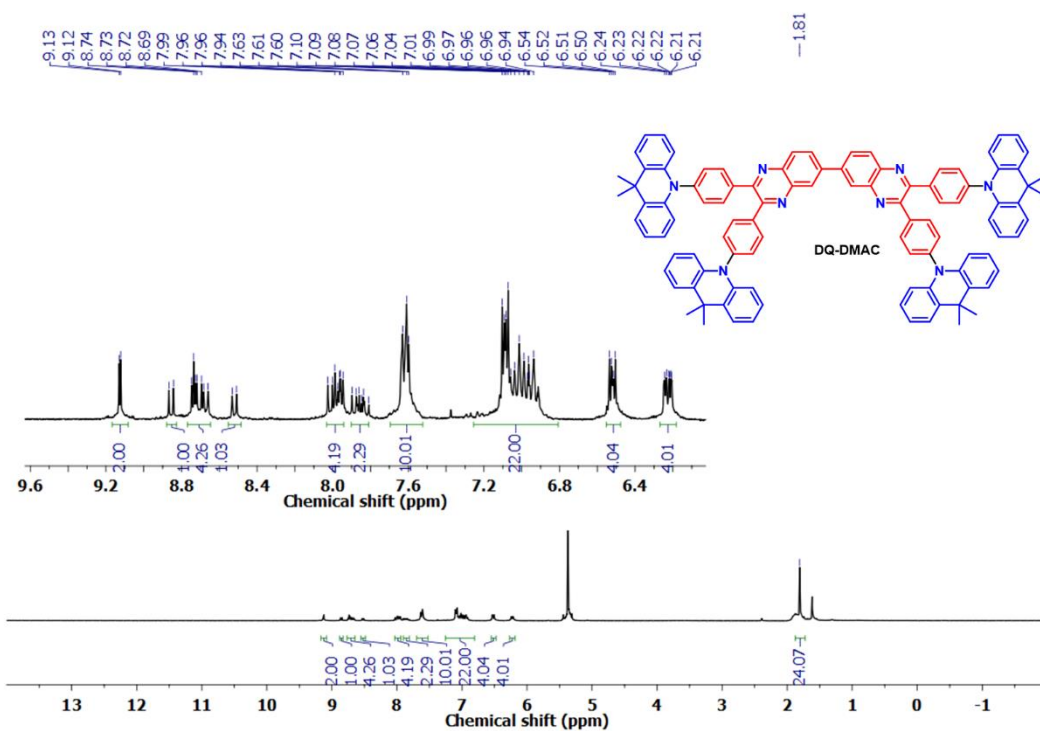
*¹H NMR (300 MHz) in CDCl₃ of the compound **DQ-DDA**.*

*¹³C NMR (75 MHz) in CDCl₃ of the compound **DQ-DDA**.*

*¹H NMR (300 MHz) in CD₂Cl₂ of the compound **DQ-DMAC.***
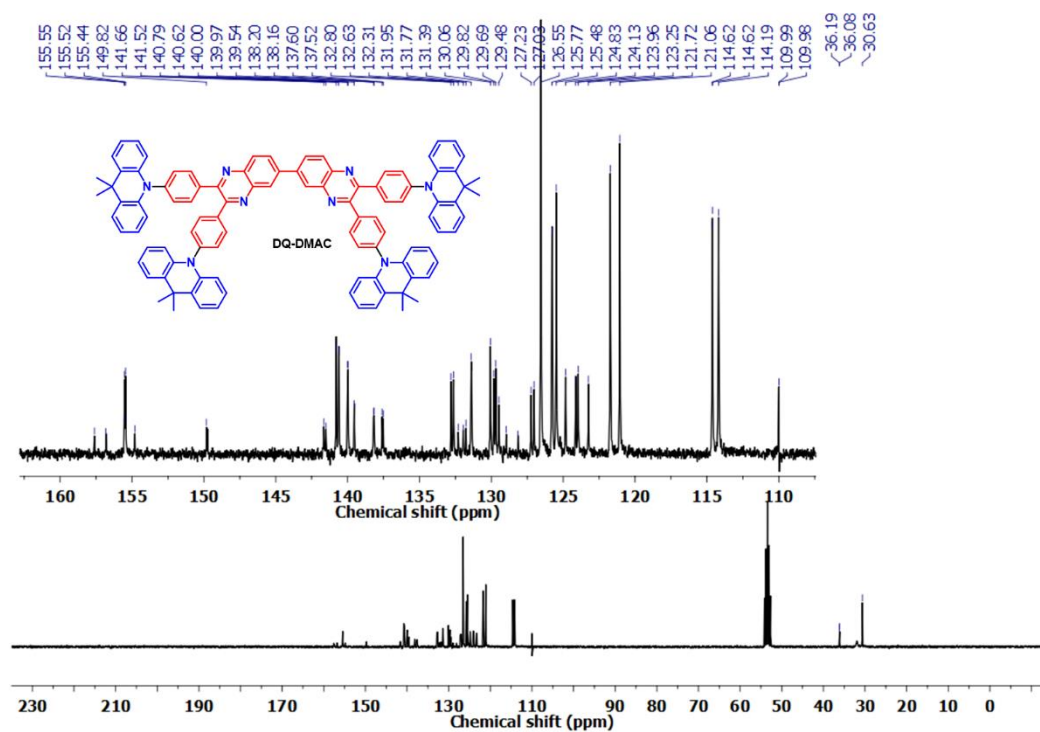
*¹H NMR (75 MHz) in CD₂Cl₂ of the compound **DQ-DMAC.***
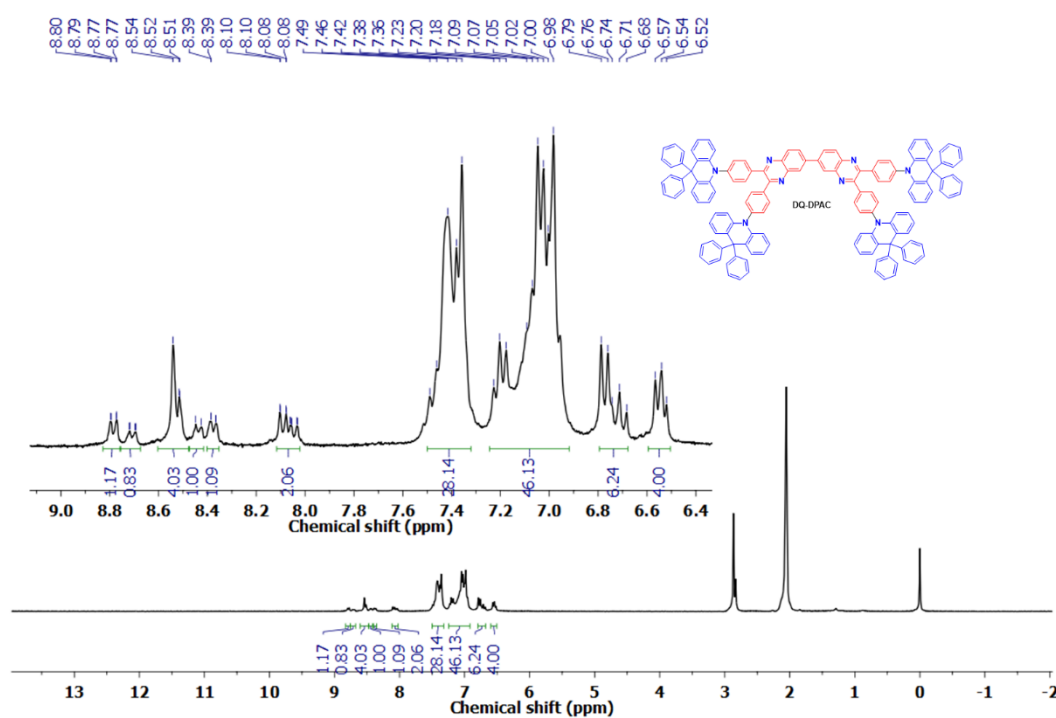
*1H NMR (300 MHz) in acetone-d6 of the compound **DQ-DPAC**.*
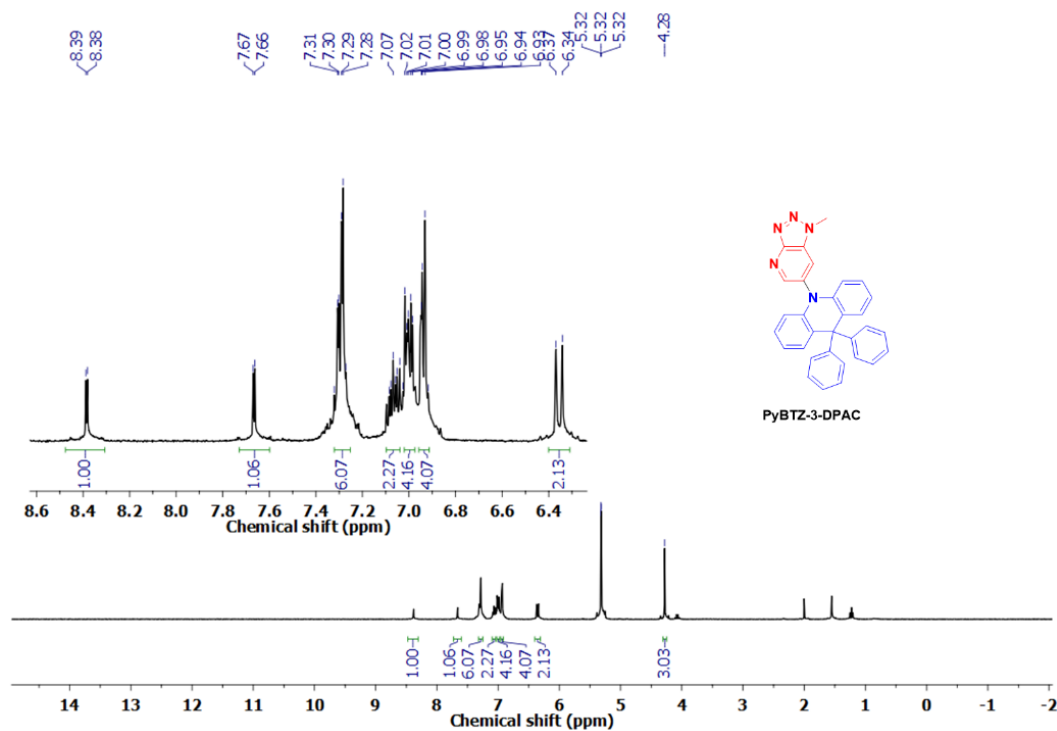
12.5 PyBTZ-1,2,3-Donor compounds
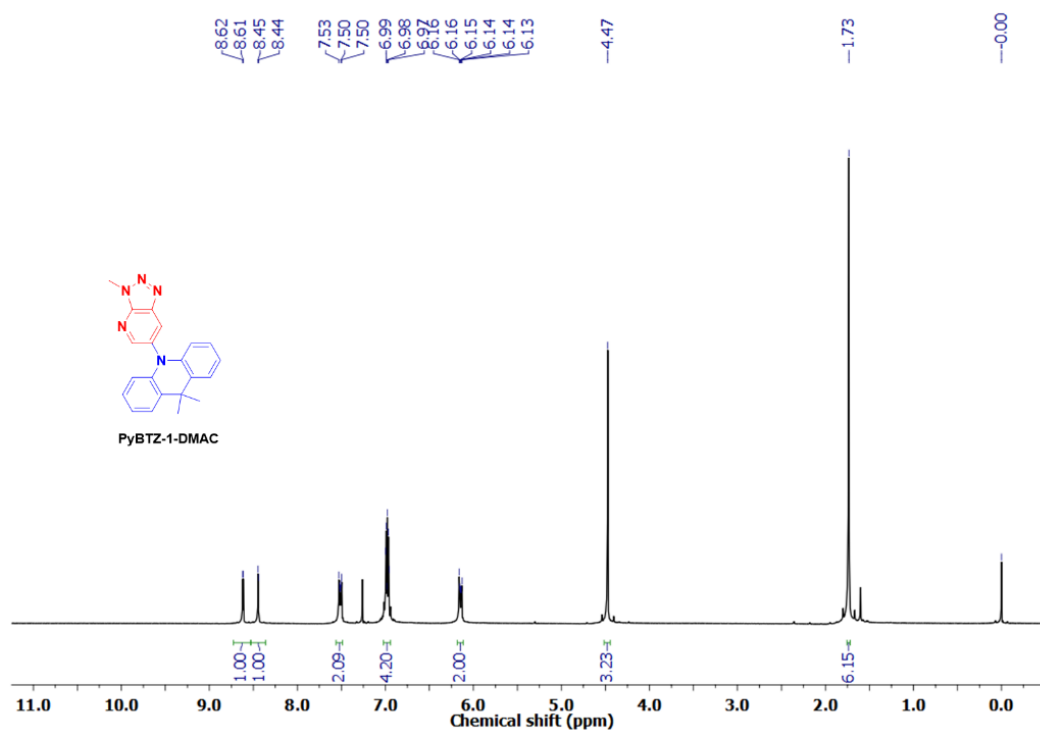
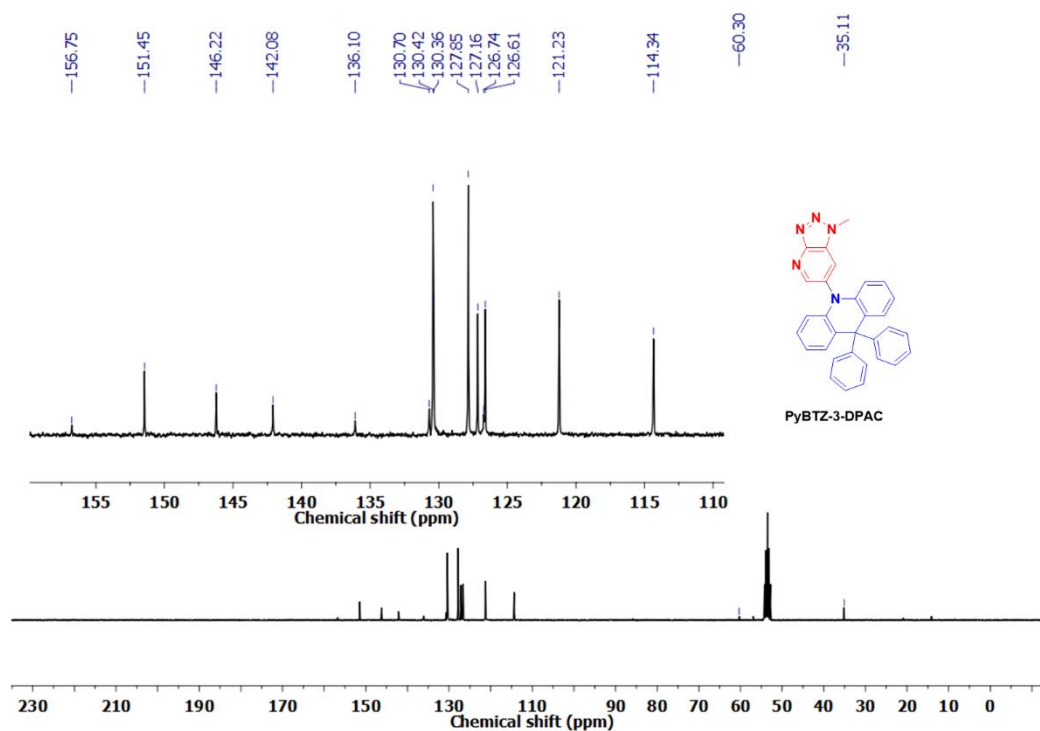*1H NMR (300 MHz) in CDCl3 of the compound **PyBTZ-1-DMAC**.*
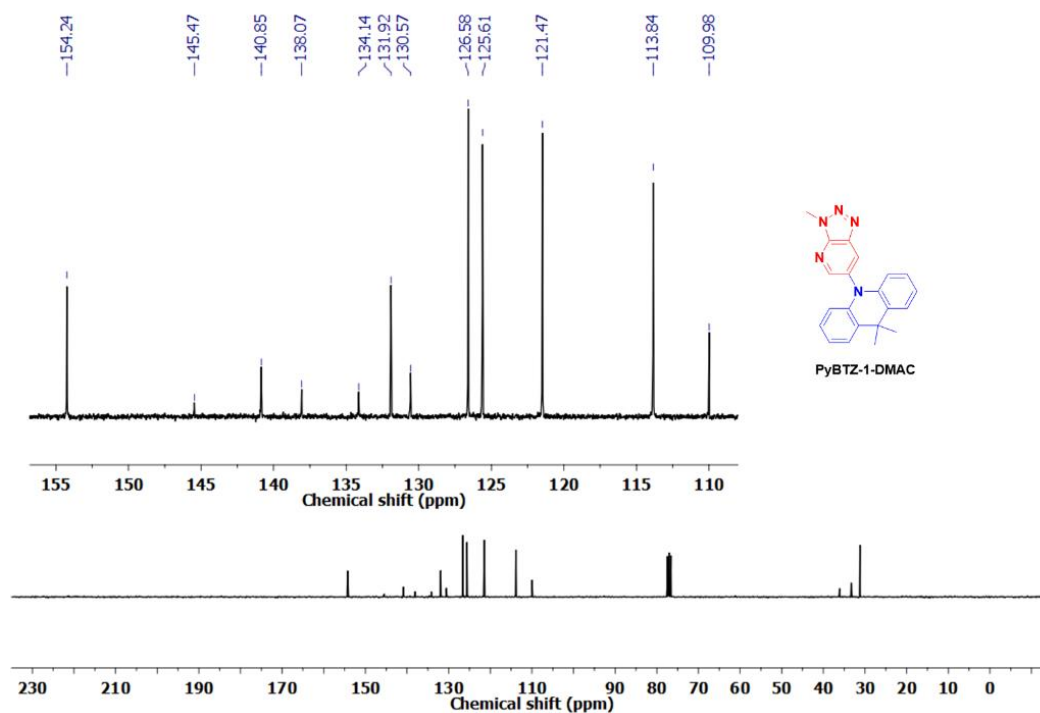
^{13}C NMR (75 MHz) in CDCl$_3$ of the compound **PyBTZ-1-DMAC.**

HRMS (TOF MS ES$^+$) of the compound **PyBTZ-1-DMAC.**

^{1}H NMR (300 MHz) in CDCl$_3$ of the compound **PyBTZ-2-DMAC.**

^{13}C NMR (75 MHz) in CDCl$_3$ of the compound **PyBTZ-2-DMAC.**

*HRMS (TOF MS ES⁺) of the compound **PyBTZ-2-DMAC.***

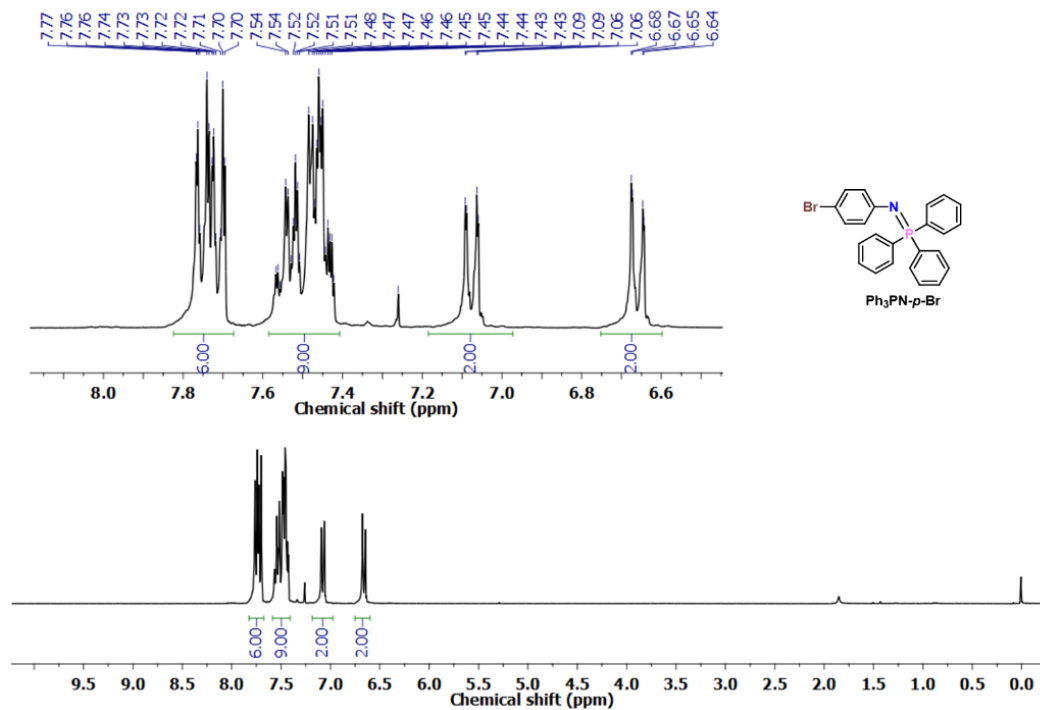*^{1}H NMR (300 MHz) in CDCl$_3$ of the compound **PyBTZ-3-DMAC.***

155.10 31.27
151.98
148.66
140.62
136.60
130.64
126.89
126.63
125.70
121.67
121.05
113.91
36.09
35.10
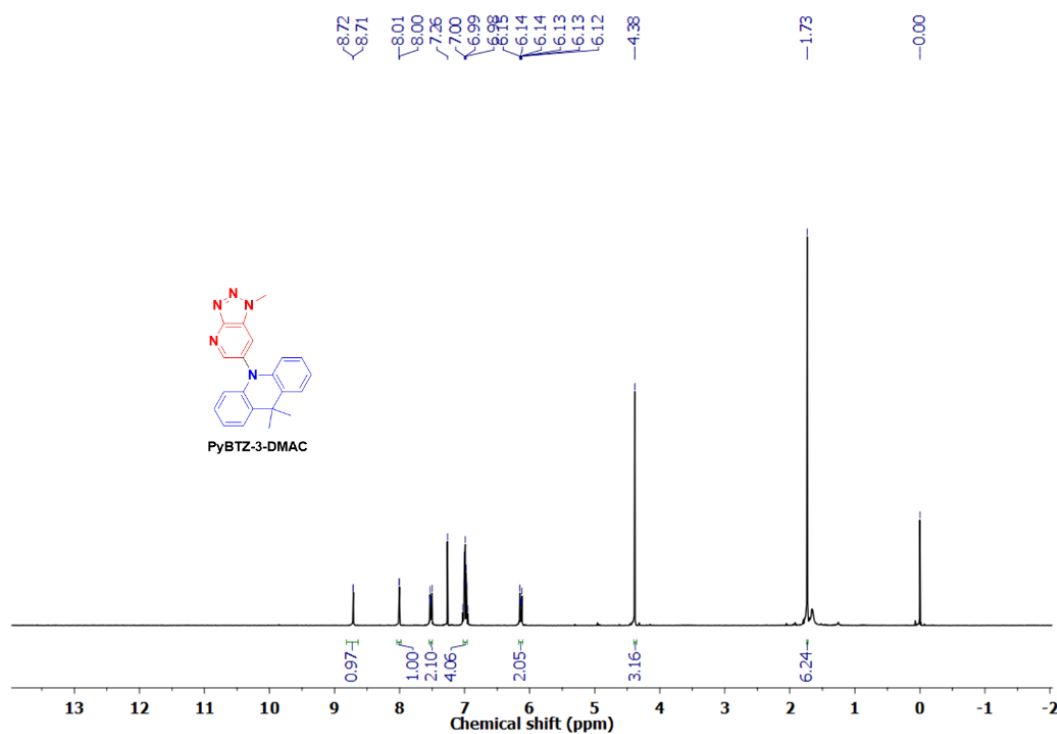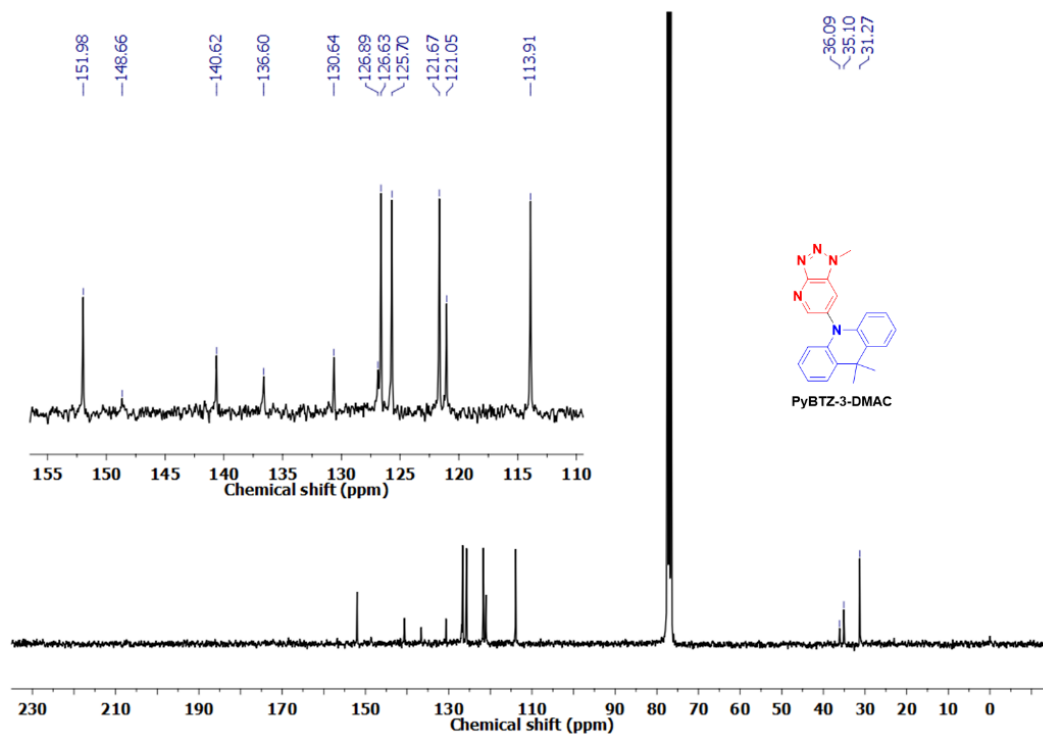
PyBTZ-3-DMAC

^{13}C NMR (75 MHz) in CDCl$_3$ of the compound **PyBTZ-3-DMAC.**

HRMS (TOF MS ES$^+$) of the compound **PyBTZ-3-DMAC.**

8.22, 8.22, 8.19, 8.18
7.32, 7.30, 7.30, 7.30, 7.29, 7.28, 7.28, 7.27
7.02, 7.01, 7.00, 6.98, 6.94, 6.93, 6.92, 6.38, 6.35

PyBTZ-1-DPAC

*1H NMR (300 MHz) in CD2Cl2 of the compound **PyBTZ-1-DPAC.***

153.72, 146.10, 145.50, 142.13, 137.65, 133.49, 131.41, 130.53, 130.33, 130.16, 127.72, 127.02, 126.50, 120.92, 114.12
56.82
33.09, 29.68

PyBTZ-1-DPAC

*13C NMR (75 MHz) in CD2Cl2 of the compound **PyBTZ-1-DPAC.***

Welisson de Pontes Silva
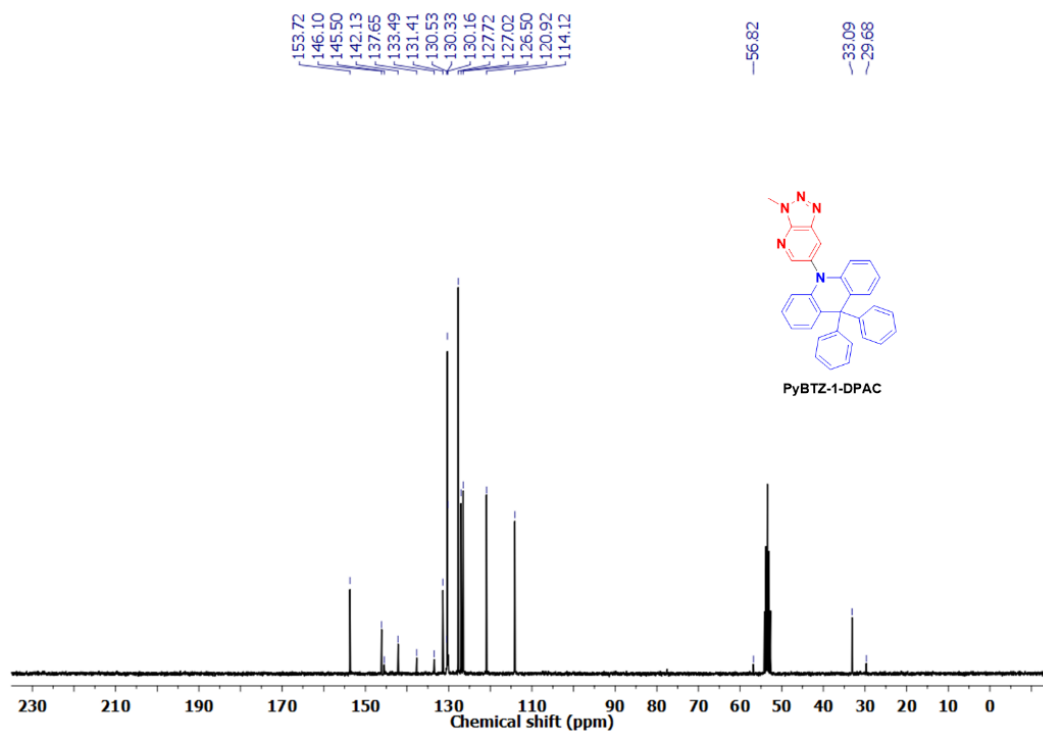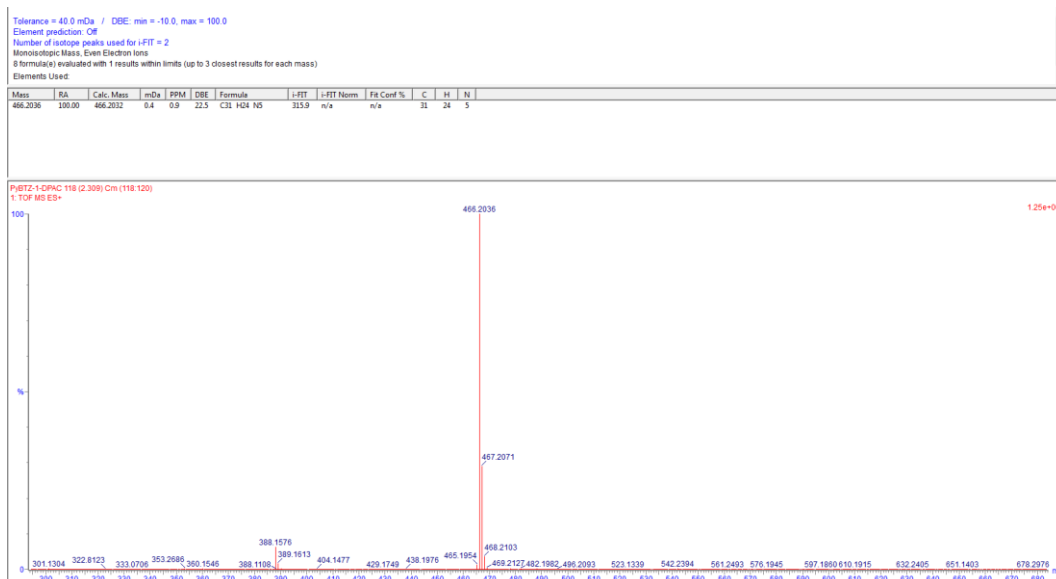
*HRMS (TOF MS ES⁺) of the compound **PyBTZ-1-DPAC**.*
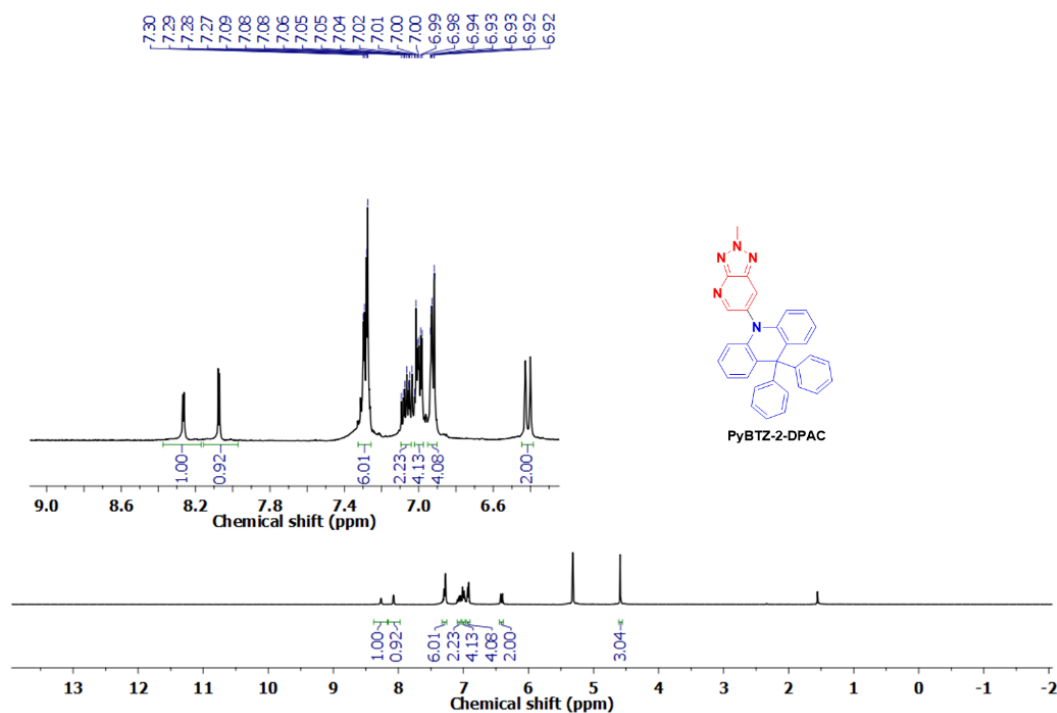
*¹H NMR (300 MHz) in CD₂Cl₂ of the compound **PyBTZ-2-DPAC**.*
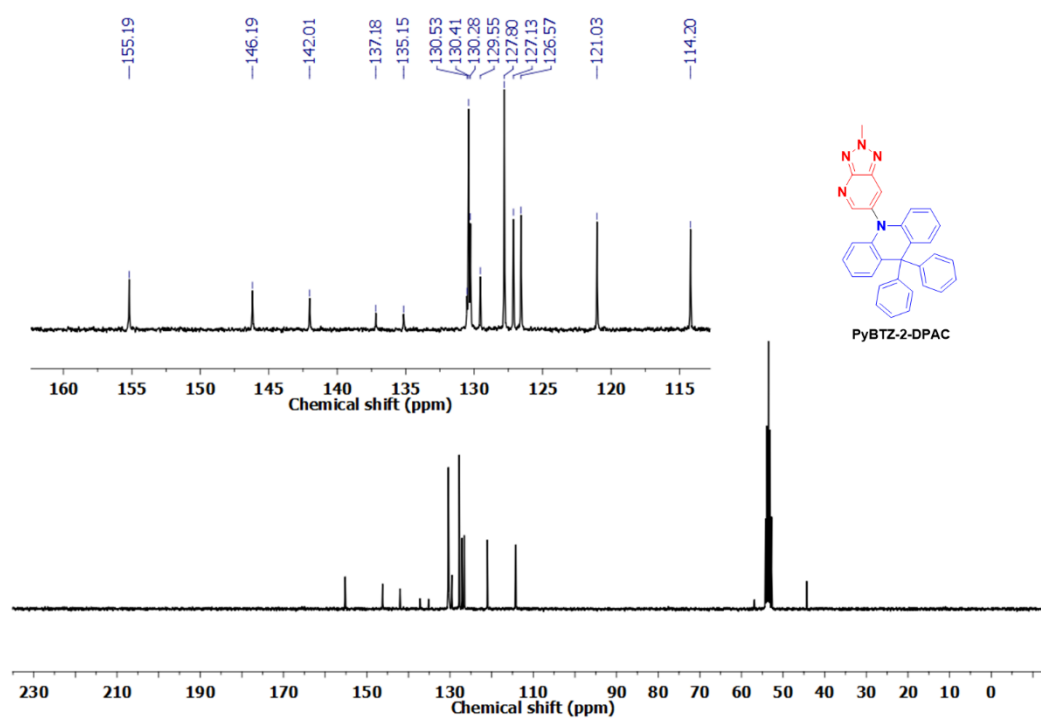
^{13}C NMR (75 MHz) in CD$_2$Cl$_2$ of the compound **PyBTZ-2-DPAC.**
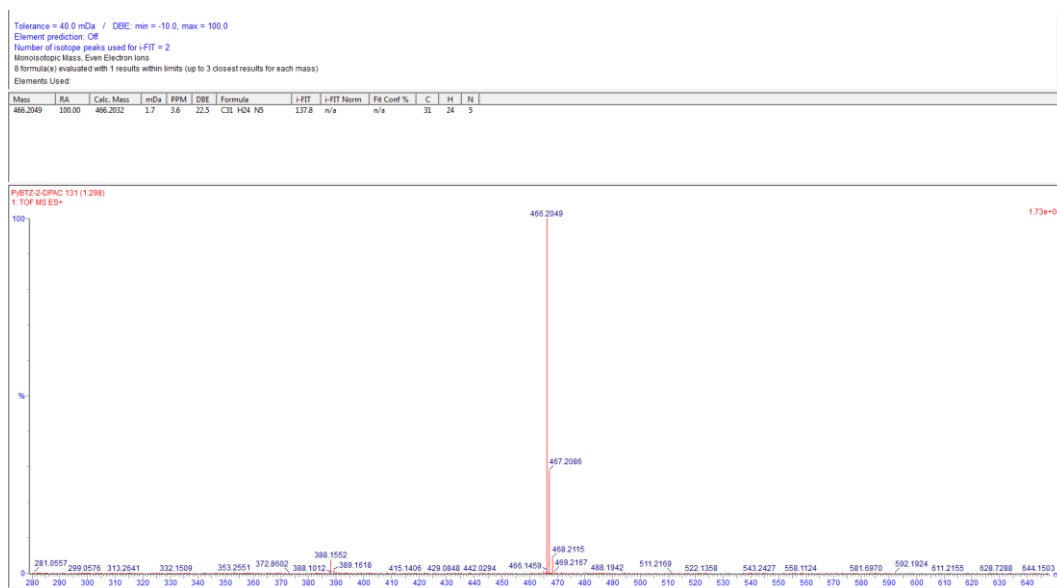
HRMS (TOF MS ES$^+$) of the compound **PyBTZ-2-DPAC.**

*¹H NMR (300 MHz) in CD₂Cl₂ of the compound **PyBTZ-3-DPAC.***

*¹³C NMR (75 MHz) in CD₂Cl₂ of the compound **PyBTZ-3-DPAC.***

*HRMS (TOF MS ES⁺) of the compound **PyBTZ-3-DPAC.***
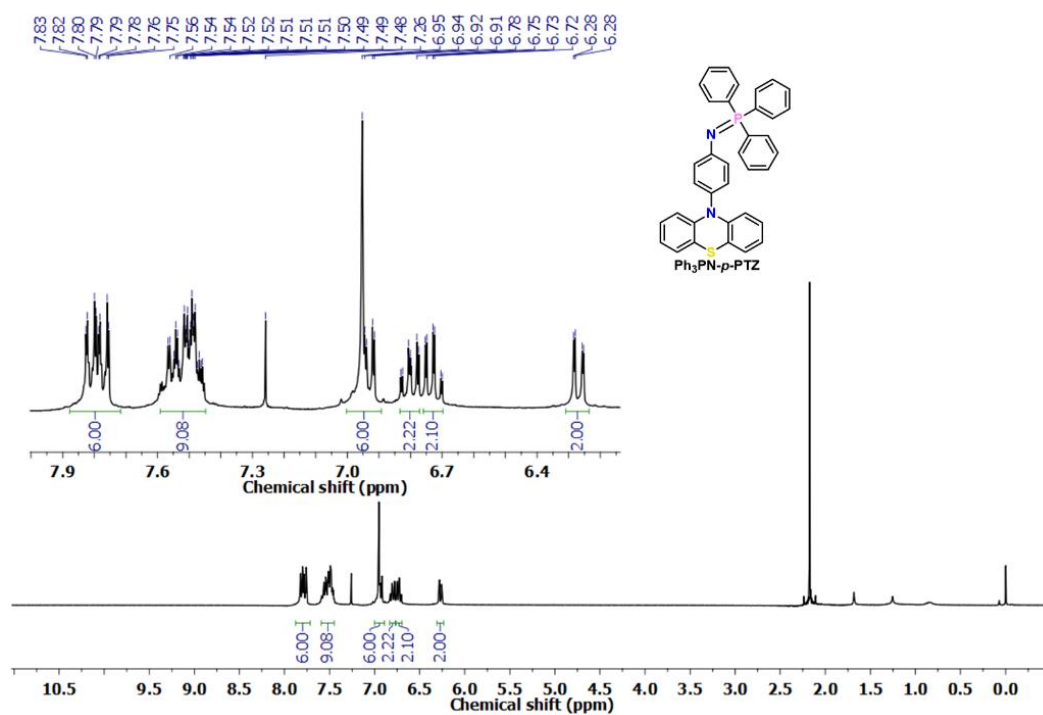
12.6 Ph3PN-p,m-PTZ compounds

^{1}*H NMR (300 MHz) in CDCl₃ of the compound **Ph₃PN-p-Br.***
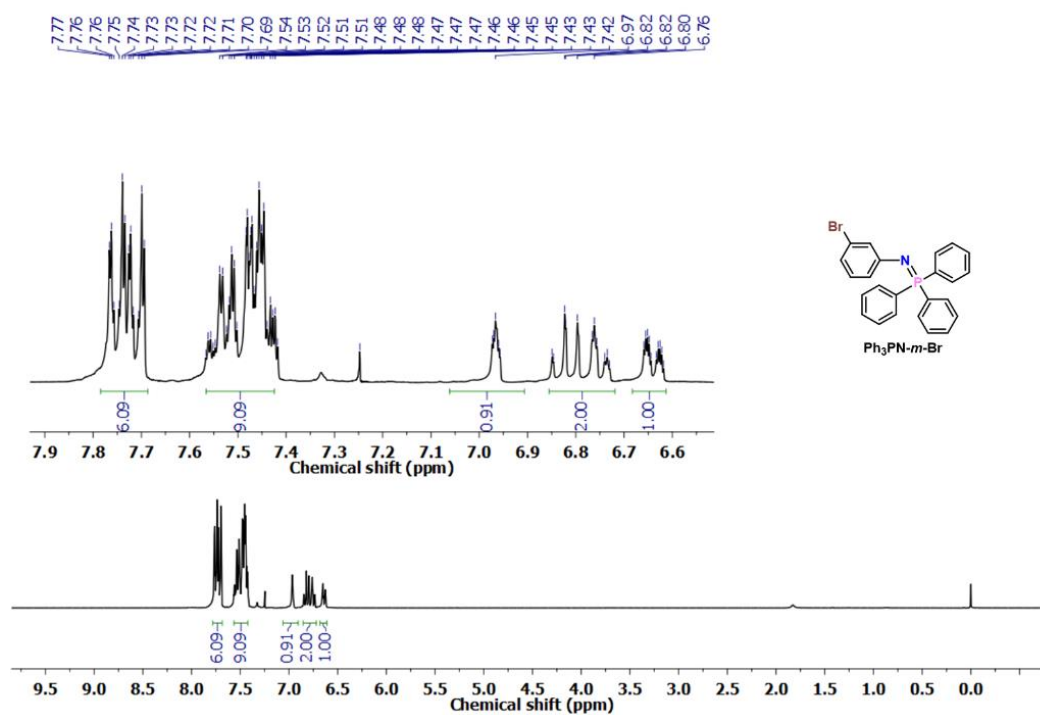
*1H NMR (300 MHz) in CDCl3 of the compound **Ph3PN-m-Br.***
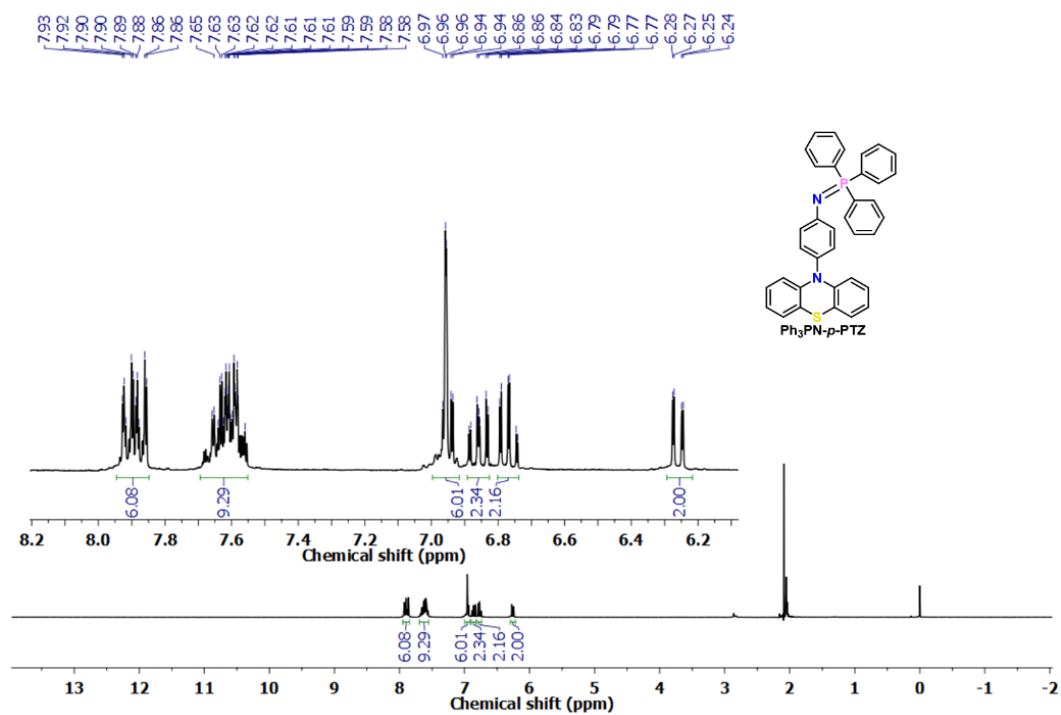
*1H NMR (300 MHz) in Acetone-d6 of the compound **Ph3PN-p-PTZ.***

*¹H NMR (300 MHz) in CDCl₃ of the compound **Ph₃PN-p-PTZ**.*
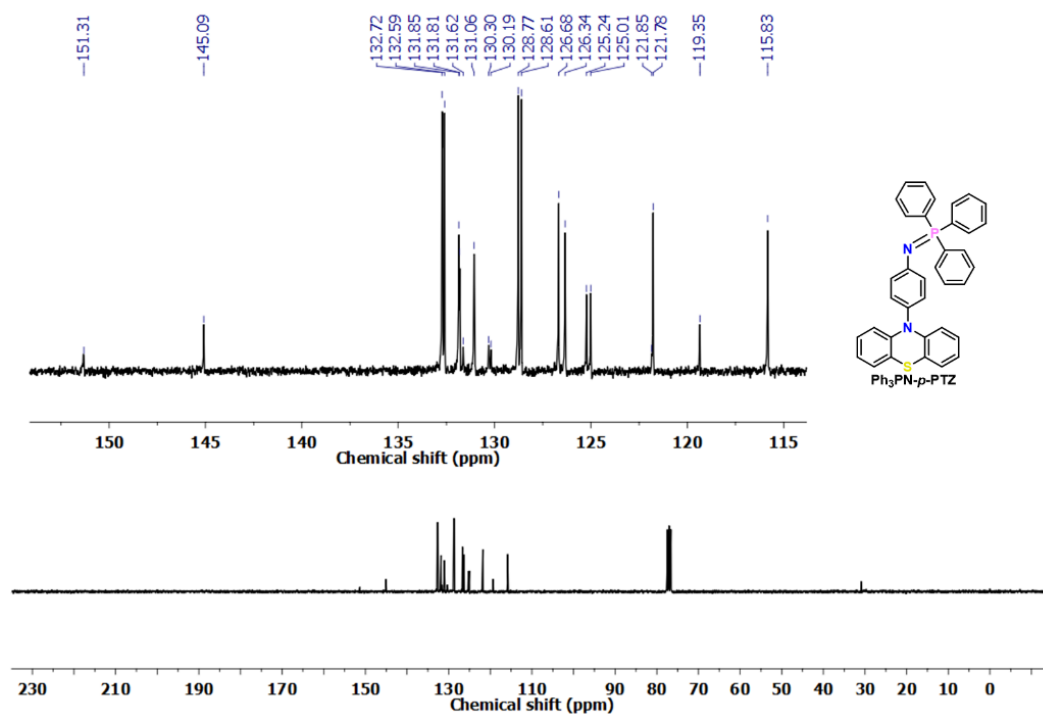
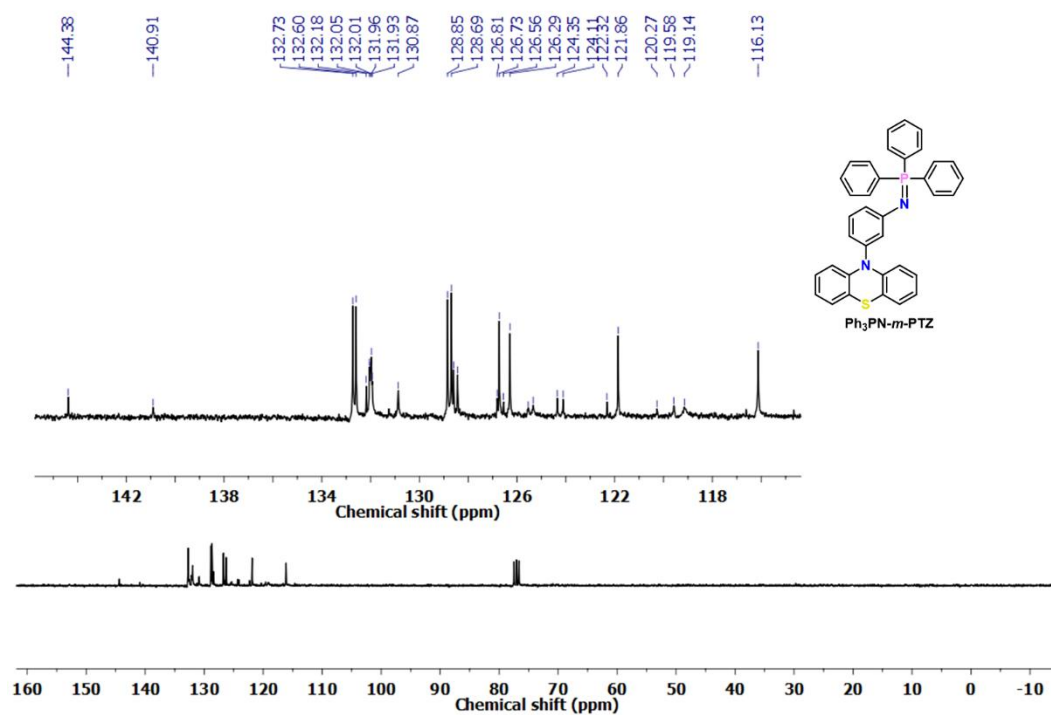*¹³C NMR (75 MHz) in CDCl₃ of the compound **Ph₃PN-p-PTZ**.*

HRMS (TOF MS ES⁺) of the compound **Ph₃PN-p-PTZ.**
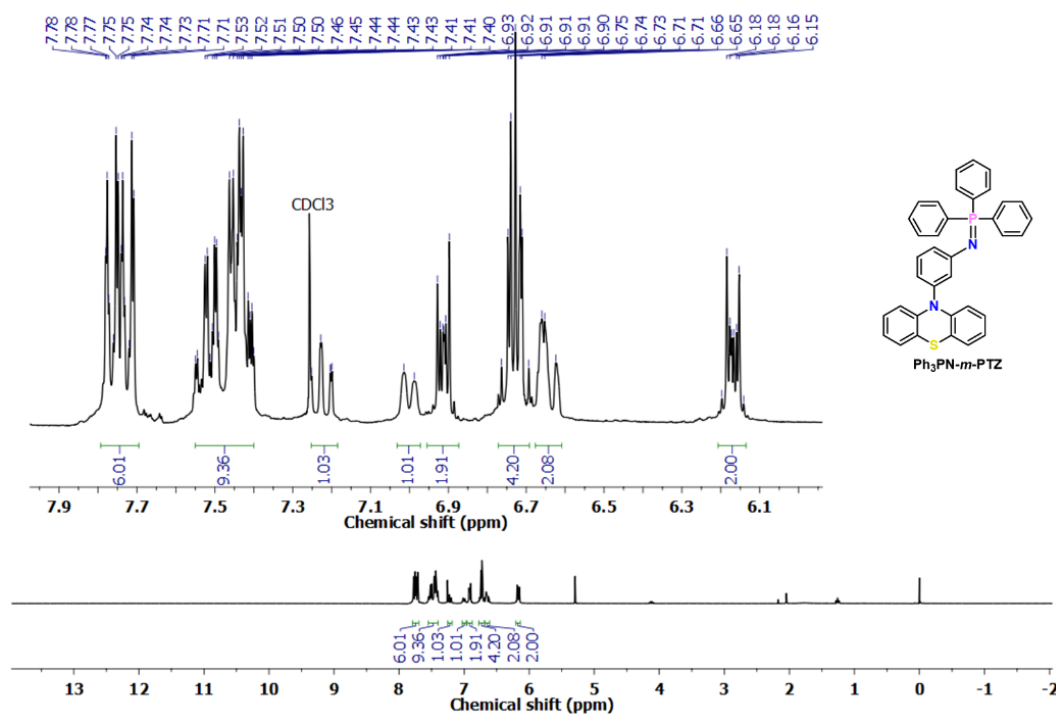
¹H NMR (300 MHz) in CDCl₃ of the compound **Ph₃PN-*m*-PTZ.**
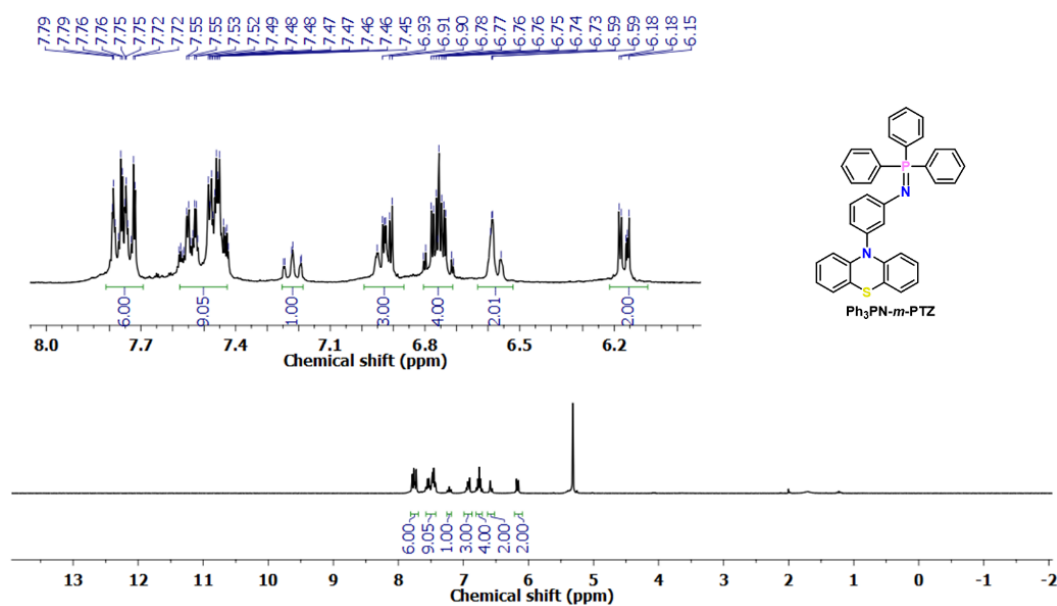
^{1}H NMR (300 MHz) in CD$_2$Cl$_2$ of the compound **Ph$_3$PN-*m*-PTZ.**
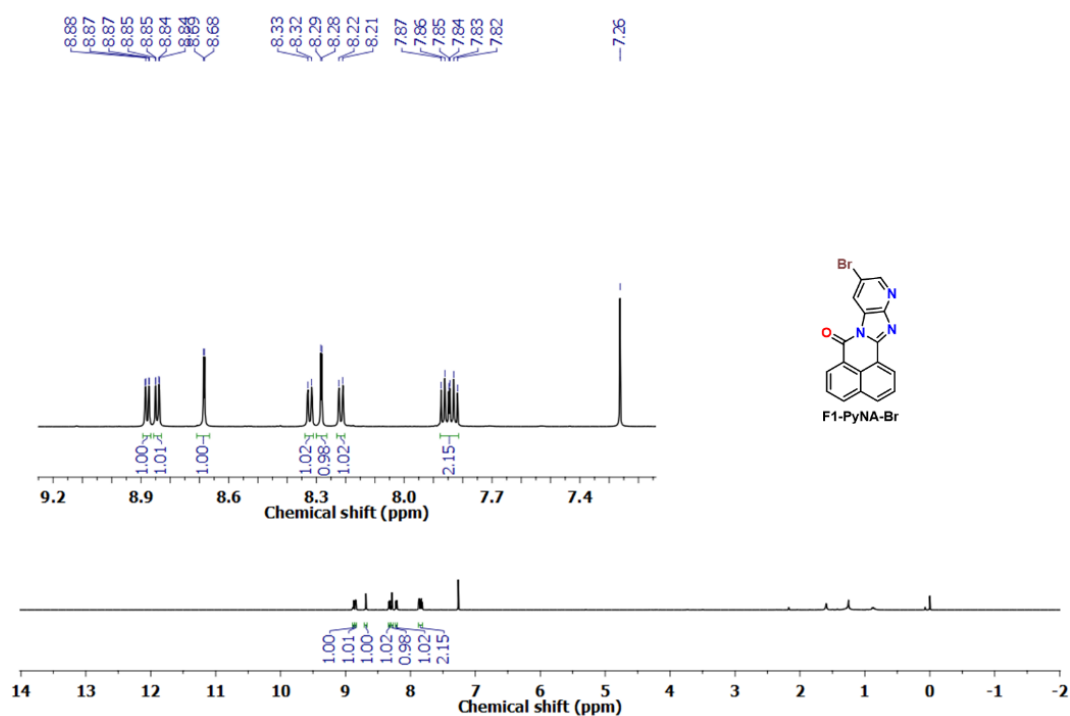

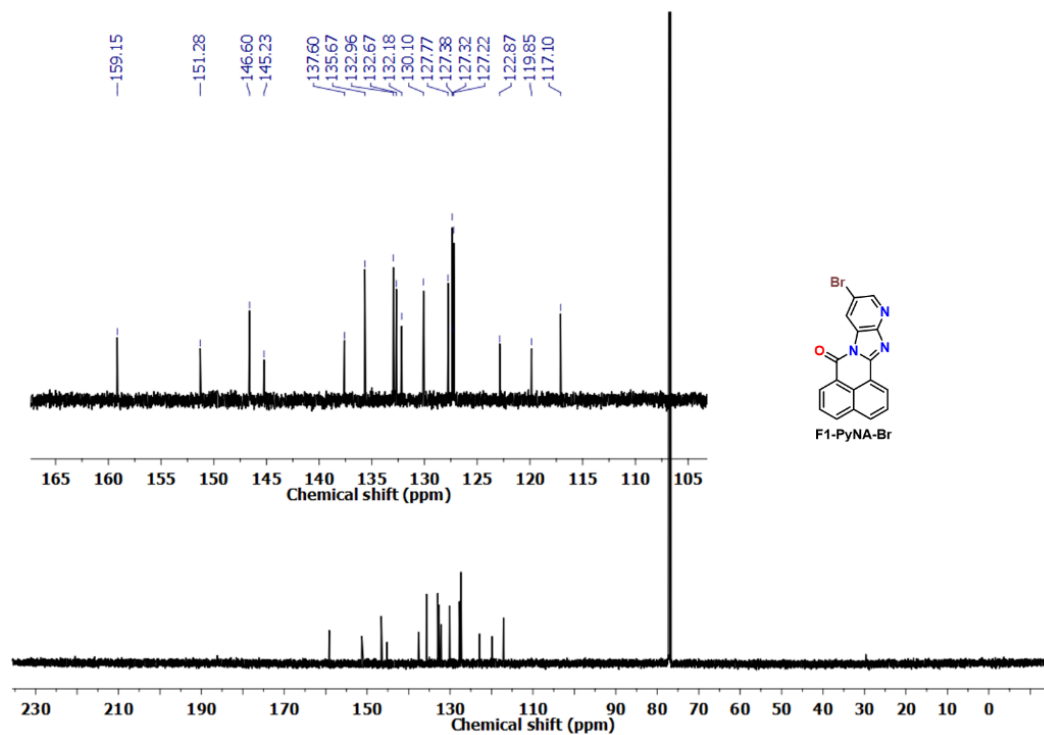^{13}C NMR (75 MHz) in CDCl$_3$ of the compound **Ph$_3$PN-*m*-PTZ.**
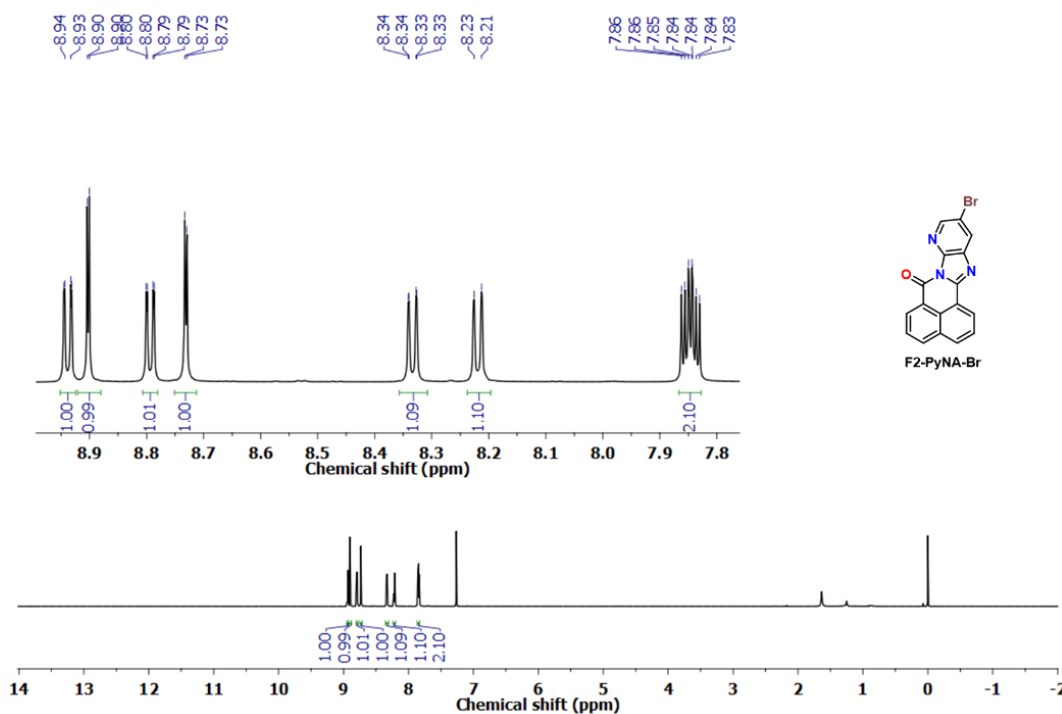
HRMS (TOF MS ES⁺) of the compound **Ph₃PN-m-PTZ**.

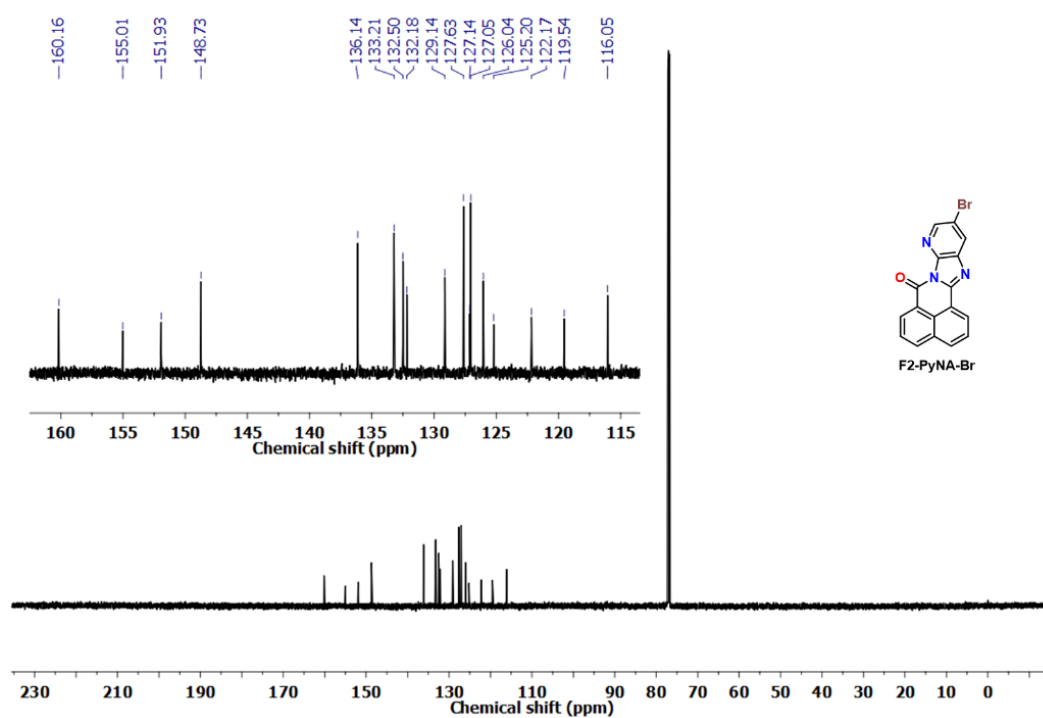## 12.7 F2-PyNA-donor compounds

^{1}H NMR (600 MHz) in CDCl₃ of the compound **F1-PyNA-Br.**
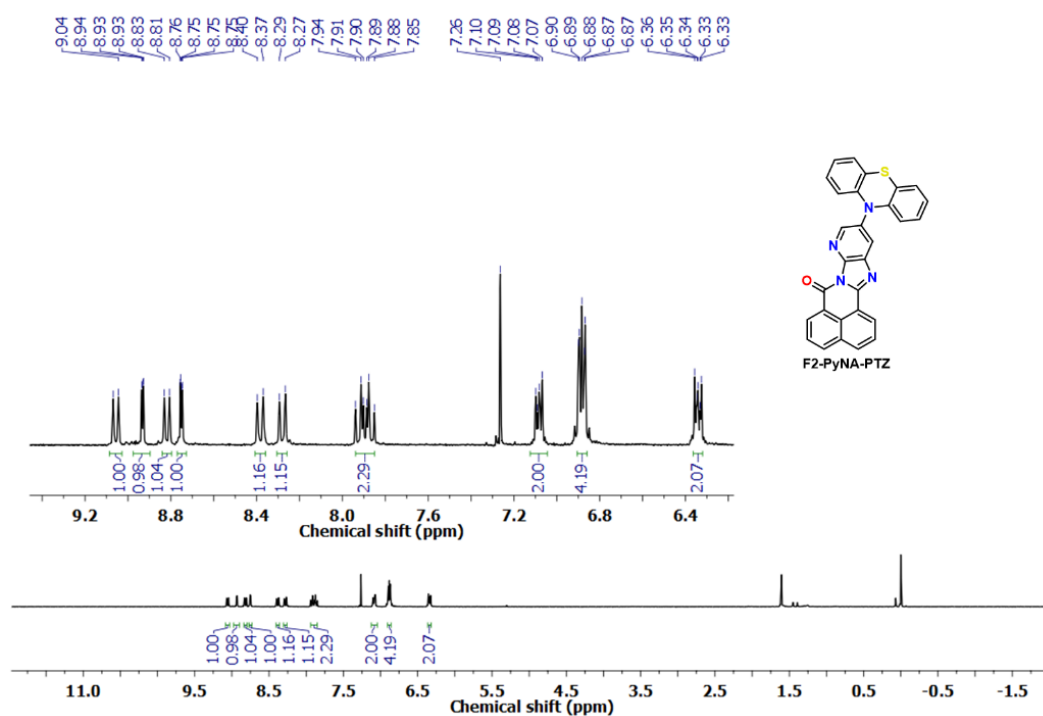
Welisson de Pontes Silva

^{13}C NMR (151 MHz) in CDCl$_3$ of the compound **F1-PyNA-Br.**

^{1}H NMR (600 MHz) in CDCl$_3$ of the compound **F2-PyNA-Br.**

^{13}C NMR (151 MHz) in CDCl$_3$ of the compound **F2-PyNA-Br.**

^{1}H NMR (300 MHz) in CDCl$_3$ of the compound **F2-PyNA-PTZ.**
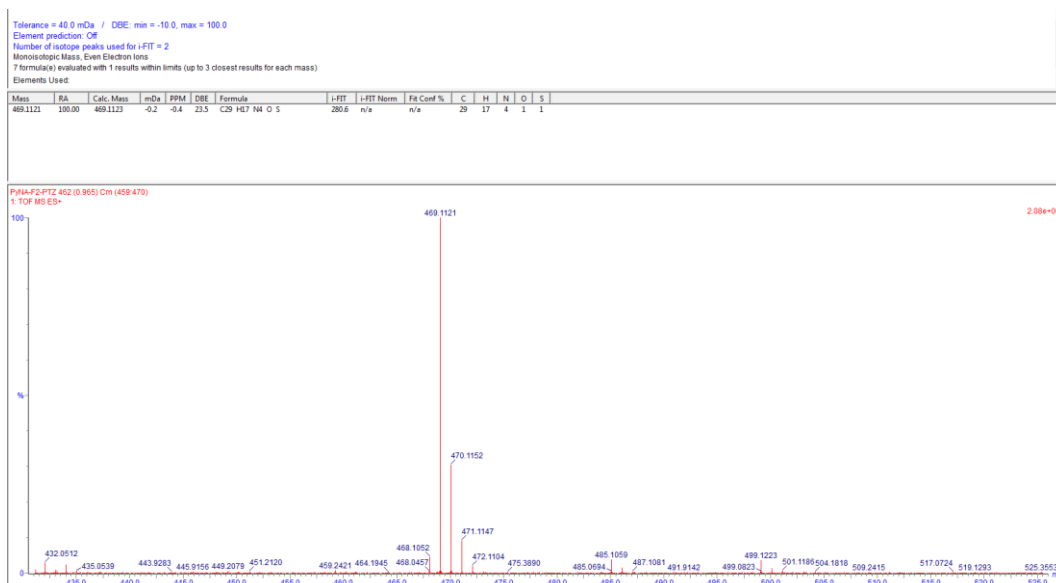
HRMS (TOF MS ES⁺) of the compound ***F2-PyNA-PTZ.***

13. Student achievements

Publications

Welisson de Pontes Silva, Nícolas Oliveira Decarli, Leandro Espíndola, Karol Erfurt, Agata Blacha-Grzechnik, Piotr Pander, Mieczyslaw Lapkowski and Przemyslaw Data. *Multifunctional Properties of D-A Luminophores Based on Acenaphtopyrido[2,3-b]pyrazine Core: Photophysics, Photochemistry, and Efficient Solution-Processed OLEDs.* **Journal of Materials Chemistry C**. 2023. DOI: 10.1039/d3tc02860g.

Welisson P. Silva; Edivandro Girotto; Hugo Gallardo; Rodrigo Cristiano. *Synthesis and characterization of photoactive columnar liquid crystals containing azobenzene and quinoxaline moieties*. **Journal of Molecular Liquids**. Volume 307, 2020. DOI: https://doi.org/10.1016/j.molliq.2020.112944.

André H. de Oliveira; **Welisson P. Silva**; Jordan K. da Silva; Júlio. C. O. Freitas; Miguel A. F. de Souza; Rodrigo Cristiano; Fabrício G. Menezes. *Non-symmetrical three and two-core ring mesogens based on quinoxaline and benzimidazole derivatives:*

Supramolecular layers through amphoteric donating/accepting H-bonds, **Journal of Molecular Structure.** Volume 1180, 2019, Pages 399-405. DOI: 10.1016/j.molstruc.2018.12.007.

Conferences

Poster: **Welisson de Pontes Silva**, Nícolas Oliveira Decarli, Leandro Espíndola, Agata Blacha-Grzechnik, Piotr Pander, Mieczyslaw Lapkowski and Przemyslaw Data. Design, synthesis and characterization of multifunctional D-A compounds to TADF-OLEDs application. International Symposium on Synthesis and catalysis (ISySyCat) 2023, 5-8 september, Évora, Portugal.

Poster: **Welisson de Pontes Silva**, Nícolas Oliveira Decarli, Leandro Espíndola, Mieczysław Łapkowski, Przemyslaw Data. *Design, synthesis and characterization of multifunctional D-A compounds based on acenaphtopyridopyrazine core*. 6 th International Workshops on Nano and Bio-Photonics (IWNBP), 25-30 september, 2022, Evian – France.

Poster**:** Nícolas Oliveira Decarli, **Welisson de Pontes Silva**, Mieczysław Łapkowski, Przemyslaw Data. *Design, synthesis and characterization of compounds based on diquinoxaline and dibenzophenazine cores*. *6 th International Workshops on Nano and Bio-Photonics (IWNBP),* 25-30 september, 2022, Evian – France.

Poster: **Welisson de Pontes Silva**; Edivandro Girotto; Hugo Gallardo; Rodrigo Cristiano. S*ynthesis of Columnar Liquid Crystals Containing Azo groups*. π-System Configuration European-Japanese Workshop 2019 (π – EJ 2019). Zabrze, Polska, 12-15.11.2019.

Poster: **Welisson de Pontes Silva**, Hugo Gallardo, Rodrigo Cristiano*. Luminescent liquid crystals derived from quinoxaline and thiophene*. XVIII Brazilian MRS Meeting, in Balneário Camboriú-SC, Brasil. 22-26.10.2019.

Poster: **SILVA, W. P**.; GIROTTO, E.; GALLARDO, H.; CRISTIANO, R. *Synthesis and Characterization of New Photoactive Columnar Liquid Crystals Containing Two Electronically Distinct Parts*. 42ª Reunião Anual da SBQ (RASBQ), in Joinville-SC, Brazil, 27-30.05.2019.

Additional Scholarships and Grants obtained

- ✓ **PRELUDIUM 20** - Design, Synthesis, and Investigation of New π-Conjugated Macrocycles with Thermally Activated Delayed Fluorescence for Organic Lighting Emitting Diodes/Transistors. Project number: 2021/41/N/ST4/03753. Amount: 209840 PLN.
- ✓ *Additional Scholarship by National Science Centre*-NCN: ***OPUS 16*** – 2018_31_B_ST5_03085 (NCN1/2020).
- ✓ Grant supporting academics starting their scientific activity in a new research field: *Synthesis and investigation of new D-A type molecules based on acenaphtopyridopyrazine as acceptor core to OLED applications.* Project number: 32/014/SDU/10-22-04. Amount: 12000 PLN.
- ✓ Research tasks carried out by young scientists SBM (BKM) - *Synthesis and spectroelectrochemical investigation of new asymmetric D-A-D molecules derived from imidazoquinoline.* Project number: 04/040/BKM21/0184 (BKM-552/RCH4/2021). Amount: 5000 PLN.

Project participation

Creation and development of an ERA Chair and Centre of Excellence in Organic Electronics as a strategic point for science and innovation development in the Silesian region and Poland*.* Exceed Research Group: http://exceedresearch.com/

OCTA-Organic Charge Transfer Applications: http://octa.organicelectronics.co.uk/

Internship participation

Brazyl, Physics department of the Federal University of Santa Catarina.

Period: 03 December, 2022 – 31 January, 2023.

Funded by Grant for the best PhD students under excellence initiative.

Welisson de Pontes Silva